

# **Development of a novel 3D culture system to understand bone – cartilage crosstalk in osteoarthritis**

**David James Hughes**



A thesis submitted in partial fulfilment of the requirements of Edinburgh  
Napier University, for the award of Doctor of Philosophy

February 2023

## **Declaration**

I declare that this thesis has been composed entirely by the candidate, David Hughes. This work has not previously been submitted for a Doctor of Philosophy, a degree, or any professional qualification. I have done all the work, unless acknowledged otherwise. All sources of information have been acknowledged.

David Hughes

## **Acknowledgements**

I would like to thank my supervisory team: Dr. Katherine Staines, Dr. Craig Stevens, Dr. Peter Barlow, Prof. Colin Farquharson, Dr. Amanda Pitkethly and Dr. Chris Allan for their guidance and support throughout the entirety of my PhD. Supervision throughout my project was the best a student could ask for and they have all helped develop and shape me as a scientist.

I would also like to thank everyone in the Edinburgh Napier School of Applied Sciences (SAS) that helped me through my time at Edinburgh Napier, including Dr. Staines' and Dr. Stevens' research groups and the technical staff from SAS. Additionally, I would like to thank Medical Research Scotland (MRS) for providing a generous research budget and stipend, whilst also providing support, encouragement, and opportunities to further shape my development as a researcher. Thanks, must also be paid to Biogelx who provided funding and support for my project. I'd like to thank my fellow students and friends who helped keep things light-hearted when challenges arose; I know I have made some friends for life.

I would like to pay special thanks to my family including my mother Linda Hughes who has always supported me in everything I do, this would not have been possible without her. I'd like to thank my brother Colin Hughes for always being there for guidance and to lighten the mood when times were tough. I'd also like to thank my grandmother Mary Paterson who has been an icon of resilience and discipline. Finally, I'd like to thank my partner Rosaleen McConville who has continually supported me through this entire endeavour and again, this would not have been possible without her love and support.

## Abstract

Osteoarthritis (OA) is a chronic degenerative disease of the articulated joint that affects approximately 10% of men and 18% of women over the age of 60 globally. There is no cure for OA, and current treatments aim to attenuate the symptoms e.g., non-steroidal anti-inflammatories are used to manage pain, and in severe cases, surgical intervention may be necessary. There is currently no validated *in vitro* model of OA, which limits understanding of the disease and makes the development of new therapies more challenging.

Animal models of OA do exist; however, scientists are now expected to adhere to the “3Rs” principle of animal experimentation: reduce, replace, and refine. The development of a physiological *in vitro* model of OA would reduce the need for animal experimentation and improve the consistency of results obtained using *in vitro* and *in vivo* models.

Development of a typical two-dimensional (2D) *in vitro* model of OA is challenging as the key cell types, in particular cartilage cells, often lose their phenotype. Additionally, *in vitro* models often focus on only one cell type (predominantly chondrocytes in the case of OA) which does not give any indication of crosstalk between cartilage and bone cells (osteoblasts) that becomes dysregulated in articulated joints during OA progression, a phenomenon which has been recognised in more recent OA research.

With the development of three-dimensional (3D) cell culture technologies, such as self-assembling supramolecular hydrogels, there is an opportunity to create a physiological *in vitro* model of OA using these new materials; 3D models have been shown to maintain cellular phenotypes and provide opportunities for the co-culture of multiple cell types and for the creation of direct cellular interfaces.

The research described here aimed to develop a 3D hydrogel co-culture model of OA by determining the most appropriate cell types and the optimal hydrogel conditions to recapitulate the articulated joint under both physiological and OA pathological conditions. Firstly, the most appropriate cell types were identified by analysis of the expression of genes and proteins associated with healthy and diseased chondrocytes and osteoblasts using RT-qPCR and immunoblotting techniques. The optimum hydrogel conditions for growing these cells were determined using RT-qPCR, immunoblotting,

immunostaining, and dye-based fluorescent staining, across a variety of hydrogel culture conditions, including hydrogels of varying stiffnesses and composition.

Finally, autophagy, a cellular degradation pathway that plays a key role in OA, and is a druggable target, was manipulated *in vitro* using the thiopurine Azathioprine, a potential novel drug for the treatment of OA.

## **Publications**

### **Review**

Samvelyan HJ, Hughes D, Stevens C, Staines KA. Models of Osteoarthritis: Relevance and New Insights. *Calcified Tissue International*. 2021 Sep;109(3):243-256.

## Abbreviations

2D	Two-dimensional
3D	Three-dimensional
AA	L-ascorbic acid
AC	Articular cartilage
ACAN	Aggrecan
ADAMTS	A Disintegrin and Metalloproteinase with Thrombospondin motifs
ADAMTS-4	A Disintegrin and Metalloproteinase with Thrombospondin motifs-4
ADAMTS-5	A Disintegrin and Metalloproteinase with Thrombospondin motifs-5
ALP	Alkaline phosphatase
AMPK	AMP-activated protein kinase
ANOVA	Analysis of variance
AP-1	Activator protein 1
ATG101	Autophagy-related 101
ATG12	Autophagy-related 12
ATG13	Autophagy-related 13
ATG14	Autophagy-related 14
ATG16	Autophagy-related 16
ATG3	Autophagy-related 3
ATG4	Autophagy-related 4
ATG5	Autophagy-related 5
ATG7	Autophagy-related 7
ATP	Adenosine triphosphate
BLC	Bone lining cells
BGLAP	Osteocalcin
BMP	Bone morphogenetic proteins
BMSC	Bone marrow stem cells
BMU	Basic multicellular unit
BRC	Bone-remodelling compartment
BSA	Bovine serum albumin
BSP	Bone sialoprotein
CCL2	Chemokine ligand 2
CCL5	Chemokine ligand 5
cFMS	Macrophage colony stimulating factor receptor
COL10A1	Collagen type 10 alpha 1 chain
COL1A1	Collagen type 1 alpha 1 chain
COL2A1	Collagen type 2 alpha 1 chain
COMP	Cartilage oligomeric protein
COX-2	Cyclooxygenase-2
CSF-1	Colony-stimulating factor 1
DAPI	4',6-diamidino-2-phenylindole
DC	Detergent compatible
DC-STAMP	Dendritic cell specific transmembrane protein

DMEM	Dulbecco's modified eagle medium
DMM	Destabilisation of the medial meniscus
DMP1	Dentin matrix protein 1
DMSO	Dimethyl sulfoxide
DNA	Deoxyribonucleic acid
ECL	Enhanced chemiluminescence
ECM	Extracellular matrix
EDTA	Ethylenediaminetetraacetic acid
ER	Endoplasmic reticulum
ERK	Extracellular signal-regulated kinases
FADD	Fas-associated death domain protein
FCS	Fetal calf serum
FGF	Fibroblast growth factor
FGF23	Fibroblast growth factor 23
FIP200	Focal adhesion kinase family interacting protein of 200 kD
GAG	Glucosaminoglycans
GFOGER	Type 1 collagen-like binding motif
GP38	Glycoprotein 38
HPA	Hydroxyapatite
IGF-I	Insulin-like growth factor 1
IHH	Indian hedgehog
IKVAV	Laminin-like binding motif
IL-1	Interleukin-1
IL-10	Interleukin-10
IL-1 $\beta$	Interleukin-1 beta
IL-6	Interleukin-6
IL-8	Interleukin-8
JNK	c-Jun N-terminal kinases
LC3	Microtubule-associated protein 1A/1B-light chain 3
LSB	Laemmli sample buffer
LSCM	Laser scanning confocal microscopy
MAPK	Mitogen-activated protein kinase
M-CSF	Macrophage colony-stimulation factor
MEPE	Matrix extracellular phosphoglycoprotein
MITF	Microphthalmia-associated transcription factor
MMP1	Matrix metalloproteinase-1
MMP13	Matrix metalloproteinase-13
MMP14	Matrix metalloproteinase-14
MMP3	Matrix metalloproteinase-3
MSC	Mesenchymal stem cells
MTOR	Mammalian target of rapamycin
MTORC1	Mammalian target of rapamycin complex 1
MV	Matrix vesicle
NCP	Non-collagenous proteins

NFATc1	Nuclear factor of activated T-cells c1
NFκB	Nuclear factor kappa-light-chain-enhancer of activated B cells
NHS	National health service
NO	Nitric oxide
NSAID	Nonsteroidal antiinflammatory drugs
NTC	No template control
OA	Osteoarthritis
OCN	Osteocalcin
OPG	Osteoprotegerin
OPN	Osteopontin
P/S	Penicillin-streptomycin
PARP	poly (ADP-ribose) polymerase
PBS	Phosphate buffered saline
PCL	Poly (ε-caprolactone)
PCR	Polymerase chain reaction
PDPN	Podoplanin
PE	Phosphatidylethanolamine
PEG	Poly (ethylene glycol)
PFA	Paraformaldehyde
PGE2	Prostaglandin E2
PGLA	Poly (D, L-lactide-co-glycolide acid)
PHEX	Phosphate-regulating gene with homologies to endopeptidases on the X chromosome
PI	Propidium Iodide
PI3K	Phosphatidylinositol 3-kinase
POSTN	Periostin
PO <sub>4</sub> <sup>3</sup>	Phosphate
PPF	Poly(propylene fumarate)
PTH	Parathyroid hormone
PU.1	Transcription factor PU.1
RANK	Receptor activator of nuclear κβ
RANKL	receptor activator of nuclear κβ ligand
RER	Rough-endoplasmic reticulum
RGD	Fibronectin-like binding motif
RIN	RNA integrity number
RIPA	Radio-immunoprecipitation buffer
RNA	Ribonucleic acid
RNA	Ribonucleic acid
ROS	Reactive oxygen species
RT	Reverse transcription
RUNX2	Runt-related transcription factor 2
SCB	Subchondral bone
SLRPS	Small leucine-rich proteoglycans
SOST	Sclerostin

SOX5	Sex-determining region Y-box 5
SOX6	Sex-determining region Y-box 6
SOX9	Sex-determining region Y-box 9
TGF- $\beta$	Transforming growth factor-beta
TGF- $\beta$ 3	Transforming growth factor-beta 3
TIMP1	Tissue inhibitor of metalloproteinase-1
TNFR-1	Tissue inhibitor of metalloproteinase-1
TNFR-2	Tissue inhibitor of metalloproteinase-2
TNF- $\alpha$	Tumour necrosis factor-alpha
TRADD	TNFR-1 associated death domain
TRAF2	TNF receptor-associated factor 2
TRAP	Tartrate-resistant acid phosphatase
UBL	Ubiquitin-like
UK	United Kingdom
ULK1	Unc-51-like kinase
UPR	Unfolded protein response
USA	United States of America
VEGF	Vascular endothelial growth factor
VEGFA	Vascular endothelial growth factor A
VPS15	Vacuolar protein sorting 15
VPS34	Vacuolar protein sorting 34
$\beta$ -GP	Beta-glycerophosphate

## Table of contents

1	Chapter 1: Background .....	17
1.1	Preface .....	17
1.2	The articular joint.....	17
1.2.1	Overview of articular joints.....	17
1.2.2	Subchondral bone and the synovial joint .....	18
1.2.3	Osteoblasts, osteoclasts, and osteocytes .....	21
1.2.3.1	Osteoblasts.....	21
1.2.3.2	Bone lining cells.....	22
1.2.3.3	Osteocytes.....	23
1.2.3.4	Osteoclasts .....	23
1.2.4	Bone matrix deposition and mineralization.....	24
1.2.5	Bone Remodelling .....	27
1.2.6	Cartilage and the articular joint .....	29
1.2.7	Chondrocytes .....	30
1.2.8	Articular cartilage formation.....	31
1.2.9	Mature articular cartilage and maintenance .....	33
1.3	Osteoarthritis overview .....	35
1.3.1	Osteoarthritis and bone .....	36
1.3.2	Osteoarthritis and cartilage .....	38
1.3.3	Bone-cartilage crosstalk in osteoarthritis .....	43
1.3.4	The role of autophagy in osteoarthritis .....	45
1.3.4.1	The autophagy pathway .....	45
1.3.4.2	Autophagy is linked to the pathogenesis of osteoarthritis.....	47
1.4	<i>In vitro</i> models of osteoarthritis .....	48
1.4.1	Two-dimensional monolayer models.....	49
1.4.2	Two-dimensional co-culture models .....	51
1.4.3	Explant culture models .....	51
1.4.4	Three-dimensional prefabricated scaffold models.....	52
1.4.5	Three-dimensional scaffold-free models .....	56
1.4.6	Biogelx.....	57
1.5	Aims.....	59
2	Chapter 2: Materials and methods .....	60
2.1	Reagents and solutions .....	60
2.2	Cell culture .....	60
2.2.1	C-28/I2 and SaOS-2 cell maintenance.....	60

2.2.2	Freezing/thawing C-28/I2 and SaOS-2 cells .....	60
2.2.3	Primary Human Chondrocytes .....	61
2.2.4	Freezing/thawing primary human chondrocytes.....	61
2.3	Hydrogel preparation.....	62
2.4	Hydrogel encapsulation .....	63
2.5	RNA methods .....	64
2.5.1	Isolation of RNA from cells.....	64
2.5.2	Determination of RNA integrity .....	64
2.5.3	Reverse transcription (RT).....	65
2.5.4	Real time quantitative polymerase chain reaction (RT-qPCR) and GeNorm analysis	65
2.5.5	GeNorm analysis .....	66
2.5.6	Quantification of gene expression .....	66
2.6	Protein methods .....	66
2.6.1	Protein extraction from two-dimensional cell cultures.....	66
2.6.2	Protein extraction from three-dimensional cell cultures. ....	67
2.6.3	Protein extraction from human articular cartilage .....	67
2.6.4	Quantification of protein .....	67
2.6.5	Immunoblotting .....	68
2.6.6	Quantification of Western blots .....	69
2.7	Cell tracker staining.....	69
2.8	Live/dead staining.....	70
2.8.1	Live/dead staining method .....	70
2.8.2	Live/dead staining analysis .....	71
2.9	Cell tracker staining.....	71
2.10	Immunofluorescence .....	72
2.11	Statistical analysis .....	72
Chapter 3: Characterization of two-dimensional chondrocyte and osteoblast cell cultures for use in a three-dimensional <i>in vitro</i> model. ....		73
3.1.	Introduction .....	73
3.2.	Aims and objectives .....	75
3.2.1.	Aim .....	75
3.2.2.	Objectives.....	75
3.3.	Methods.....	75
3.3.1.	Cell culture .....	75
3.3.1.1.	C-28/I2 optimizing media conditions.....	76
3.3.1.2.	C-28/I2 time course .....	76

3.3.1.3. SaOS-2 time course .....	76
3.3.2. RNA extraction, cDNA synthesis and RT-qPCR.....	77
3.3.3. Protein extraction and quantification.....	77
3.3.4. Immunoblotting .....	77
3.3.5. Statistical analysis .....	78
3.4. Results.....	78
3.4.1. Characterisation of primary chondrocytes .....	78
3.4.2. Characterisation of C-28/I2.....	78
3.4.2.1 Optimization of C-28/I2 growth conditions .....	78
3.4.2.2. Morphology of C-28/I2 under differing serum conditions .....	79
3.4.2.3. Analysis of chondrocyte-associated gene expression under differing serum conditions.....	80
3.4.2.4. Analysis of chondrocyte-associated protein expression under differing serum conditions.....	81
3.4.3. Characterization of C-28/I2 over a 12-day time course.....	85
3.4.3.1. Morphology of C-28/I2 over a 12-day time course. ....	85
3.4.3.2. Analysis of chondrocyte-associated gene expression over a 12-day time course. ....	85
3.4.3.3. Analysis of chondrocyte-associated protein expression over a 12-day time course.....	85
3.4.4. Characterization of SaOS-2 cells .....	90
3.4.4.1. Morphology of SaOS-2 cells over a 12-day time course .....	90
3.4.4.2. Analysis of osteoblast-associated gene expression over a 12-day time course	93
3.4.4.3. Analysis of osteoblast-associated protein expression over a 12-day time course .....	96
3.5. Discussion.....	98
Chapter 4: The impact of hydrogel encapsulation on C-28/I2 chondrogenic and SaOS-2 osteoblastic cell lines .....	105
4.1. Introduction .....	105
4.2. Aims and objectives .....	107
4.2.1. Aim .....	107
4.2.2. Objectives.....	107
4.3. Methods.....	108
4.3.1. Hydrogel preparation.....	108
4.3.2. Acellular hydrogel modelling and co-culture suitability .....	108
4.3.3. Cell culture .....	108
4.3.4. Hydrogel encapsulation .....	108
4.3.5. RNA extraction .....	109

4.3.5.1. RNeasy kit extraction (also used as a method for testing different gel volumes)	109
4.3.5.2. Standard Trizol extraction	110
4.3.5.3. Trizol + RNeasy kit extraction	111
4.3.5.4. Alternate Trizol method	111
4.3.6. cDNA synthesis and RT-qPCR	111
4.3.7. Protein extraction and quantification	112
4.3.8. Immunoblotting	112
4.3.9. Cell Tracker staining	112
4.3.10. Immunostaining	113
4.3.11. Live/Dead staining	113
4.3.12. Image processing and analysis	113
4.3.13. Statistical Analysis	114
4.4. Results	115
4.4.1. Acellular three-dimensional constructs	115
4.4.2. Optimising RNA extraction from hydrogel encapsulated cells	116
4.4.3. Comparison of two-dimensional and three-dimensional culture conditions on C-28/I2 cells	119
4.4.3.1. The effect of three-dimensional culture on the expression of chondrocyte associated genes	119
4.4.3.2. The effect of three-dimensional culture on the expression of chondrocyte associated proteins	121
4.4.3.2. The impact of culture substrate on C-28/I2 cell morphology	122
4.4.5. Comparison of three-dimensional and two-dimensional culture conditions on SaOS-2 cells	123
4.4.5.1. The effect of three-dimensional culture on the expression of osteoblast associated genes	123
4.4.5.2. The effect of three-dimensional culture on the expression of osteoblast associated proteins	125
4.4.5.3. The effect of hydrogel encapsulation on SaOS-2 cell morphology	126
4.4.6. C-28/I2 and Saos-2 functionalised hydrogel screening	127
4.4.10. The impact of long-term encapsulation of C-28/I2 and SaOS-2 cells in GFOGER and IKVAV hydrogels	130
4.4.11. The impact of short-term encapsulation of C-28/I2 and SaOS-2 cells in GFOGER and IKVAV hydrogels	135
4.5 Discussion	138
Chapter 5: Development of an inflammation-based co-culture model of osteoarthritis and investigation of autophagy as a potential therapeutic pathway	145
5.1. Introduction	145

5.2. Aims and objectives .....	147
5.2.1. Aims.....	147
5.2.2. Objectives.....	147
5.3. Methods.....	148
5.3.1. Cell culture .....	148
5.3.2. Cytokine and drug treatments.....	148
5.3.3. RNA extraction .....	148
5.3.4. cDNA synthesis and RT-qPCR.....	149
5.3.5. Protein extraction and quantification.....	149
5.3.6. Immunoblotting .....	149
5.3.7. Immunofluorescence .....	149
5.3.8. Statistical analysis .....	150
5.4. Results.....	151
5.4.1. Development of a cytokine-based inflammation model in C-28/I2 chondrocytes.	151
5.4.1.1. The effect of 24 hour cytokine treatment on C-28/I2 morphology.....	151
5.4.1.2. Nuclear Factor Kappa B activation in response to 24 hour cytokine treatment on C-28/I2 chondrocytes.....	152
5.4.1.3. The impact of 24 hour cytokine treatment on Matrix Metalloproteinase 13 gene expression in C-28/I2 chondrocytes.....	153
5.4.1.4. The impact of 24 hour cytokine treatment on Matrix Metalloproteinase 13 protein expression in C-28/I2 chondrocytes.....	154
5.4.2. 48 hour time course analysis of cytokine-induced inflammation in C-28/I2 chondrocytes.....	154
5.4.2.1. The effect of cytokine treatment on C-28/I2 morphology over a 48 hour time course.....	154
5.4.2.2. Nuclear Factor Kappa B activation in C-28/I2 cells treated with Tumour Necrosis Factor- $\alpha$ and Interleukin-1 $\beta$ over a 48 hour time course .....	156
5.4.2.3. The impact of cytokine treatment on gene expression associated with the chondrocyte phenotype over a 48 hour timecourse .....	158
5.4.2.4. Expression of chondrocyte and apoptosis associated proteins in C-28/I2 cells treated with Tumour Necrosis Factor- $\alpha$ and Interleukin-1 $\beta$ over a time course of 0 to 48 hours .....	160
5.4.2.5. Induction of autophagy in C-28/I2 cells treated with Tumour Necrosis Factor- $\alpha$ and Interleukin-1 $\beta$ over a time course of 0 to 48 hours .....	162
5.4.3. The effect of drug induced autophagy induction on C-28/I2 cells .....	164
5.4.3.1. The effect of autophagy induction on C-28/I2 cell morphology.....	164
5.4.3.2. The impacts of azathioprine and rapamycin on autophagy induction in C-28/I2 cells .....	165
5.4.3.3. Analysis of chondrocyte associated gene expression by C-28/I2 cells treated with rapamycin and azathioprine for 8 and 24 hours.....	167

5.4.3.4. Analysis of chondrocyte and autophagy associated protein expression by C-28/I2 cells treated with rapamycin and azathioprine for 8 and 24 hours. ....	168
5.5. Discussion.....	171
Chapter 6. General Discussion .....	178
6.1. Introduction .....	178
6.2. Determination of optimum cell lines and growth conditions.....	178
6.3. Development of a three-dimensional in vitro model of osteoarthritis .....	179
6.4. Viability of three-dimensional cell cultures .....	180
6.5. Phenotype of three-dimensional cell cultures.....	182
6.6. Autophagy as a potential therapeutic target.....	182
6.7. Development of novel therapeutics for osteoarthritis.....	183
6.8. Further applications.....	<b>Error! Bookmark not defined.</b>
6.9. Conclusions .....	186
6.9. Directions for future research.....	187
References .....	191
Appendix .....	223

# 1 Chapter 1: Background

## 1.1 Preface

Osteoarthritis (OA) is a chronic degenerative disease that impacts over one-third of UK residents over the age of 45, with this number increasing due to growing rates of obesity and an ageing population [1]. Various risk factors exist for OA including age, obesity, physical trauma [2], genetic disposition [3] and “wear and tear” on articular - particularly synovial joints. Patients who suffer from OA experience progressive loss of articular cartilage (AC) and thickening of subchondral bone (SCB). These processes are perpetuated by abnormal cartilage restoration and bone remodelling that ultimately leads to patient disability [4]. OA presents clinical symptoms such as pain, stiffness, swelling and decreased range of motion and eventually, disability [4–6]. Unfortunately, there are currently no effective treatments for OA. Management of the condition typically involves the attenuation of symptoms via anti-inflammatory medications with disease progression resulting in invasive surgical interventions such as arthroplasty. Previous research has primarily considered AC degradation as the main driving factor in OA pathogenesis however more recently, research has shown that SCB also plays a key role in this process. This has led to the hypothesis that OA should be considered a disease of the whole joint manifesting as a result of interactions between both the SCB and AC. There are currently no *in vitro* models available to test this hypothesis, potentially due to the drawbacks associated with two-dimensional (2D) *in vitro* modelling of the disease, therefore this thesis will aim to detail the development of a novel three-dimensional (3D) *in vitro* model of OA to investigate bone-cartilage crosstalk under pathological conditions.

## 1.2 The articular joint

### 1.2.1 Overview of articular joints

Joints exist within the body to connect the individual bones of the skeleton, providing support and leverage that allows for locomotion by facilitating the movement of multiple components of the musculoskeletal system as a single functional unit. The synovial joint or, diarthrodial joint, is a highly specialised anatomical region that allows

for simple as well as complex movement, these joints can be found throughout the body in a variety of locations including the hip and knee. Synovial joints are defined by the variety of tissues found throughout the joint space and the conglomeration of these tissues with each providing important components integral to joint stability, movement, and flexibility [7]. Within the diarthrodial joint space, a cartilaginous interface can be found between the bones involved in articulated movement and this interface is encased in a synovial membrane filled with synovial fluid. Each of these tissues possesses unique structural properties that collectively provide support, strength and shock absorption against compressive forces and impact, which occur during normal movement and locomotion (**Figure 1**).

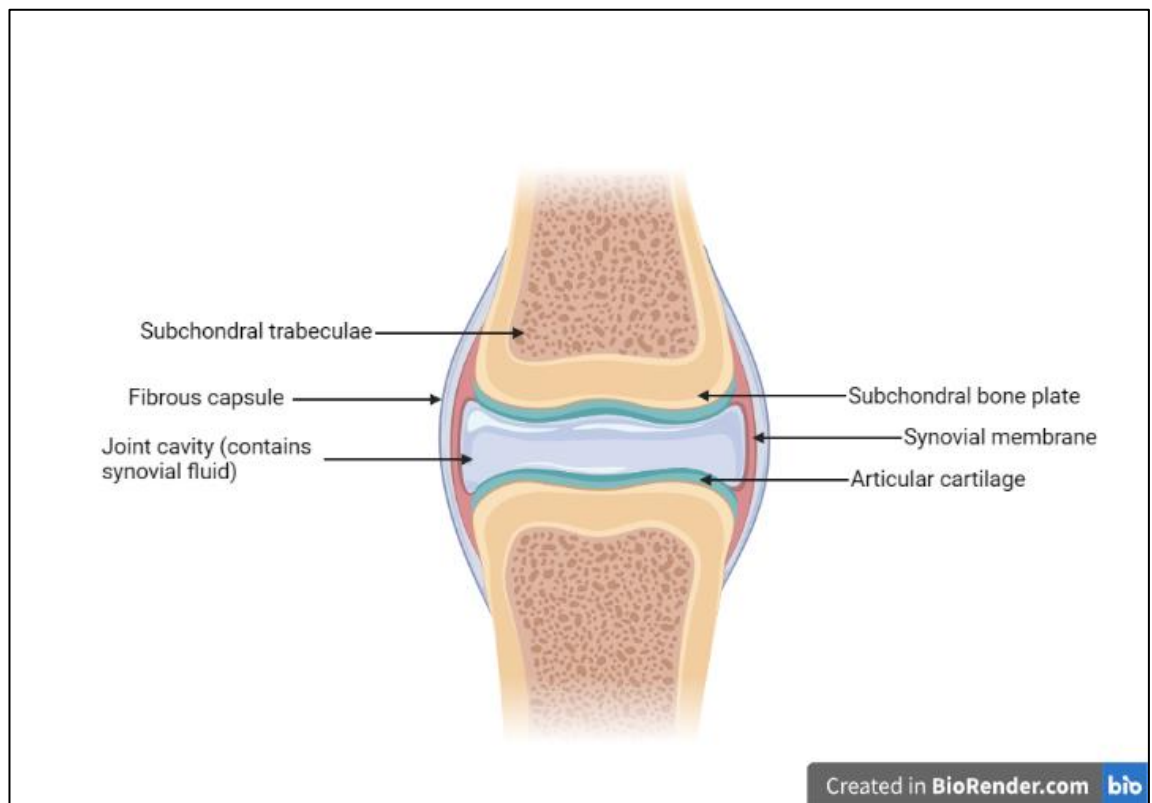


**Figure 1. General synovial joint.** Figure adapted from Prekasan and Saju (2016) [8] and created using BioRender.

### 1.2.2 Subchondral bone and the synovial joint

Bone is an adaptive tissue that serves a variety of functions within the body; some of which are apparent, for example, structural support, permission of movement and protection. Additionally, bone enacts several complex functions including mineral

homeostasis, growth factor and cytokine regulation [9], and haematopoiesis linking this tissue to immune processes [10]. Within the synovial joint, bone is found below the articular cartilage and here it is known as the subchondral bone (SCB). This SCB provides mechanical strength to the joint and is directly linked to the calcified cartilage and hard diaphysis in long bones, giving it a critical role in impact absorption; a function derived from its unique architecture (**Figure 2**) [11].

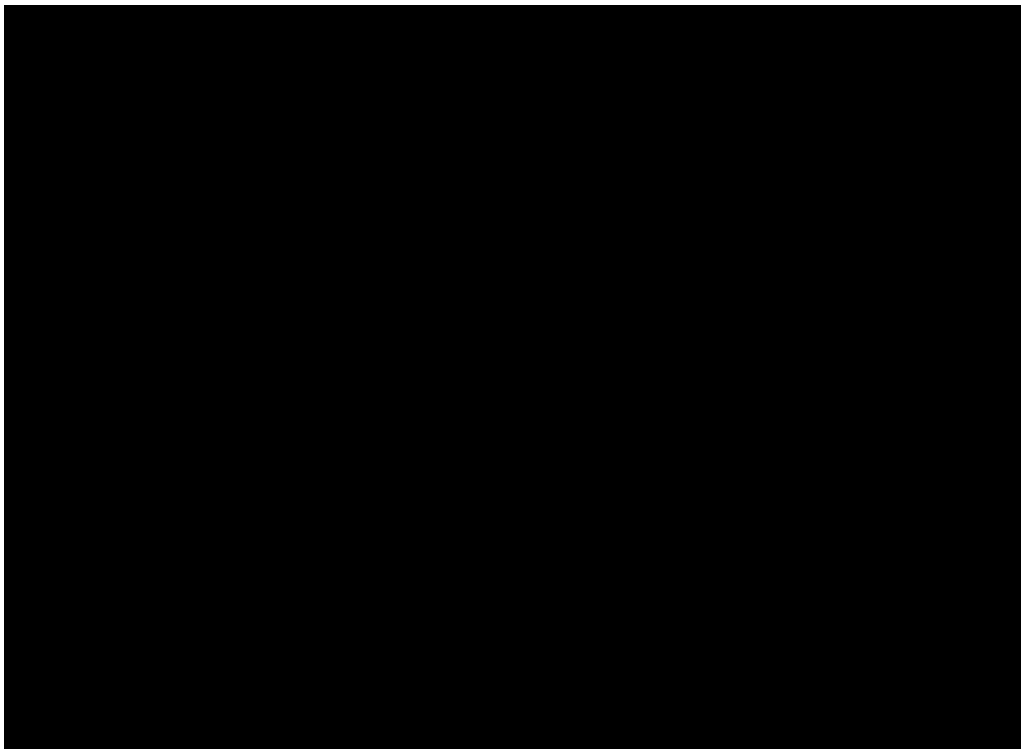


**Figure 2. The AC-SCB interface.** Four distinct regions of AC can be found within a synovial joint, these are found interfacing with the bone underneath the cartilage known as subchondral bone. Figure adapted from Mahjoub *et. al.* (2012) [12] using Servier Medical Art.

The SCB is separated from the calcified cartilage by a region known as the tidemark which interfaces directly with what is known as the SCB plate; a layer of bone with location-dependent variation in thickness ranging from 10 $\mu$ m to 3mm. Thinner regions of the SCB plate are generally comprised of appositional layers of trabecular bone with low numbers of haversian canals [13]. Trabecular bone is also found in the medullary cavity (**Figure 3**) and is known for its complex networked structure, around 20% of this tissue is comprised of bone with the remaining volume being made up of bone marrow and fat [14]. Trabecular bone provides flexibility and load transference and is also important for bone and cartilage nutrient supply, as inferred by its metabolic activity,

porosity, vascularization, and innervation [14–16]. Thicker regions of the SCB plate are structurally like compact bone. Compact bone is an extremely strong and dense material characterised by the presence of high numbers of osteons (**Figure 3**) [13, 17]. These osteons are comprised of concentric lamellae of cortical bone that provide strong support against multi-directional shearing and permit the direct connection between arteries, veins and nerves of SCB to the AC [15, 18]. Notably, the shape and diameter of these osteons are governed by both ageing and compressive forces being relayed through the joint [19].

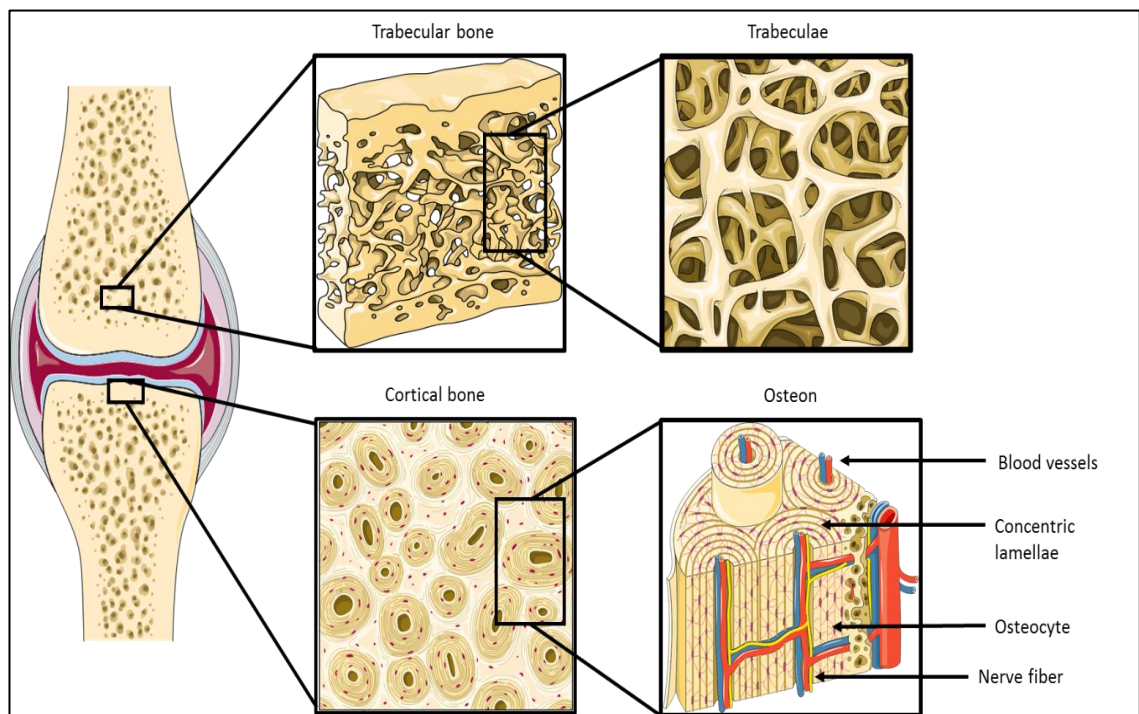


**Figure 3. Ultrastructure of trabecular and cortical bone.** Note that cortical bone image details structures in a transverse orientation however osteons are shown from a sagittal axial view. Figure adapted from El-Ganzuri *et. al.* (2016) [20]. using Servier Medical Art.

It is the combined assets of both trabecular and cortical bone that give the SCB its unique load-bearing properties with the compact SCB plate providing a solid platform for support, and the trabecular bone providing elasticity and shock absorption. These properties stem from the SCB being biphasic; it possesses both inorganic and organic components which yield specific, beneficial mechanical properties. The inorganic matrix consists of calcium ( $\text{Ca}^{2+}$ ) and phosphate ( $\text{PO}_4^{3-}$ ) crystals deposited on an organic matrix in the form of hydroxyapatite ( $\text{Ca}_5(\text{PO}_4)_3(\text{OH})$ ) which provides a rigid structure. The

organic component of the matrix (osteoid) is comprised primarily of collagen type I (~90% of the osteoid) as well as proteoglycans and glycosaminoglycans that form an elastic, supple material [13, 18]. Additionally, the organic matrix contains other non-collagenous proteins (NCPs) such as periostin, osteocalcin and alkaline phosphatase; markers of extracellular matrix formation and mineralization [21–24]. Synthesis of this organic matrix and subsequent mineralization is achieved via tightly regulated processes that can be induced in response to mechanical bone loading. This allows for the resorption of old bone and deposition of new bone in response to stress in accordance with Wolff's Law. Wolff's Law states that bone will adapt in response to the loading under which it is subjected, thus resulting in the formation of new bone along lines of stress [13]. This process of modelling and remodelling primarily involves three different terminally differentiated cell types: osteoblasts (bone-building cells), osteoclasts (bone-resorbing cells) and osteocytes (bone-signalling cells) [24, 25].

### **1.2.3 Osteoblasts, osteoclasts, and osteocytes**

#### **1.2.3.1 Osteoblasts**

The synthesis of a new organic matrix and its subsequent mineralization is carried out by cells known as osteoblasts. Osteoblasts are mononuclear, cuboidal cells derived from mesenchymal stem cells (MSCs) [26]. These cells can be found around the surface of the bone and display features commonly associated with protein-synthesising cells such as plentiful rough-endoplasmic reticulum (RER) and prominent Golgi apparatus and a variety of secretory vesicles [27]. Osteoblast differentiation is regulated by a variety of transcription factors including runt-related transcription factor-2 (Runx2), osterix (Osx), the activator protein (AP-1) family, activating transcription factor 4 (Atf4),  $\beta$ -catenin. Runx2 and Osx are considered the two primary transcription factors for maturation with Runx2 being considered a master regulator of osteoblast differentiation as Runx-2 knockout mice are found bereft of osteoblasts entirely [28]. The differentiation process itself is influenced by hormones, growth factors (GFs) and cytokines such as parathyroid hormone (PTH), parathyroid hormone-related proteins (PTHrPs), insulin-like growth factor I (IGF-I), bone morphogenetic proteins (BMPs), fibroblast growth factors (FGFs), as well as Wingless (Wnt) and notch signalling.

Both Runx2 and Osx factors have a role in early-stage differentiation with Runx2 upregulating the expression of genes associated with matrix production including bone sialoprotein (BSP), collagen I (COL1A1), osteocalcin (OCN), alkaline phosphatase (ALP) and osteopontin (OPN); with Osx potentiating this process [29, 30]. It is worth noting that during late-stage differentiation, Runx-2 has been shown to inhibit the final maturation of bone cells resulting in the impairment of bone matrix production and mineralization, whereas Osx has been shown to be necessary for these processes [30, 31].

Osteoblast differentiation is characterised by the formation of a collection of osteoblast progenitor cells which express both Runx2 and Col1A1, this is then followed by proliferation with osteoblast progenitors expressing ALP activity and are at this stage considered pre-osteoblasts [27]. The transition to mature osteoblast is characterised by an increase in Osx expression [30], subsequent secretion of bone matrix proteins such as collagen I, OCN and bone sialoproteins I and II (BSP-I, BSP-II) [29] as well as an accompanying cuboidal morphological change [32].

#### **1.2.3.2 Bone lining cells**

Bone lining cells (BLC) are osteoblasts which have become quiescent and can be found upon most trabecular and cortical bone surfaces. These cells are observed as a flat layer with a seam of the non-mineralized matrix. The cytoplasm is found to be extended along the bone surface with cell processes extending into the canaliculi and forming gap junctions with other BLCs and osteocytes [33]. Once stimulated the quiescent cells are activated, becoming larger, cuboidal in shape, and reacquiring their secretory activity. Activated BLCs can produce a variety of matrix-degrading enzymes and their associated inhibitors including matrix-metalloproteinase-13 (MMP-13), MMP14 and tissue inhibitor of metalloproteinase-1 (TIMP1) [34]. Additionally, BLCs can promote and inhibit osteoclastogenesis by expressing receptor activator of nuclear  $\kappa\beta$  ligand (RANKL) and osteoprotegerin (OPG). It is suggested that these cells may act as a mechanical barrier preventing inappropriate resorption of bone during remodelling whilst isolating osteoclastic activity from the bone marrow by creating a bone-remodelling compartment (BRC) [35]

### 1.2.3.3 Osteocytes

Osteocytes comprise around 95% of all bone cells present in mammalian bones. These cells are considered to have critical roles in bone remodelling, displaying mechanosensory properties and the ability to interact with both osteoblasts and osteoclasts [36, 37]. These cells are derived from osteoblasts which become embedded within the osteoblastic organic matrix that they secrete; ultimately becoming entombed once this matrix mineralizes [38]. Entombed osteocytes are found within lacunae displaying a dendritic morphology. These dendrites spread throughout canaliculi in bone – tunnels that connect cells on the bone to the vasculature, creating what is known as the lacunocanalicular network [39, 40]. Interestingly, the morphology of the cell body differs depending on what type of bone they are found within; trabecular bone-derived osteocytes have a rounded shape whereas those found in cortical bone display an elongated morphology [41]. It is considered that osteocytogenesis is marked by four individual stages of transition from the osteoblast precursor: osteoid-osteocyte, preosteocyte, young osteocyte and mature osteocyte [38]. The shift from osteoblast to osteocyte is accompanied by a distinct shift in genetic profile with a downregulation in osteoblast markers such as collagen I and alkaline phosphatase, and an upregulation of specific genes and their associated proteins such as dentin matrix protein 1 (DMP1), E11/GP38/podoplanin, FGF-23, matrix extracellular phosphoglycoprotein (MEPE), phosphate-regulating gene with homologies to endopeptidases on the X chromosome (PHEX) [42–45]. Once maturation has been achieved, the expression of genes such as SOST and its protein counterpart sclerostin can also be detected [46]. In addition to upregulating the aforementioned genes and their protein counterparts, osteocytes are found upregulating proteins related to cytoskeletal function such as destrin, macrophage capping protein (CapG), and E11 [47, 48].

### 1.2.3.4 Osteoclasts

Osteoclasts are the product of the fusion of mononuclear cells of a hematopoietic stem cell lineage, creating large multinucleated, terminally differentiated cells that are responsible for the resorption of bone [27]. This fusion is driven by cytokines such as macrophage colony-stimulation factor (M-CSF) which is produced by osteoprogenitor

mesenchymal cells (MSCs) and osteoblasts, and receptor-activator of nuclear factor  $\kappa$ - $\beta$  ligand (RANKL) which is also produced by osteoblasts, osteocytes and stromal cells. M-CSF targets the receptor cFMS which works to promote proliferation of osteoclast precursor cells and inhibit their apoptosis [49]. RANKL is part of a resorption regulating system alongside its receptor, receptor activator of nuclear factor- $\kappa$   $\beta$  (RANK), the inhibitor of RANKL, and OPG. RANKL directly binds to RANK inducing osteoclast formation [50]. However, the soluble receptor OPG, produced by osteoblasts and osteocytes can directly bind to RANKL and inhibit the RANK/RANKL interaction, preventing its osteoclastogenic effects [51, 52]. In addition to directly promoting osteoclastogenesis, the RANK/RANKL interaction induces the upregulation of other osteoclastogenic transcription factors such as the nuclear factor of activated T-cells c1 (NFATc1). NFATc1 interacts with transcription factors PU.1, cFos and MITF to induce osteoclast genes TRAP and cathepsin K [53]. It also upregulates the expression of DC-STAMP, a transcription factor that is vital for precursor fusion [54]. Once osteoclasts have formed and become activated upon a bone substrate, these cells polarize and subsequently form four distinct domains: the sealing zone, the ruffled border, the basolateral domain, and the functional secretory domain [55]. Both the sealing zone and ruffled border are in direct contact with the bone surface, and it is here resorption takes place. The sealing zone is an organelle-free zone that is characterised by the presence of an F-actin ring [56] and separates the osteoclast cell body and organelles from the ruffled border [55]. The ruffled border is formed due to lysosome and endosome trafficking, a vacuolar-type  $H^+$ -ATPase proton pump helps acidify the area of resorption [56], known as the lacuna, allowing the breakdown of apatite crystals via osteoclastic release of protons and enzymes such as tartare-resistant acid phosphatase (TRAP), cathepsin K and matrix metalloproteinase-9 (MMP-9) [57, 58].

#### **1.2.4 Bone matrix deposition and mineralization**

Formation of the bone matrix by osteoblasts occurs in two phases: the deposition of an organic matrix, followed by the mineralization of this matrix. The organic matrix also known as, "osteoid" is a dense substance comprised of cross-linked type I collagen supplemented with smaller non-collagenous proteins such as osteocalcin in addition to proteoglycans such as decorin and biglycan [59]. In this matrix, collagen I is arranged

into fibrillar structures with characteristic periodic banding, appearing as large rod-like structures. This macrostructure is achieved by the formation of a collagen triple helix. The triple helical structure here is achieved by the assembly of three parallel polypeptide strands forming a left-handed helix that is facilitated by repeating sequences of Xaa-Yaa-glycine in which X and Y are often proline or hydroxyproline residues followed by any amino acid [60, 61]. These polypeptides are arranged in a heterotrimeric fashion with two similar  $\alpha$ -1 chains and an  $\alpha$ -2 chain [59] and are configured in large parallel arrays with overlapping regions and “gap” or “hole” zones [59]. These zones are important for the mineralization process. NCPs such as osteocalcin are also important for the mineralization process. Osteocalcin is a low molecular weight protein (~5.8kDa) found only in bone and teeth. The presence of three  $\gamma$ -carboxyglutamic acid residues within the structure of OCN provides calcium-binding properties conveying an affinity for hydroxyapatite [62]. Research has shown that impairment of OCN function via incomplete carboxylation leads to an increased chance of osteoporosis [63] however OCN deficient mice display increased bone mass and functional quality [64]. Therefore, a regulatory role has been suggested for this protein which is further highlighted by its ability to act in an endocrine fashion by stimulating the  $\beta$ -cells of the pancreas to produce insulin which may be a pro-osteoblastic agent [65]. Proteoglycans such as decorin and biglycan belong to the small leucine-rich proteoglycans (SLRPs) family and have been shown to have an established function in regard to matrix structure and mineralization. Decorin is found throughout most collagenous matrices with its key function being that of collagen fibril assembly [66], disruption of the gene responsible for decorin production yields abnormal collagen structure and was shown to induce skin fragility in rat models [67]. Additionally, it has been shown that decorin may play a role in mineralization with high levels delaying and low levels accelerating the mineralization process [68]. Studies have shown decorin localizing to collagen fibrils at the osteoid border with calcification fusing these fibrils and causing a decrease of decorin around these fibrils [69]. Biglycan similarly to decorin is involved in collagen fibril assembly with ablation variation in collagen fibre size, shape, and arrangement [70] but may also affect osteogenesis. Biglycan deficiency has been shown to effect bone morphogenetic protein-4 (BMP-4) signalling – a member of the TGF- $\beta$  family of cytokines – reducing Runx2 expression and therefore reducing osteoblast differentiation.

Bone mineralization involves the deposition of minerals onto the organic matrix substrate. In this process, calcium ( $\text{Ca}^{2+}$ ) and phosphate ( $\text{PO}_4^{3-}$ ) crystals are deposited in the form of hydroxyapatite ( $\text{Ca}_5(\text{PO}_4)_3(\text{OH})$ ). These mineral deposits have been found to be site specific within the collagen fibril: in the intrafibrillar gap spaces where carboxy- and amino-terminal ends of serially arranged collagen triple helices meet and interfibrillar spaces between the fibrils [71]. The exact mechanism by which mineralization occurs is unknown; however, there are two main theories that account for this process: collagen template-mediated mineralization and matrix vesicle-mediated matrix mineralization.

Collagen template-mediated mineralization involves the direct nucleation and deposition of  $\text{CaPO}_4$  crystals onto specific regions within the collagen fibrils. These crystals then diffuse throughout the collagen fibrils creating an amorphous phase which is then transformed into oriented apatite crystals which is coordinated by the collagen fibre arrangement [72].

Alternatively, the matrix vesicle (MV)-mediated mineralization process involves the secretion of extracellular vesicles from cells such as osteoblasts, chondrocytes and odontoblasts [73]. These MVs are small (~100nm in diameter) particles that are produced via budding from the cell membrane [74]. MVs initiate mineralization by drawing  $\text{Ca}^{2+}$  that is pulled into the MV structure such as calcium-binding acidic phospholipids i.e., phosphatidyl serine [75]. Local intravesicular and perivesicular phosphate concentrations are raised by membrane-bound enriched phosphohydrolases such as alkaline phosphatase (ALPL) [76]. The uptake of phosphate is also facilitated by a sodium-dependent phosphate transporter that is present in MVs [77]. This accumulation of  $\text{Ca}^{2+}$  and  $\text{PO}_4^{3-}$  leads to the precipitation of the first  $\text{CaPO}_4$  mineral deposits within the MV, eventually leading to hydroxyapatite formation [74]. Once hydroxyapatite crystals have been formed, these are released from the MV into the extravesicular environment, MV binding to ECM collagens II and X which may act as a bridge for crystal propagation into the extravesicular matrix [78]. Upon mineral release, vesicular mineralization would occur followed by extravesicular collagen mineralization [79] which possesses distinct temporospatial characteristics. The mineral is first seen deposited in and on the collagen in a localized manner, and subsequently engulfing the remainder of the fibre as time progresses [79].

Mineralization processes are regulated by serum concentrations of both calcium and phosphate. Deprivation of calcium can be seen to cause rickets, with symptoms including progressive genu valgum due to the bone being soft and under-mineralized [80]. Inorganic pyrophosphate (PPi) acts as an inhibitor to mineralization by preventing the incorporation of calcium and inorganic phosphate into apatite crystals however the ectoenzyme alkaline phosphatase (ALPL) acts to hydrolyse PPi into inorganic phosphate (Pi). With an increasing Pi/PPi ratio, the mineralization process is promoted [81].

### **1.2.5 Bone Remodelling**

Bone remodelling is a multi-step process involving osteoblasts, osteoclasts and osteocytes. Osteoblasts and osteoclasts form a basic multicellular unit (BMU) which is responsible for osteoclastic degradation (resorption) of old bone matrix and subsequent osteoblastic deposition of new bone matrix. This process is regulated by factors in the cellular microenvironment or in response to mechanical stimulation of osteocytes achieved by locomotion or trauma [24, 25]. Remodelling is a multi-step process that involves an activation phase, a resorption phase, a reverse phase, a formation phase, and a termination phase [82].

The activation phase involves the stimulation of bone lining cells via mechanical stimulation detected by osteocytes [83], or by factors released into the bone microenvironment such as the serum-calcium regulator: parathyroid hormone (PTH). Stimulation of the bone lining cells results in a cascade of signalling events that begins the process of bone resorption.

The resorption phase involves the recruitment of osteoclast precursors via osteoblast-produced chemokines such as monocyte chemoattractant protein-1 (MCP-1) [84]. In addition to this, increased osteoblastic expression of colony-stimulating factor-1 (CSF-1) and receptor activator of nuclear  $\kappa\beta$  ligand (RANKL). CSF-1 expression results in an increase in proliferation and survival of osteoclast precursors whilst RANKL interacts with its receptor, receptor activator of nuclear  $\kappa\beta$  (RANK) [85, 86]. RANK is present on the surface of pre-osteoclasts and RANK-RANKL interaction drives these cells toward a differentiated multinucleated state via pre-osteoclast fusion. Throughout this phase expression of osteoprotegerin (OPG) a known osteoclastogenesis inhibitor is down-

regulated [86]. Subsequently, a catabolic phenotype is induced in which osteoblasts upregulate matrix metalloproteinases (MMPs) [87] such as MMP-13 [88]. These MMPs degrade the unmineralized osteoid that lines the bone surface and exposes arginine, glycine and aspartate (RGD) adhesion sites found on the underlying mineralized bone which facilitates osteoclast attachment [89]. Once bound to these sites the osteoclasts create a clear zone, or sealed zone – a microenvironment in which controlled resorption of the bone can occur. Osteoclasts will then work to acidify this microenvironment via the release of hydrogen ions ( $H^+$ ). In this instance, acidification serves two functions: to leech the mineral component of the bone and to increase the activity of specific osteoclast-derived enzymes such as the collagenolytic cathepsin K [90]. This bipartite process ensures that the mineral and organic components of bone are appropriately degraded and resorbed, leaving resorption pits known as Howship's lacunae [91]. This leads to the reversal phase.

Once resorption and formation of the Howship's lacunae have occurred, the reversal phase occurs. Reversal is conducted by a mononuclear cell of unknown origin and there is contention as to whether this process is undertaken by cells derived from an osteoblastic lineage [92], monocytic lineage [93] or is in fact conducted by cells from both lineages in tandem [89]. This unknown cell clears any undigested, de-mineralized matrix and then prepares the leftover mineralized surface for new bone formation achieved by the creation of an osteopontin-rich cement line upon which collagen is deposited.

The formation phase of bone remodelling may be induced by resorption-formation coupling factors released from resorbed bone, or from cells actively involved in the remodelling process. Growth factors such as the osteotropic transforming growth factor beta-1 (TGF- $\beta$ ) may be liberated from resorbed bone and have been shown to induce coupling between resorption and formation [94]. Osteoclasts have been shown to directly produce coupling signals in the form of soluble molecules such as sphingosine 1-phosphate which induces osteoblast precursor recruitment and promotes mature osteoblast survival [95]. Additionally, osteoclasts may be responsible for coupling via direct interactions with osteoblasts via the EphB4-ephrin-B2 bidirectional signalling complex. Osteoclasts express the ephrin-B2 ligand with which osteoblastic EphB4 receptors interact; this interaction is bidirectional and can either: enhance osteogenic

differentiation whilst also inhibiting osteoclastogenesis, or conversely, enhance osteoclastogenesis and inhibit osteogenesis [96]. Mechanical or PTH stimulation of osteocytes may also link the resorption-formation process as both stimuli have been found to decrease the production of sclerostin – a known inhibitor of bone formation produced in osteocytes [97, 98].

Once formation has been induced osteoblastic precursors will return to the resorption lacunae and differentiate. At this stage, they will produce molecules associated with the organic bone matrix such as collagen I as well as non-collagenous proteins and this matrix will subsequently become mineralized with the mature osteoblasts either becoming apoptotic, transitioning to a bone lining cell phenotype, or becoming embedded within the bone and differentiating into an osteocyte [89].

### **1.2.6 Cartilage and the articular joint**

In articulated joints, hyaline cartilage is found in the joint space sheathing bone surfaces – acting as a barrier providing lubrication and shock absorption [99]. This cartilage is comprised of sparsely distributed chondrocytes surrounded by a thick extracellular matrix (ECM), split into four distinct zones: superficial, intermediate, radial, and calcified, with each of these zones possessing properties that are unique and necessitated by cartilage function (**Figure 4**) [12, 100].

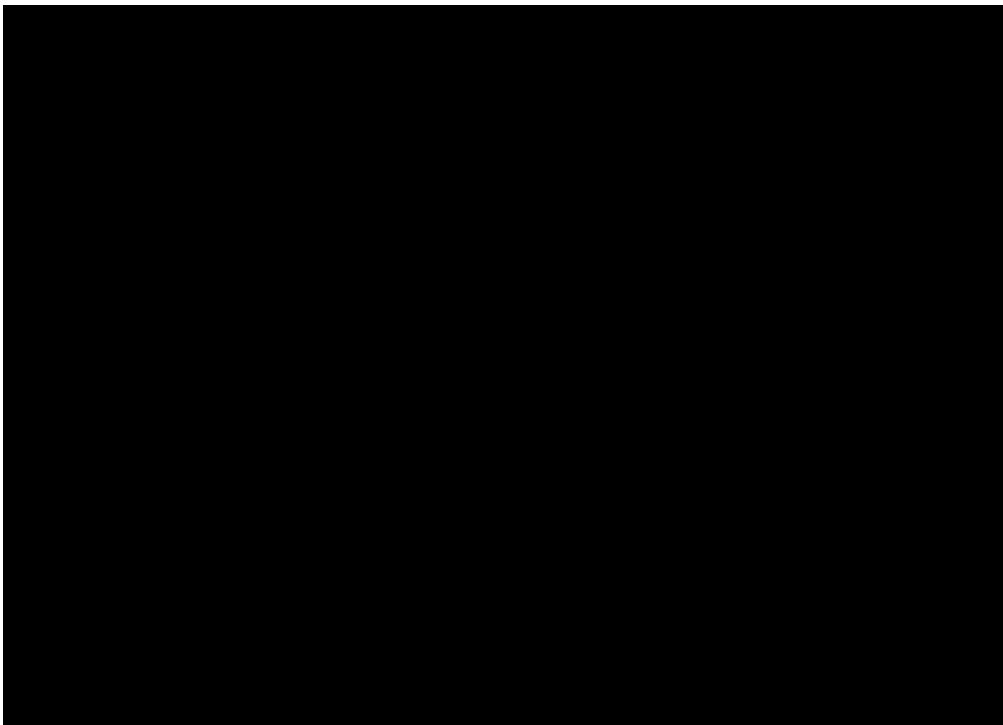


**Figure 4. Three-dimensional representation of the AC-SCB interface.** The articular cartilage is split into four distinct zones, the superficial zone, intermediate zone, radial zone, and calcified zone. The tidemark denotes the interfacial region between the AC and SCB. Main structural molecules are highlighted along with their appropriate orientations which can be seen to be unique in each separate cartilage region. The orientation and phenotype of chondrocytes can also be seen to differ throughout the AC. Figure adapted from Baumann *et. al.* (2019) [101]. using Servier Medical Art.

### 1.2.7 Chondrocytes

Development of the articular joint and cartilage is dependent on MSCs that progressively differentiate through various chondrocyte stages, each with a different role and function in development [100, 102]. Chondrocytes are mononuclear cells responsible for the deposition of the cartilaginous matrix; synthesising collagen, glycoproteins, proteoglycans and hyaluronan [103]. During the process of endochondral ossification and articular cartilage formation, these cells transition through various stages of activity, altering their morphology, as well as gene and protein expression profiles. Once a limb has fully developed these cells are then only active in regions known as the growth plate and AC [102, 104]. Although AC chondrocytes are metabolically active, the level of metabolic turnover they experience is low due to their aneural, avascular, alymphatic microenvironment which is particularly hypoxic. Chondrocytes are therefore dependent on nutrient diffusion through the ECM [105].

### 1.2.8 Articular cartilage formation

AC is produced because of the embryonic development of the appendicular skeleton. Most of the appendicular human skeleton is formed during embryonic development as a hyaline cartilaginous anlage (**Figure 5**) [102], with AC forming at the end of many of these ossified structures to facilitate skeletal movement and provide support creating articular joints. Endochondral ossification is initiated via the condensation of MSCs characterised by an increase in expression of the transcription factor *SOX9*, a key chondrogenic regulator. This condensation eventually produces a cartilage primordium containing immature chondrocytes [106, 107]. These immature chondrocytes no longer undergo the regular cell cycle and increase in volume dramatically becoming what is known as hypertrophic chondrocytes [108]. As cartilage grows longitudinally, chondrocytes continually differentiate into hypertrophic chondrocytes and are eventually replaced by bone in the primary ossification centre. Production and maturation of chondrocytes then become limited to the epiphysis of the developing structure a region known as the growth plate; a secondary ossification centre forms here and separates the growth plate from the distal region of long bones. Throughout the process of chondrocyte hypertrophy, longitudinal extension, growth plate formation and resultant AC formation, chondrocytes change between distinct expression profiles in a progressive manner, altering the properties of the developing skeletal element and articular joint [106]. Small, rounded chondrocytes in the epiphyseal region give rise to flattened immature chondrocytes expressing chondrogenic transcription factors *SOX5*, *SOX6* and *SOX9*, as well as *Col2 $\alpha$ 1* and aggrecan (*ACAN*). These cells mature into pre-hypertrophic chondrocytes that are characterised by the expression of the parathyroid hormone 1 receptor (*Pth1r*) and the cell signalling protein Indian hedgehog (*IHH*). Further maturation occurs with pre-hypertrophic chondrocytes becoming early hypertrophic chondrocytes characterised by expression of *Col10 $\alpha$ 1*. Throughout this transition through hypertrophic states, the expression of *SOX5*, *SOX6* and *SOX9* as well as *Col2 $\alpha$ 1* and *Acan*. Pre-hypertrophic chondrocytes eventually mature once more into late hypertrophic chondrocytes expressing vascular endothelial growth factor (*VEGFA*), *MMP-13* and *OPN*. The expression of *VEGFA* and *MMP-13* promotes blood vessel formation and matrix remodelling, allowing endothelial cells, osteoblasts, and osteoblast precursors to infiltrate the tissue. These cells work in tandem with perichondrium-derived osteoblasts to remodel the growth plate and form trabecular

bone [109, 110]. These endochondral structures are mapped during articular joint formation, with presumptive articular joint spaces in the cartilaginous anlagen becoming marked by an inter-zone of mesenchyme which will act as the site of stable articular cartilage formation. This area is indicated by the presence of flat mesenchymal cells [102] and the removal of this site results in no joint formation, highlighting its importance [111]. These interzone cells are chondrocyte-derived, however, they can be characterised by a cessation in *Col2 $\alpha$ 1* expression [112] and expression of growth differentiation factor-5 (*Gdf-5*) and versican at each presumptive articular joint site [113, 114]. These inter-zones differentiate into three layers: two chondrogenic layers which will cover the surfaces of the opposing developing skeletal structures and an intermediate layer that exists between these chondrogenic layers [102]. The exact mechanism of articular cartilage formation following these processes is not fully elucidated, however, it has been suggested that the aforementioned chondrogenic layers are incorporated into bone epiphysis, whereas cells from the intermediate layer differentiate to become articular chondrocytes, creating a layered structure that eventually transitions into mature articular cartilage creating two distinct borders between anlagen structures and resulting in joint cavitation [115]. Research has suggested that articular cartilage develops in an appositional manner, with new articular cartilage chondrocytes developing at the articular surface, expanding in the intermediate zone, and becoming terminally differentiated in the radial zone creating mature articular cartilage [116]. Upon maturation, AC takes on a very distinct and varied phenotype and genotype within the tissue itself, creating a unique structure necessitated by its' function [100].

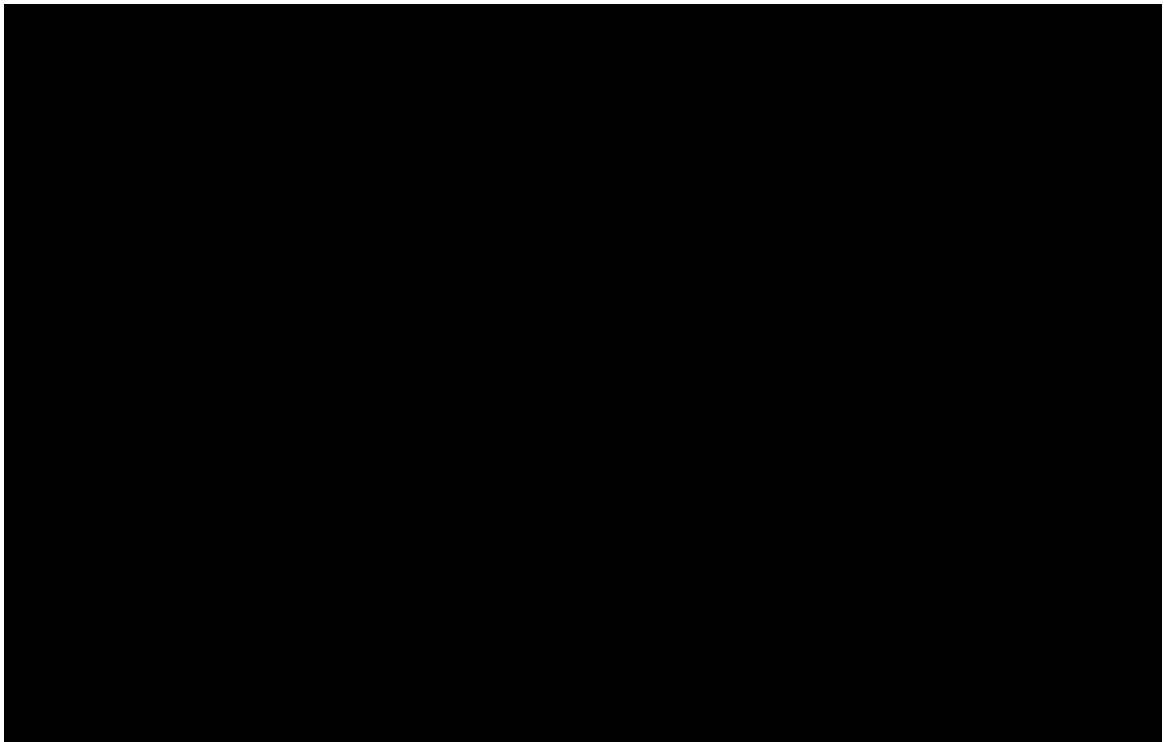


**Figure 5. Schematic showing synovial joint formation using the digit as an example articulated structure (A-F).** (A) Initial condensations of mesenchymal chondroprogenitors forming an uninterrupted anlage. (B) The joint site is determined by currently unknown mechanisms, potentially Hox genes. (C) The interzone forms via the clustering of mesenchymal cells creating a distinct region in which the joint will form, simultaneously mesenchymal cells making up the remainder of the anlage differentiate into chondrocytes and produce the cartilaginous template for the skeleton. (D) Cavitation begins and leads to the separation of the anlagen. (E) Anlagen at each side of the newly formed cavity begins to change shape and form complimentary interlocking structures. (F) Distinct tissues form and create a cohesive joint structure. This entire process is continuous, and the above schematic highlights a stepwise process for descriptive purposes. Figure adapted from Pacifi *et. al.* (2005) [104] using Servier Medical Art.

### **1.2.9 Mature articular cartilage and maintenance**

The mature AC ECM consists of predominantly type II collagen, glycoproteins, proteoglycans such as aggrecan, and water; these yield strong tensile properties whilst keeping the matrix flexible [99]. Type II collagen exists as the main structural component of the AC. It is structurally similar to type I collagen as detailed in section 1.1.4. existing as a large, fibrillar, trimeric molecule. However, type II collagen is a homotrimeric molecule comprised of three  $\alpha$ -1 collagen chains compared to type I collagen's heterotrimeric two  $\alpha$ -1 chains and one  $\alpha$ -2 chain [117]. The most abundant proteoglycan in cartilage is aggrecan. Aggrecan directly binds to hyaluronan which is bound to collagen fibrils [118]. Aggrecan contains many glycosaminoglycans including chondroitin

and keratan sulphate which provide this molecule with an overall negative charge which helps the cartilage retain water and therefore create osmotic pressure giving cartilage properties that allow it to resist deformation and compression [118]. AC contains other non-collagenous molecules such as the glycoproteins lubricin and cartilage oligomeric matrix protein (COMP). Lubricin functions to provide lubrication of the articular surface [119] whereas COMP interacts with a variety of other ECM components such as collagen type I and II helping retain matrix structure and microfibril formation within the ECM [120, 121]. Glycosaminoglycans such as hyaluronan are also key components of the ECM. Hyaluronan has lubricant properties [122], but in addition to this, provides mechanical stiffness and acts as an intermediate binding molecule between aggrecan and the collagen network [123].

The AC can be split into four distinct zones: superficial, intermediate, radial, and calcified. Chondrocyte morphology, as well as ECM matrix composition and structure, has been found to change depending on which region in the articular cartilage the chondrocytes are located. The superficial zone contains flattened chondrocytes arranged amongst collagen fibres that run parallel to the joint surface providing shear stress resistance [100]. In the intermediate zone, chondrocytes are found to be more rounded and dispersed amongst a randomly organised collagen network. In both the superficial and intermediate zones, the chondrocytes show a differentiated phenotype with the high secretion of collagen type II, IX and XI as well as proteoglycans [12, 124]. In contrast, the radial zone is characterised by collagen fibres which extend through the matrix arranged perpendicular to the joint surface, where terminally differentiated, chondrocytes are found arranged in columns and expressing hypertrophy markers: predominantly collagen type X [12, 124, 125]. Below the radial zone, the tidemark can be found which splits non-mineralized cartilage from the calcified cartilage [126]. Finally, the calcified zone acts as an interface between mineralized cartilage and subchondral bone. This region contains hypertrophic chondrocytes which also express collagen type X [12, 125]. Collagen type X is associated with the regulation of proteolytic enzymes which act to remove the cartilage ECM paving the way for vascularisation, innervation and calcification ultimately facilitating bone growth and turnover [12, 124, 127].

Once developed, mature AC exists as a permanent tissue, which differs from the transient cartilage involved in the process of skeletal development and endochondral

ossification; their capacity to undergo proliferation, maturation and hypertrophy is greatly diminished. However, under disease conditions, such as those found in OA [100]. Under OA conditions articular chondrocytes can take on a genotypic profile similar to those found in the growth plate and can display a hypertrophic phenotype as well as a catabolic activity associated with bone-cartilage remodelling, this ultimately results in the degradation of the AC [100, 128, 129].

### **1.3 Osteoarthritis overview**

OA is a chronic degenerative disease that results in the progressive loss of articular joint cartilage and thickening of SCB and is perpetuated by abnormal cartilage restoration and bone remodelling that ultimately leads to patient disability (**Figure 6**) [4, 130]. As OA progresses the condition is characterised by joint space narrowing, as well as the formation of bone marrow lesions, cysts, and tidemark duplication [131–133]. Additionally, the calcified cartilage region is found to increase in volume and is subject to vascular penetration which eventually reaches the non-calcified articular cartilage. Outside of the osteochondral tissues, the synovium surrounding these tissues is often found inflamed, undergoing fibrosis and vascularisation [134, 135]. OA presents clinical symptoms such as pain, stiffness, swelling and decreased range of motion [5, 130]. Various risk factors exist for OA including age, obesity, physical trauma, and genetic disposition [2, 3]. Despite this obscured aetiology, the pathology of osteoarthritis follows a similar phenotype regardless of cause. Cartilage degradation and bone remodelling are key driving factors in disease onset and progression.

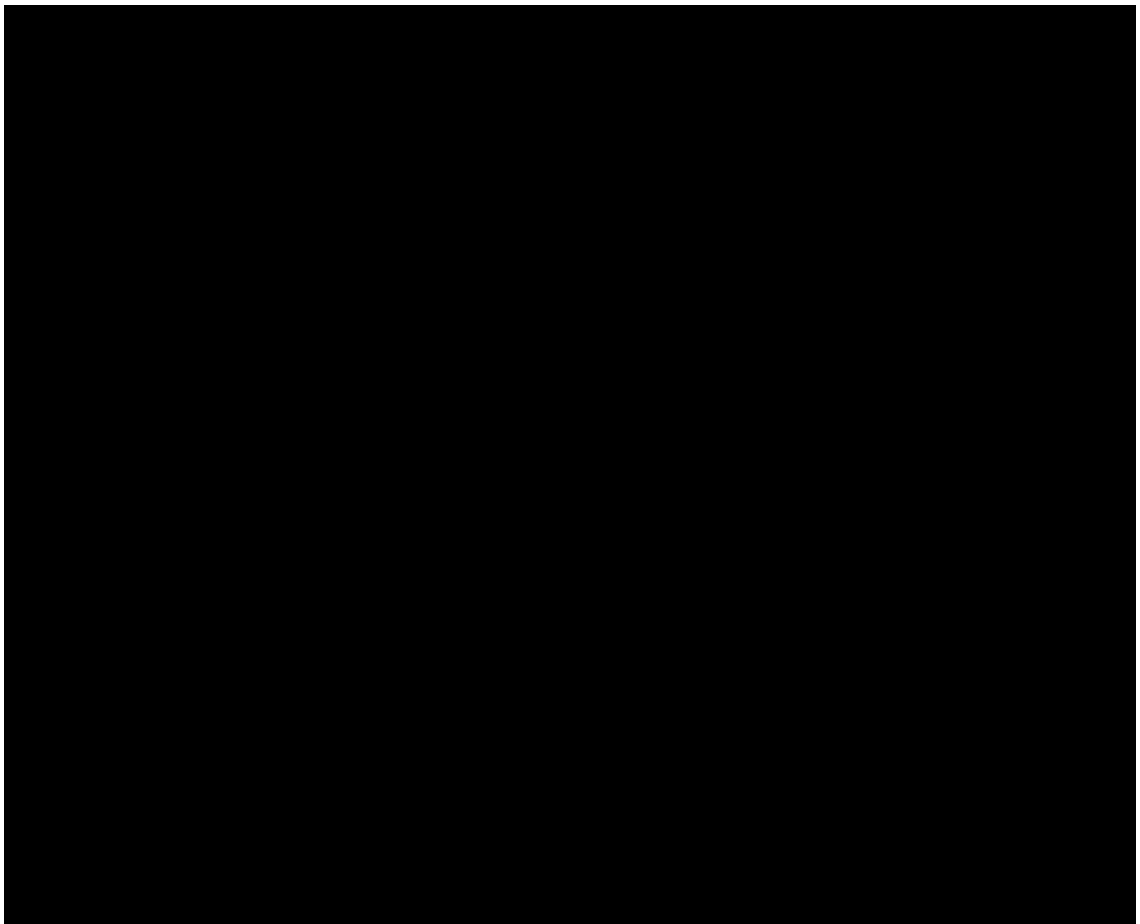


**Figure 6. Three-dimensional diagram displaying the structure of the AC-SCB interface and how these differ between healthy and OA cartilage.** OA results in the loss of superficial and intermediate cartilage. Blood vessels can be seen to penetrate the articular cartilage from the underlying subchondral bone. Additionally, subchondral bone may also penetrate the articular cartilage space in the form of osteophytes. These processes can result in loss of mobility and further degradation of the joint tissues. Figure adapted from Baumann *et. al.* (2019) [101] using Servier Medical Art.

### **1.3.1 Osteoarthritis and bone**

OA impacts both bone and cartilage and therefore should be considered a disease of the whole joint. Beneath the AC and tidemark region SCB exists in two discrete structures – the SCB plate and the subchondral trabeculae [136]. The SCB plate is a porous calcified bone plate through which many blood vessels and nerve fibres extend. These blood vessels and nerve fibres are responsible for providing nutritional support to the cartilage and the SCB calcified plate and trabeculae provide structural support [136]. Increasing evidence is suggesting that bone may in fact play a role in early OA development, radiographical scans have indicated increased SCB turnover is evident prior to the appearance of radiographically detectable knee OA [137]. Additionally, markers of bone

and cartilage turnover: bone sialoprotein (BSP) and cartilage-oligomeric matrix protein (COMP) were both found to be elevated in the early stages of knee OA suggesting that turnover processes between these tissues are occurring simultaneously [138]. Animal models have shown that induced SCB damage can lead to degradation of the articular cartilage [139], and spontaneous animal OA models show the thickening of the SCB plate and increased urinary markers of OA [140].

In osteoarthritic bone, abnormal mineralisation can be observed, this may be due to abnormalities in type I collagen fibres. Increased levels of TGF- $\beta$ 1 may be responsible for this process, type I collagen exists as a heterotrimer of  $\alpha$ 1 and  $\alpha$ 2 chains at a ratio of 2.4:1, in OA this is elevated to between 4:1 and 17:1 [141, 142]. Deposition of this abnormal collagen and its associated high osteoid volume contributes toward hypomineralized SCB which is compensated for by an increase in the number of trabeculae and volume of these structures, providing a stiff structure. These abnormal properties may cause altered mechanical loading and subsequently weakening of the SCB further perpetuating pathological bone development this weakening has been associated with the development of bone marrow lesions. These lesions are characterised by trabecular bone abnormalities, fibrosis of the bone marrow and oedema [143–145]. These bone marrow lesions often pre-exist in locations that become sites of bone marrow cysts and develop into bone cysts [146]. Bone marrow lesions have been shown to be associated with predictions of OA progression and cartilage loss, and cysts have been associated with articular cartilage degradation [147]. Certainly, once the loading mechanics exerted on bone are altered SCB remodelling will also occur according to Wolff's law. Increases in bone turnover have been indicated by *In vitro* studies, demonstrated by increased alkaline phosphatase activity, osteocalcin, and insulin-like growth factor (IGF-I) release in SCB derived from human OA patients [148, 149]. IGF-I acts to promote osteoblast differentiation and production of type I collagen and has bone-protective effects [150]. Additionally, TGF- $\beta$  has been suggested as a potential contributor to aberrant bone anabolism in OA as a correlation between total TGF- $\beta$  and severity of OA has been highlighted in previous research; SCB derived from OA patients has also shown increases in mRNA of TGF- $\beta$ 1 and TGF- $\beta$ 3 [151, 152]. Under OA conditions it has been shown that osteocytes and chondrocytes act as sources of influence for bone remodelling by producing RANKL [153, 154]. The association of RANKL-RANK is known to induce

osteoclast progenitor differentiation into mature osteoclasts whilst promoting osteoclast survival and bone resorption [155, 156]. This leads to aberrant bone remodelling under OA conditions. Further pathologic behaviours may also be induced by a variety of cytokines, including IL-1 $\beta$  [157]. IL-1 $\beta$  is a regulator of bone formation and has shown the ability to inhibit the production of mineralized nodules *in vitro* [158]. Additionally, IL-1 $\beta$  has been shown to promote bone resorption [159] and is a potent osteoclast activation factor [160] potentially acting via the production of prostaglandin E<sub>2</sub> (PGE<sub>2</sub>) a known inflammatory mediator [161].

### **1.3.2 Osteoarthritis and cartilage**

Under physiological conditions, this cartilage undergoes regular turnover, with degradation and restoration occurring in a homeostatic manner. However, under osteoarthritic conditions, there are a variety of pathological changes that result in increased levels of both cartilage synthesis and degradation (**Figure 7**) [162].

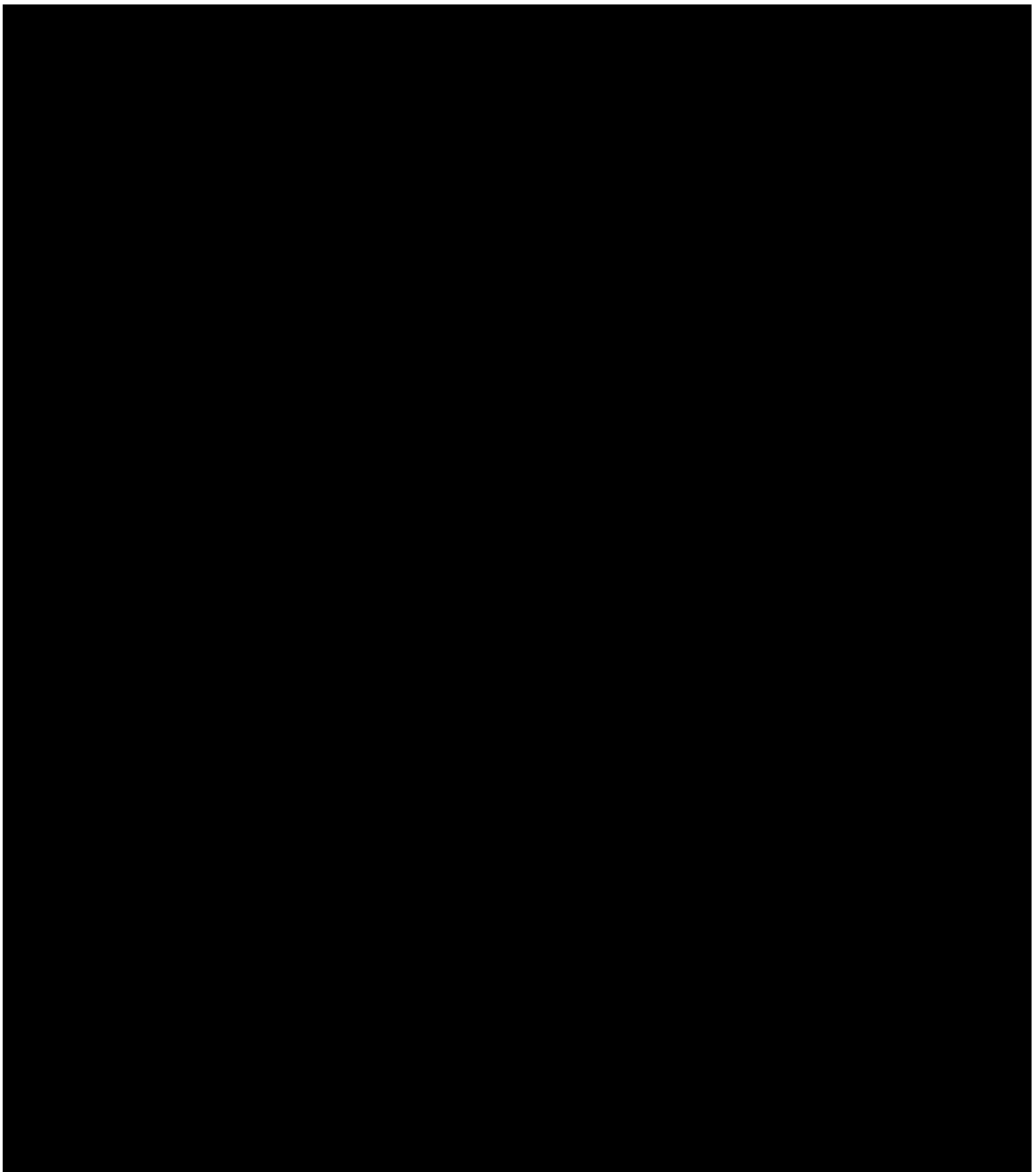


**Figure 7. Impact of common OA-associated risk factors on the AC and chondrocytes (A-B).** (A) shows the direct effects of OA risk factors such as mechanical insult, joint instability and cytokine signalling on the AC; anabolic processes are indicated by green text and catabolic processes are indicated by red text. (B) details the impacts of these OA risk factors on chondrocytes directly; anabolic effects are indicated by green arrows and catabolic effects are indicated by red arrows. Figure adapted from Sandell and Aigner (2001) [162] using Servier Medical Art.

In the osteoarthritic joint, anabolic synthesis of key proteins has been linked to several well-characterised growth factors. Transforming Growth Factor  $\beta$  (TGF- $\beta$ ) has been shown to increase secretion of ECM components including type II collagen whilst having a regulatory role in articular chondrocyte hypertrophy and maturation under an OA phenotype [163]. Prevention of canonical TGF- $\beta$  signalling is characterized by chondrocyte hypertrophy and expression of type X collagen, an indicator of chondrocyte terminal differentiation. The presence of TGF- $\beta$  can inhibit IL-1 protease-inducing activity and directly inhibit nitric oxide (NO) another characteristic degradative factor of OA [164, 165]. Bone morphogenetic proteins (BMPs) are part of the TGF- $\beta$  family and research has highlighted a potential role for BMPs such as BMP-2 and BMP-7 in OA progression. Bone morphogenetic protein-7 has been implicated in the stimulation of type II collagen and aggrecan secretion as well as counteracting inflammatory IL-1 activity [166, 167]. It has been shown that insulin-like growth factor (IGF-I) expression is lost with OA progression and that this results in increased OA severity, a loss of chondrocytes and ECM integrity [168]. However, despite the anabolism found under OA conditions, it is overshadowed by catabolic activity, which ultimately results in an overall degradative phenotype. Chondrocytes show a decrease in cartilage-specific genes such as those responsible for collagen type II (*COL2A1*) and aggrecan (*ACAN*) [169]. Expression of the key chondrogenic transcription factor *SOX9* is also found to greatly decrease with OA severity [169]. In conjunction with this, there is an upregulation in genes that indicate chondrocyte hypertrophy such as *Runx2* [28, 170], and *COL10A1* [169]. Additionally, in OA cartilage, type II collagen and type X collagen are shown to have an inverse relationship – OA reduces type II collagen as a function of disease severity, whilst increasing collagen type X expression [169]. This process coincides with chondrocytes and the synovium-producing pro-inflammatory factors that contribute to OA pathology, including cytokines: IL-1, IL-6, IL-10, TNF- $\alpha$ , and chemokines such as MCP-1 [171]. Amongst a variety of pro-inflammatory effects, cytokines such as IL-1 $\beta$  and TNF- $\alpha$  have been shown to increase the levels of a variety of matrix metalloproteinases (MMPs) such as collagenase MMP-13 and gelatinase MMP-3 [172]. Matrix metalloproteinase-13 is responsible for the breakdown of the collagen type II components of the ECM [173] whereas MMP-3 hydrolyses aggrecan [174]. MMP-13 may be considered one of the key degradative players in articular cartilage destruction as it specifically targets AC resident collagen type II fibres [175]. The presence of IL-1 $\beta$  also

stimulates the ADAMTS (a disintegrin and metalloproteinase with thrombospondin motifs) family of metalloproteinases, particularly aggrecanases: ADAMTS-4 and ADAMTS-5 [176]. Under osteoarthritic conditions, chondrocytes form clusters that highly express vascular endothelial growth factor (VEGF) and VEGF receptors [177]. Possessing many functions, VEGF has been found to induce MMP-3 and MMP-13 and decrease levels of MMP and ADAMTS inhibitors TIMP-1, TIMP-2, and TIMP-3 [177, 178]. Furthermore, VEGF facilitates vascular penetration in the SCB and extension into AC [179] and is associated with endochondral ossification via the stimulation of osteoblast migration and the hypertrophic terminal differentiation of chondrocytes [180].

Due to both IL-1 $\beta$  and TNF- $\alpha$  playing a role in osteoarthritic pathology of both bone and cartilage, this study will focus on these cytokines when considering the creation of an *in vitro* model of OA disease. Notably, both IL-1 $\beta$  and TNF- $\alpha$  can elicit a potent inflammatory response via the nuclear factor kappa B (NF $\kappa$ B) pathway. IL-1 $\beta$  and TNF- $\alpha$  stimulation of the NF $\kappa$ B pathway has been shown to inhibit type II collagen expression and upregulate the expression of a variety of MMPs including the OA hallmark MMP-13 in a synergistic fashion [181–185]. Stimulation of the NF- $\kappa$ B pathway has also been shown to induce the production of the ADAMTS enzymes, as well as a variety of other inflammatory mediators that can inhibit cartilage proteoglycan synthesis such as PGE<sub>2</sub> [186]. Stimulation of NF- $\kappa$ B by both IL-1 $\beta$  and TNF- $\alpha$  also increases autocrine production of proinflammatory molecules such as IL-6 and TNF- $\alpha$  and also drives the production of chemotactic IL-8 [186]. TNF- $\alpha$  has also been shown to induce apoptosis, a currently debated process in OA pathology [186]. A more comprehensive overview of the impacts of IL-1 $\beta$  and TNF- $\alpha$  in OA can be seen in **Figure 8** and **9**.

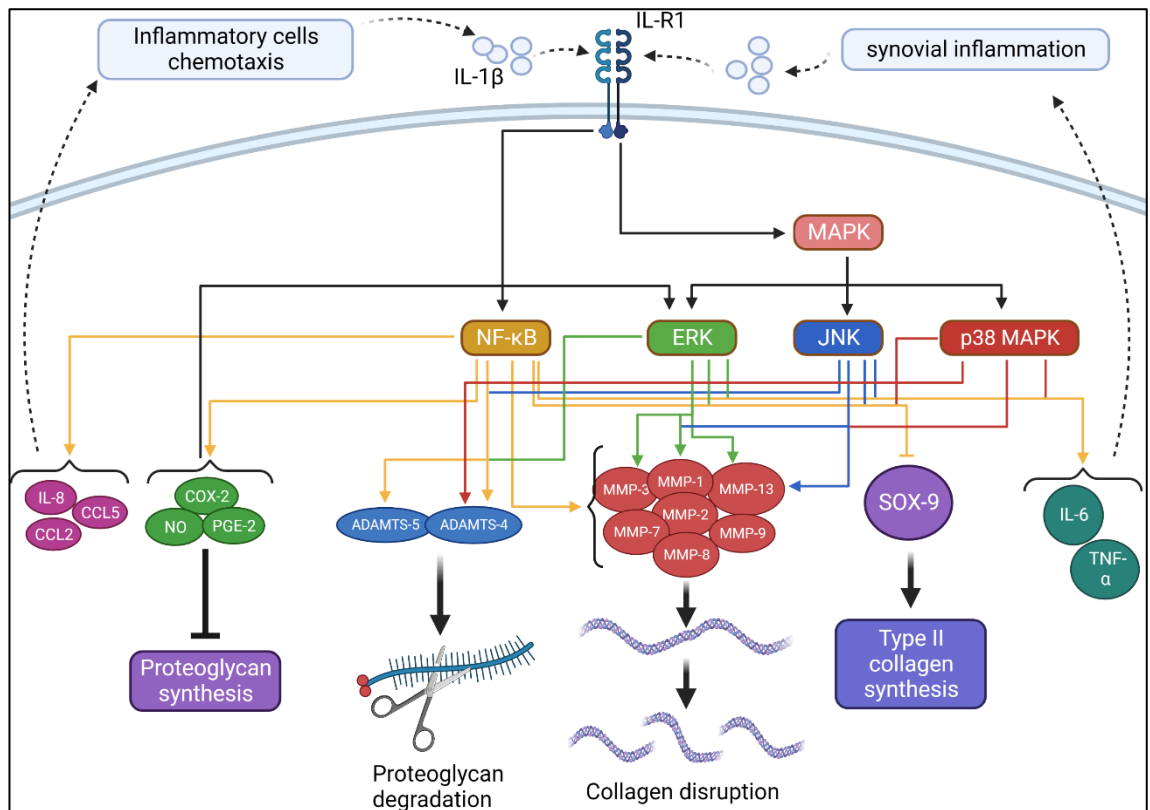


**Figure 8. The function of IL-1 $\beta$  in OA pathogenesis.** Upon binding to its receptor, IL-1 $\beta$  exerts a signalling cascade via NF- $\kappa$ B (nuclear factor kappa-light-chain-enhancer of activated B cells) and MAPK (mitogen-activated protein kinase) pathways. MAPK is responsible for further stimulation of ERK (extracellular signal-regulated kinases), JNK (c-Jun N-terminal kinases) and p38 MAPK. Overall, these pathways act to inhibit the production of and degrade key AC ECM components. NF- $\kappa$ B and MAPK activation causes the inhibition of type II collagen synthesis via SOX-9 inhibition, additionally, proteoglycan synthesis is inhibited via NF- $\kappa$ B mediated increases in COX-2 (cyclooxygenase-2), NO (nitric oxide) and PGE-2 (prostaglandin E2). The NF- $\kappa$ B and MAPK are also responsible for upregulating the ADAMTS and MMP family of enzymes which are responsible for the degradation of proteoglycans and collagens respectively. Cytokines and chemokines are upregulated via NF- $\kappa$ B and MAPK activation; IL-6 and TNF- $\alpha$  act to promote inflammatory cell migration and inflammation in the synovium, whereas chemokines IL-8, CCL5 (chemokine ligand 5) and CCL2 (chemokine ligand 2) further influence chemotaxis. Figure adapted from Molnar *et al.* (2006) [186] using Servier Medical Art.

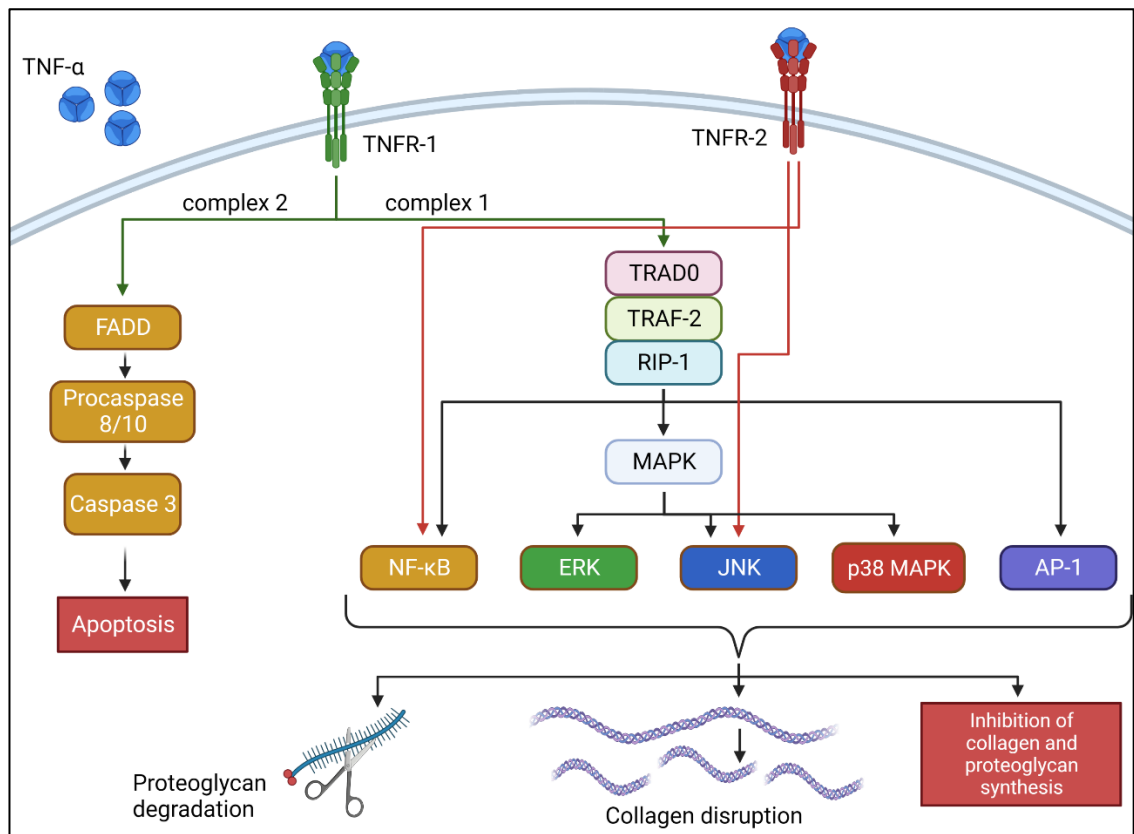


**Figure 9. The function of TNF- $\alpha$  in OA pathogenesis.** TNF- $\alpha$  acts upon two receptors: TNFR-1 and TNFR-2. Binding of TNF- $\alpha$  to TNFR-1 can result in the formation of two different complexes: complex 1 and complex 2. Complex 1 promotes cell survival and the activation of NF- $\kappa$ B, MAPK and AP-1 pathways, resulting in the degradation of proteoglycans, disruption of collagens, as well as the inhibition of the synthesis of collagens and proteoglycans. Alternatively, complex 2 leads to the formation of FADD (Fas-associated death domain protein) and the activation of procaspase 8/10 and caspase 3, resulting in apoptosis of the cell. TNFR-2 activation results in the activation of both NF- $\kappa$ B and JNK pathways, further driving proteoglycan degradation, collagen disruption and inhibition of the synthesis of these key structural molecules. Figured adapted from Molnar *et. al.* (2006) [186] using Biorender.

### 1.3.3 Bone-cartilage crosstalk in osteoarthritis

While previous research has considered bone or cartilage pathology individually, more recent research has focused on the potential crosstalk between bone and cartilage and how they may share a role in the pathology of OA. Evidence has shown that in healthy patients un-calcified cartilage dips through calcified cartilage and is able to interface with bone and bone marrow spaces presenting direct connections between AC and SCB [187]. Initially, it was thought that the SCB plate was impenetrable, however, it has been shown that there are in fact holes present throughout the plate, additionally, these

holes are in an area normally covered by the meniscus in healthy patients which may become exposed under degradative OA conditions [188]. There are also a variety of canals between AC and SCB which can act as a passageway for fluorescent dyes such as sodium fluorescein (376Da) which can diffuse between bone marrow and articular space in mouse models. Further research has shown larger molecules, such as those as large as 12.3kDa can pass through the lacuna-canalicular network which houses osteocytes and allows for their signalling functionality, notably this transport is enhanced under loading conditions [189]. This highlights the potential of AC-derived signalling molecules to directly influence the SCB and vice versa, for example, IGF-I [189, 190]. Additional research into the impacts of loading on solute diffusion shows that large molecules specifically, such as human serum albumin (66.5kDa), have enhanced diffusion through cartilage under cyclic loading [191]. Abnormal bone remodelling may play a role in increasing crosstalk between the bone and cartilage as revealed by a mouse model of instability-induced knee OA which showed an increase in porosity in the subchondral bone plate due to increased OA-induced osteoclast activity leading to further vascular penetration of the SCB plate associated with OA progression [192]. This is further highlighted by research conducted by Sanchez et. al. [193] in which osteoblasts derived from “sclerotic” and “non-sclerotic” tissue were co-cultured with healthy chondrocytes. Chondrocytes cultured with “sclerotic” osteoblasts were found to show reduced expression of aggrecan whilst increasing levels of MMP3 and MMP13. Further investigation showed that “sclerotic” osteoblasts also reduced mRNA expression of Collagen II, as well as increased expression of ADAMTS-4 and ADAMTS-5 [194]. Alternatively, loss of homeostasis may be induced by cellular signalling from diseased cartilage in the form of metabolic cytokines such as RANKL/OPG expression [195]; OA-driven increased permeability of the SCB plate may allow for these factors to transfer to the SCB and alter bone remodelling. Additionally, growth factors such as TGF- $\beta$  are highly active in healthy AC; degradation of the cartilage and potential transferral of these proteins to the SCB can result in altered bone remodelling increasing osteoclastic activity [196].

### 1.3.4 The role of autophagy in osteoarthritis

#### 1.3.4.1 The autophagy pathway

Macroautophagy henceforth referred to as autophagy, is an intracellular degradation system that breaks down and recycles aged and damaged macromolecules, proteins, and organelles. Autophagy plays a critical role in the regulation of cell homeostasis and is activated in response to a variety of pathological conditions including nutrient deprivation, hypoxia, and endoplasmic reticulum stress [197]. Autophagy is a membrane system that can be broken down into 5 main steps: initiation, nucleation, elongation, maturation, and degradation (**Figure 10**). This process results in the formation of double-membrane vesicles called autophagosomes which then fuse with lysosomes to form autolysosomes, where cargo is degraded into its constituent parts such as amino acids, aliphatic acids, nucleotides, and saccharides, which can then be recycled to support cell survival and maintenance [197, 198].

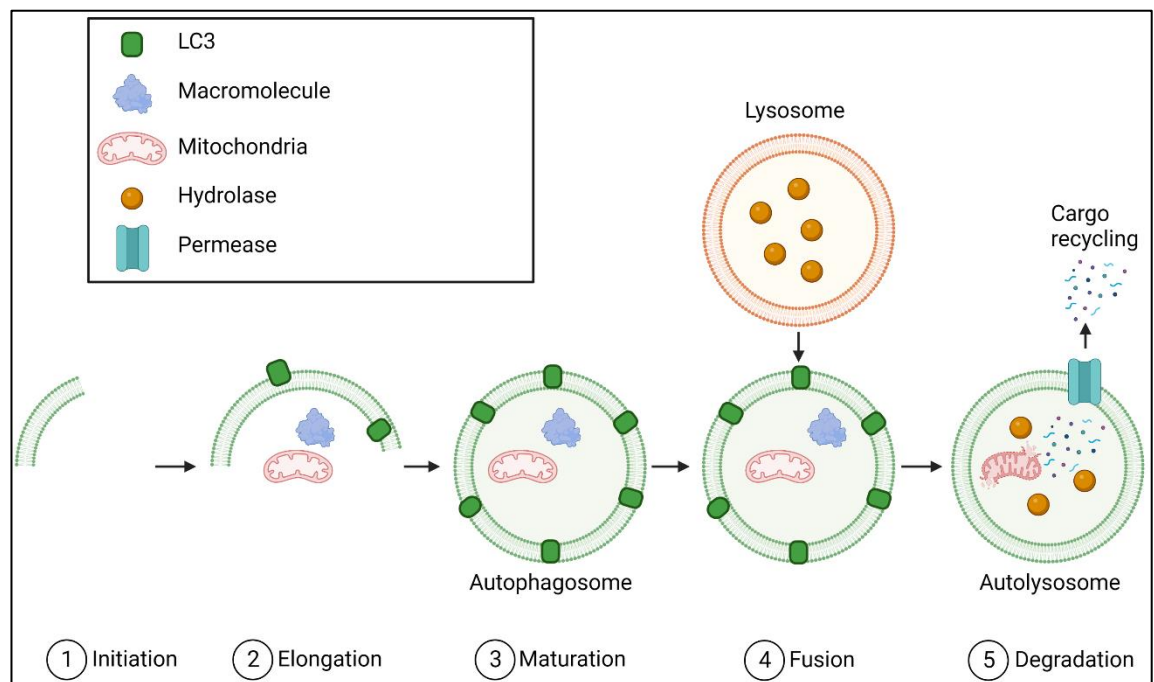


**Figure 10. Key steps in mammalian autophagy.** There are five key steps in the process of autophagy: initiation, elongation, maturation, fusion, and degradation. Initiation of the autophagy process begins with the formation of a double-membraned vesicle which will extend to engulf cargo such as damaged organelles and other macromolecules. This membrane continually elongates forming a mature autophagosome which will fuse with a lysosome containing degradative hydrolases. Upon fusion the contents of the lysosome are mixed with the contents of the autophagosome resulting in their degradation. These contents are released into the cell cytosol via lysosomal permeases for recycling. Figure adapted from Sun et. al. (2013) [199] using Biorender.

The regulation of autophagy is complex; initiation involves the formation of an isolation membrane around the cargo to be degraded and is directly regulated by the unc-51-like kinase (ULK1) complex, comprised of ULK1, FIP200, ATG13 and ATG101 [200]. The ULK1 complex is in turn regulated by the mammalian target of rapamycin (mTORC1) complex, a major regulatory hub balancing cell growth and protein translation with the control of autophagy [201]. mTORC1 is responsible for protein synthesis, cell size, cell-cycle progression, and glucose homeostasis via S6 kinase (S6K1) which phosphorylates a variety of substrates, the most studied of which is ribosomal protein S6 (rpS6) [202]. When cell stress occurs such as starvation, hypoxia, or organelle damage mTORC1 dissociates from ULK1 to allow initiation of autophagy [203]. Once ULK1 is liberated from mTORC1 control, the ULK1 complex activates the class III phosphatidylinositol 3-kinase (PI3K) complex, comprised of PI3K, beclin 1, VPS15, VPS34 and ATG14, which in turn triggers vesicle nucleation [204]. Elongation and maturation are regulated by two ubiquitin-like ATG conjugation pathways, ATG5-ATG12 and LC3/Atg8. ATG5 and ATG12 form a conjugate with ATG16, and this complex specifies the site of LC3-I lipidation for autophagosome formation [205]. LC3 is then processed to LC3-I via ATG4, and this complex is conjugated to phosphatidylethanolamine (PE) via ATG7 and ATG3 producing LC3-II, a lipidated molecule. As LC3-I is being conjugated, LC3-II associates with the inner membrane of the autophagosome as closure occurs and autophagosomes then fuse with lysosomes to achieve cargo degradation; the products of which are made available within the cell cytosol for re-use [197]. Due to the involvement of LC3-II in the process of autophagosome formation, this protein is a commonly used marker for the assessment of autophagy levels in cells including the induction of this process [206].

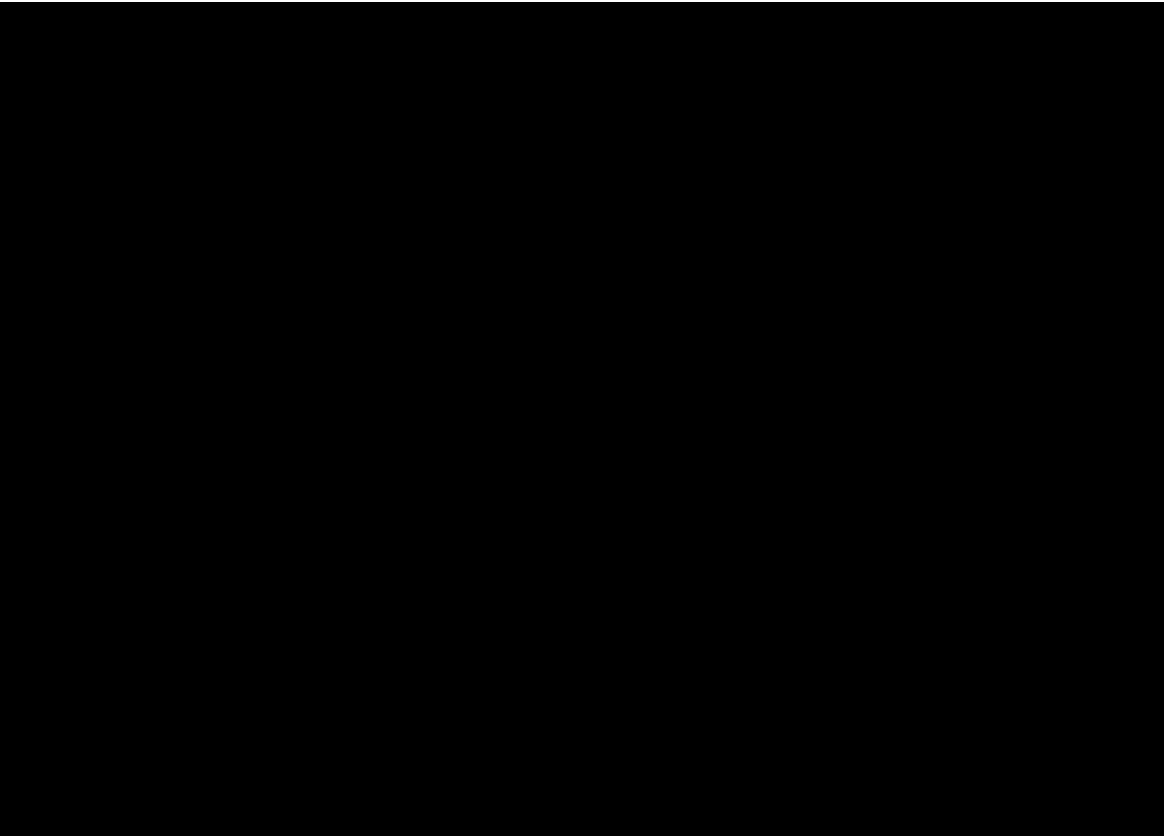


**Figure 11. Regulation of mammalian autophagy.** ULK1 is a protein kinase that acts as the key initiator of autophagy. ULK1 is inhibited by mTORC1, under a change of conditions such as nutrient deprivation, mTORC1 will dissociate from ULK1 allowing ULK1 to initiate the autophagy process. An initiation membrane is formed from the endoplasmic reticulum (ER) or other cellular membrane sources; the nucleation of which is promoted by the beclin-1 complex containing the lipid kinase Vps34. The ubiquitin like (UBL) conjugation systems ATG12UBL and LC3UBL work together to facilitate the conjugation of phosphatidylethanolamine (PE) to LC3, converting cytosolic LC3-I to LC3-II which is translocated to the membrane of the autophagosome. The vesicle matures forming a sealed autophagosome which fuses with lysosomes creating autolysosomes which degrade the autophagosome cargo via lysosomal proteases. Figure taken from Dikic and Elazar (2018) [207].

#### **1.3.4.2 Autophagy is linked to the pathogenesis of osteoarthritis**

Research has shown that autophagy levels are reduced with ageing; this prevents the removal of malfunctioning or damaged intracellular macromolecules and is therefore associated with a variety of aging-related diseases, including OA [208]. It has been shown that overall levels of autophagy are decreased in OA cartilage resulting in cartilage degeneration and apoptosis [209]. Therefore, autophagy may play a protective role in age-related disease including OA. Induction of autophagy via mTORC1 knockout, or pharmacological intervention, results in a decrease in chondrocyte apoptosis and cartilage degeneration in surgically induced OA [210, 211]. Specifically, autophagy has

been implicated directly in the amelioration of MMP13 activity. Increased MMP-13 expression, a hallmark symptom of OA, is accompanied by a concomitant reduction in expression of LC3-II a key indicator of autophagy activity [212, 213]. Further amelioration of MMP-13 activity has been shown through the use of isoimperatorin, which also worked to reduce expression of Col X and VEGF, an effect achieved via autophagy induction both *in vitro* and *in vivo* using destabilisation of the medial meniscus (DMM) mouse models [214]. Additionally, the ablation of key autophagy genes such as ATG7 has been shown to result in the impairment of type II collagen secretion and ECM formation [215].

It is known that the processes of inflammation and autophagy are closely connected, and it has been shown that TNF- $\alpha$  and IL-1 $\beta$  are both inducers of autophagy [216] and that the pathway acts to specifically inhibit the production of IL-1 $\beta$  cytokines *in vitro* and *in vivo* via targeting pro-IL-1 $\beta$  for degradation [217]. Autophagy has also been shown to attenuate the impacts of TNF- $\alpha$  and IL-1 $\beta$  on cells via inhibition of NF- $\kappa$ B activity directly, preventing translocation of p65, a key cellular subunit involved in NF- $\kappa$ B activation [218].

The NF $\kappa$ B pathway has been shown to have key pathological effects on OA pathogenesis and disease progression promoting the degradation of proteoglycans, disruption of collagen synthesis, down regulation of chondrogenesis and promotion of inflammation. Therefore, modulation of the autophagy pathway may allow for attenuation of NF- $\kappa$ B activation and expression, presenting a potential therapeutic avenue for one of the key contributors to OA pathology.

#### **1.4 *In vitro* models of osteoarthritis**

Several *in vitro* models have been developed to study the pathogenesis of OA at both tissue and cellular levels, however, no single model has proved to be the gold standard for OA research [219]. To date, studies using 2D cell culture primarily consider the chondrocyte as the “model” for OA with little consideration of the role of other cells relevant to the articular joint such as osteoblasts and osteocytes found in the SCB, which have been found to be aberrant in OA [195]. This may be due to the lack of funding for the investigation into mechanosensory stimulation in monolayer cell culture systems, which is also limited in its use in investigating cell-cell interactions and cell-ECM interactions [220]. Therefore, to create a robust and reliable model of OA, the variety of

articular joint tissues must be considered as a biological unit. Furthermore, *in vitro*, and *in vivo* models often produce conflicting results. Thus, there is a need for an *in vitro* model that generates results consistent with *in vivo* studies, and that overcomes the limitations of the current 2D and 3D models.

#### **1.4.1 Two-dimensional monolayer models**

2D monolayer models are inexpensive, permit the use of a single source of cells for multiple experimental treatments, and allow for rigorously controlled investigational conditions. Typically, 2D monolayer models involve the culturing of either primary cells or immortalised cell lines on a flat surface in polystyrene culture flasks, which exposes the cultured cells to an equal volume of the surrounding media containing the various nutrients and growth factors essential for cell development and proliferation [221, 222]. 2D *in vitro* models have routinely allowed for the screening of chondroprotective compounds to attenuate the catabolic factors involved in AC degradation. The usage of primary cells including osteoblasts and chondrocytes in 2D models provides a system that is associated with higher secretion of ECM and a phenotype more akin to that found *in vivo* for the respective cell lineage. However, it is of note that primary cell culture is substantially more expensive than the use of cell lines, with the primary cell source material being difficult to obtain and limited in terms of how often they can be sub-cultured before they undergo de-differentiation and lose their distinct phenotype. The usage of cell lines provides a much less limited source of cell material however due to their immortalized nature; these cells have evaded cellular senescence and are associated with alterations in the expression of markers typically associated with their non-immortalized counterpart. This can be exemplified by immortalized chondrocytes which display a marked reduction in the secretion of ECM components compared to primary cells, thus reducing their reliability as true cell models. 2D *in vitro* models have routinely been used for cytokine stimulation such as IL-1 $\beta$  to induce an OA phenotype which has allowed for the screening of chondroprotective compounds to attenuate the catabolic factors involved in AC degradation (e.g., IL-1 $\beta$ , TNF- $\alpha$ , NO, PGE<sub>2</sub>, COX-2, MMP3, MMP-13, ADAMTS-4 and ADAMTS-5) [223, 224]. Manipulation of 2D culture can also allow for the investigation of individual signalling pathways. For example, recent interrogation of the Wnt/ $\beta$ -catenin signalling pathway with a novel inhibitor highlighted

the critical role of the Wnt/ $\beta$ -catenin pathway in chondrogenesis and chondroprotection [225]. Additionally, monolayer cultures are easily transfected to manipulate gene and protein expression. For example, a proteomics study conducted on IL-1 $\beta$ /TNF- $\alpha$  stimulated human primary chondrocytes that were transfected with microRNAs (miRNA) identified proteins of the complement cascade, mediators of the NF- $\kappa$ B pathway and several regulators of autophagy that may be important in the pathology of OA [226].

Despite the benefits of 2D cell culture, there are numerous drawbacks that are inherent in the nature of the system itself. When using primary cells in 2D culture such as primary chondrocytes, little consideration is given as to the location from which these cells are derived, be it from articular, costal or fibrillar cartilage, or a specific layer of the cartilaginous matrix. Notably, 2D cell culture results in altered cell morphology as cells are forced to grow in a planar environment where nutrient and oxygen gradients are non-existent [227]. This can result in cellular polarisation due to limited connections with surrounding cells. Polarisation is known to alter cell mechanotransduction; directly impacting cell signalling and therefore the phenotype of the cell [228]. Chondrocyte cultures are no exception to this as they have been found previously to de-differentiate and adopt an elongated fibroblast-like shape that has been associated with an altered genetic profile, including a reduction in the expression of aggrecan and other matrix-specific genes [229]. Additionally, prolonged monolayer culture of chondrocytes results in the increased expression of *Col1a1* mRNA, thus, signifying de-differentiation [230]. Furthermore, incongruous results are often found between *in vivo* and *in vitro* studies. To date, publications using 2D cell culture primarily consider the chondrocyte as the “model” for OA with little consideration of the role of other cells relevant to the articular joint such as osteoblasts and osteocytes found in the SCB, which have been found to be aberrant in OA [195]. This may be due to the lack of support for the investigation into mechanosensory stimulation in monolayer cell culture systems, which is also limited in its use in investigating cell-cell interactions and cell-ECM interactions. Therefore, to create a robust and reliable model of OA, the variety of articular joint tissues must be considered as a biological unit.

### **1.4.2 Two-dimensional co-culture models**

2D co-culture models allow the investigation of cell-cell interactions in a shared environment. Like monolayer models, these can be used to investigate multiple experimental treatments at once and have the potential to generate extensive data on pathological mechanisms. Transwell plate models may be used which involve seeding cells in the lower chamber of multi-well plates, with additional cells being seeded in transwell plates suspended above each well. This allows for the investigation of cell-cell communication via the secretion of soluble factors into the surrounding media [231, 232]. Using this method, it has been shown that when chondrocytes and synoviocytes are co-cultured alongside adipose-derived mesenchymal stem cells, their expression of pro-inflammatory cytokines including IL-1 $\beta$ , IL-6, IL-8 and TNF- $\alpha$  significantly decreases [231]. A similar method revealed that chondrocytes cultured in the presence of adipose-derived stem cells have higher viability following TNF- $\alpha$  challenge, thus highlighting a paracrine chondroprotective role for adipose-derived stem cells [232]. As detailed, these experiments allow for the exploration of a variety of factors in OA development. However, it should be noted that many of the limitations associated with 2D monolayer culture also exist in 2D co-culture, including altered cell morphology and an inability to investigate direct cell-cell or cell-ECM contact.

### **1.4.3 Explant culture models**

Explant models are derived directly from *in vivo* tissue and maintain cells in their 3D surroundings, and both animal (e.g., murine femoral heads) and human (e.g., articular cartilage, or whole osteochondral plugs) explant systems are used within the OA field. These models still allow for the experimental manipulation provided by *in vitro* culture, with experimental evidence suggesting tissue viability is maintained [233]. Explant models have certain benefits such as enabling the investigation of compressive overload on AC and providing insight into the impact of cartilage loading in disease progression; a facet of OA that cannot be investigated by monolayer models [234]. Comparable to monolayer culture, explants may undergo multiple treatments *in vitro* allowing for the investigation of a variety of factors in a controlled environment. Unlike monolayer culture, osteochondral explant models may be more readily used to investigate the relationship between AC and the underlying SCB tissue. Osteochondral explants

challenged with IL-1 $\beta$  have been found to express a significantly lower level of MMP-13 than cartilage explants alone; results from this study also indicate that osteochondral explant expression of alkaline phosphatase may differ from chondrocyte explants [235]. Additionally, cartilage explants challenged with IL-1 $\beta$  produced an elevated level of TNF- $\alpha$  compared to controls, whereas osteochondral explant TNF- $\alpha$  secretion was unchanged, suggesting the presence of bone or synovium may reduce TNF- $\alpha$  expression and highlighting the need to consider all joint tissues in the analysis of OA pathophysiology [235]. In agreement, bone explants have been found to secrete increased levels of pro-Col-I, IL-6 and MCP-1 compared to osteochondral explants when challenged with lipopolysaccharide, suggesting that different cells within the osteochondral tissues can attenuate one another [233]. Furthermore, Haltmayer et. al. [236] detail a co-culture model in which horse osteochondral plugs and synovium membrane explants were cultured *in vitro* and stimulated using IL-1 $\beta$  and TNF- $\alpha$ . This study showed that the osteochondral-synovium co-culture enabled upregulation of MMP1 expression, subsequently attenuating genetic expression of MMP3, MMP-13, and IL-6 expression, as well as increasing gene expression of ECM products such as collagen type II.

Clearly, explant models provide benefits over monolayer culture, particularly regarding interactions between tissues, however, there are still shortcomings that must be addressed when using these models. For example, cells at the surgical edge may die when tissue is removed from specimens, and tissue from any single same biological source is finite; with different sources potentially eliciting different responses [235]. Importantly, explanted tissues are cultured in artificial settings which limits the investigation of mechanical loading effects or angiogenic effects following surgical resection [233]. Additionally, cells derived from explant outgrowths are susceptible to the de-differentiation and morphology changes observed over time in 2D culture, and there is still a requirement for use of culture media which may contain components that have undesirable effects on the tissues [233].

#### **1.4.4 Three-dimensional prefabricated scaffold models**

3D tissue scaffolds provide a platform in which biochemistry, matrix elasticity and micro-architecture can be altered [237]; this is important as polarity, pore size and pore

interconnectivity affect cell fate and the ability of cells to secrete ECM products. Additionally, biologic hydrogels have the ability to support chondrocyte proliferation and ECM production, as well as osteoblast growth and mineralisation, providing a potential model for investigating activity at the osteochondral interface [237–239].

Biologic hydrogels represent a scaffold-based system that is derived from natural resources, have a large water component, and are used due to their similarities to ECM modifiability, bioactivity, biodegradability, porosity, biocompatibility and low immunogenicity. Biologic hydrogels derived from materials such as alginate, gelatin, chitosan and hyaluronan promote chondrocyte viability and proliferation, as well as collagen type II, aggrecan and Sox9 expression, markers which normally diminish in monolayer culture [240–242]. Additionally, biologic hydrogels have the ability to support chondrocyte proliferation and ECM production, as well as osteoblast growth and mineralisation, providing a potential model for investigating activity at the osteochondral interface an area important in OA pathology [243]. Remarkably, certain biologic hydrogels can be manufactured through 3D printing, increasing availability and reducing the need for fabrication and crosslinking with potentially toxic reagents and hazardous processes [244]. Recent work on developing an *in vitro* 3D model of OA by Galuzzi et. al. [245] has shown that nasal chondrocytes encapsulated within alginate beads are able to produce increasing levels of glycosaminoglycans (GAG), however, culture in these beads had no effect on AC chondrocyte GAG secretion, highlighting a potential limitation for their use as a model of OA. Unfortunately, biological hydrogels can suffer from variations in batch-to-batch manufacturing, as with explants, single biological sources can vary which can impact the properties of the gel. These must be considered when choosing a biological hydrogel culture system.

Synthetic hydrogels are prevalent in 3D tissue culture, and like biological hydrogels, they possess desirable features for tissue culture [246, 247]. Importantly, synthetic hydrogels do not originate from a finite source meaning variability between manufactured products is reduced [248]. Synthetic hydrogels have been shown to facilitate chondrogenesis and increased expression of key chondrocyte markers such as collagen type II, and non-collagenous proteins such as osteocalcin, compared to 2D controls [249, 250]. Synthetic hydrogels can also be finely tuned via chemical modification, such as the inclusion of chondrogenic molecules which are delivered to hydrogel-embedded cells

such as biotinylated TGF- $\beta$ 3 which promotes chondrogenesis, as well as collagen type II and GAG expression [251]. Stüdle et. al. describes a model in which bone marrow stem cells (BMSCs) seeded in Poly (ethylene glycol) (PEG) hydrogels are layered with non-functionalised PEG-seeded nasal chondrocytes. This 3D construct results in a calcified bottom layer of BMSCs and a cartilaginous top layer of chondrocytes producing a 3D co-culture model interface of SCB and AC-like tissues which could be adapted for an investigation into OA pathology [251]. Similarly, a hydrogel co-culture system has been produced [252] using transwell plates to elucidate the relationship between chondrocytes and macrophages in OA. Research has also shown synthetic hydrogels such as those derived from PEG dimethacrylate are able to be integrated into a mechanical loading system which was able to direct human mesenchymal stem cell differentiation into AC, calcified cartilage and SCB tissues [247]. Preliminary data, therefore, support the potential of a synthetic 3D hydrogel co-culture system that includes multiple cell types involved in OA to investigate cell-cell interactions at a molecular level in the context of OA development.

Hydrogels thus provide materials that have a variety of suitable characteristics for *in vitro* modelling however, certain disadvantageous features exist and must be considered. *In vitro* modelling must consider the composite parts of these hydrogels as they are comprised of materials that are dissimilar to those found in the natural ECM which may alter cell behaviour. Moreover, these hydrogels contain a large water component, which has implications for the structural integrity of the gel as an anchoring substrate and while this may be suitable for mimicking certain *in vivo* environments such as AC, it may be unsuitable for others such as SCB which has very little ECM water content *in vivo*.

Prefabricated scaffolds, comprised of biodegradable polymers, are favoured for their biocompatibility, allowing for easy integration into biological systems as exemplified using PCL (poly( $\epsilon$ -caprolactone)) in surgical sutures and implants. Prefabricated scaffolds also possess a low melting point, providing desirable thermoplastic properties which facilitate 3D printing. Additionally, the viscoelastic properties of these scaffolds provide benefits for cell culture as substrate stiffness can determine cell growth [253, 254]. However, it has been noted that polymers such as PCL are non-osteoinductive and therefore their use in the culture of bone tissues is considered limited, limiting their

potential to be used to investigate an osteoblastic OA phenotype [255]. To remedy this, recent research has taken to altering PCL scaffold biochemistry and fabrication methods. Indeed, osteoinductive and mechanically supportive molecules such as hydroxyapatite (HPA) and Poly (propylene fumarate) (PPF) have been included to facilitate bone growth [238]. PCL/HPA/PPF scaffolds were found to boost BMSC osteoinduction increasing levels of calcium deposition and *Runx2* expression, a marker of osteoblast differentiation, and were particularly non-cytotoxic [238]. In consideration of improving manufacturing methods, Brennan et. al. [256] developed a novel jet-spraying technique as an alternative to the commercially accepted electrospinning technique. Electrospinning produces nanofiber scaffolds that closely resemble the native bone ECM; however, cell infiltration is a common problem with these scaffolds. Jet-spraying manufacturing produced scaffolds that boost alkaline phosphatase levels and calcium deposition whilst maintaining collagen production at similar levels to commercially available electro-spun scaffolds – this is due to jet-spraying producing scaffolds with smaller pore diameters and a greater variety of fibre thickness within the scaffold. Notably, these scaffolds resulted in higher osteogenesis than their 2D counterparts [256].

Pre-fabricated scaffolds also include microcarriers which do not possess the mesh-like physical properties expected of a scaffold, but instead anchor cells on their surface providing 3D support [257]. Thus far, microcarriers have shown desirable chondrogenic qualities. Galuzzi et. al. [245] described the development of a silk/alginate microcarrier model in which silk anchors human nasal chondrocytes to the surface of the silk/alginate manufactured beads avoiding encapsulation and negating issues associated with cell infiltration. These cells retained a chondrocyte phenotype via the expression of markers such as collagen type II and were metabolically active even after cryopreservation [245]. Microcarriers have also been shown to support biochemical modification [258]. A microcarrier consisting of PGLA (poly (D, L-lactide-co-glycolide acid) coated with fibronectin and poly-D-Lysine to promote cell adhesion and loaded with TGF- $\beta$  was shown to upregulate chondrogenic markers, whilst downregulating osteogenic proteins [258]. This highlights the ability of 3D culture models to be tailored to guide stem cells to a specific lineage giving more control over differentiation than can be found in 2D models.

By showing the chondrogenic and osteogenic potential that can also facilitate cell-cell and cell-ECM interaction, scaffold-based systems, therefore, offer great potential as *in vitro* systems to model OA. Notably, cell proliferation is typically found to be slower in scaffold-based systems [259], as is cell migration [260]. However, research involving these models is still in relative infancy compared to 2D *in vitro* models. Further work is needed to establish the implications of these characteristics on model development as well as the robustness and reliability of these systems.

#### **1.4.5 Three-dimensional scaffold-free models**

Pellet culture provides an alternative to a typical 3D culture that carries less of a financial burden than other 3D systems such as hydrogels and scaffolds. Typically, pellet culture involves maintaining centrifuged cell pellets in conical tubes, or multiwell plates, in such a manner that the cells are clumped together, adding a 3D aspect to the culture system. De-differentiated human AC chondrocytes cultured as a pellet have shown increased expression of chondrogenic SOX9 as well as *Col2a1* and aggrecan mRNAs [261]. Additionally, pellet cultured chondrocytes exhibit reduced expression of hypertrophy markers such as collagen type X, as well as a reduction in calcification markers such as *Runx2* and alkaline phosphatase. Pellet culture also induces collagen type II expression to a higher level than both 3D alginate bead culture and monolayer culture, however, expression of collagen type X and *Runx2* protein did not differ between monolayer, pellet, or alginate bead culture [261].

In contrast to the benefits described, pellet culture has inherent systematic disadvantages that must be considered when using this *in vitro* culture method, particularly for OA. Cells cultured in a pellet show a large reduction in proliferative capacity, whilst cells in the centre of the pellet may be deprived of nutrients and oxygen; providing an environment for maintaining non-hypertrophic chondrocytes-for *in vitro* analysis [262].

However, these conditions can cause apoptosis; and more recent research has provided an alternative chondrogenic model using transwell plates. Whilst these hypoxic and low-nutrient conditions may be suitable for chondrogenesis, it has been shown that hypoxia can reduce osteogenesis [263]. If an *in vitro* model of OA is to be fully comprehensive it

must suitably support the variety of cell types that are found within an articular joint including chondrocytes and osteoblasts.

Hanging drop cell culture involves pelleting cells and culturing them in an inverted fashion against a 2D surface, allowing gravity to help maintain the cells in suspension reducing the chance of polarisation. *In vitro* culture using the hanging drop technique has been shown to promote an *in vivo*-like rounded morphology accompanied by increased levels of *Sox9* mRNA compared to both monolayer and typical pellet culture methods. Additionally, hanging drop culture has been shown to induce upregulation of proteoglycan 4 (Prg4) mRNA and its associated protein lubricin – which is found in healthy AC joint space, providing lubrication [264]. Hanging drop models present similar advantages as pellet culture systems, but notably, share the same disadvantages therefore further research is required to determine their suitability as a potential adaptable model for the *in vitro* investigation into OA.

#### 1.4.6 Biogelx

Biogelx (Biogelx Ltd, UK) are commercial manufacturers of synthetic hydrogel products that provide hydrogel cell culture systems. These systems derived from supramolecular self-assembling peptides that form a fibrous, porous network that is designed to mimic the ECM [265]. The scaffold component of the hydrogel is comprised of two peptides, Fmoc-diphenylalanine (Fmoc-FF) and Fmoc-serine (Fmoc-S) (**Figure 12**) [265, 266]. In the presence of water, Fmoc-diphenylalanine (Fmoc-FF) gelator peptides form nanoscale fibres via non-covalent interactions and combine with Fmoc-serine (Fmoc-S) surfactant peptides, engaging in a cooperative assembly process forming a nanoscale fibre with a polar surface (**Figure 13**). The nanoscale fibrous network is crosslinked with ions such as  $\text{Ca}^{2+}$  forming a nanoscale fibre network that arranges itself via  $\pi$ - $\pi$  stacking interactions resulting in an interlocked  $\beta$ -sheet architecture [265–267]. Biogelx hydrogels have been shown to support a variety of cell types including hepatocytes [266], fibroblasts and chondrocytes [268] as well as promote the expression of osteogenic *RUNX2* and chondrogenic *SOX9* transcription factors in pericytes [265]. Tuneable stiffness provides Biogelx hydrogels with characteristics for the culture of cells derived from a variety of tissues of varying stiffness such as bone and cartilage. Furthermore, Biogelx hydrogels can be formulated with a variety of additional structural motifs that are known to

promote cell adhesion, including GFOGER, IKVAV and RGD [269]. These properties make Biogelx hydrogels an attractive candidate for the culture of bone and cartilage cells with the intent of creating a 3D co-culture model of OA.

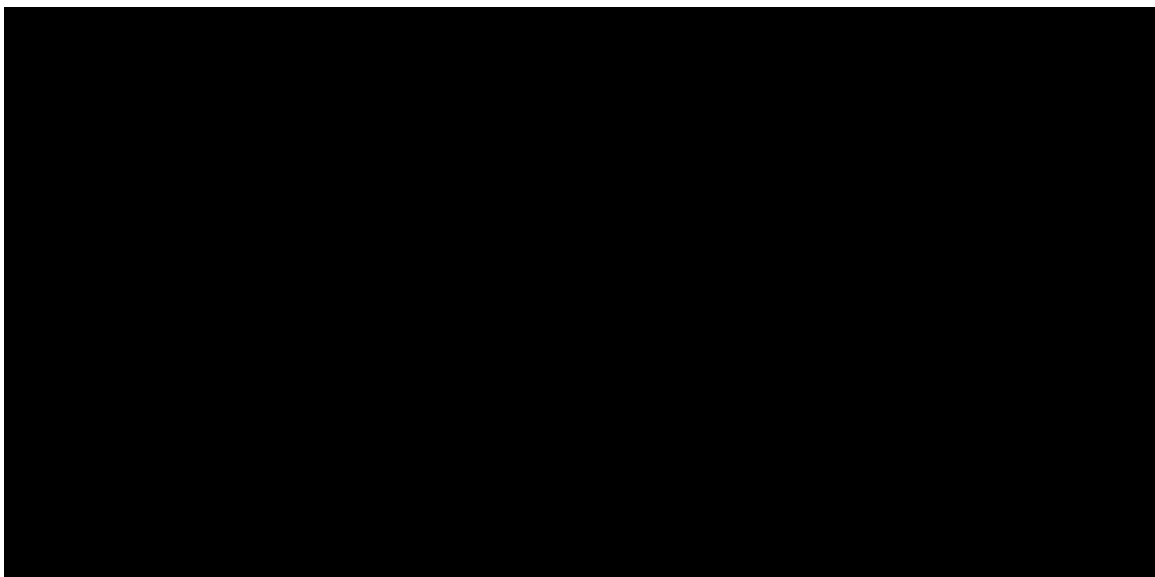


**Figure 12. Chemical structure of gelator and surfactant peptides and their role in fibre assembly.** In the presence of water Fmoc-FF and Fmoc-S peptides combine to form a nanoscale fibre. Fmoc-FF peptides form the core structure of the fibres during assembly with Fmoc-S peptides coating the fibre surface. Image provided by Biogelx (Biogelx, UK).

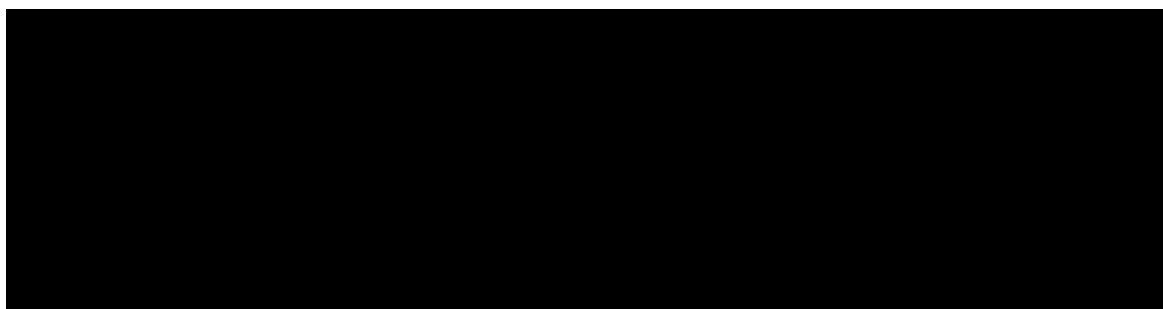


**Figure 13. Nanoscale fibre assembly and crosslinking of the nanoscale matrix.** Gelator and surfactant peptides combine in the presence of water to form a network of nanoscale fibres, this network is then crosslinked via the presence of ions such as  $\text{Ca}^{2+}$  which is commonly found in cell culture media. Crosslinking results in a mesh network that is designed to mimic the ECM. Image provided by Biogelx (Biogelx, UK).

## 1.5 Aims

The overarching aim of this study is to establish a 3D *in vitro* co-culture model of OA that will enable the investigation of bone-cartilage crosstalk. This 3D model will be developed using commercially available hydrogel systems provided by the industrial collaborator for this PhD project, Biogelx. The utility of the 3D model will be investigated in the context of autophagy, as this pathway has been linked to OA pathogenesis. In the longer term, the development of a physiological *in vitro* model may facilitate the identification of novel therapeutic targets and the development of new drugs for OA.

Specific aims are to:

1. Determine the most appropriate osteoblast and chondrocyte cell lines to use in the novel 3D model, confirmed by the expression of key bone and cartilage genes and proteins.
2. Determine the optimum 3D hydrogel culture conditions for each cell line as dictated by cell viability and the expression of key bone and cartilage genes and proteins.
3. Develop a co-culture system using 3D encapsulated osteoblasts and chondrocytes that mimics OA and use this model to investigate the effects of modulating the autophagy pathway.

## **2 Chapter 2: Materials and methods**

### **2.1 Reagents and solutions**

All chemicals were purchased from Sigma-Aldrich (Dorset, UK) and tissue culture media and buffers were purchased from Invitrogen (Paisley, UK) unless otherwise stated. All buffer recipes are shown in appendix.

### **2.2 Cell culture**

#### **2.2.1 C-28/I2 and SaOS-2 cell maintenance**

Cells of the C-28/I2 and SaOS-2 cell lines were provided as a gift from Professor Colin Farquharson (The Roslin Institute, Scotland). C-28/I2 and SaOS-2 cells were maintained in culture flasks (Corning, Surrey, UK) containing growth medium: dulbecco's modified eagle's medium (DMEM) F12 Glutamax + 10% fetal calf serum (FCS) + 1% penicillin-streptomycin (10,000µm/L penicillin and 10,000µm/L streptomycin) + 110mg/L sodium pyruvate. Growth media was changed every 2-3 days and cells were passaged once flasks had reached sub-confluence. Cells were passaged at a ratio of 1:3-1:8 depending on experimental requirements. Passaging cells was achieved by washing cells grown in flasks with sterile PBS and then adding 1X trypsin for 3 minutes at 37°C; the volume of trypsin added was dependent on flask size and was added at a ratio of 3mL per 25cm<sup>2</sup> of flask culture area. After 3 minutes, flasks were gently agitated by hand to ensure cell detachment and growth media was added to the cell-trypsin suspension to inactivate the trypsin. Growth media was added at 5mL per 3mL of trypsin. Cell suspensions were then aspirated in to a 50mL falcon tube (Corning, Surrey, UK) and spun at 230 x *g* for 5 minutes to pellet cells. Cell pellets were then re-suspended in a desired volume of media and split to a desired ratio in new cell culture flasks. For experiments requiring differentiation media, this was created using (DMEM) F12, Glutamax + 10% fetal calf serum (FCS) + 1% penicillin-streptomycin (10,000µm/L penicillin and 10,000µm/L streptomycin) + 110mg/L sodium pyruvate supplemented with 5mM β-glycerophosphate and 50 µg/mL L-ascorbic acid.

#### **2.2.2 Freezing/thawing C-28/I2 and SaOS-2 cells**

Freezing C-28/I2 and SaOS-2 cells was achieved by trypsinizing and centrifugating a confluent flask of cells as described in section 2.2.1. However, cell pellets were

resuspended in a cryogenic media comprised of growth media and DMSO (Fisher Scientific). Cells were re-suspended in cryoprotectants: 95% growth media + 5% DMSO for C-28/I2 cells, and SaOS-2 cells were re-suspended in 90% growth media + 10% DMSO. Cryogenic cell suspensions were then aspirated into nunc cryovials (Gibco, Paisley, UK) at a ratio of 1:6. Cryovials were placed in a Mr. Frosty freezing container (Fisher Scientific, Paisley, UK) containing 100% isopropanol (Fisher Scientific, Paisley, UK). Mr. Frosty containers were then placed in a -80°C freezer for at least 24 hours to ensure cells were frozen. Cryovials were then transferred to liquid nitrogen for long term storage.

Frozen cell stocks were revived in T25/T75 tissue culture flasks. Cells were defrosted briefly in a 37°C water bath and subsequently gently aspirated into a 50ml falcon tube (Corning, Surrey, UK) which was then centrifuged at 220 x G for 3 minutes to pellet cells. The supernatant was then discarded, and the cell pellet was re-suspended in 1ml growth medium. This 1ml suspension was then aspirated into a T25 flask, topped up with 9mls fresh growth medium and stored at 37°C in an atmosphere of 5%CO<sub>2</sub>.

### **2.2.3 Primary Human Chondrocytes**

Human primary chondrocytes (Promocell, Heidelberg, Germany) were maintained as described for C-28/I2 cells in section 2.2.2., however Human Chondrocyte Growth Medium (Promocell, Heidelberg, Germany) supplemented with Growth Medium Supplement Mix (Promocell, Heidelberg, Germany) was used as a general culture media as purchased from the manufacturer.

### **2.2.4 Freezing/thawing primary human chondrocytes**

Human primary chondrocytes (Promocell, Heidelberg, Germany) were frozen as described for C-28/I2 cells in section 2.2.2. however, PromoCell Freezing Medium Cryo-SFM (Promocell, Heidelberg, Germany) was used instead of cell growth media + DMSO as a cryoprotectant.

### 2.3 Hydrogel preparation

Biogelx lyophilized hydrogel powder (Biogelx, Glasgow, UK) was weighed out and reconstituted in distilled water as per the manufacturer's instruction to yield the known stiffness of each hydrogel formulation (Table 2.1 – Table 2.4). Following the reconstitution of lyophilized powders, each gel solution (referred to now as the pre-gel solution) was vortexed for 15 seconds, and this was repeated until all lyophilized powders had dissolved. Pre-gel solutions were then UV sterilized within a biological safety cabinet class 2 hood for 30 minutes.

**Table 2.1 Biogelx recommended solute-solvent ratios to give known stiffnesses of Standard hydrogel product.**

Stiffness range of standard gel required (kPa)	Weight of lyophilized powder per 1mL dH <sub>2</sub> O
Low (0.5-1.5 kPa)	4.4mg
Medium (2.0-4.5 kPa)	8.8mg
High (6.0-10.0 kPa)	13.2mg

**Table 2.2 Biogelx recommended solute-solvent ratios to give known stiffnesses of GFOGER hydrogel product.**

Stiffness range of GFOGER gel required (kPa)	Weight of lyophilized powder per 1mL dH <sub>2</sub> O
Low (0.5-2.5 kPa)	5.8mg
Medium (4.5-7.0 kPa)	11.6mg
High (7.5-10.5 kPa)	17.4mg

**Table 2.3 Biogelx recommended solute-solvent ratios to give known stiffnesses of IKVAV hydrogel product.**

Stiffness range of IKVAV gel required (kPa)	Weight of lyophilized powder per 1mL dH <sub>2</sub> O
Low (0.8-1.1 kPa)	4.9mg
Medium (3.0-4.0 kPa)	9.8mg
High (8.0-9.2 kPa)	14.7mg

**Table 2.4 Biogelx recommended solute-solvent ratios to give known stiffnesses of RGD hydrogel product.**

Stiffness range of RGD gel required (kPa)	Weight of lyophilized powder per 1mL dH <sub>2</sub> O
Low (0.5-2.5 kPa)	5.0mg
Medium (5.5 kPa-8.0 kPa)	9.9mg
High (9.0-15.0 kPa)	14.9mg

## 2.4 Hydrogel encapsulation

Before encapsulation, hydrogels were warmed to 37°C. To achieve encapsulation, C-28/I2 and SaOS-2 cells were trypsinized and counted using a haemocytometer. Desired cell numbers were then pelleted via centrifugation at 230g for 5 minutes and re-suspended in cell culture media at 10% of the volume of pre-gel solution within which cells will be encapsulated. Cells were mixed at a desired number with 100µl of pre-gel solution. Pre-gel/cell suspensions were then pipetted into 96-well plates at 100µl per well and subsequently incubated at 37°C for 30 minutes. Crosslinking of the hydrogel constructs was then encouraged through the addition of 100µL of growth medium to the surface of the constructs for 2 hours at 37°C. Finally, fresh growth media was added to the surface of the cross-linked hydrogel and cell-laden constructs were incubated at 37°C overnight. After 24 hours (day 0) remaining cultures were grown in differentiation media (as described in section 2.2.1.). Media was replenished every 3 days for the duration of each experiment unless otherwise stated.

## **2.5 RNA methods**

### **2.5.1 Isolation of RNA from cells**

RNA was isolated from monolayer cultured cells via TRIZOL (Invitrogen, Paisley, UK) and Qiagen RNeasy Mini Kit (Qiagen, Manchester, England) column extraction. Monolayer cells were washed with 3mL ice-cold PBS and scraped on ice in 1mL of TRIZOL reagent using a cell scraper. The resultant suspension was then aspirated into a 1.5mL Eppendorf tube (Eppendorf, Stevenage, UK) and stored at -80°C until RNA extraction was necessary. Upon requirement of RNA extraction TRIZOL suspensions were removed from -80°C freezers and defrosted on ice. Once defrosted suspensions were left on ice for a further 10 minutes. Next, 200µl of chloroform was added to the suspension and mixed vigorously by hand for 30 seconds. Following mixing, Eppendorfs were left at room temperature for 3 minutes and then centrifuged at 12000 x *g* for 10 minutes at 4°C. The resultant top layer of supernatant was aspirated from the Eppendorf (avoiding the interphase and organic layers) and RNA was extracted through Qiagen columns as per manufacturer's instructions provided with the Qiagen RNeasy Mini Kit. RNA was concentrated via running the final eluate through the column twice.

### **2.5.2 Determination of RNA integrity**

RNA concentration and purity (260/280 >1.8, 260/230 >1.8) was then assessed using a Thermo Scientific NanoDrop One (ThermoFisher, Paisley, UK). Briefly, 1µl of RNA sample was loaded on to the Nanodrop loading platform and assessed on concentration and absorbance at wavelengths of 260nm and 280nm. Ratios of 260/280 and 260/230 absorbances were then used to determine RNA purity with ratios over 1.8 being considered low in DNA and exogenous contaminants.

Samples were then bioanalysed using an Agilent 2100 bioanalyser (Agilent, California, USA) to determine a definitive RNA concentration and RNA integrity. Bioanalysis was conducted as per manufacturer's instructions. Samples with a RIN of  $\geq 7.5$  were used for downstream analysis.

### **2.5.3 Reverse transcription (RT)**

cDNA synthesis was conducted using Primer Design Nanoscript (Primer Design, Chandler's Ford, UK) reverse transcription kits and prepared as per manufacturer's instructions. The resultant cDNA was diluted to 5ng/ul with RNase/DNase free water and frozen at -20°C. A -RT reaction was also conducted, this involved substituting reverse transcriptase with water whilst synthesising cDNA, creating a final product that should have no cDNA replication thus acting as an indicator of genomic DNA contamination during downstream RT-qPCR assays.

### **2.5.4 Real time quantitative polymerase chain reaction (RT-qPCR) and GeNorm analysis**

All PCR reagents including cDNA were defrosted on ice and pulse spun prior to conducting the assay. PCR was conducted on 96 well bright white plates. A master mix was created for each housekeeping gene and gene of interest. Master mixes contained 10µl of primer design SYBR green (Primer Design, Chandler's Ford, UK), 4µl of RNase/DNase free water (Primer Design, Chandler's Ford, UK) and 1µl of desired primer (Appendix II) creating a master mix with a primer concentration of 300nM. Note, PDPN master mixes contained 10µl of primer design SYBR green, 4.5µl of RNase free water and 0.5µl of primer mix, giving a final primer concentration of 250nM. Next 15ul of master mix was plated in triplicate for each sample in a 96 well bright white plate (Primer Design, Chandler's Ford, UK); no template control (NTC) and -RT wells were also prepared. 5µl of cDNA was added to test wells and -RT wells, while 5µl of RNase/DNase free water was added to each NTC well. The 96 well plate was then sealed and centrifuged at 300 x *g*. Following centrifugation RT-qPCR was conducted using an Applied Biosystems StepOnePlus thermocycler (Thermofisher, Paisley, UK) and v2.2.3 OneStep software (Thermofisher, Paisley, UK).

### **2.5.5 GeNorm analysis**

GeNorm (Primer Design, Chandler's Ford, UK) analysis was performed on both cell lines to determine the most suitable housekeeping targets for gene data normalisation. This process involved performing RT-qPCR on samples from selected time points. C-28/12 and SaOS-2 cells were cultured for 0, 6, and 12 days in growth media containing 5mM  $\beta$ -GP and 50 $\mu$ g/mL L-ascorbic acid, cells were then harvested for RNA as per section 2.4.1., RNA integrity was assessed as per 2.4.2 and cDNA was synthesised as per section 2.4.3. RT-qPCR was then performed as per section 2.4.4. using 12 pre-selected genes as per GeNorm manufacturer guidelines (Appendix II). GeNorm data was then generated via the use of qbase+ (Biogazelle, Canada) as per manufacturer's guidelines.

### **2.5.6 Quantification of gene expression**

Following thermocycling qPCR data was exported and Microsoft Excel was used to conduct calculations to determine gene expression values. Relative gene expression calculations were conducted using the  $2^{(-\Delta\Delta Ct)}$  method described by Livak and Schmittgen [270].

## **2.6 Protein methods**

### **2.6.1 Protein extraction from two-dimensional cell cultures.**

Cell monolayers were washed with 3mL ice-cold PBS and subsequently scraped on ice in 1mL ice-cold PBS. Scraped suspensions were aspirated into a 1.5mL Eppendorf tube and centrifuged at 800 x *g* for 5 minutes to create a cell pellet. The resultant supernatant was gently aspirated with care to not disturb the pellet which was then stored at -80°C until protein extraction was required. To achieve protein extraction, pellets were agitated and re-suspended in Radioimmunoprecipitation assay (RIPA) lysis buffer containing 1X cComplete Mini EDTA-free protease inhibitor cocktail. These suspensions were left on ice for 30 minutes, with intermittent agitation to allow for total lysis of all cell materials. Suspensions were then centrifuged at 16,813 x *g* for 5 minutes at 4°C, pelleting insoluble materials and allowing proteins to solubilise in the supernatant. Subsequently, protein lysates were stored at -20°C until required for quantification and analysis.

### **2.6.2 Protein extraction from three-dimensional cell cultures.**

3D constructs were washed gently with 200µl ice-cold PBS and lysed via vortexing directly in 300µl of urea buffer (appendix I) + 1X cOmplete Mini EDTA-free Protease Inhibitor Cocktail. 3D construct suspensions were then left on ice for 30 minutes to allow for full sample lysis. Subsequently, 3D construct suspensions were then centrifuged at 16,000g for 5 minutes to remove debris and obtain sample supernatants for analysis.

### **2.6.3 Protein extraction from human articular cartilage**

Human cartilage samples were obtained from patients undergoing total knee replacement with Mr Amish Amin (University of Edinburgh) diagnosing OA based on clinical and radiographic OA features. Samples are obtained with patient consent and all procedures with ethical approval by NHS Lothian in collaboration with Mr. Anish Amin. The collection, storage, and subsequent use of human tissues are regulated in Scotland by The Human Tissue Act (Scotland) 2006. The study of these tissues was in compliance with all necessary UK licenses and ethical approvals. Thin slices of cartilage were placed into a 2mL Eppendorf tube and submerged in 500µL urea buffer. The cartilage was then homogenised using an IKA T10 homogenizer (IKA, Oxford, England) for 10 seconds at speed 6. This homogenisation step was repeated 3 times. Cartilage homogenates were then left for 30 minutes allow lysis of cells. Following lysis, lysates were centrifuged at 16,813 x *g* for 5 minutes at 4°C pelleting insoluble materials and allowing proteins to solubilise in the supernatant. Subsequently, cartilage lysates were stored at -20°C until required for quantification and analysis.

### **2.6.4 Quantification of protein**

For RIPA lysed cell materials, the colorimetric Bio-Rad DC (Detergent Compatible) assay (Bio-rad, Hertfordshire, UK) was used as a means of quantification and was conducted as per manufacturer's instructions. Standard curves were created using bovine serum albumin (BSA) dissolved in de-ionized H<sub>2</sub>O. Samples and standards were incubated within 96-well plates with assay reagents for 15 minutes at room temperature to allow colorimetric reactions. Absorbances of each well was read at 600nm using a Tecan Sunrise plate reader (Tecan, Crailsheim, Germany) and protein concentrations were

determined using linear regression methods. For 3D samples lysed in urea buffer, protein was quantified using the Bradford method. 1µl of the samples and BSA standards were incubated with 200µl of Bradford reagent at room temperature for 15 minutes and colorimetric changes were read at 600nm using a Tecan Sunrise plate reader (Tecan, Crailsheim, Germany) and protein concentrations were determined using linear regression methods.

### **2.6.5 Immunoblotting**

For immunoblotting, samples were first prepared in loading sample buffer (LSB). Desired concentration of proteins was re-suspended in 3X LSB buffer (Appendix I) to give a final concentration of 1X LSB. Samples were then heated for 3 minutes at 99°C. Following heating, samples were then loaded into pre-cast Tris-glycine gels (Bio-rad, Hertfordshire, UK) unless stated otherwise, and PageRuler Prestained Protein Ladder (ThermoFisher Scientific, Paisley, UK) was used as a molecular weight standard. Electrophoresis was performed using Mini-Protean Tetra Cell apparatus (Bio-rad, Hertfordshire, UK). Gels were set inside the Tetra-Cell module assembly and placed in a Bio-Rad Tetra Cell tank. The outside and inside of the assembly was submerged in running buffer (Appendix I) and electrophoresis was conducted in two steps. Power packs were first set to 80V at 400mA, voltage constant, for 10 minutes. After two minutes voltage was increased to 120V until protein had completely migrated through the gel (confirmed by LSB dye front). Proteins were then transferred to Amersham Protran Premium 0.45µm nitrocellulose membranes (GE Healthcare, United Kingdom). To achieve this, membranes, filter paper and sponges were pre-soaked in transfer buffer (Appendix I) and then assembled into a gel holder cassette. The cassette was then loaded into the Tetra Cell blotting module and placed inside the Tetra Cell tank. The module was then submerged in transfer buffer and an ice pack was also inserted into the tank to ensure cool temperatures during the transfer process. A magnetic stirrer was placed in the tank which was then positioned on a stirring platform ready for the transfer process. Transfer of the protein was achieved by applying 200V with a current of 400mA to the gel assembly for 2 hours. The blotting module/gel assembly was then disassembled, and protein transfer was confirmed via the use of Ponceau S staining. Membranes were then washed twice for 10 minutes in 0.1% PBS-Tween. Following wash steps, membranes

were incubated overnight at 4°C with antibodies for relevant targets. Antibodies (Appendix III) were diluted in 0.1% PBS-Tween containing 5% skimmed-milk (Sainsbury's, Edinburgh, UK) unless stated otherwise. After the overnight incubation, membranes were washed 3 times for 10 minutes with 0.1% PBS-Tween. Licor Odyssey secondary antibodies (Appendix III) were then diluted in 0.1% PBS-Tween containing 5% skimmed-milk and membranes were stained for 45 minutes in the dark, at room temperature. Proteins of interest were stained with Licor 800CW secondary antibodies and loading controls were stained with Licor 680LT unless stated otherwise. For E11 probing, secondary HRP antibodies were incubated in the same manner. Following secondary antibody staining, membranes were washed three times for 10 minutes using PBS-T and subsequently imaged and analysed using a Licor Odyssey 9120 (Licor, Nebraska, USA) and the associated Image Studio software (Licor, Nebraska, USA). E11 visualisation was performed using Immobilon Western Chemiluminescent HRP substrate (Merck, Poole, UK). Luminol and Peroxide solutions were mixed 1:1 and added to HRP stained blots for 5 minutes. Images were then captured using Syngene G:Box Chemi XX6 (Syngene, Cambridge, UK).

#### **2.6.6 Quantification of Western blots**

Western blots were quantified using the Licor Odyssey 9120 system and its associated Image Studio software (Licor, Nebraska, USA). The Image Studio "Western Blot" analysis function was used to generate background subtracted densitometry values for each immunoblot. Densitometry values for each treatment were then normalised to  $\beta$ -actin expression and expressed as arbitrary units of fluorescence. Data processing was conducted using Microsoft Excel (Microsoft, Redmond, United States of America).

#### **2.7 Cell tracker staining**

Cells were cultured in Ibidi 35mm culture-insert 4 well  $\mu$ -dishes (Thistle Scientific, Uddingston, UK). SaOS-2 cells were seeded in monolayer culture at a density of  $1.66 \times 10^4$  in 100 $\mu$ L growth medium or encapsulated in hydrogel as detailed in section 4.3.3., however, these were seeded as 50 $\mu$ L constructs covered with 50 $\mu$ L growth medium. After 24 hours of incubation at 37°C, 2D and 3D cultures were washed with 3mL and

200µL of PBS respectively. CellTracker™ Deep Red dye (1000X) was diluted to a working concentration of 1X in growth media and added to both 2D and 3D cultures and incubated for 45 minutes at 37°C. After 45 minutes cell tracker solutions were removed, and cultures were washed with PBS. Fresh growth media was added to each culture which was then imaged using a Zeiss LSCM 880 (Zeiss, Dresden, Germany) and ZEN Black software (Zeiss). Images were then processed using ZEN Blue software (Zeiss, Dresden, Germany).

## **2.8 Live/dead staining**

### **2.8.1 Live/dead staining method**

C-28/I2 and SaOS-2 cells were cultured and stained in both 2D and 3D conditions. Live/Dead staining was achieved with the use of Calcein AM and Propidium Iodide respectively. 2D cell cultures were seeded in an Ibidi µ-Slide Angiogenesis Glass Bottom microscopy slide at a density of  $1.8 \times 10^4$  in 50µL of growth media per well described in section 4.3.3. 3D cultures were also seeded in an Ibidi µ-Slide Angiogenesis Glass Bottom microscopy slides (Thistle Scientific, Uddingston, UK) at a volume of 10µL of pre-gel-cell solution per well containing  $2 \times 10^5$  cells. Cells were encapsulated in hydrogels as per sections 2.3. and 2.4. 50µL of media was then added dropwise to the top of the hydrogel to not disturb the construct. This pre-gel-cell solution was left for 10 minutes at room temperature and then incubated at 37°C in an incubator for 2 hours to allow crosslinking to occur. After 2 hours, the 50µL of media on top of the construct was replaced with a fresh 50µL and left over night in an incubator at 37°C. For functionalised hydrogel live/dead screening, cells were cultured for 24 hours in growth medium. For hydrogel time-course culture, cells were cultured in growth media for the first 24 hours and then subsequently in differentiation media (as described in section 2.2.1.) for up to 12 days with the media being replenished every 2 days. Live/dead stain was prepared by diluting a 1µg/µL calcein AM stock solution and 1µg/µL propidium iodide solution in 300µL growth media pre-warmed to 37°C. 50µL of the stain mix was then added to each well and incubated for 1 hour at 37°C. Finally, stained samples were gently washed twice with 50µL phosphate-buffered saline (PBS) and then covered with 50µL PBS for microscope visualisation. Cell cultures were then visualised using 488nm (calcein AM) and 568nm (propidium iodide) channels. Stained cultures were imaged via the creation

of a 2x2 tile scan of each culture to provide a comprehensive image that was representative of 4 fields of view using a Zeiss LSCM 880 (Zeiss, Dresden, Germany) and ZEN Black software (Zeiss, Dresden, Germany).

### **2.8.2 Live/dead staining analysis**

Live/dead cell images were produced and captured using a Zeiss LSCM 880 (Zeiss, Dresden, Germany) and ZEN Black software (Zeiss, Dresden, Germany). Images were then processed using ZEN Blue software (Zeiss, Dresden, Germany) and cell counts were performed using ImageJ. ImageJ processing involved converting images to grayscale using “scale when converting” and 16-bit options in the ImageJ toolbar. Next, thresholds were set to include all cell structures in the image. Automated cell counts were then produced, excluding everything smaller than  $5^2$  pixels to mitigate background staining. Count masks were used to ensure reliable and robust counting was performed. During the analysis of 2D cultures, the “watershed” feature was used to construct a reliable representation of the number of cells due to the confluence of these cultures.

## **2.9 Cell tracker staining**

Cells were cultured in Ibidi 35mm culture-insert 4 well  $\mu$ -dishes. SaOS-2 cells were seeded in monolayer culture at a density of  $1.66 \times 10^4$  in 100 $\mu$ L growth medium or encapsulated in hydrogel as detailed in section 2.4., however, these were seeded as 50 $\mu$ L constructs covered with 50 $\mu$ L growth medium. After 24 hours of incubation at 37°C, 2D and 3D cultures were washed with 3mL and 200 $\mu$ L of PBS respectively. CellTracker™ Deep Red dye (1000X) was diluted to a working concentration of 1X in growth media and added to both 2D and 3D cultures and incubated for 45 minutes at 37°C. After 45 minutes cell tracker solutions were removed, and cultures were washed with PBS. Fresh growth media was added to each culture which was then imaged using a Zeiss LSCM 880 and ZEN Black software. Images were then processed using ZEN Blue software.

## **2.10 Immunofluorescence**

Immunofluorescent staining was conducted for both 2D and 2.5D (on top of hydrogel constructs) cultured cells. 2D cultured cells were stained using coverslips, C-28/12 cells were seeded in monolayer culture in a 6-well plate on top of borosilicate coverslips (VWR, Pennsylvania, USA) or on top of a 300 $\mu$ L acellular hydrogel solution (referred to as 2.5D) and incubated for 24 hours at 37°C. Following 24 hours of incubation, 2D coverslips were washed via dipping in PBS 10 times and the surface of 2.5D cultures were washed three times with PBS. Cultures were then fixed for 15 minutes using 4% PFA. Wash steps were repeated using PBS and cells were then permeabilised with 0.1% Triton-X (in PBS) for 10 minutes and washed again with PBS. Fixed cells were then incubated with 10% FCS-PBS for 30 minutes to block the nonspecific binding of antibodies. Primary antibodies were diluted in 1% FCS-PBS and added to fixed cultures overnight at 4°C. The following day, cultures were washed with PBS and 1% FCS-PBS. Again, 2D cover slips were dipped in each solution 10 times and 2.5D cultures were washed 3 times with each solution. Secondary antibodies were diluted in 10% FCS-PBS and added to fixed cultures for 45 minutes at room temperature. Cultures were washed as before with PBS and 1% FCS-PBS and then mounted on slides with Vectashield DAPI mounting medium (2bScientific, Kirtlington, UK). 2D culture slides were sealed with nail varnish. Slides were then imaged using a Zeiss LSCM 880 and ZEN Black software. Images were then processed using ZEN Blue software.

## **2.11 Statistical analysis**

Statistical analysis was performed using GraphPad Prism 9.3.0 (GraphPad Software, California, USA). Data distribution was checked for normality using the Shapiro-Wilk test. One-way analysis of variance (ANOVA) was used to analyse statistical differences within an experiment and Tukey's post-hoc multiple comparisons test was performed to determine statistically significant differences between conditions. When data was not normally distributed the non-parametric Kruskal-Wallis ANOVA was used to analyse statistical differences within an experiment and Dunn's post-hoc multiple comparison's test was performed to determine statistically significant differences between conditions.

## **Chapter 3: Characterization of two-dimensional chondrocyte and osteoblast cell cultures for use in a three-dimensional *in vitro* model.**

### **3.1. Introduction**

Development of a novel 3D *in vitro* model of osteoarthritis (OA) first requires the establishment of suitable cell models that will allow for investigation into characteristics of the OA phenotype. It is therefore important that chondrocyte and osteoblast cells are represented as these cells are important in the formation and maintenance of articular cartilage and subchondral bone respectively; these cells also play a key role in the pathogenesis of OA. Ultimately it is the disruption of cell phenotype and extracellular matrix (ECM) produced by these cells that leads to severe disease symptoms and outcomes. It is therefore important that cells included within this cell model express the genes and proteins associated with physiological chondrocyte and osteoblast phenotypes and their respective ECM.

Human primary cells are generally considered the optimal 2D *in vitro* cell model as they behave most similarly to cells in physiologic *in vivo* conditions. These cells are not immortalized and therefore do not suffer the potential disadvantages associated with cell lines such as genetic drift, variations in protein expression and proliferation dynamics [271, 272]. Primary human chondrocytes (PHCs) have been found to express substantially higher levels of chondrocyte-associated genetic markers such as *COL2A1*, *ACAN*, *SOX9*, *MMP1*, *MMP13* and *ADAMTS5* compared to immortalized cell lines [273, 274]. However, in 2D culture, these cells will eventually de-differentiate as indicated by increased collagen I expression, whilst also displaying slower growth characteristics compared to cell lines [230, 272, 275]. Notably, PHCs will ultimately become senescent, limiting their subculture potential. The inevitable senescence coupled with high sample costs can result in a PHC model that is expensive to maintain in the longer term, which may present a challenge when trying to develop a novel 3D *in vitro* model.

Alternatively, chondrocyte cell lines are less costly and show rapid growth, whilst maintaining detectable expression of key genes and proteins associated with the chondrocyte phenotype and ECM production [273]. These characteristics can be seen in

the immortalized, juvenile costal cartilage-derived C-28/I2 chondrocyte cell line. The C-28/I2 clonal cell line displays an expression of the normally labile *COL2A1*, as well as *ACAN*, *SOX9*, *MMP-13* and *ADAMTS-5*. Notably, these cells display an expression profile more like primary chondrocytes compared to immortalized alternatives T/C-28a2, T/C28a4 and chondrosarcomas JJ012, H-ECM-SS, and produce higher yields of glycosaminoglycans (GAGs) [274, 276, 277]. It has been reported that culturing C-28/I2 immortalized chondrocytes in serum-free conditions with an insulin-containing supplement such as ITS+ can help to stabilize this chondrocyte phenotype [278, 279]. This is thought to be due to a decrease in the proliferative rate of cells under serum-starved conditions which allows the expression and deposition of proteins [276]. Additionally, the serum contains growth factors such as platelet-derived growth factor (PDGF) which may inhibit *COL2A1* expression. Substitution of serum with ITS+ provides C-28/I2 cells provides a source of insulin which may mimic the effects of IGF-I; a known chondrogenic molecule [280]. Further, if the chondrocyte phenotype is lost, it can be restored through 3D culture as exemplified by micromass culture [274].

Primary osteoblasts (POB) adapt well to monolayer culture. These cells express genetic and protein markers associated with osteoblast maturation and matrix production such as collagen I (*COL1A1*), alkaline phosphatase (AP-TNAP) and osteocalcin (*BGLAP*) [281, 282] Additionally these cells have been shown to produce a mineralised matrix with the formation of distinct mineralised nodules [281]. However, as is the case with all primary cells, they have limited subculture potential and will eventually undergo senescence, suggesting they may not be appropriate for novel model development.

A potential alternative to POB cells can be seen in the human osteosarcoma SaOS-2 cell line. These cells have a higher proliferative capacity compared to POBs and express osteoblast-specific genes in a profile similar to that of POB including *COL1A1*, *ALPL* and *BGLAP* [281, 283]. SaOS-2 cells follow this POB profile in a manner more consistent than other human cell lines such as the MG-63 and U2OS osteosarcoma lines [271, 281]. Expression of proteins such as collagen type I and AP-TNAP have previously been shown in SaOS-2 cells, with AP-TNAP activity being elevated in this cell line compared to POB, MG-63 and U2OS cells [271, 281, 284]. This seems to promote rapid mineralization in SaOS-2 monolayer cultures compared to POB and MG-63 cells, with SaOS-2 cells also forming distinct nodules and depositing calcium [281, 283, 285]. Additionally, research

has highlighted the ability of these cells to differentiate from mature osteoblast into an osteocyte-like cell in monolayer, expressing markers such as *PHEX*, *MEPE*, *DMP1* and *SOST*; with *PHEX* and *MEPE* expression being enhanced in 3D culture. However, expression of the osteocyte hallmark protein podoplanin has not been detected [286].

Therefore, to determine the suitability of C-28/I2 and SaOS-2 lines for use in a novel 3D *in vitro* model of OA these cells were first characterized in 2D culture. This allowed for the optimization of growth conditions, as well as the determination of the effects of serum and osteogenic media on C-28/I2 cells. Importantly, the expression of key chondrocyte and osteoblast markers that will be used to assess a 3D model of OA were examined.

## **3.2. Aims and objectives**

### **3.2.1. Aim**

To establish and characterise chondrocyte and osteoblast cell culture models for subsequent use in a 3D *in vitro* model of OA.

### **3.2.2. Objectives**

1. Characterise the expression of key genes and proteins in C-28/I2 chondrocytes in 2D culture, and determine the suitability of these cells for use in a 3D OA model
2. Characterise the expression of key genes and proteins in SaOS-2 osteoblasts in 2D culture, and determine the suitability of these cells for use in a 3D OA model
3. Determine the optimum conditions for the co-culture of C-28/I2 chondrocytes and SaOS-2 osteoblasts for use in a 3D OA model

## **3.3. Methods**

### **3.3.1. Cell culture**

Cells were maintained as detailed in section 2.2.1. Briefly, all cells were maintained in tissue culture flasks and sub-cultured via trypsinization at 70-80% confluency. PHCs were maintained in PromoCell Chondrocyte Growth Medium as per section 2.2.3. and C-28/I2 and SaOS-2 cells were maintained in Dulbecco's modified eagle's medium (DMEM)/F12 GlutaMAX, + 10% fetal calf serum (FCS), + 1% penicillin-streptomycin (P/S), + an

additional 55mg/L sodium pyruvate to give a final concentration of 110mg/L sodium pyruvate.

#### **3.3.1.1. C-28/I2 optimizing media conditions**

C-28/I2 cells were seeded in 6-well plates at a density of  $2.5 \times 10^5$  cells per well in 3mL of growth media and grown until confluent (48 hours). Cells were gently washed twice with sterile saline solution and their media was then changed to either DMEM F-12 GlutaMAX growth medium or DMEM F-12 GlutaMAX serum-free medium (DMEM F/12 GlutaMAX, + 1% insulin transferrin selenium plus (ITS+) + 55mg/L sodium pyruvate), and subsequently cultured for an additional 48 hours. For investigation of protein expression, media was also supplemented with an additional 50 $\mu$ g/ml L-ascorbic acid. Following these two days of culture in serum or serum-free conditions, cells were harvested for RNA and protein.

#### **3.3.1.2. C-28/I2 time course**

C-28/I2 cells were seeded in 6-well plates at a density of  $2.5 \times 10^5$  cells per well in 3mL of growth media and grown until confluent (48 hours). Upon reaching confluency (day 0), cells were treated with DMEM F-12 GlutaMAX osteogenic medium (growth medium supplemented with 50 $\mu$ g/ml L-ascorbic acid and 5mM  $\beta$ -glycerophosphate). RNA and protein were harvested on days 0, 3, 6, 9 and 12. All C-28/I2 cells used for time course analysis were seeded between passages 4 and 6.

#### **3.3.1.3. SaOS-2 time course**

SaOS-2 cells were seeded in 6-well plates at a density of  $4.5 \times 10^5$  cells per well in 3mL of growth media and grown until confluency (24 hours). Upon reaching confluency (day 0), cells were treated with DMEM F-12 GlutaMAX osteogenic media (growth medium supplemented with 50 $\mu$ g/ml L-ascorbic acid and 5mM  $\beta$ -glycerophosphate). RNA and protein were harvested on days 0, 3, 6, 9 and 12 days. All SaOS-2 cells used for time course analysis were seeded between passages 10-12.

### **3.3.2. RNA extraction, cDNA synthesis and RT-qPCR**

Cells were washed twice with 3mL ice-cold PBS and then scraped on ice in 1mL TRIZOL. Samples were frozen at -80°C until 3 biological replicates for each experimental condition had been harvested, at which point RNA extraction was performed as per section 2.5.1. and RNA integrity was assessed as per section 2.5.2. cDNA was synthesised as per section 2.5.3 and frozen at -20°C for storage.

RT-qPCR was used to determine the expression of chondrocyte and osteoblast genes. Prior to the analysis of genes of interest, geNorm analysis was performed and determined *B2M* and *SDHA*, and *TOP1* and *ATP5B* as the most suitable housekeeping genes to use for the normalization of C-28/I2 and SaOS-2 RT-qPCR data, respectively (section 2.5.4).

RT-qPCR was performed on chondrocyte (*ACAN*, *COL10A1*, *COL1A1*, *COL2A1*, *COMP* and *MMP13*) and osteoblast (*ALPL*, *BGLAP*, *COL1A1*, *PDPN* and *POSTN*) target genes. Primer sequences are detailed in Appendix II. RT-qPCR was performed over 3 biological replicates as detailed in section 2.5.4. Data were normalized to the geometric mean of appropriate housekeeping genes as determined by geNorm analysis, and target gene data were analysed as per section 2.5.5 and 2.5.6.

### **3.3.3. Protein extraction and quantification**

Cells were washed twice with 3mL ice-cold PBS and then scraped on ice into 1mL PBS. Cells were pelleted via centrifugation at 145 *g*, 4°C for 5 minutes. PBS was aspirated and pellets were then frozen at -80°C until 3 biological replicates for each experimental condition had been harvested. Once all biological replicates were acquired, protein was extracted and quantified as per sections 2.6.1 and 2.6.4.

### **3.3.4. Immunoblotting**

Following quantification of protein concentration in whole cell lysates, samples were loaded onto Tris-Glycine gels prepared by the operator (reagents specified in Appendix I). Where possible, 10µg of whole cell lysate from human articular cartilage was loaded as a positive control for chondrocytes. Immunoblotting was performed as per section 2.6.5. with membranes probed using primary antibodies as detailed in Appendix III.

Secondary antibody staining was performed, and proteins visualized using the Licor Odyssey system for anti-rabbit antibodies or enhanced chemiluminescence (ECL) blotting for anti-sheep secondary antibodies (Appendix III). The expression of a protein of interest was then normalized to  $\beta$ -actin expression. Immunoblotting images were quantified as per section 2.6.6.

### **3.3.5. Statistical analysis**

Statistical analysis was performed using GraphPad Prism 9.3.0 (GraphPad Software, USA) as per section 2.11.

## **3.4. Results**

### **3.4.1. Characterisation of primary chondrocytes**

Primary chondrocytes were grown in monolayer conditions from passage 2 to passage 6. Within this time cells underwent a noticeable morphological change from a standard polygonal chondrocyte-like morphology to a more fibroblast-like morphology as indicated by increased numbers of spindle-shaped cells (**Figure 3.1**). This morphological change was accompanied by slower growth rates observed with increasing passage numbers. For these reasons it was determined that the use of primary cells was not suitable for the development of a reproducible, cost-effective novel model due to the demand for a high number of cells.

### **3.4.2. Characterisation of C-28/I2**

#### **3.4.2.1 Optimization of C-28/I2 growth conditions**

The C-28/I2 chondrocyte cell line was investigated as these cells produce hyaline cartilage, express markers associated with articular, including labile markers such as *COL2A1* [287]. It has been reported that culturing immortalized chondrocytes in the absence of FCS can promote the chondrocyte phenotype, preserving the expression of markers such as *COL2A1* in monolayer culture [287]. Ultimately, a co-culture of chondrocytes and osteoblasts with one universal growth media is required. Therefore,

it was first necessary to investigate their potential for growth in differing serum conditions.

#### 3.4.2.2. Morphology of C-28/I2 under differing serum conditions

To investigate the effect of serum on the chondrocyte phenotype, C-28/I2 cells were grown for 2 days until sub-confluence in growth media containing FCS and then cultured for a further 2 days in either: media containing FCS, or media without FCS supplemented with ITS+. During this time no morphological differences were observed, and cells were growing at the same rate in both conditions; however, C-28/I2 cells cultured in the absence of FCS were becoming less adherent and potentially apoptotic (**Figure 3.2**).

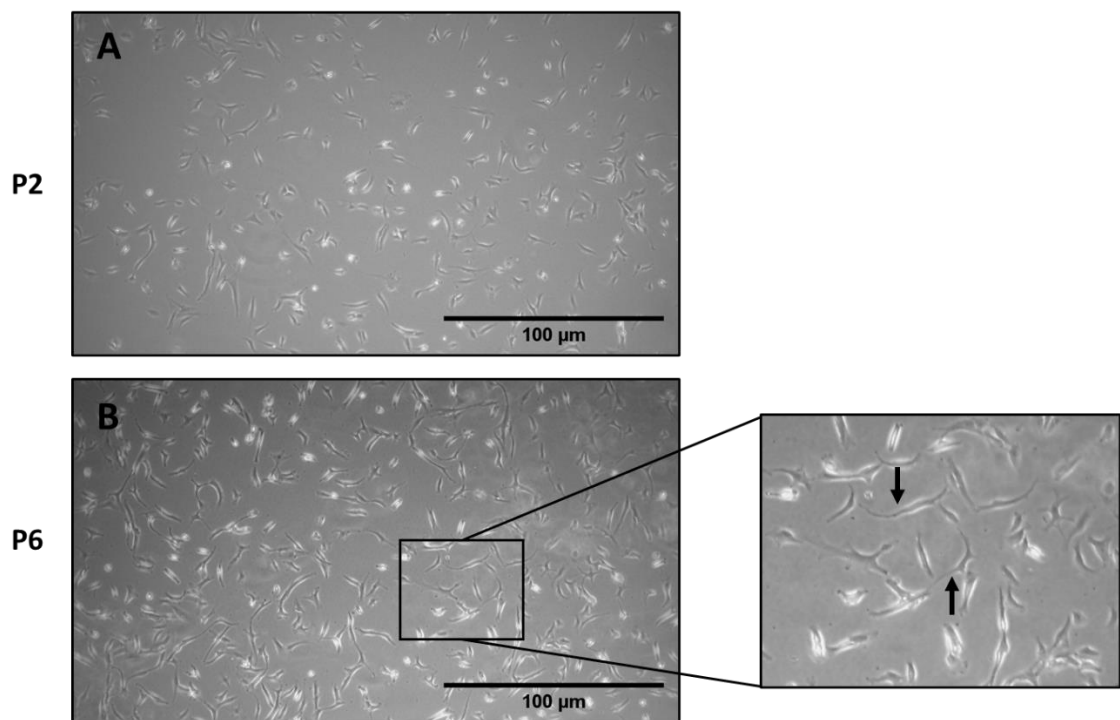


**Figure 3.1. The effect of 2D cell culture on primary human chondrocyte morphology.** (A) PHCs displayed a typical polygonal morphology at early passage numbers (P2). (B) Passage 6 (P6) PHCs began to display a fibroblast-like morphology (indicated by black arrows) with these cells showing an increased number of spindle-shaped cells, suggestive of de-differentiation. Images were taken at 4X magnification, and the scale bar represents 100μm.

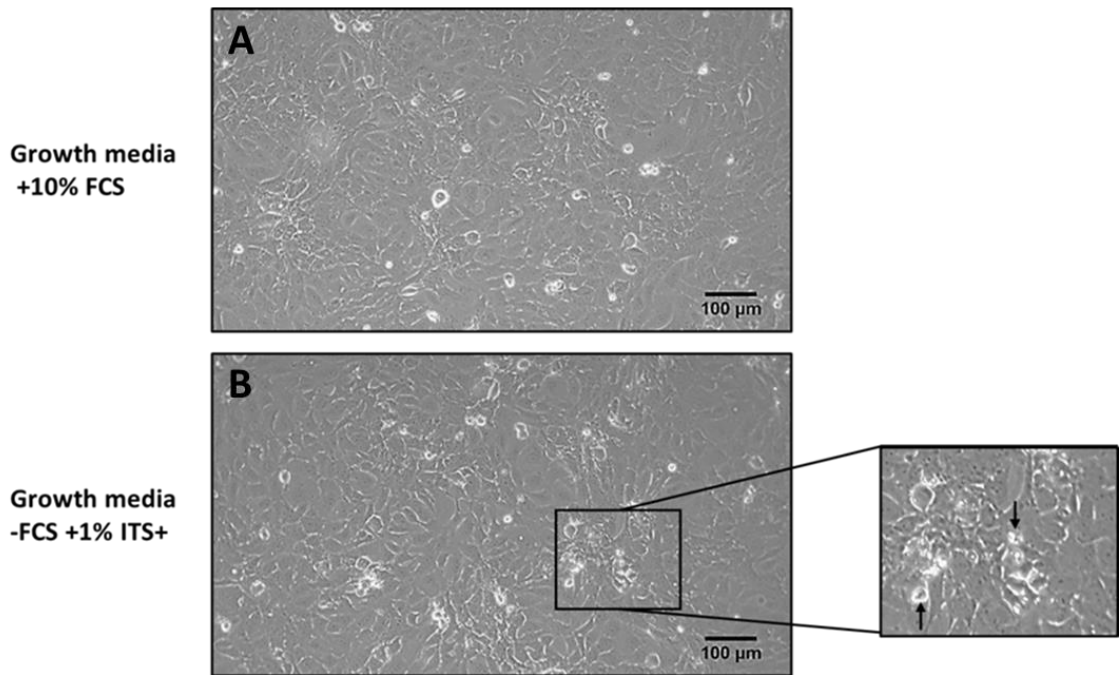


**Figure 3.2. The effect of serum on C-28/I2 cell morphology.** Cells after 2 days in growth media with FCS and then a further 2 days in either growth media +10% FCS (A), or growth media -FCS + 1% ITS+ (B). C-28/I2 displayed polygonal morphology under both conditions, however in the FCS-free conditions cells appeared to become less adherent and potentially more apoptotic (indicated by black arrows) than cells cultured in the presence of FCS. Images were taken at 10X magnification, and the scale bar represents 100µm.

#### 3.4.2.3. Analysis of chondrocyte-associated gene expression under differing serum conditions

Initially, a geNorm analysis was performed to ensure appropriate housekeeping reference genes were used for normalization (**Figure 3.3**). GeNorm analysis indicated that the appropriate reference genes for analysis were *B2M* and *SDHA* as determined by geNorm M and V values. GeNorm M highlights the average expression stability value (M) of reference genes at each step during stepwise exclusion of the least stably expressed reference gene, with stability increasing from left to right (**Figure 3.3A**). GeNorm V indicates the number of reference genes required for reliable analysis of qPCR data (**Figure 3.3B**). Therefore, the geometric mean of the expression of these two reference genes was used in calculations when analyzing RT-qPCR output data.

Following geNorm analysis, the determination of target gene expression was investigated (**Figure 3.4**). Target Ct values were normalized to the geometric mean of *B2M* and *SDHA* and changes in gene expression were determined by comparing gene

expression between all conditions. Expression of *COL2A1* (**Figure 3.4B**), and *COMP* (**Figure 3.4C**) did not significantly change when comparing media containing FCS and FCS-free ITS+ supplemented medium. Expression of *COL1A1* was also found to be stable between conditions indicating that FCS did not influence cell de-differentiation (**Figure 3.4F**). FCS starvation significantly decreased the expression of *AGG* ( $P < 0.05$ ; **Figure 3.4A**) whilst increasing the expression of both the hypertrophy marker *COL10A1* ( $P < 0.05$ ; **Figure 3.4D**) and the catabolic factor *MMP13* ( $P < 0.05$ ; **Figure 3.4E**). This suggests that FCS starvation has an anti-anabolic effect and drives the C-28/I2 cells towards hypertrophy.

#### **3.4.2.4. Analysis of chondrocyte-associated protein expression under differing serum conditions**

Following the determination of the expression of genes associated with the chondrocyte phenotype, immunoblotting was performed to determine the effects of serum conditions on the expression of chondrocyte-associated proteins. Immunoblotting analysis revealed that the expression of key markers *COL2 $\alpha$ 1* (**Figure 3.5A** compare lanes 1 to 2 & **Figure 3.5B**) and *COMP* (**Figure 3.5C** compare lanes 1 to 2 & **Figure 3.5D**) remained relatively stable between different FCS conditions. Expression of the catabolic *MMP13* protein was seen to slightly decrease under FCS-deprived conditions (**Figure 3.5E** compare lanes 1 to 2 & **Figure 3.5F**). Finally, the protein expression of the chondrocyte hypertrophy marker *COL10 $\alpha$ 1* could not be detected in C-28/I2 cultures (**Figure 3.5G**), confirmed using human articular cartilage as a positive control for *COL10 $\alpha$ 1* expression. These results suggest that under the experimental conditions tested, FCS deprivation has a negligible effect on the expression of chondrocyte-associated proteins in C-28/I2 cells.

Taken altogether, results suggest that C-28/I2 chondrocytes do not need FCS deprivation to maintain expression of chondrocyte associated genes and proteins and will display a chondrocyte-like phenotype in 2D culture in growth media with supplemented with FCS.

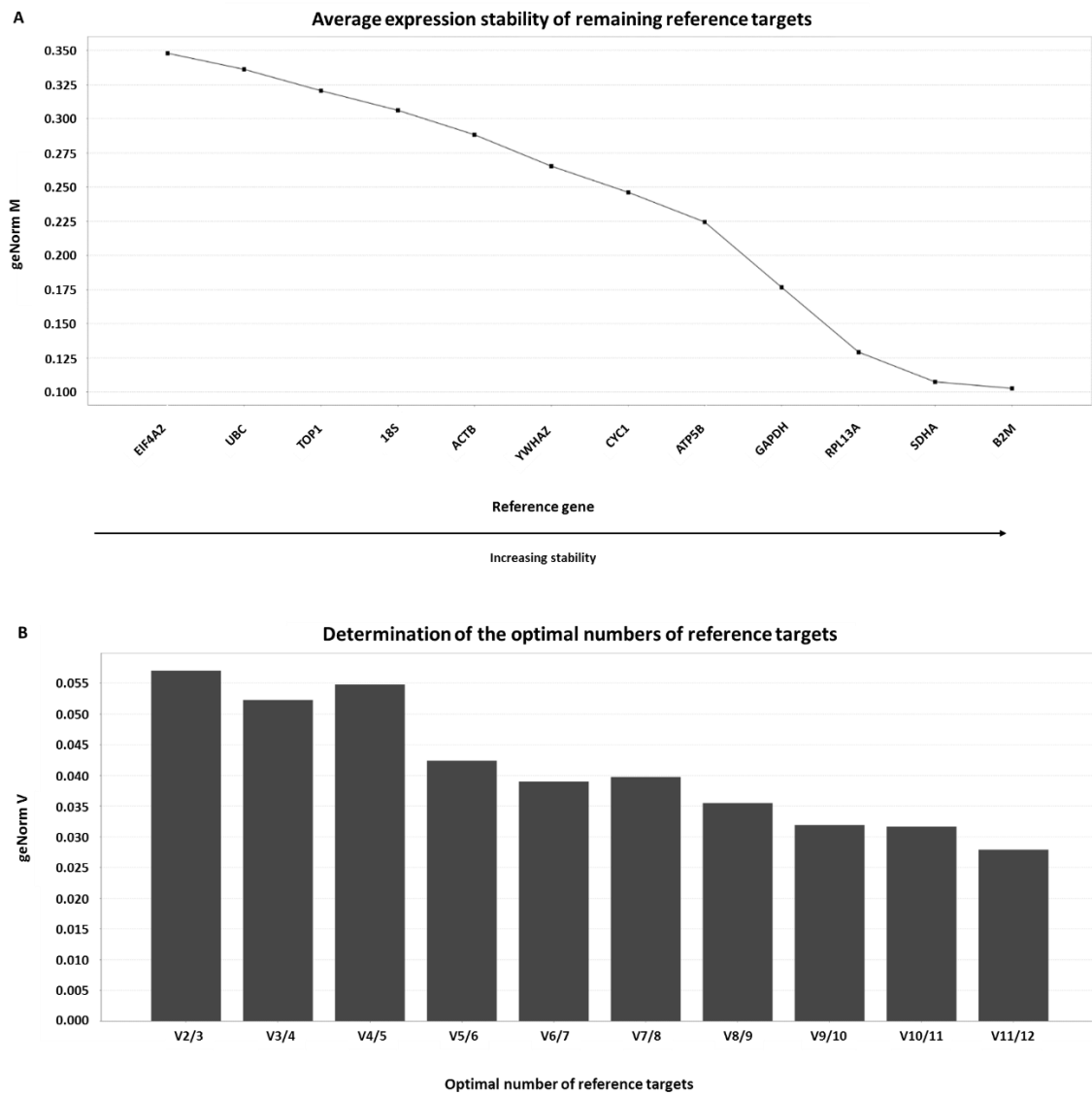


**Figure 3.3. The presence of serum alters housekeeping gene expression over a 4-day timecourse.** GeNorm analysis of RNA harvested from C-28/12 cells over a 4-day time course comparing differing media conditions (+10 % FCS vs. no FCS +1% ITS+). (A) geNorm M highlights the average expression stability value (M) of reference genes at each step during stepwise exclusion of the least stably expressed reference gene, with stability increasing from left to right. (B) geNorm V indicates the number of reference genes required for reliable analysis of qPCR data. The optimal number of gene values <0.15 are considered stable (i.e., V2/3 <0.15 therefore using 3 reference genes instead of 2 will not impact analysis). Data are from a dataset of n=3.

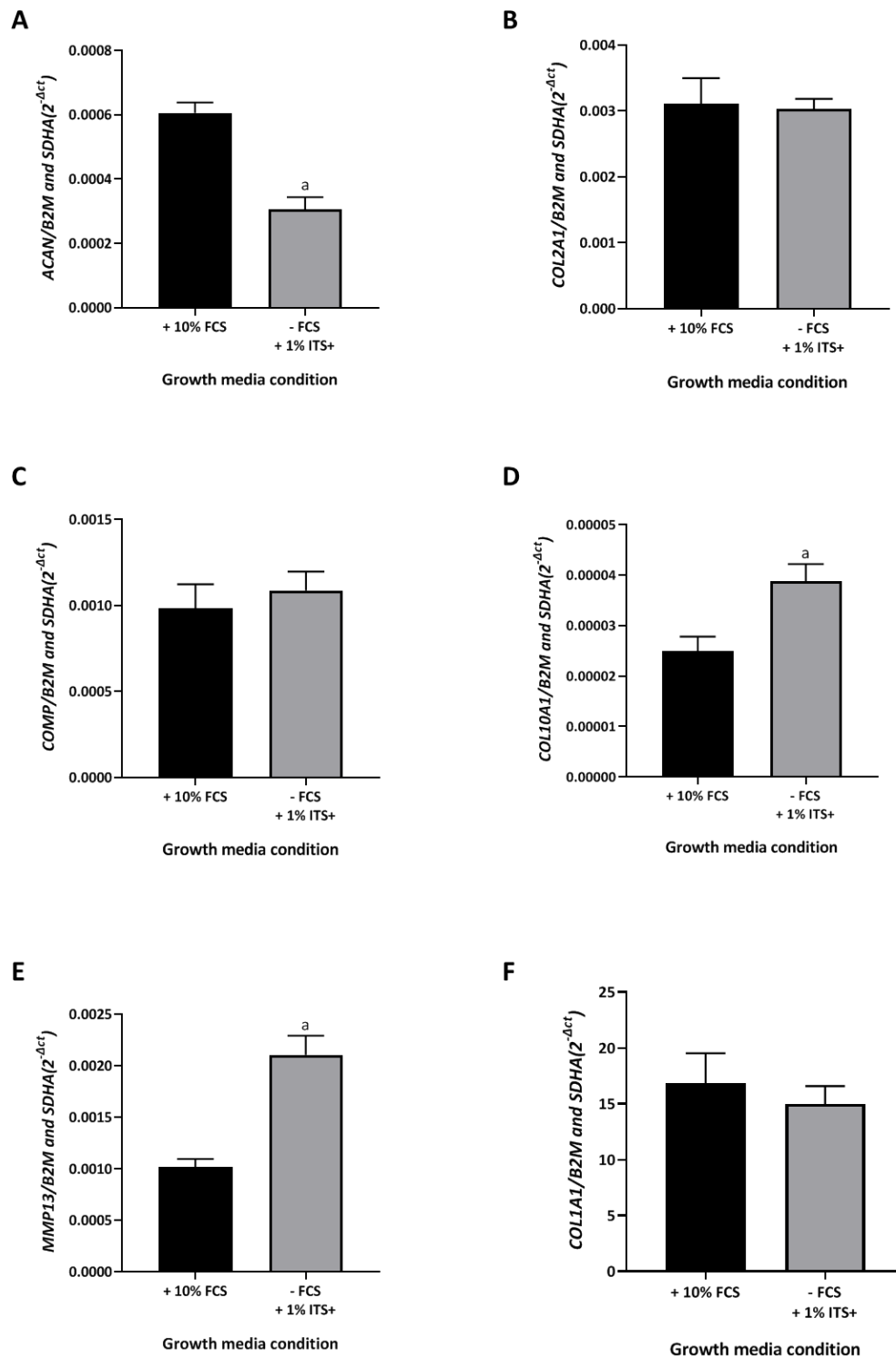


**Figure 3.4. Serum deprivation drives the expression of genes associated with a hypertrophic phenotype in C-28/I2 cells.** C-28/I2 cells were cultured with or without serum and RNA was harvested 3 days post-confluence. The expression of chondrocyte associated genes was determined via RT-qPCR (A) ACAN, (B) COL2A1, (C) COMP, (D) COL10A1, (E) MMP13, (F) COL1A1. Data are presented as  $2^{-\Delta Ct}$  mean values  $\pm$  SEM for n=3; significant differences between conditions denoted by a =  $P < 0.05$ .

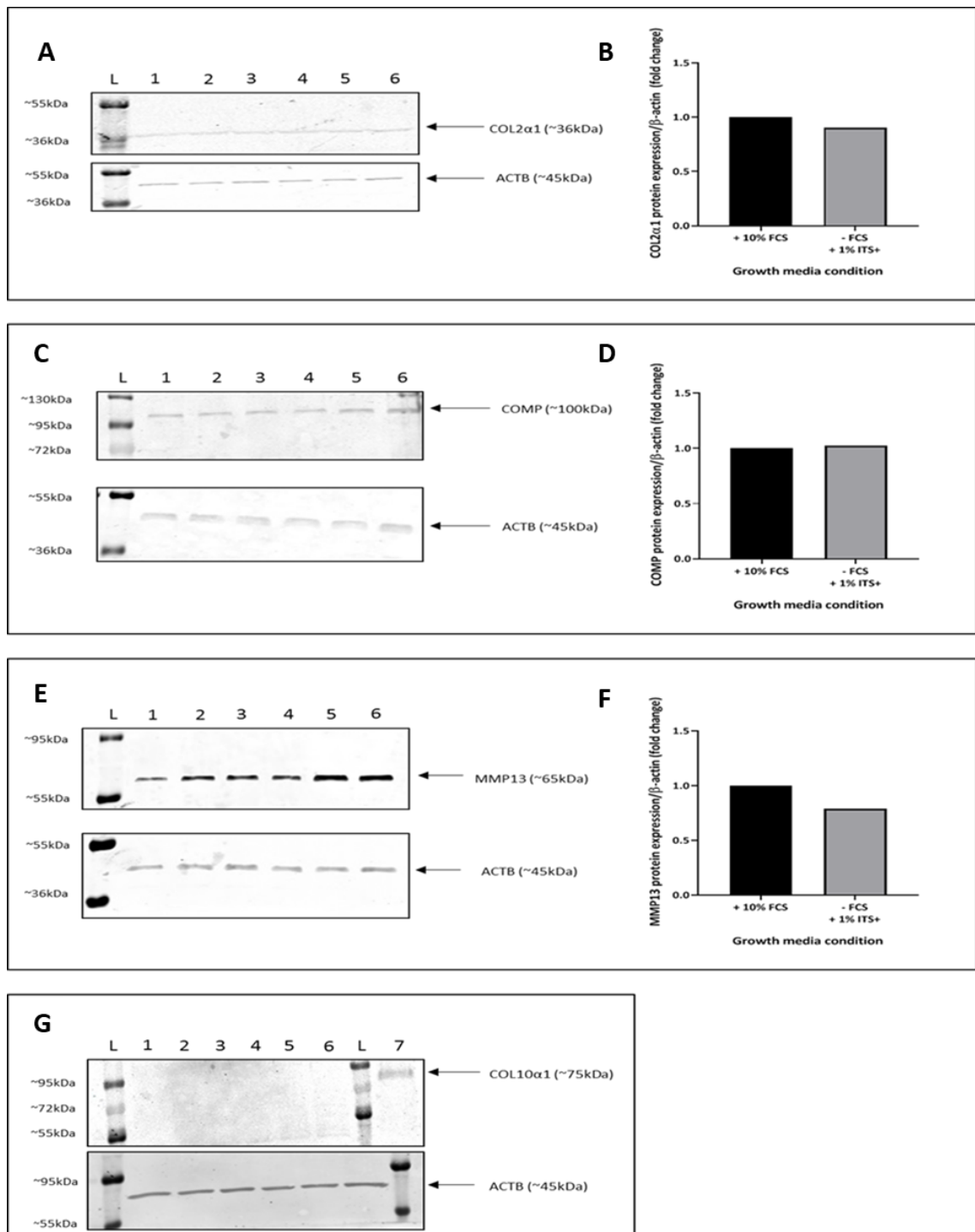


**Figure 3.5. Serum deprivation has no impact on proteins associated with the chondrocyte ECM.** Cells were cultured with or without serum and protein was harvested 3 days post-confluence. Immunoblotting was used to determine protein expression (A) COL2 $\alpha$ 1 immunoblot, (B) COL2 $\alpha$ 1 quantification (C) COMP immunoblot, (D) COMP quantification, (E) MMP13 immunoblot (F) MMP13 quantification and (G) COL10 $\alpha$ 1 immunoblot. Lanes: (L) Ladder. (1, 3 & 5) Growth medium + 10% FCS, with each lane representing one biological replicate. (2, 4 & 6) Growth medium -FCS + 1% ITS+, with each lane representing one biological replicate. (7) Human cartilage positive control. Immunoblotting was performed in triplicate and normalised to  $\beta$ -actin expression. Densitometry was performed on the representative images shown.

### **3.4.3. Characterization of C-28/I2 over a 12-day time course.**

#### **3.4.3.1. Morphology of C-28/I2 over a 12-day time course.**

Following optimization of culture conditions for the C-28/I2 cell line, these cells were grown over a 12-day time course in osteogenic media. These conditions are required by osteoblasts to effectively undergo differentiation *in vitro*, therefore, to facilitate a co-culture model, C-28/I2 cells must be able to tolerate these conditions whilst maintaining their chondrocyte phenotype. Light microscopy images show that the C-28/I2 cells form a dense, adherent monolayer under these conditions, with no observable changes in C-28/I2 polygonal morphology over time (**Figure 3.6**).

#### **3.4.3.2. Analysis of chondrocyte-associated gene expression over a 12-day time course.**

To determine the effects of osteogenic media on C-28/I2 expression of chondrocyte-associated genes, RT-qPCR was performed on C-28/I2 cells cultured under osteogenic conditions for up to 12 days. Expression of *ACAN* significantly decreases between days 0 and 6 ( $P < 0.05$ ; **Figure 3.7A**), before returning to baseline levels. *COL2A1* expression significantly decreases over days 6, 9 and 12 compared to day 0 ( $P < 0.05$ ; **Figure 3.7B**). *COMP* expression significantly decreases between days 0 and 3 ( $P < 0.05$ ; **Figure 3.7C**) and returned to basal levels at subsequent time points, as did *COL10A1* expression ( $P < 0.05$ ; **Figure 3.7D**). *MMP13* expression did not significantly change over the time course, however, a trend towards increased expression is observed (**Figure 3.7E**). Finally, *COL1A1* expression significantly decreases when comparing days 0 to days 6, 9 and 12 ( $P < 0.05$ ; **Figure 3.7F**).

#### **3.4.3.3. Analysis of chondrocyte-associated protein expression over a 12-day time course.**

Western blotting was performed to determine the expression of target proteins associated with the chondrocyte phenotype and cartilaginous ECM production over a 12-day time course (**Figure 3.8**). Immunoblotting revealed that *COL2 $\alpha$ 1* production decreased between days 0 and 3 (**Figure 3.8A** compare lanes 1 to 2 & **Figure 3.8B**),

increased between days 3 and 6 (**Figure 3.8A** compare lanes 2 to 3 & **Figure 3.8B**) and finally decreased in a linear fashion over days 9 and 12 (**Figure 3.8A** compare lanes 4 to 5 & **Figure 3.8B**). COL2 $\alpha$ 1 expression follows a similar trend to the COL2A1 gene expression which shows an overall decrease by the end of the time course. Expression of COMP can be seen to increase in a time-dependent manner from days 0 to day 9 (**Figure 3.8C** lanes 1-4 & **Figure 3.8D**) and decrease between days 9 and 12 (**Figure 3.8C** compare lanes 4 and 5 & **Figure 3.8D**); the same trend is observed in the expression of MMP13 (**Figure 3.8E** lanes 1-5 & **Figure 3.8F**). Notably, *COMP* gene expression followed a trend like COMP protein aside from an initial drop in expression, whereas MMP13 expression followed a trend inverse to that of the *MMP13* gene. Active COL1 $\alpha$ 1 protein expression was not found to be expressed in C-28/I2 cells with immunoblotting only showing pro-collagen I expression which is consistent with *COL1A1* qPCR data (**Figure 3.8G**).

The results presented show that over a 12-day time course in osteogenic media C-28/I2 cells can maintain their chondrocyte phenotype; despite overall drops in the expression of markers such as *COL2A1*, the gene and its associated protein COL2 $\alpha$ 1 are still detectable even after 12 days of monolayer culture. Intermittent drops of other chondrocyte-associated genes are recoverable, and all other proteins are upregulated throughout the time course. These results suggest that monolayer culture in osteogenic media does not significantly impact the overall cartilage phenotype of the C-28/I2 cell and that these cells can be successfully cultured in this media which will be carried forward into future chondrocyte-osteoblast co-culture experiments.

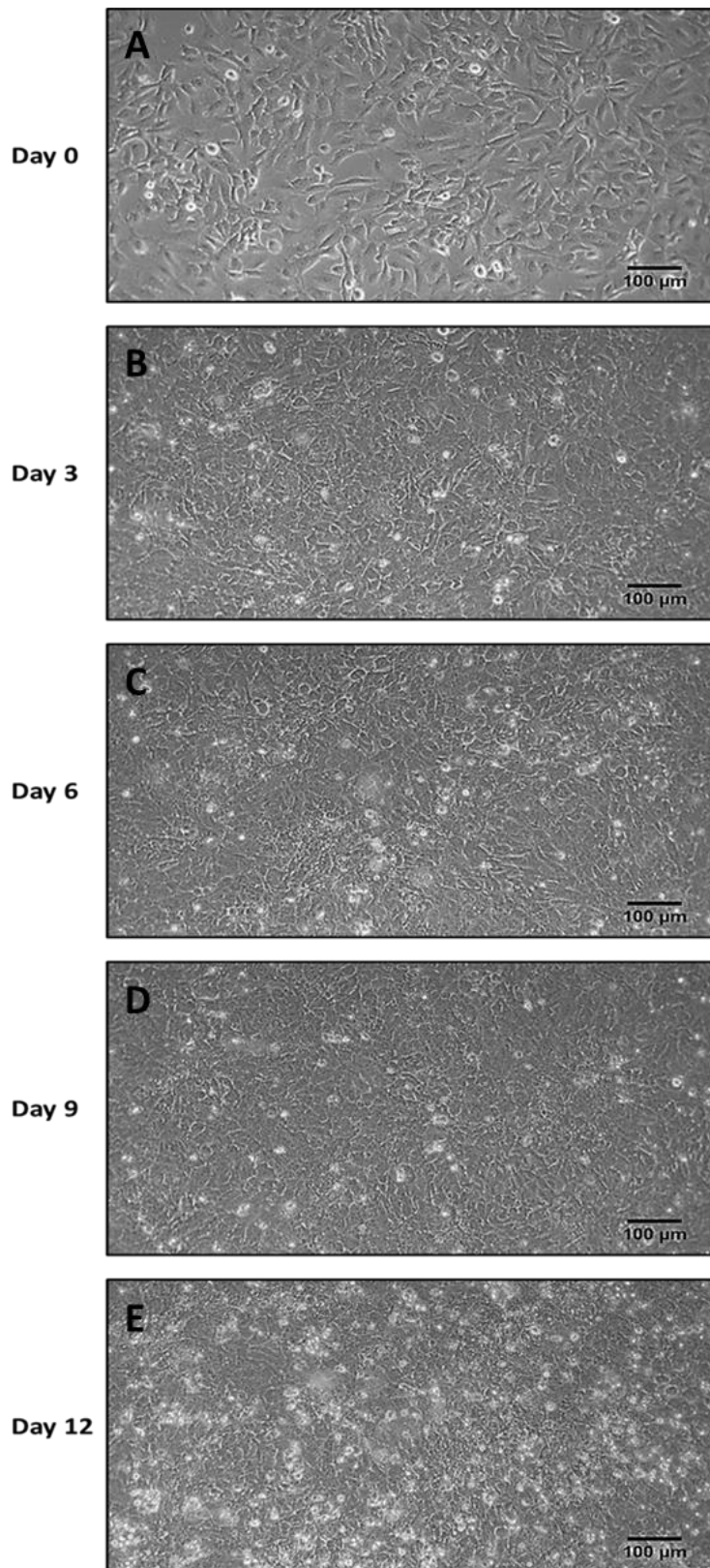


**Figure 3.6. The effect of sustained 2D culture on C-28/I2 morphology.** (A) Cells were grown to confluence (Day 0) in DMEM F-12 GlutaMAX growth media. Once confluent, cells were subsequently cultured in DMEM F-12 GlutaMAX osteogenic media for (B) 3 days, (C) 6 days, (D) 9 days, (E) 12 days. Images were taken at 10X magnification, and the scale bar represents 100μm.

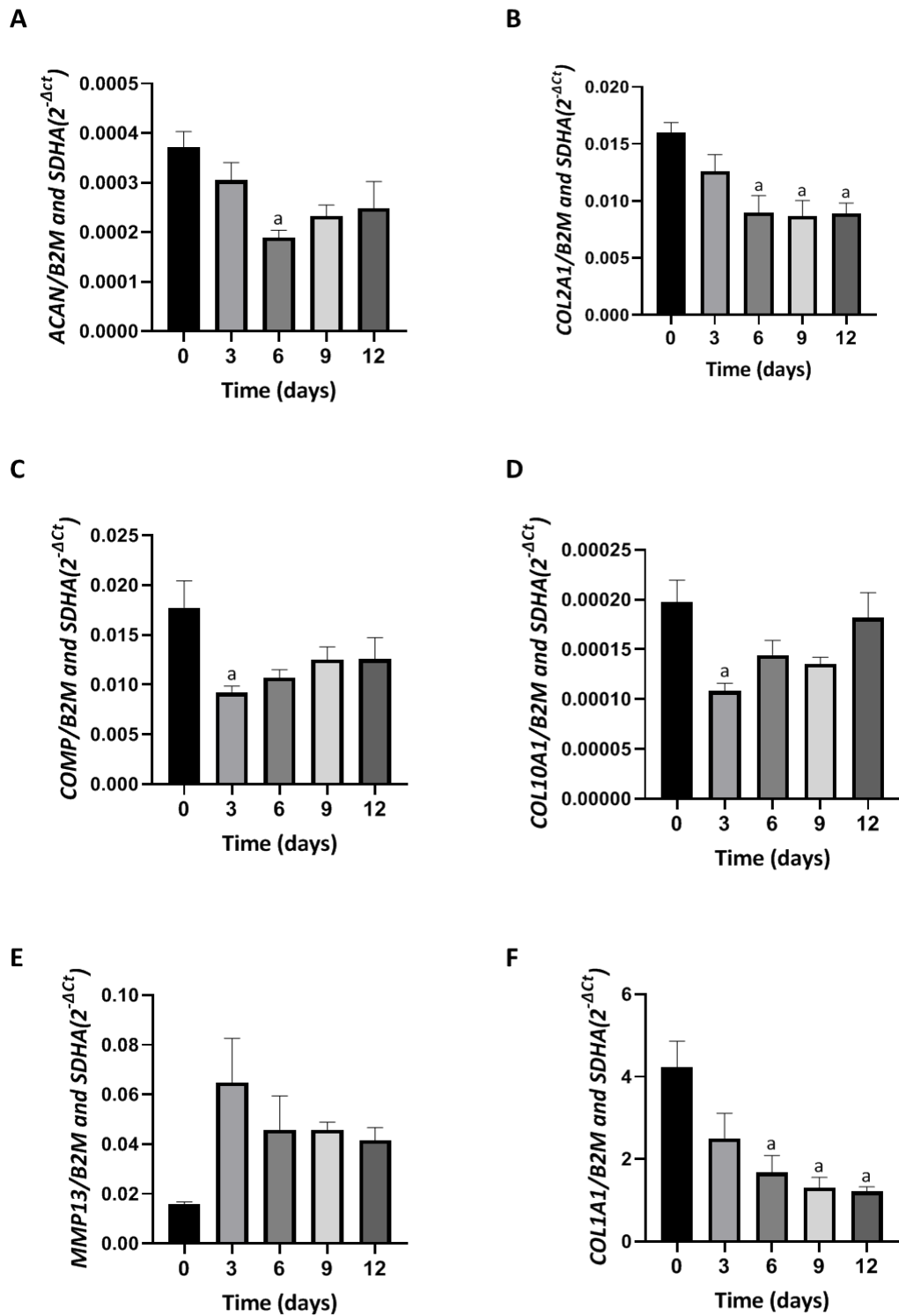


**Figure 3.7.** 2D culture of C-28/I2 over 12 days cells is associated with a reduction in expression of genes associated with the chondrocyte phenotype. C-28/I2 cells were cultured from 0 to 12 days and expression of chondrocyte associated genes was determined via RT-qPCR. Data is presented as  $2^{-\Delta Ct}$  mean values  $\pm$  SEM showing normalized changes in expression of target genes. Results obtained from a dataset of n=3. (A) ACAN, (B) COL2A1, (C) COMP, (D) COL10A1, (E) MMP13, (F) COL1A1. Differences between conditions denoted by a = compared to day 0 ( $P < 0.05$ ).

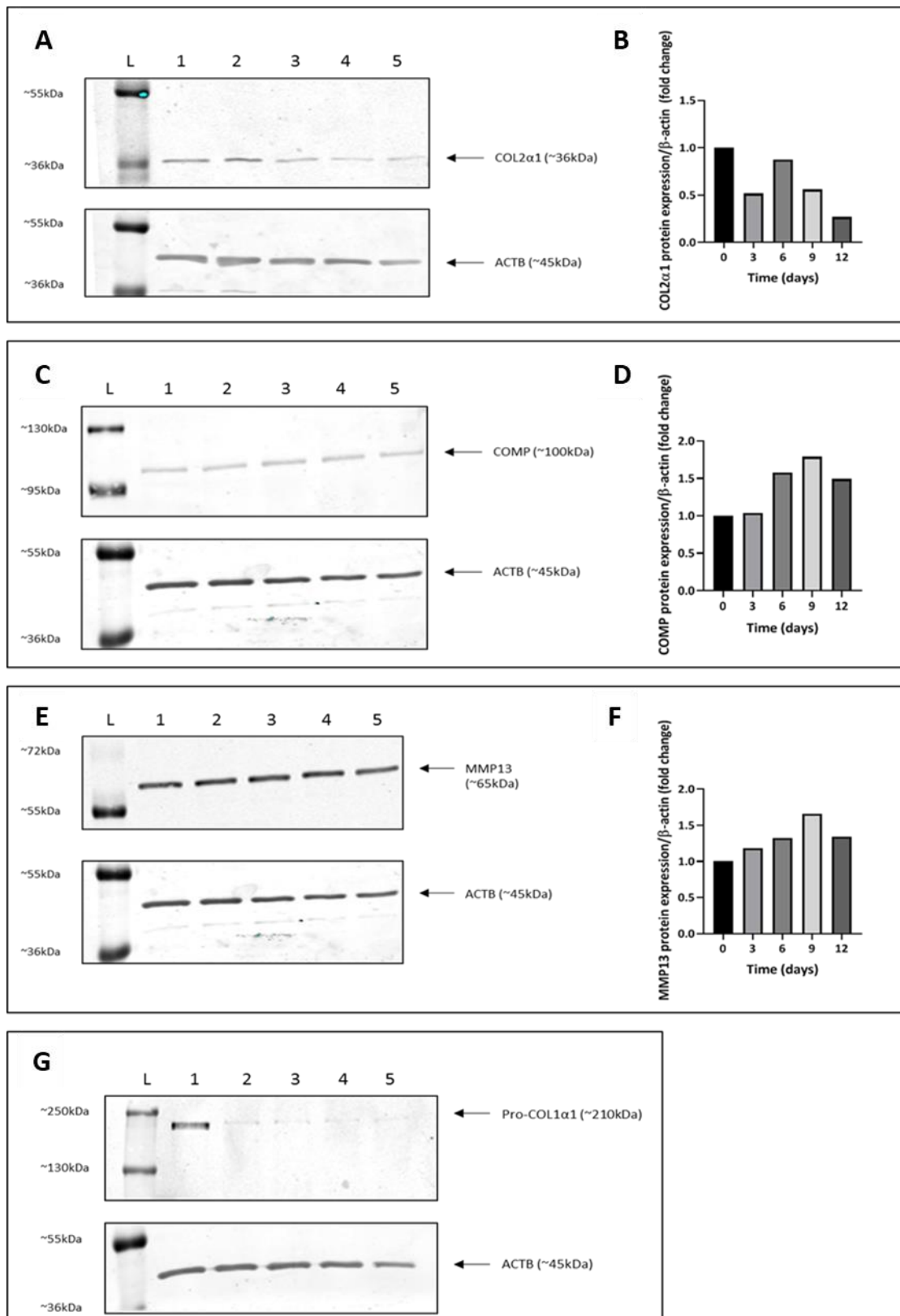


**Figure 3.8.** 2D culture of C-28/I2 over 12 days cells is associated with a reduction in expression of proteins associated with the chondrocyte phenotype. C-28/I2 cells were cultured from 0 to 12 days and expression of chondrocyte associated genes were determined via immunoblotting (A) COL2 $\alpha$ 1 immunoblot, (B) COL2 $\alpha$ 1 quantification (C) COMP immunoblot, (D) COMP quantification, (E) MMP13 immunoblot (F) MMP13 quantification and (G) COL1 $\alpha$ 1 immunoblot. Lanes: (L) = ladder, (1) = day 0, (2) =

day 3, (3) = day 6, (4) = day 9, (5) = day 12. Immunoblotting was performed in triplicate and normalised to  $\beta$ -actin expression. Densitometry was performed on the representative images shown.

#### **3.4.4. Characterization of SaOS-2 cells**

It was previously determined that primary cells would not be suitable for the development of a novel 3D *in vitro* model, therefore an osteoblast counterpart must be selected. SaOS-2 cells were chosen as these cells have been shown to express a variety of osteoblast-related genes such as *COL1A1*, *ALPL* and *BGLAP* as well as their protein counterparts. Additionally, these cells have been shown to produce a mineralized matrix under 2D *in vitro* conditions. Typically, it is recommended that SaOS-2 cells are cultured in McCoy's 5A medium, however, future co-culture experiments necessitate the use of DMEM F-12 GlutaMAX as required by C-28/I2 cells. SaOS-2 cells were grown in both DMEM F-12 GlutaMAX media and McCoy's 5A media to assess suitability of growth conditions (**Figure. 3.9**) This was performed over a 7-day time course, and it was observed that SaOS-2 cells were able to successfully grow in both types of media with no observable differences between conditions. SaOS-2 cells must be able to both grow and express the osteoblast phenotype in DMEM F-12 GlutaMAX if they are to be included in a co-culture *in vitro* model of OA therefore this was assessed over a 12-day time course under osteogenic conditions.

##### **3.4.4.1. Morphology of SaOS-2 cells over a 12-day time course**

Initially SaOS-2 Following from this SaOS-2 cells were grown over a 12-day time course in DMEM F-12 GlutaMAX osteogenic media to determine expression of osteoblast associated genes and proteins. Light microscopy images show that SaOS-2 cells can be effectively cultured in DMEM F-12 GlutaMAX differentiation media forming a dense, adherent monolayer with cells changing from an initial polygonal shape to a more elongated morphology (**Figure 3.10**).

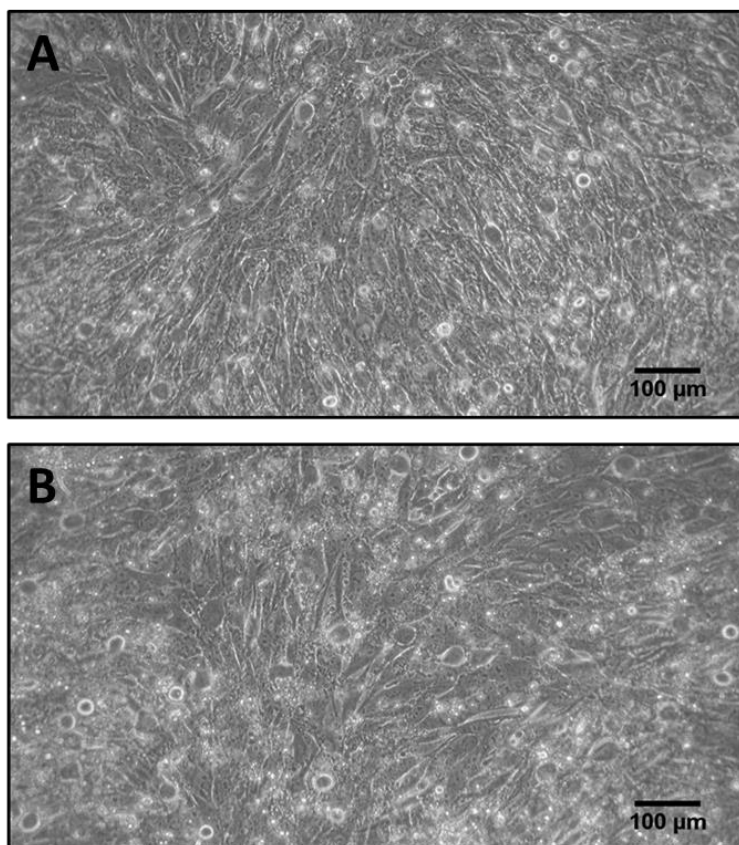


**Figure 3.9. The effect of growth media on SaOS-2 morphology.** SaOS-2 cells were grown over 7 days comparing DMEM F-12 GlutaMAX and McCoy's 5a Media. SaOS-2 cells were grown for 7 days in either (A) DMEM F-12 GlutaMAX growth media or (B) McCoy's 5a growth media and imaged via light microscopy. Images were taken at 10X magnification, and the scale bar represents 100µm.

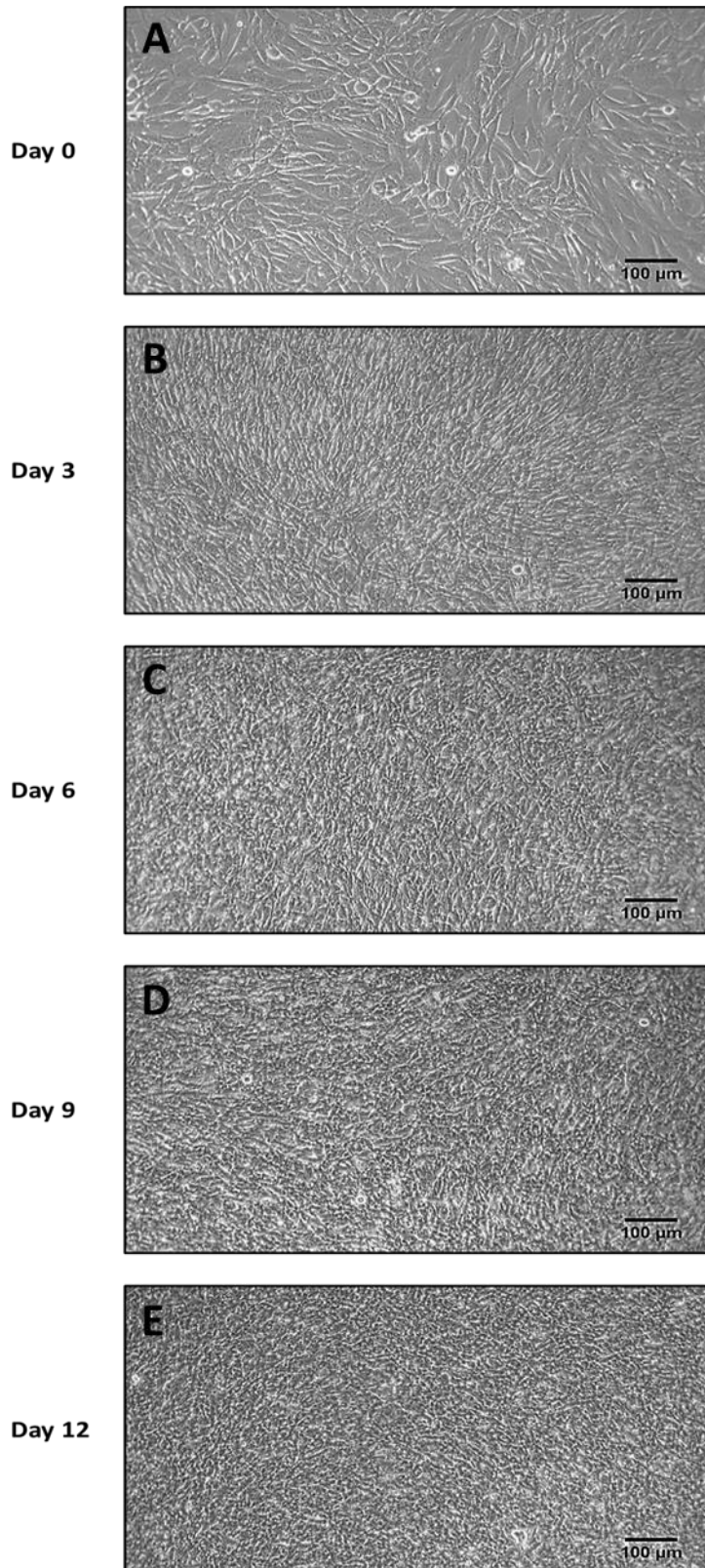


**Figure 3.10. The effect of sustained 2D culture on SaOS-2 cell morphology.** (A) Cells were grown to confluence (Day 0) in DMEM F-12 GlutaMAX growth media. Once confluent cells were subsequently cultured in DMEM F-12 GlutaMAX osteogenic media and grown for up to 12 days (B-E). Images were taken at 10X magnification, and the scale bar represents 100μm.

#### 3.4.4.2. Analysis of osteoblast-associated gene expression over a 12-day time course

To determine the genetic expression of osteoblast maturation and bone matrix production markers over a 12-day time course, SaOS-2 cells were grown in a differentiation growth medium, and RNA was extracted for qPCR analysis at time points 0 (untreated), 3, 6, 9 and 12 days. Target genes were those associated with bone matrix production, mineralisation, and osteoblast maturation.

Firstly, a geNorm analysis was performed to ensure the appropriate reference genes were used for normalization (**Figure 3.11**). GeNorm analysis indicated that the appropriate reference genes for analysis were *TOP1* and *ATP5B* as determined by geNorm M and V values. Therefore, the geometric mean of the expression of these two reference genes was used in calculations when analyzing qPCR output data for SaOS-2 cells.

Following geNorm analysis, the determination of target gene expression was investigated (**Figure 3.12**). Expression of *COL1A1* increased from day 0 to day 6 ( $p < 0.05$ ) with no other differences observed between any other time points (**Figure 3.12A**). *ALPL* remained stable over 12 days with no significant changes in mRNA expression (**Figure 3.12B**). *PDPN* expression showed an increase when comparing day 0 to days 6, 9 and 12 ( $P < 0.001$ ; **Figure 3.12C**) as well as when comparing day 3 to days 6, 9 and 12 ( $P < 0.05$ ; **Figure 3.12C**). Similarly, *BGLAP* expression was seen to increase when comparing day 0 to days 6, 9 and 12 ( $P < 0.001$ ; **Figure 3.12D**) with days 6 and 9 showing significantly higher expression than day 3 ( $P < 0.05$ ; **Figure 3.12D**). Finally, *POSTN* expression was increased when comparing days 0 to days 9 and 12 ( $P < 0.001$ ) with days 9 and 12 showing increased expression over days 3 ( $P < 0.05$ ) and 6 ( $P < 0.05$ ) (**Figure 3.12E**). Over time, critical matrix markers such as *COL1A1* as well as *BGLAP* and *POSTN* are being upregulated alongside the osteoblast maturation marker *PDPN* whilst *ALPL* expression remains stable suggesting these cells are differentiating as expected.

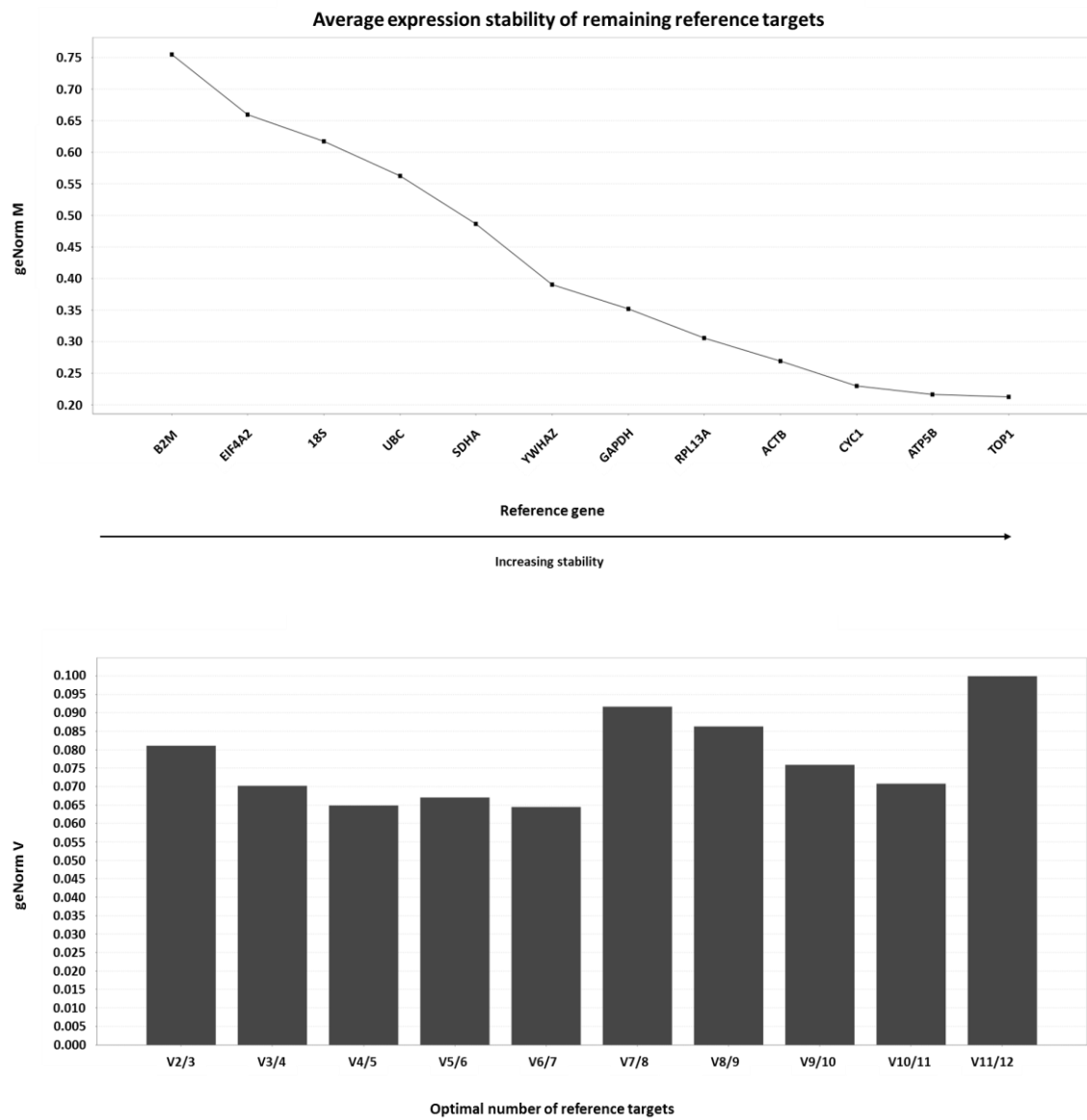


**Figure 3.11. 2D culture of SaOS-2 cells in differentiation media alters housekeeping gene expression.** GeNorm analysis of RNA harvested from SaOS-2 cells over a 12-day time course in differentiation media. (A) geNorm M highlights the average expression stability value (M) of reference genes at each step during stepwise exclusion of the least stably expressed reference gene, with stability increasing from left to right. (B) geNorm V indicates the number of reference genes required for reliable analysis of qPCR data. The optimal number of gene Values <0.15 are considered stable (i.e., V2/3 <0.15 therefore using 3 reference genes instead of 2 will not impact analysis). Data are from a dataset of n=3.

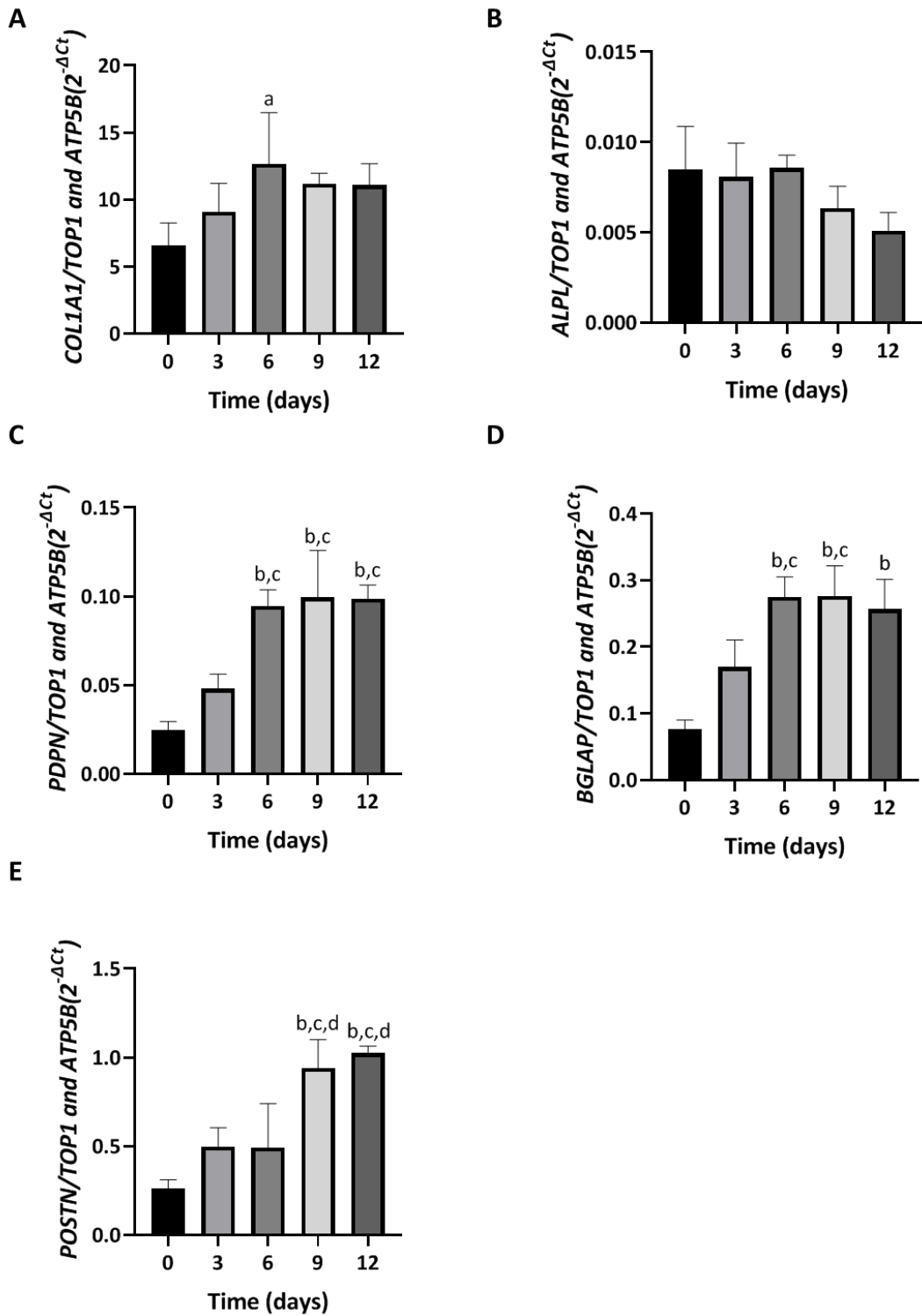


**Figure 3.12. 2D culture of SaOS-2 cells over 12 days is associated with an increase in gene expression associated with osteoblast maturation and mineral deposition.** SaOS-2 cells were cultured from 0 to 12 days in differentiation media. RNA was harvested and RT-qPCR performed to determine expression of genes associated with the osteoblast maturation and ECM production. Data is presented as 2<sup>-ΔCt</sup> mean values ± SEM showing normalized changes in expression of target genes over n=3 replicates. (A) COL1A1, (B) ALPL, (C) PDPN, (D) BGLAP, (E) POSTN. Differences between conditions are denoted by a = compared

to day 0 ( $P < 0.05$ ), b = compared to day 0 ( $P < 0.001$ ), c = compared to day 3 ( $P < 0.05$ ) and d = compared to day 6 ( $P < 0.05$ ).

#### **3.4.4.3. Analysis of osteoblast-associated protein expression over a 12-day time course**

Following the determination of gene expression, immunoblotting was performed to determine the expression of target proteins associated with osteoblastic maturation and bone ECM production over a 12-day time course (**Figure 3.13**). COL1 $\alpha$ 1 immunoblotting shows clear processing of the protein from its pro- to its active form with COL1 $\alpha$ 1 being observed by day 6 (**Figure 3.13A** compare lanes 1 and 2 to lane 3 & **Figure 3.13B**), expression then increases by day 9 (**Figure 3.13A** compare lane 3 to 4 & **Figure 3.13B**) and reduces slightly at day 12 (**Figure 3.13A** lane 5 & **Figure 3.13B**). AP-TNAP can be observed across all time points with expression slightly increasing in a time-dependent manner (**Figure 3.13C** lanes 1-5 & **Figure 3.13D**). Finally, podoplanin expression was detectable from day 0 with expression increasing until day 6 (**Figure 3.13E** lanes 1-3 & **Figure 3.13F**), slightly decreasing by day 9 (**Figure 3.13E** lane 4 & **Figure 3.13F**) and increasing again by day 12 (**Figure 3.13E** lane 5 & **Figure 3.13F**).

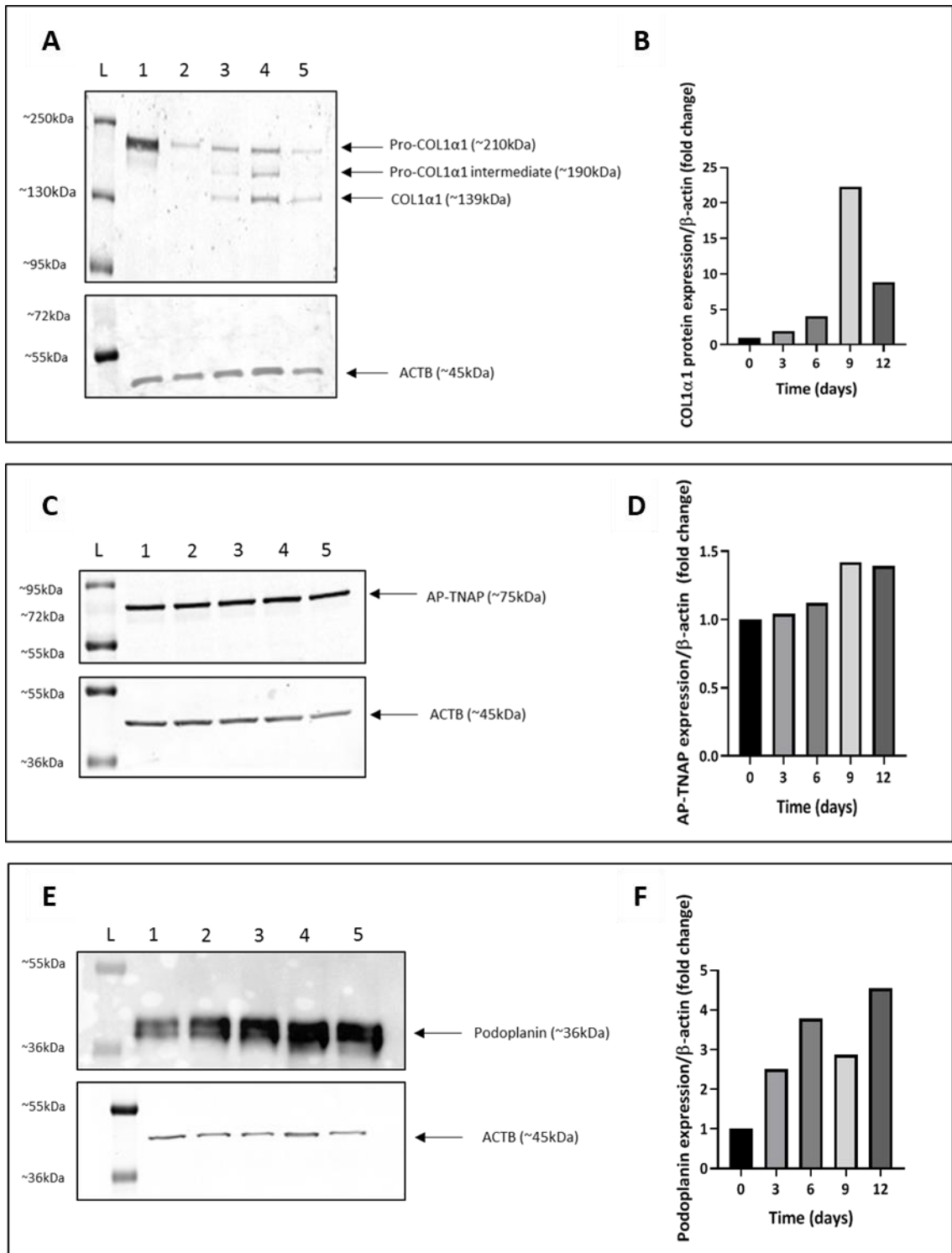


**Figure 3.13. 2D culture of SaOS-2 cells over 12 days is associated with an increase in protein expression associated with osteoblast maturation and mineral deposition.** SaOS-2 cells were cultured from 0 to 12 days in differentiation media. Protein was harvested and immunoblotting performed to determine expression of genes associated with the osteoblast maturation and ECM production. (A) COL1 $\alpha$ 1 immunoblot, (B) COL1 $\alpha$ 1 quantification (C) AP-TNAP immunoblot, (D) AP-TNAP quantification, (E) Podoplanin immunoblot (F) Podoplanin quantification. Lanes: (L) = ladder, (1) = day 0, (2) = day 3, (3) = day 6, (4) = day 9, (5) = day 12. Blotting was performed in triplicate and quantification was performed

relative to  $\beta$ -actin expression. Densitometry was performed on one replicate representative of the dataset.

### 3.5. Discussion

The aim of this chapter was to determine the suitability of chondrocyte and osteoblast cell lines for use in a 3D *in vitro* model of OA. This was achieved by determining the expression of key cellular and ECM genes and proteins in 2D culture.

The use of primary cells as a model cell system is considered the gold standard for *in vitro* models. This is due to primary cells being derived directly from *in vivo* conditions thus most reliably reflecting the *in vivo* physiologic or pathologic environment. However, here it was shown that culture of PHCs in monolayer conditions results in a change in PHC morphology with cells shifting from a typical polygonal chondrocyte shape to a spindle-like fibroblast shape, suggestive of de-differentiation. Additionally, it was observed that PHCs have slow growth rates. These findings are consistent with published literature regarding the monolayer culture of PHCs where it has been highlighted that de-differentiation can be induced via low-density plating and monolayer culture, with cell sub-culture exacerbating the severity of the de-differentiation [288, 289]. For these reasons, it was determined that PHCs were not suitable for the development of the 3D *in vitro* model.

Immortalised cell lines were then considered for use with the human chondrocyte cell line C-28/I2 investigated as a potential candidate for the chondrocytes. First, it was necessary to optimize the culture conditions for these cells. Previous research has reported that growing these cells in the absence of serum but in the presence of insulin-containing supplements can boost the chondrocyte phenotype [278, 279]. However, it is important to note that serum starvation can induce apoptosis and cell detachment which is not ideal for the osteoblast co-culture [290, 291].

Light microscopy revealed that C-28/I2 cells grown in serum-free conditions begin to exhibit signs of potential detachment and apoptosis. Further analysis of gene expression highlights a catabolic effect of serum starvation on the chondrocyte phenotype, exemplified by the reduction in *ACAN*, and an increase in the expression of *COL10A1* and *MMP13*. Previous studies suggest that serum has no effect on the expression of *ACAN* in monolayer culture, however, both studies were performed using end-point PCR and

a semi-quantitative form of end-point PCR [278, 279]. The current study uses the more sensitive RT-qPCR method, which may highlight small changes in gene expression that are not detectable using end-point PCR. Results presented in this chapter show for the first time that serum starvation induces the expression of *COL10A1*, contrary to findings that serum starvation should preserve the C28/I2 chondrocyte phenotype [279]. Notably, overall expression of *COL10A1* was low, a finding seen in other immortalized chondrocyte cell lines [292]. Expression of COL10 $\alpha$ 1 protein could not be detected in C-28/I2 cells suggesting these cells are not undergoing hypertrophy, which is consistent with the very low, but detectable, levels of the *COL10A1* gene in this study. Similarly, this is the first report of the effects of serum on the expression of *MMP13* by C-28/I2 cells, however, studies using high-density monolayers of primary cells have shown that the induction of *MMP13* via IL-1 $\beta$  is exacerbated under serum-free conditions [293]. *MMP13* immunoblotting suggested that serum condition slightly decreased expression of this protein, indicating serum starvation is not optimal for *MMP13* production.

In the current study, no significant change was detected in *COL2A1*, *COMP* or *COL1A1* expression. Immunoblotting revealed that the expression of COL2 $\alpha$ 1 and COMP proteins did not differ when comparing media with and without serum. Expression of *COL2A1* was previously shown to be induced by serum starvation [278], however once again, the methods used were less sensitive than the methods employed in this study. Previous research shows immunoblotting for Col2 $\alpha$ 1 expression is achievable, but available studies do not consider the comparison between serum conditions [294] Additionally, the cells used in the current study were at a low passage number (P4-P6) which may have preserved the chondrocyte phenotype. Previous key studies do not detail the passage number used, a factor which is critical in chondrocyte de-differentiation and phenotype retention [230, 295]. This is the first study to consider COMP mRNA and protein expression in the C-28/I2 cell line with results suggesting that expression of both markers is not impacted by serum starvation; COMP gene and protein markers may not be as labile as *COL2A1*, therefore its expression may not be impacted by the presence of serum. Expression of *COL1A1* was also stable when comparing serum conditions, suggesting the absence of serum may have no impact on de-differentiation under the conditions tested.

It was determined that growing cells in the presence of serum did not affect C-28/I2 expression of key chondrocyte markers and that in some cases serum deprivation was not optimal. Therefore, for the purpose of ongoing model development, it was considered that serum starvation was not necessary and would not need to be incorporated. This is beneficial as osteoblast lines have been shown to become more apoptotic under serum-free conditions [296].

The next stage in determining the suitability of C-28/I2 cells to be included in a 3D *in vitro* model of OA was to investigate their ability to grow and maintain the chondrocyte phenotype under osteogenic conditions; a reliable model of OA would require C-28/I2 cells to share a culture environment with osteoblasts undergoing differentiation over a 12-day time course. Research performed in this study is the first to monitor C-28/I2 cells over a 12-day time course in osteogenic media containing ascorbic acid and beta-glycerophosphate. Chondrocytes require ascorbic acid to produce collagens and proteoglycans *in vivo* and *in vitro* therefore, the innocuous effects of this molecule are to be expected [276, 279]. Beta-glycerophosphate acts as a source of inorganic phosphate and has been shown to promote chondrocyte hypertrophy and subsequently mineralization as seen in the ATDC5 murine chondrocyte line [297]. In human chondrocytes, it has been shown that  $\beta$ -glycerophosphate results in increased collagen type X synthesis and mineralization only when applied directly to chondrocytes that are already hypertrophic [298]. This may eventually result in mineralisation-associated apoptosis, however, C-28/I2 cells appeared to tolerate the presence of  $\beta$ -GP with no observable signs of mineralization.

Analysis of gene expression showed that expression of all target genes was altered over the 12-day period. *ACAN* expression was seen to initially decrease before returning to baseline levels, and this may be due to a slight loss of phenotype through prolonged monolayer culture which was then recovered via the addition of L-ascorbic acid which has been shown to have chondrogenic effects in ATDC5 cells [299]. A similar pattern was observed *COMP* and *COL10A1* genes. *COMP* protein expression increases between days 0 and 9 and slightly decrease between days 9 and 12. *COMP* has been shown to aid in the regulation of chondrocyte proliferation and collagen fibril assembly therefore its increase over time in culture may be indicative of chondrogenesis and cartilaginous matrix synthesis [300, 301]

Expression of *COL2A1* and *COL1A1* genes were both found to significantly decrease when comparing day 0 to days 6, 9 and 12. Decreasing levels of *COL2A1* is consistent with previous research that suggests monolayer culture can reduce expression of the labile *COL2A1*; here no recovery of expression is observed within the time course [278]. Protein analysis revealed COL2 $\alpha$ 1 expression fluctuated across the twelve-day time course. Between day 0 and day 3 COL2 $\alpha$ 1 expression dropped. This was then increased again between days 3 and 6, dropping off again over days 9 and 12. The initial drop in COL2 $\alpha$ 1 expression may be due to an intolerance for monolayer growth, with COL2 $\alpha$ 1 expression being recovered following the application of ascorbate [299]. Overall reduction in the expression of COL2 $\alpha$ 1 may be due to prolonged monolayer culture resulting in a significant reduction of expression of the labile *COL2A1*. Reduction in *COL1A1* expression over the time course suggests that C-28/12 cells are suited to culture under these conditions as *COL1A1* is a common marker for de-differentiation. Expression of the COL1 $\alpha$ 1 protein could not be detected; only the precursor pro-collagen molecule could be seen at day 0. Studies have shown that monolayer culture results in a shift from type II collagen to type I collagen expression however work regarding this have been performed under the influence of IL-1 $\beta$  [276, 302]. Therefore, COL1 $\alpha$ 1 expression may be dependent on a synergistic effect of IL-1 $\beta$  and monolayer conditions with the current conditions being insufficient for COL1 $\alpha$ 1 induction as corroborated by *COL1A1* expression patterns. Expression of *MMP13* did not significantly change over the time course. This may be due to *MMP13* being a stably expressed gene; studies have shown that IL-1 $\beta$  stimulation of PHCs results in increased levels of *MMP13* mRNA, however, this effect is not detectable in immortalized lines including C-28/12 cells [272, 293]. *MMP13* protein expression increased in a time-dependent manner between days 0 and 9, with both markers slightly dropping off between days 9 and 12. This pattern of expression for *MMP13* is concurrent with that found in micromass-cultured ATDC5 cells [299].

Together, these results suggest that C-28/12 cells can grow under osteogenic conditions with serum, whilst maintaining their chondrocyte phenotype. They also suggest that an early culture time point (e.g., day 3) is most representative of the articular cartilage chondrocytes. The purpose of the novel 3D model development is to provide a means by which subchondral bone (SCB) and articular cartilage (AC) crosstalk may be

investigated. Therefore, the findings presented here are crucial as model development is dependent on incorporating a reliable cell model of the articular cartilage chondrocyte, which is characterised by expression of collagen type II and aggrecan, whereas chondrocytes expressing markers such as collagen type X are restricted to the deep zones of the articular cartilage and calcified cartilage (CC). If future co-culture experiments aimed to consider interactions between the CC and SCB then incorporating C-28/I2 cells cultured for 12 days may be more appropriate due to downregulation in type II collagen expression, as well as increases in expression of the catabolic MMP13 protein [102].

Following the characterisation of a representative chondrocyte cell line, this study set out to find a suitable osteoblast cell type to be included in the development of the 3D *in vitro* model of OA. Due to the drawbacks encountered when working with PHCs, it was decided that the use of an osteoblast cell line would be appropriate, with the human osteosarcoma SaOS-2 cell line being screened as a candidate.

SaOS-2 cells are typically grown in McCoy's 5A media, however, for co-culture purposes, these cells must tolerate culture in DMEM F-12 GlutaMAX media, therefore it was first shown that SaOS-2 cells were able to tolerate culture in DMEM F-12 GlutaMAX media. Subsequently, SaOS-2 cells were grown in osteogenic media over a 12-day time course, in identical conditions to those examined in the C-28/I2 time course. SaOS-2 cells tolerated these conditions well, growing continuously forming dense monolayers with observably low levels of cell death. This is to be expected as these cells are commonly grown under such conditions with ascorbic acid and  $\beta$ -GP acting as promoters of the osteogenic phenotype in a variety of studies [283, 303–305].

Notably, overall expression of COL1A1 mRNA was consistently high throughout the time course. Results indicated that SaOS-2 COL1A1 expression increased between days 0 and 6, with no differences between any other time points; this dataset followed a similar trend to findings in published literature [283]. This was corroborated by immunoblotting in which three clear distinct bands were observed, indicative of pro-collagen to active collagen processing and COL1 $\alpha$ 1 increased over the time course with expression peaking at day 9. ALPL mRNA expression was consistent throughout the time course with no significant changes detected, this is consistent with previous findings that suggest ALPL expression is relatively stable [306]. Increases in AP-TNAP protein expression were

however observed and this may be due to the need for alkaline phosphatase to aid in the provision of inorganic phosphate for mineral deposition. For the first time, the expression of PDPN in SaOS-2 cells was examined. PDPN mRNA significantly increased by day 6 of culture and this was maintained throughout the time course. Concomitant increases were seen in podoplanin protein expression. These results indicate that SaOS-2 cells are undergoing the process of maturation towards a differentiated osteocyte-like phenotype [286]. Expression of BGLAP in the SaOS-2 line was also increased over the time course. Literature has shown that BGLAP expression is detectable in SaOS-2 cells, however, there has been little consideration for a time course of expression of this gene. BGLAP has a variety of functions related to the regulation of biomineralization, notably it has strong calcium-binding properties with an affinity for hydroxyapatite [62]. It has been highlighted that SaOS-2 cells express BGLAP even at the early stages of cell culture experiments, therefore its increase with time under osteogenic conditions is not necessarily surprising [271]. Expression of POSTN was also seen to be significantly higher. Whilst this is the first study to investigate POSTN expression in SaOS-2 cells, it is logical to deduce that increased expression of POSTN under osteogenic conditions is to be expected as previous studies have shown that the periostin protein plays a key role in processes such as collagen fibrillogenesis, cross-linking and incorporation of the pro-osteogenic tenascin-C into the organic matrix [21, 22].

The overall analysis of SaOS-2 cells cultured over a 12-day time course in osteogenic media suggests that these cells do not only tolerate the culture conditions tested but begin to undergo differentiation. This process is indicated by a time-dependent increase and drop-off of collagen type I protein expression, as well as time-dependent increases in BGLAP, POSTN and podoplanin, markers associated with matrix deposition, mineralization, and osteoblast maturation. Considering these findings, future experiments should involve culturing SaOS-2 osteoblasts for 9 days to achieve optimal expression of target markers to be considered in an *in vitro* model of OA.

Taken altogether, the results reported in this chapter suggest that primary human cells are not appropriate for use in the development of a novel 3D *in vitro* model of osteoarthritis and that cell lines should be used as a cost-effective alternative. This chapter also effectively demonstrates that C-28/12 cells do not need to be serum starved to achieve expression of chondrocyte-associated genes and proteins. Additionally, it has

been shown that osteogenic media also does not have a negative impact on the expression of these target genes and proteins. SaOS-2 cells were cultured in osteogenic conditions identical to C-28/I2 cells and not only did these cells proliferate under these conditions, but they also expressed a variety of osteoblast-associated genes and proteins and began to take on a profile of a mature osteoblast undergoing further differentiation. Further, SaOS-2 cells must be cultured for 9 days to allow for optimal marker detection, whereas C-28/I2 cells express most target genes and proteins at day 3 (~2 days monolayer culture). These findings will directly inform the optimal culture conditions and timings for C-28/I2 and SaOS-2 cells embedded within hydrogels for the development of a 3D model of OA.

## Chapter 4: The impact of hydrogel encapsulation on C-28/I2 chondrogenic and SaOS-2 osteoblastic cell lines

### 4.1. Introduction

To establish a three-dimensional (3D) model of osteoarthritis (OA), a suitable 3D cell culture system must be selected. A variety of 3D systems are commercially available, many of which have been shown to maintain the *in vivo* phenotype of chondrocyte cell cultures to a higher degree than their two-dimensional (2D) counterparts [240–242, 249, 250, 261, 307]. Similarly, many 3D models exist that promote the osteogenic phenotype with some showing promise beyond their 2D counterpart [238, 256]. Many systems have shown suitable properties for both chondrocyte and osteoblast culture, however, hydrogel-based culture methods have been a key focus of recent research, particularly with the increasing prevalence of bioink production [308, 309]

Hydrogel systems provide a platform with tuneable micro-environment characteristics that may be adjusted to alter matrix elasticity, polarity, pore size and pore interconnectivity; factors important for cell fate and phenotype [237]. Additionally, hydrogels are comprised of a water/polymer biphasic construct that is like the extracellular matrix (ECM) found in many tissues [310]. Hydrogels can broadly be broken down into two categories, biological and synthetic.

Biological hydrogel systems are derived from known natural systems such as alginate, gelatin and chitosan and exhibit suitable characteristics for cell culture including biocompatibility, modifiability, as well as support for chondrogenic and osteogenic activity [240–242]. However, due to the biological nature of these systems, they may suffer from batch-to-batch variability as no single biological source will be the same, which may impact the properties of the gel. To overcome this problem, research groups and commercial entities have worked toward the development of synthetic hydrogel systems.

Like biological hydrogels, synthetic hydrogel systems display desirable features for tissue culture but are not derived from a finite source. Synthetic hydrogel systems are reproducibly manufactured polymer/water constructs that have been shown to support chondrogenesis including the induction of higher levels of collagenous and non-

collagenous matrix proteins such as collagen type II and osteocalcin compared to typical 2D monolayer culture [249, 250]. They have also shown beneficial chemical modification capabilities, for example through the inclusion of chondrogenic molecules such as TGF- $\beta$  in Poly (ethylene glycol) (PEG) hydrogel systems [251]. Notably, synthetic hydrogel systems have already shown promise in a co-culture model using bone marrow stem cells (BMSCs) encapsulated in a chondrocyte laden PEG hydrogel which resulted in the production of distinct cartilaginous cartilage and calcified bone like tissues producing an interface that is a mimic of the subchondral bone (SCB) – articular cartilage (AC) interface found within the articular joint, the site of OA development [251].

Biogelx hydrogel products (Biogelx Ltd, UK) are reproducible hydrogel cell culture systems that yield the qualities expected of synthetic hydrogels using a technology that is simple to handle. The products are derived from self-assembling Fmoc-diphenylalanine (Fmoc-FF) gelator peptides that form nanoscale fibres via non-covalent interactions. These Fmoc-FF peptides are combined with a Fmoc-serine (Fmoc-S) surfactant peptide that engages in cooperative assembly with Fmoc-FF forming a nanoscale fibre with a polar surface. These fibres are then cross-linked via the coordination of divalent  $\text{Ca}^{2+}$  ions forming a nanoscale fibre network that arranges itself via  $\pi$ - $\pi$  stacking interactions resulting in an interlocked  $\beta$ -sheet architecture [265, 267, 268]. Biogelx hydrogels have shown promise in promoting the survivability and functionality of hepatocytes including upregulation of P450 enzyme gene expression [311], as well as pericyte differentiation using stiffness alone as a substrate, allowing for the derivation of cells expressing a variety of markers including SOX-9 and RUNX-2 markers of chondrogenesis and osteogenesis respectively [265]. Additionally, Biogelx hydrogel systems allow for further microenvironment manipulation via the incorporation of functional groups that mimic properties of the native cellular environment such as fibronectin (RGD), collagen (GFOGER) and laminin (IKVAV) which may promote cellular adhesion [269].

Due to the favourable characteristics of Biogelx hydrogels detailed in publications thus far, as well as their ease of handling, customizable properties, and commercial availability, it is considered that Biogelx hydrogels may be a suitable environment for the culture of cells relevant to OA, namely the chondrocytes (C-28/I2) and osteoblastic (SaOS-2) cell lines characterised in results Chapter 3. This chapter aims to determine the

suitability of these hydrogel systems for integration into a 3D model of OA by assessing the expression of key chondrocyte and osteoblast markers of C-28/I2 and SaOS-2 cells respectively.

## **4.2. Aims and objectives**

### **4.2.1. Aim**

To determine the effects of hydrogel encapsulation on C-28/I2 chondrocytes and SaOS-2 osteoblasts, including the impact on cell viability and the expression of key cellular markers linked to OA.

### **4.2.2. Objectives**

1. Demonstrate proof of concept for hydrogel culture and the potential for future co-culture models of OA.
2. Optimise the purification of RNA from hydrogel encapsulated C-28/I2 and SaOS-2 cells and perform RT-qPCR, comparing expression of target genes between 2D and 3D culture conditions.
3. Optimise the purification of protein from hydrogel encapsulated C-28/I2 and SaOS-2 cells and perform immunoblotting, comparing expression of target proteins between 2D and 3D culture conditions.
4. Assess the viability of chondrocytes and osteoblast cells cultured in Biogelx functionalised hydrogels.
5. Establish the optimal Biogelx hydrogel culture system to integrate this into a 3D *in vitro* culture model of OA

### **4.3. Methods**

#### **4.3.1. Hydrogel preparation**

Hydrogels were prepared as per section 2.3.

#### **4.3.2. Acellular hydrogel modelling and co-culture suitability**

Biogelx standard high-stiffness hydrogels were prepared as in section 2.3 These were then plated in a variety of cell culture vessels to allow for visual assessment of their physical properties and handling for potential use in a co-culture model. Briefly, pre-gel solutions were plated into a target vessel and incubated for 15 minutes at 37°C. Pre-gel solutions were then cross-linked using cell growth media for 2 hours at 37°C and imaged using a Sony Xperia 5 camera (Sony, Japan). Hydrogel constructs were used to create 3 distinct co-culture models, a vertical co-culture system using 24-well transwell inserts as moulds, a horizontal co-culture system using silicone plugs, and a non-contact cell signalling co-culture system using 24-well transwell plates and inserts.

#### **4.3.3. Cell culture**

Cells were maintained as detailed in section 2.2.1. For RT-qPCR, immunoblotting and immunostaining experiments, C-28/I2 cells cultured in 2D were seeded at a density of  $5 \times 10^5$  cells per well in 6-well culture dishes, and SaOS-2 cells were seeded at a density of  $4.5 \times 10^5$  cells per well in 6-well culture dishes. After 24 hours control cells were harvested (day 0) and remaining cultures were grown in differentiation media ((DMEM)/F12 GlutaMAX, + 10% fetal calf serum (FCS), + 1% penicillin-streptomycin (P/S), + an additional 55mg/L sodium pyruvate + 50µg/mL ascorbic acid and 5mM β-GP) for 3 and 9 days to allow for the induction of matrix related proteins for both C-28/I2 and SaOS-2 respectively. Growth media was changed every 3 days.

#### **4.3.4. Hydrogel encapsulation**

C-28/I2 and SaOS-2 cells were encapsulated as per section 2.4. Briefly, cells were mixed at a density of  $2 \times 10^6$  cells per 100µl of pre-gel solution and pipetted into 96-well plates at 100µl per well and subsequently incubated at 37°C for 30 minutes, crosslinked and

cultured further. After 24 hours (day 0) remaining cultures were grown in differentiation media (as described in section 2.2.1.). Media was replenished every 3 days for the duration of each experiment unless otherwise stated.

#### **4.3.5. RNA extraction**

RNA was extracted using a variety of methods and at different time points. The effect of gel volume on RNA yield was first analysed using a standard RNeasy kit method on SaOS-2 cells encapsulated for 24 hours. Subsequently, a variety of RNA extraction methods were compared on encapsulated SaOS-2 cells after 24 hours in 3D culture. Following the determination of a suitable RNA extraction method SaOS-2 cells were encapsulated for several days as determined by the outcome of Chapter 3; this would ensure cells could be cultured for long enough in 3D to permit expression of key SaOS-2 ECM markers such as collagen type I. RNA extraction methods tested are listed below.

##### **4.3.5.1. RNeasy kit extraction (also used as a method for testing different gel volumes)**

2D cultured cells were washed twice with 3mL ice-cold PBS, scraped in 1mL ice-cold PBS, and aspirated into 1.5mL microcentrifuge tubes. Cell aspirates were then spun at 800g to generate a cell pellet, supernatants were removed, and cell pellets were lysed in 350 $\mu$ l of RLT buffer containing 0.01%  $\beta$ -mercaptoethanol. 3D culture constructs were washed twice with 3mL ice-cold PBS and directly lysed in 350 $\mu$ l of RLT buffer containing 0.01%  $\beta$ -mercaptoethanol and vortexed vigorously for 30 seconds (or until construct entirely dissolved in solution). 3D construct lysates were centrifuged at full speed for 3 minutes and supernatants were transferred to new 1.5mL microcentrifuge tubes. At this stage, both 2D and 3D constructs were handled in the same manner.

One volume of 70% ethanol was added to each lysate and mixed via pipetting, the total volume was then transferred to a RNeasy spin column placed in a 2mL collection tube which was centrifuged at 8000g for 15 seconds, flow through was then discarded (if lysate + ethanol mix exceeds 700 $\mu$ L run samples through columns up to 700 $\mu$ l at a time until the entire sample has been passed through the column). Columns were washed via the addition of 700 $\mu$ L of buffer RW1 and centrifugation at 8000g for 15 seconds.

Subsequently, column membranes were washed, and 500 $\mu$ L of buffer RPE (containing 20% ethanol) was added to each column which was centrifuged at 8000g for 15 seconds, a subsequent second membrane wash was performed with an 8000g 2-minute centrifugation which also ensured membranes were dried and to prevent ethanol carryover. Spin columns were removed from collection tubes and placed into a new 2mL collection tube and centrifuged at 16000g for 1 minute to ensure complete removal of ethanol contaminants. Finally, the column was placed in a new 1.5mL collection tube and RNA was eluted, 30 $\mu$ L of RNase-free water was added to each column followed by centrifugation at 8000g for 1 minute. This final step was repeated using the sample eluates to increase RNA yields. Samples were then quantified using the NanoDrop 2000 (Thermo Scientific) and stored at -80°C until required.

#### **4.3.5.2. Standard Trizol extraction**

2D cultured cells were washed twice with 3mL ice-cold PBS and scraped on ice in 1mL Trizol. Lysates were then kept on ice until 3D supernatants were collected. 3D culture constructs were submerged in 1mL trizol and vortexed vigorously for 30 seconds (or until the construct was entirely dissolved in solution). Solutions were then centrifuged at 12,000xg for 10 minutes to remove any insoluble material, supernatants were then transferred to a fresh tube. At this stage, 2D and 3D solutions were handled in the same manner. 200 $\mu$ l of chloroform was added to each sample, mixed via vigorous shaking for 5-10 seconds and incubated at room temperature for 15 minutes. Samples were then centrifuged at 12,000xg for 10 minutes at a temperature of 4°C to facilitate phase separation. The aqueous phase was then transferred to a fresh tube. 500 $\mu$ l of isopropanol was added to the aqueous phase and samples were vortexed for 10 seconds and incubated at room temperature for 10 minutes. RNA was then precipitated via centrifugation at 12,000g for 8 minutes at 4°C, supernatants were carefully removed and 1mL of 75% ethanol was added to the RNA pellet, which was then centrifuged at 7,500g for 5 minutes to remove the ethanol and pellets were then air dried for 5 minutes. The resultant precipitate was re-suspended in 100 $\mu$ l of Rnase-free water and stored at -80°C until required for analysis. RNA concentration, 260/280 and 260/230 values were determined via Nanodrop measurement.

#### **4.3.5.3. Trizol + RNeasy kit extraction**

2D cultured cells were washed twice with 3mL of ice-cold PBS and scraped on ice in 1mL of ice-cold Trizol. 3D cultured constructs were submerged in 1mL of ice-cold trizol and vortexed vigorously for 30 seconds (or until the construct was entirely dissolved in solution). Samples were frozen at -80°C until 3 biological replicates for each experimental condition had been harvested, at which point RNA extraction was performed as per section 2.5.1.

#### **4.3.5.4. Alternate Trizol method**

2D cultured cells were washed twice with 3mL ice-cold PBS and scraped on ice in 1mL Trizol. Lysates were then kept on ice until 3D supernatants were collected. 3D culture constructs were submerged in 1mL trizol and vortexed vigorously for 30 seconds (or until the construct was entirely dissolved in solution). 200µl of chloroform was added to each sample, mixed via vigorous shaking for 10-15 seconds and incubated on ice for 5 minutes. Samples were then centrifuged for 12,000g for 15 minutes at 4°C to facilitate phase separation, the upper aqueous phase was collected in a new Eppendorf, mixed with the same volume of isopropanol, and incubated overnight at 4°C. After overnight incubation samples were centrifuged at 12000g for 30 minutes at 4°C to produce an RNA precipitate. Supernatants were discarded and the RNA pellet was washed with 1mL of 75% ethanol and vortexed briefly to detach the pellet. Samples were left on ice for 5 minutes and then centrifuged for 15 minutes at 4°C. Supernatants were then discarded and the pellet was air-dried at room temperature. Subsequently, RNase-free water was added to each tube and pellets were resuspended via gentle pipetting and scraping. Once resuspended pellets were incubated for 10 minutes at 60°C and then stored at -80°C until required for analysis. RNA concentration, 260/280 and 260/230 values were determined via Nanodrop measurement.

#### **4.3.6. cDNA synthesis and RT-qPCR**

cDNA was synthesised as per section 2.5.3 and frozen at -20°C for storage. RT-qPCR was performed on chondrocyte (*ACAN*, *COL10A1*, *COL1A1*, *COL2A1*, *COMP* and *MMP13*) and osteoblast (*ALPL*, *BGLAP*, *COL1A1*, *PDPN* and *POSTN*) target genes. Primer sequences are

detailed in Appendix II. RT-qPCR was performed over 3 biological replicates as detailed in section 2.5.4. Data were normalized to the expression of CYC1 and GAPDH for SaOS-2 and C-28/I2 cell lines respectively. Target gene data were analysed as per section 2.5.6.

#### **4.3.7. Protein extraction and quantification**

2D cell cultures were washed with 3mL ice-cold PBS and scraped on ice in 1mL ice-cold PBS and aspirated. Cell suspensions were then pelleted via centrifugation at 800g for 5 minutes at 4°C and stored at -80°C until required for analysis. Protein was subsequently extracted and quantified as per section 2.5.1. Protein extraction and quantification of 3D encapsulated cells was achieved as per sections 2.5.2 and 2.5.4.

#### **4.3.8. Immunoblotting**

Gel electrophoresis was conducted using Tris-glycine gels prepared by the operator (reagents specified in Appendix I) and immunoblotting was performed as per section 2.6.5. by the operator (reagents specified in Appendix I) with membranes being probed for primary antibodies as detailed in Appendix III. Secondary antibody staining was performed using the Licor Odyssey system. (Section 2.6.5. & Appendix III). The protein of interest expression was then normalized to  $\beta$ -actin expression. Images were quantified as per section 2.6.6. Where possible, 10 $\mu$ g of whole protein lysate from human articular cartilage was loaded as a positive control for chondrocyte immunoblotting.

#### **4.3.9. Cell Tracker staining**

Cell tracker staining was performed as per section 2.9. Cells were cultured in Ibidi 35mm culture-insert 4 well  $\mu$ -dishes. SaOS-2 cells were seeded in monolayer culture or encapsulated in hydrogel as detailed in section 2.4. After 24 hours of incubation at 37°C, 2D and 3D cultures were washed and stained with CellTracker™ Deep Red dye at a working concentration of 1X in growth media. Cultures were then imaged using a Zeiss LSCM 880 (Jena, Germany) and ZEN Black software (Zeiss). Images were then processed using ZEN Blue software (Zeiss).

#### **4.3.10. Immunostaining**

Immunostaining was conducted as per section 2.10. C-28/I2 cells were seeded in monolayer culture in a 6-well plate on top of 22mm coverslips at a density of  $8.3 \times 10^4$  cells in 1mL growth medium, or on top of 300 $\mu$ L acellular hydrogel solution (henceforth referred to as 2.5D). Cells were fixed, permeabilised, blocked and subsequently stained with an F-actin primary antibody. Secondary antibody staining was performed using Alexa Fluor 647 and stained cultures were then mounted on slides with vectashield DAPI mounting medium. Slides were then imaged using a Zeiss LSCM 880 (Jena, Germany) and ZEN Black software (Zeiss). Images were then processed using ZEN Blue software (Zeiss).

#### **4.3.11. Live/Dead staining**

C-28/I2 and SaOS-2 cells were cultured and stained in both 2D and 3D conditions. Live/Dead staining was achieved with the use of Calcein AM and Propidium Iodide respectively. 2D cell cultures were seeded in an Ibidi  $\mu$ -Slide Angiogenesis Glass Bottom microscopy slide at a density of  $1.8 \times 10^4$  in 50 $\mu$ L of growth media per well described in section 4.3.3. 3D cultures were prepared as per sections 2.3 and 2.4. and seeded in an Ibidi  $\mu$ -Slide Angiogenesis Glass Bottom microscopy slides at a volume of 10 $\mu$ L of pre-gel-cell solution per well containing  $2 \times 10^5$  cells. Cultures were processed as per section 2.8.1. Live/dead staining was achieved using calcein AM and propidium iodide solutions which were visualised using 488nm (calcein AM) and 568nm (propidium iodide) channels. Stained cells were imaged via the creation of a 2x2 tile scan of each culture to provide a comprehensive image that was representative of 4 fields of view using a Zeiss LSCM 880 (Jena, Germany) and ZEN Black software (Zeiss).

#### **4.3.12. Image processing and analysis**

Live/dead cell images were produced and captured using a Zeiss LSCM 880 (Jena, Germany) and ZEN Black software (Zeiss). Images were then processed using ZEN Blue software (Zeiss) and cell counts were performed using ImageJ as per section 2.8.2.

#### **4.3.13. Statistical Analysis**

Statistical analysis was performed using GraphPad Prism 9.3.0 (GraphPad Software, USA) as per section 2.11.

## 4.4. Results

### 4.4.1. Acellular three-dimensional constructs

High stiffness acellular Biogelx hydrogel constructs were gelled and cross-linked in a variety of culture vessels and shapes (**Figure 4.1**). Hydrogel constructs were used to create 3 distinct co-culture models, a horizontal co-culture system using silicone plugs, a vertical co-culture system using 24-well transwell inserts as moulds, and a non-contact cell signalling co-culture system using 24-well transwell plates and inserts as detailed by Alsaykhan and Paxton (2020) [312]. All culture methods were deemed suitable as potential co-culture candidates at an early stage. Each gel retained its shape and showed no visual leakage characteristics, allowing for direct assessment of the interface between two individual hydrogel constructs, and assessment of cell signalling via a transwell model.

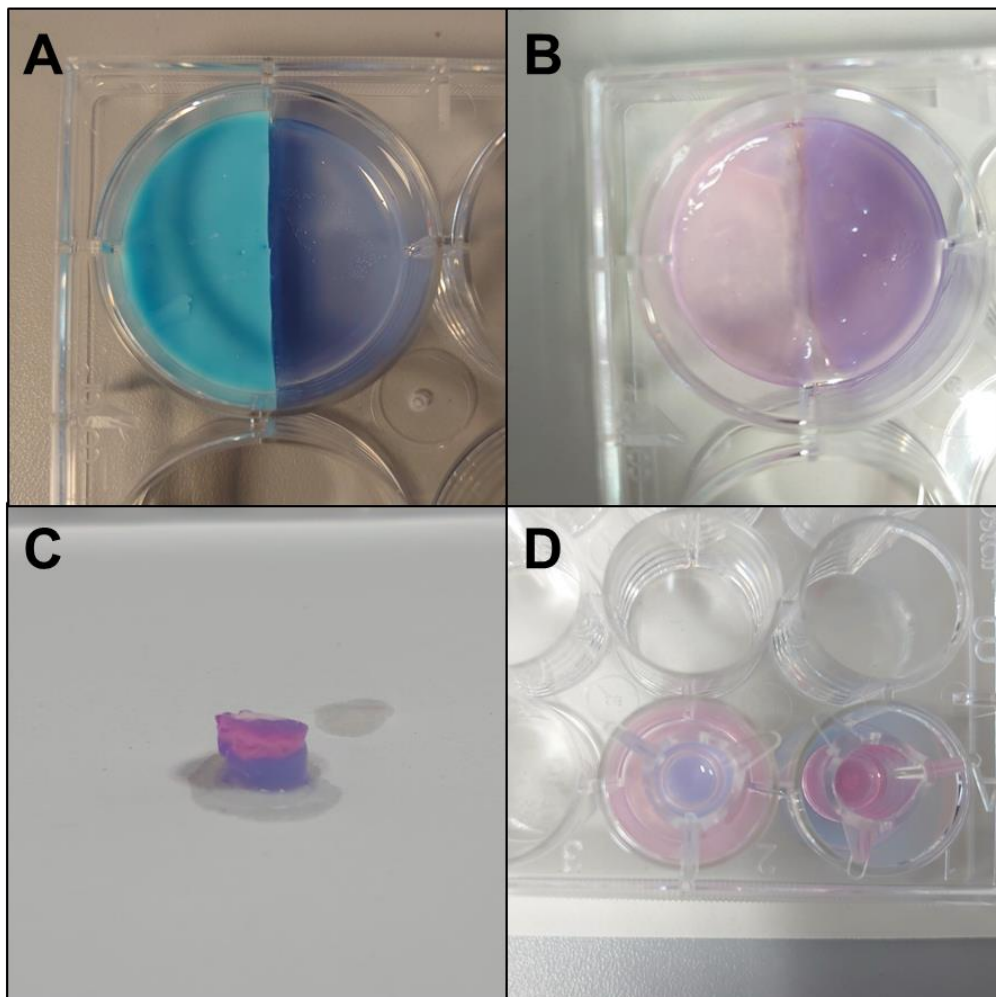


**Figure 4.1.** Co-culture model potential was considered using Biogelx standard high stiffness hydrogels (A-D). Pre-gel solutions were seeded in to (A-B) a 6-well plate with a silicone plug allowing for two halves of the well to be filled with separate hydrogel constructs in direct contact. (C) Pre-gel solutions were

moulded in 24-well transwell culture inserts and then removed and used to create a direct contact vertical gel construct. (D) pre-gel solutions were seeded in to 24-well inserts and suspended above in-well pre-gel solutions to create a non-contact 3D co-culture system.

#### **4.4.2. Optimising RNA extraction from hydrogel encapsulated cells**

A variety of culture and RNA extraction methods were tested to ensure the successful retrieval of workable RNA from cells encapsulated in 3D hydrogel constructs. Hydrogel volume was shown to greatly influence RNA yield (**Figure 4.2**) when using RNeasy Kit extraction methods. Increasing hydrogel construct size whilst keeping cell number consistent drastically decreased the amount of RNA obtained from encapsulated cells. Subsequently, cells were encapsulated in 100 $\mu$ L of hydrogel and different RNA extraction methods were tested upon cell-laden constructs. Standard Trizol extraction methods resulted in minimal RNA retrieval from encapsulated cells. All other methods tested resulted in acceptable RNA yields and 280/260 values; notably, 260/230 values were low for all methods (**Table 4.1-4.3**). The two most efficacious methods (RNeasy Kit and Alternate Trizol) were then taken forward for a time course analysis (**Figure 4.2**). RNA yields dropped considerably over time using both extraction methods, however, the use of the alternate Trizol method resulted in the best RNA yields from cells after 9 days of encapsulated cell culture (**Figure 4.2**).

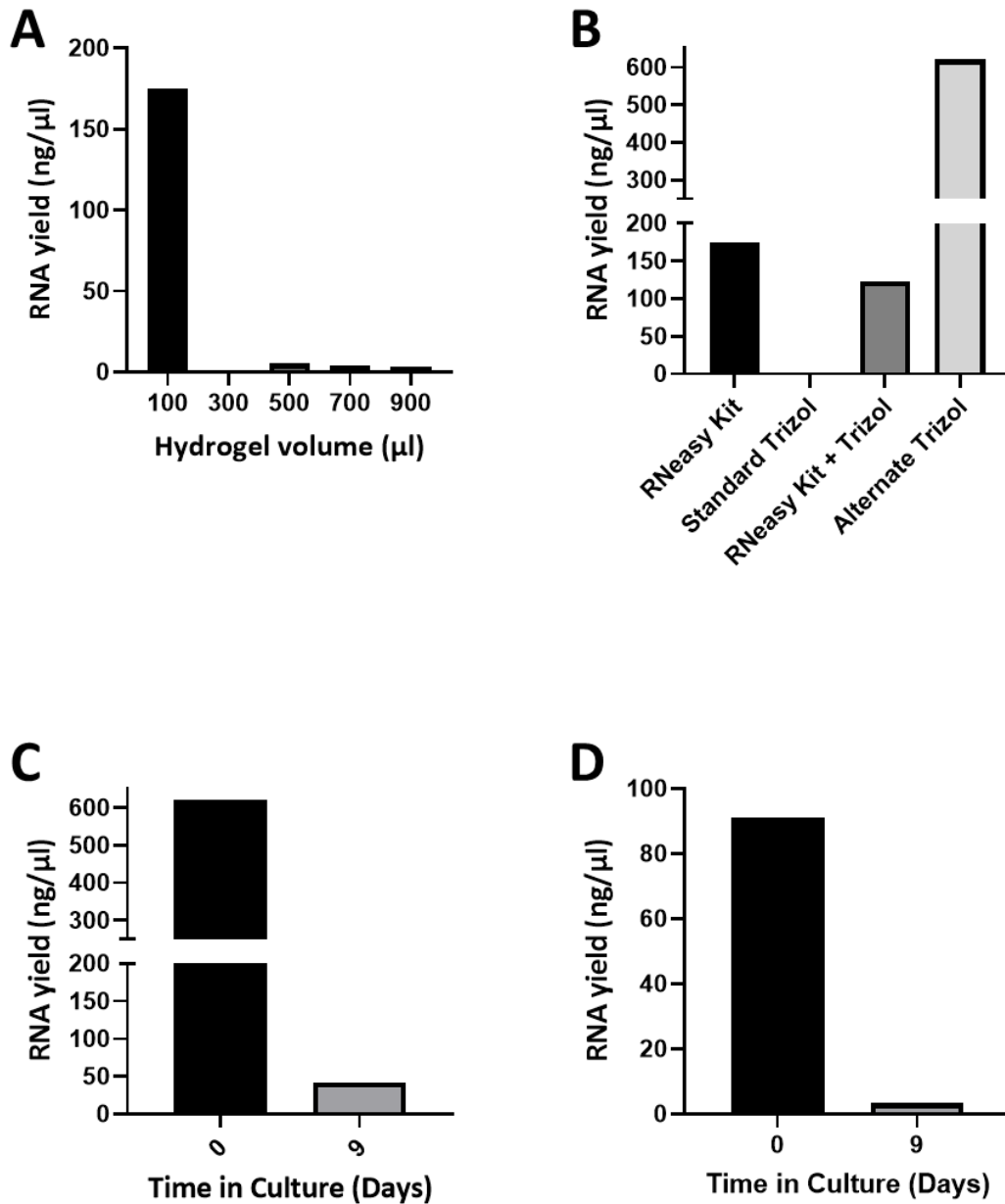


**Figure 4.2. Assessment of RNA extraction methods from Biogelx standard high stiffness hydrogels.** Extraction methods were assessed across a variety of culture conditions using SaOS-2 cells as a model. (A) The impact of hydrogel volume on RNA yields was assessed with any volume above 100 $\mu\text{l}$  of pre-gel resulting in retrieval of unworkable concentrations of RNA. (B) Extraction methods were then compared using 100 $\mu\text{l}$  pre-gel constructs. (C-D) Two extraction methods that provided the highest RNA yields were tested over the culture time period determined in chapter 3 and RNA yields were then assessed.

**Table 4.1. RNA concentrations and relevant 260/280, 260/230 ratios retrieved from cells encapsulated in Biogelx high stiffness hydrogels of increasing volume.**

<b>Hydrogel volume (μl)</b>	<b>RNA concentration (ng/μl)</b>	<b>260/280 ratio</b>	<b>260/230 ratio</b>
<b>100</b>	174.8	2.08	1.36
<b>300</b>	1.4	3.56	0.07
<b>500</b>	5.2	2.3	0.08
<b>700</b>	4	2.17	0.13
<b>900</b>	3.3	1.6	0.15

**Table 4.2. The impacts of extraction method on RNA concentrations and relevant 260/280, 260/230 ratios retrieved from cells encapsulated in Biogelx high stiffness hydrogels.**

<b>Extraction method</b>	<b>RNA concentration (ng/μl)</b>	<b>260/280 ratio</b>	<b>260/230 ratio</b>
<b>Trizol</b>	2.1	2.35	0.5
<b>Alternate Trizol</b>	619.9	1.88	0.63
<b>Trizol + kit</b>	122.9	1.76	0.6
<b>RNeasy Kit</b>	175.1	2.07	1.43

**Table 4.3. RNA yields and relevant 260/280, and 260/230 ratios retrieved from cells encapsulated in Biogelx high-stiffness hydrogels of increasing volume.**

<b>Extraction method</b>	<b>RNA Concentration (ng/μl)</b>	<b>260/280 ratio</b>	<b>260/230 ratio</b>
<b>Alternate Trizol Day 0</b>	619.9	1.88	0.63

<b>Alternate Trizol Day 9</b>	41.6	1.69	0.63
<b>RNeasy Kit Day 0</b>	91	2.02	1.12
<b>RNeasy Kit Day 9</b>	3.3	2.01	0.04

#### **4.4.3. Comparison of two-dimensional and three-dimensional culture conditions on C-28/I2 cells**

##### **4.4.3.1. The effect of three-dimensional culture on the expression of chondrocyte associated genes**

RT-qPCR was performed on cDNA derived from both 2D and 3D cultures of C-28/I2 cells and considered whether the expression of target genes characterised in chapter 3 are suitable readouts for both physiological and pathological chondrocyte activity (**Figure 4.3**). These genes were assessed and analysed between two different time points: day 0 (basal level) and day 3 and target gene expression were normalised to the geometric mean of *TOP1* and. No statistical significance was found for any gene of interest between conditions when comparing each time point to its relative control (i.e., 3D day 0 vs. 3D day 3).

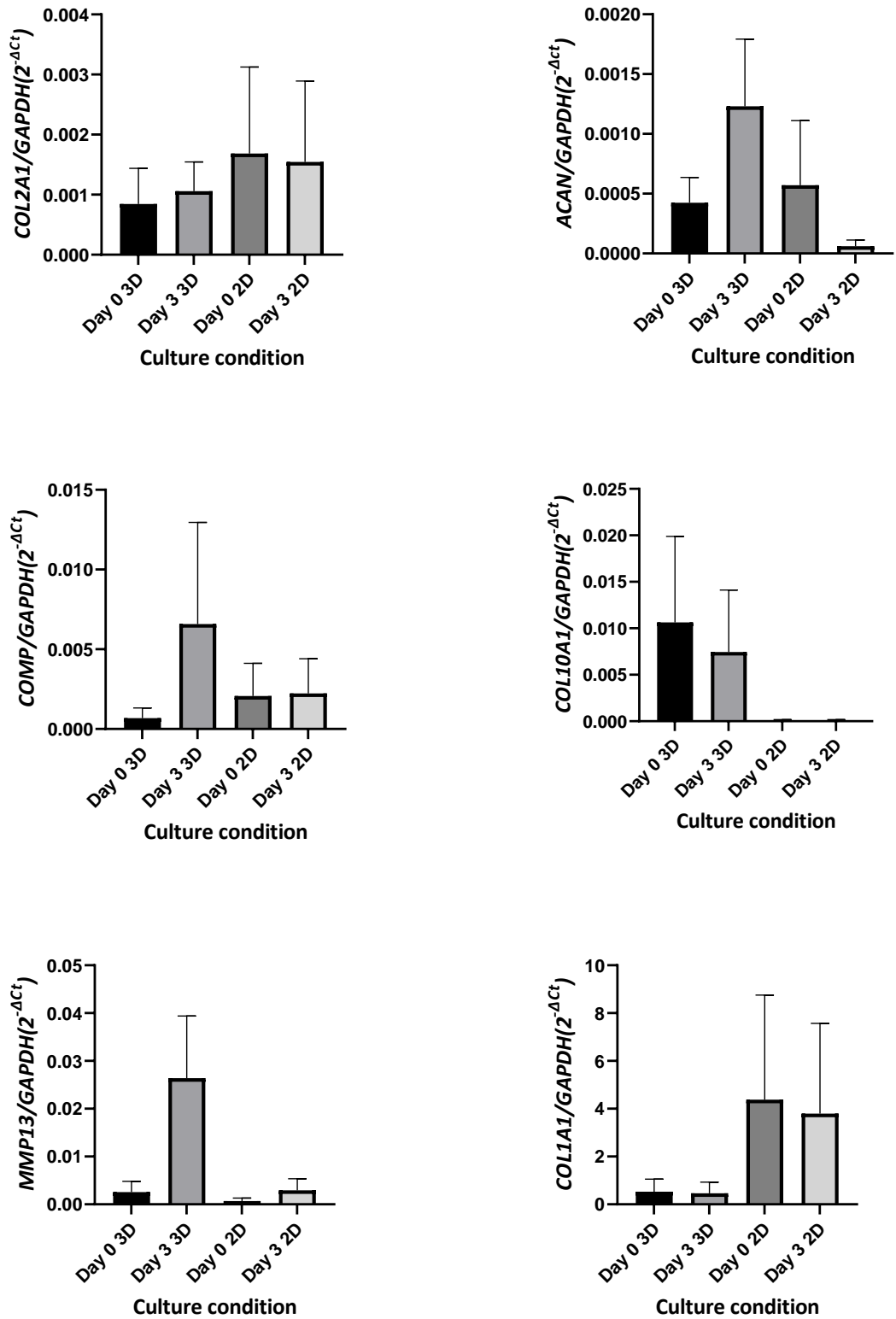


**Figure 4.3. 3D culture using Biogelx high stiffness standard hydrogels does not impact the expression of chondrocyte associated genes compared to 2D culture.** Expression of chondrocyte and cartilage ECM-associated genes by C-28/12 cells were cultured over 0-3 days in 2D and Biogelx standard high stiffness hydrogels were assessed via RT-qPCR. Data is presented as  $2^{-\Delta Ct}$  mean values  $\pm$  SEM showing normalized changes in the expression of target genes. Results were obtained from a dataset of n=3. (A) ACAN, (B)

COL2A1, (C) COMP, (D) COL10A1, (E) MMP13, (F) COL1A1. No statistically significant differences were found between culture time courses and their relevant controls.

#### **4.4.3.2. The effect of three-dimensional culture on the expression of chondrocyte associated proteins**

C-28/12 cell culture total protein lysates harvested from 2D and 3D cultures were analysed via immunoblotting (**Figure 4.4**). COMP protein expression increases over time in 3D culture when comparing day 0 to day 3 (**Figure 4.4A** lanes 1 & 2), whereas 2D culture results in a slight decrease in expression of COMP across both times tested (**Figure 4.4A** lanes 3 & 4). However, COMP is detectable at an overall higher level in 2D. MMP13 expression slightly increases over time in 3D culture when comparing day 0 and day 3 of culture (**Figure 4.4B** lanes 1 & 2). When comparing day 0 with day 3 of 2D culture MMP13 expression increases dramatically (**Figure 4.4B** lanes 3 & 4). Again, MMP13 expression is found to be overall higher in 2D conditions. Notably, ACTB staining indicated that loading was not equal between 3D and 2D conditions suggesting that hydrogel culture may interfere with protein quantification methods and could account for the discrepancy between protein expressions levels observed when comparing 3D vs. 2D.

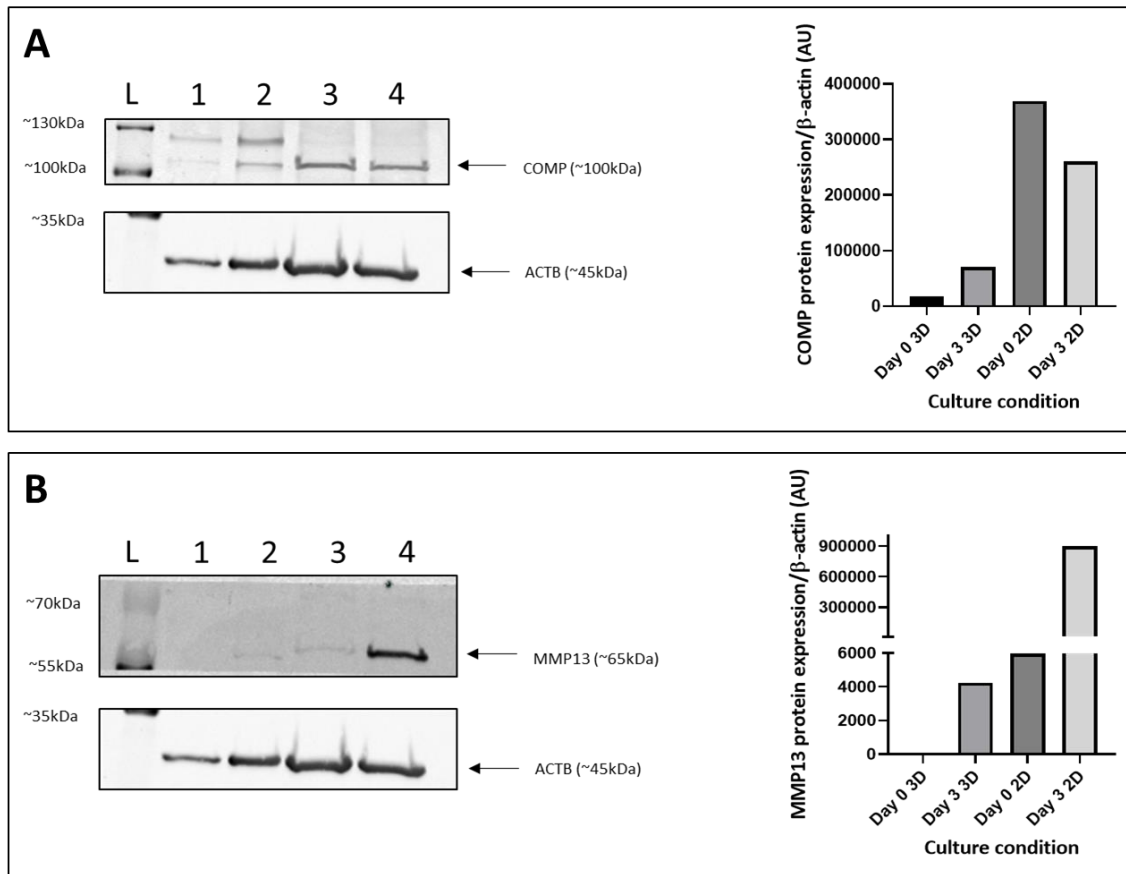


**Figure 4.4. 3D culture using Biogelx high stiffness standard hydrogels promotes a catabolic phenotype in C-28/I2 cells.** Expression of proteins associated with the chondrocyte phenotype and cartilaginous ECM produced by C-28/I2 cells cultured over 0-3 days in 2D and Biogelx standard high stiffness hydrogels were assessed via immunoblotting. Lanes are indicated by (L) ladder, (1) Day 0 3D, (2), Day 3 3D, (3) Day 0 2D and (4) Day 3 2D. Blotting was performed in triplicate and quantification was performed relative to  $\beta$ -actin expression. Densitometry was performed on one replicate representative of the dataset.

#### 4.4.3.2. The impact of culture substrate on C-28/I2 cell morphology

C-28/I2 cells were grown in 2D and 2.5D cultures and cell morphology was assessed using immunostaining of F-actin (**Figure 4.5**). In 2D, cells exhibit a typical chondrocyte polygonal morphology; cell nuclei are shown stained with DAPI. When cultured in 2.5D, chondrocytes drastically changed their morphology to a rounded shape and displayed bleb-like structures, indicative of apoptosis [313].

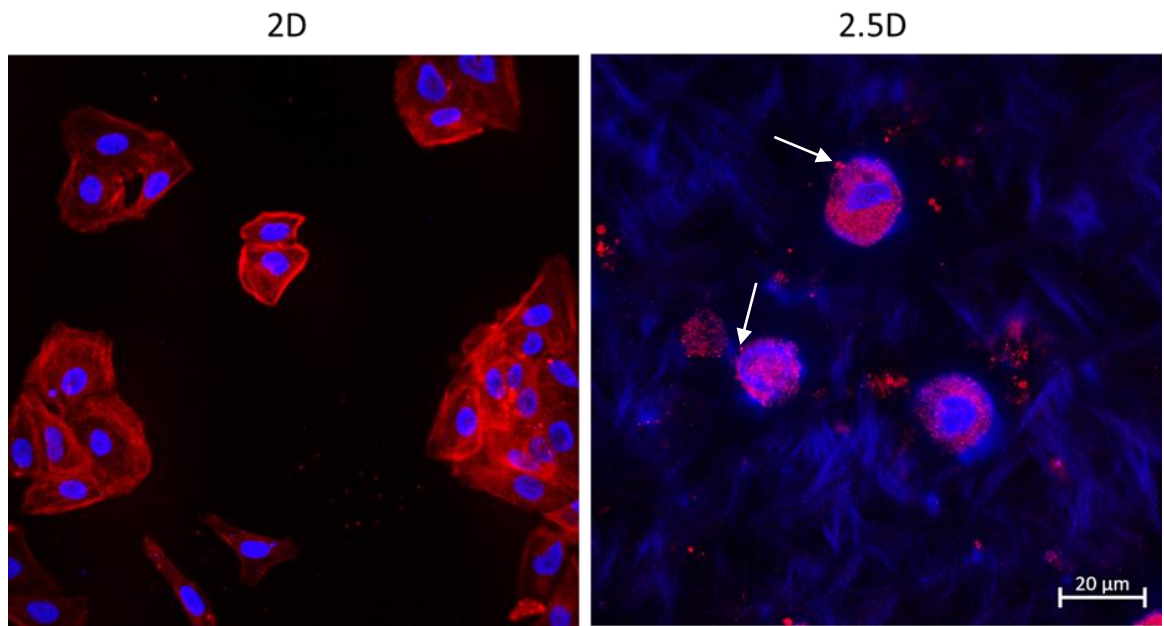


**Figure 4.5.** The effect of standard, high stiffness, Biogelx hydrogels as cell culture substrates on cell morphology. Immunostaining of the cytoskeletal protein F-actin (Red) and cell nuclei with DAPI (Blue) in C-28/I2 cells after 24 hours of culture in 2D conditions and 2.5D conditions (on top of Biogelx high stiffness standard hydrogels). White arrows indicate cell blebbing. The scale bar represents 20 $\mu$ m.

#### 4.4.5. Comparison of three-dimensional and two-dimensional culture conditions on SaOS-2 cells

##### 4.4.5.1. The effect of three-dimensional culture on the expression of osteoblast associated genes

RT-qPCR was performed on cDNA derived from both 2D and 3D SaOS-2 cultures and considered whether the expression of target genes characterised in chapter 3 are suitable readouts for both physiological and pathological osteoblast activity (**Figure 4.6**). These genes were assessed and analysed between two different time points: day 0 (basal) and day 9 and target gene expression were normalised to the geometric mean of *TOP1* and *ATP5B*. No statistical significance was found for *COL1A1*, *ALPL*, *PDPN* or *BGLAP* when comparing each time point to its relative control (i.e., 2D day 0 vs. 2D day 9). However, when considering *POSTN*, there was a significant decrease in expression from Day 0 3D and Day 9 3D ( $P < 0.05$ ).

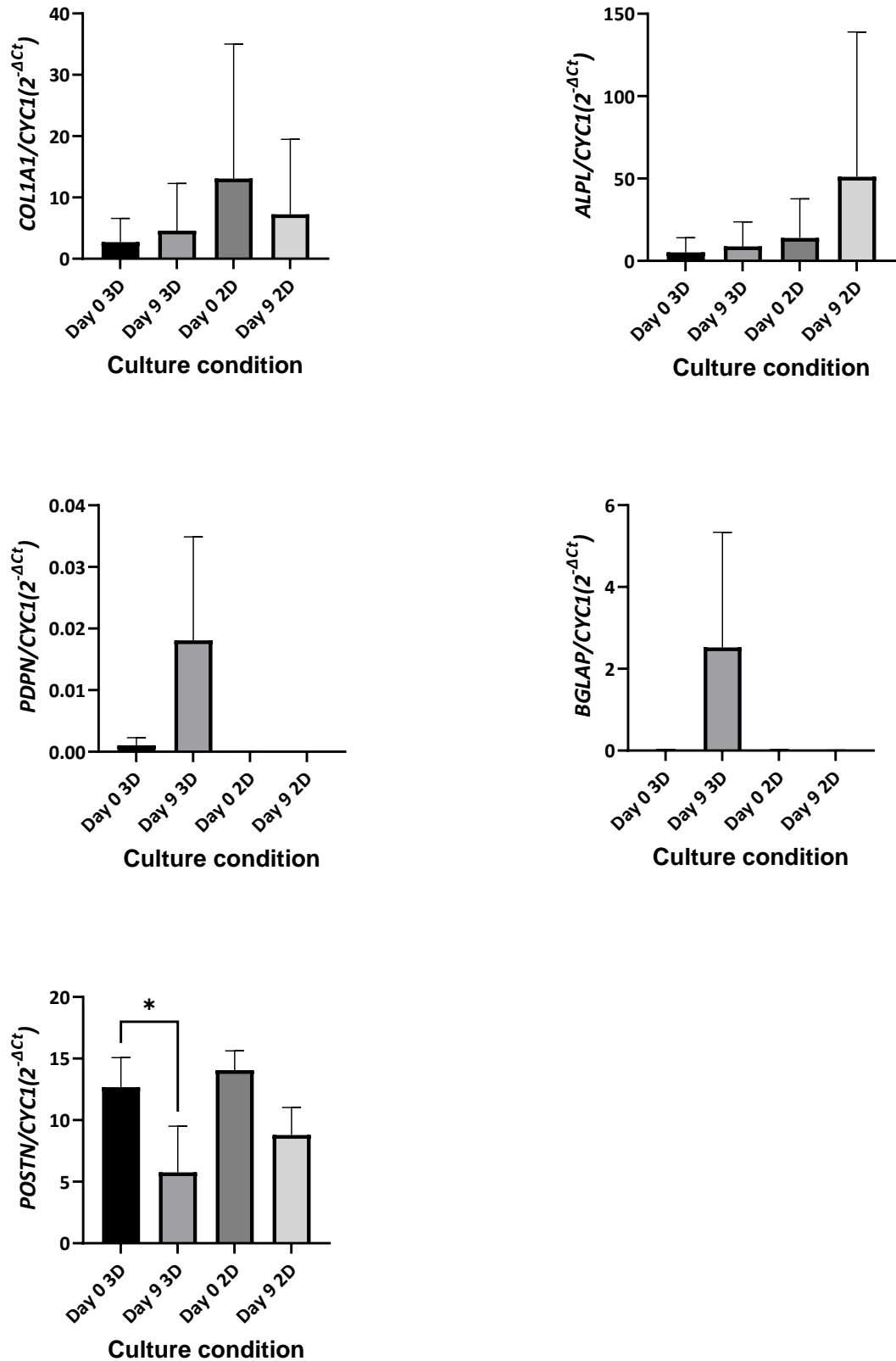


**Figure 4.6. 3D culture using Biogelx high stiffness standard hydrogels does not impact the expression of osteoblast associated genes compared to 2D culture.** Expression of osteoblast and bone ECM-associated genes by SaOS-2 cells cultured over 0-9 days in 2D and Biogelx standard high stiffness hydrogels was assessed using RT-qPCR. Data is presented as  $2^{-\Delta Ct}$  mean values  $\pm$  SEM showing normalized changes in the

expression of target genes. Results were obtained from a dataset of n=3. (A) COL1A1, (B) ALPL, (C) PDPN, (D) BGLAP, (E) POSTN. Only POSTN showed a significant change in expression, with 3D culture resulting in an overall reduction of POSTN expression when comparing Day 0 to Day 9.

#### **4.4.5.2. The effect of three-dimensional culture on the expression of osteoblast associated proteins**

SaOS-2 cell culture total protein lysates harvested from 2D and 3D cultures were analysed via immunoblotting (**Figure 4.7**).

It was observed that COL1 $\alpha$ 1 processing in 3D cultured cells shares an inverse relationship with 2D cultured cells. Between days 0 and 9 3D cultured SaOS-2 cells expression of fully processed COL1 $\alpha$ 1 slightly decreases (**Figure 4.7A** lanes 1 & 2) whereas in 2D this protein becomes detectable following 9 days of culture (**Figure 4.7A** lanes 3 & 4). Additionally, COL1 $\alpha$ 1 expression in 3D is detectable in larger quantities at both time points.

AP-TNAP expression appears to share the same relationship between 2D, and 3D culture. Between day 0 and 9 3D cultures show an increase in expression (**Figure 4.7B** lanes 1 & 2), as do 2D cultures with increased overall levels of AP-TNAP (**Figure 4.7B** lanes 3 & 4). Again, it is notable that ACTB staining indicated that loading was not equal between 3D and 2D conditions suggesting that hydrogel culture may have interfered with protein quantification methods and could account for the discrepancy between protein expression levels when considering 3D vs. 2D.

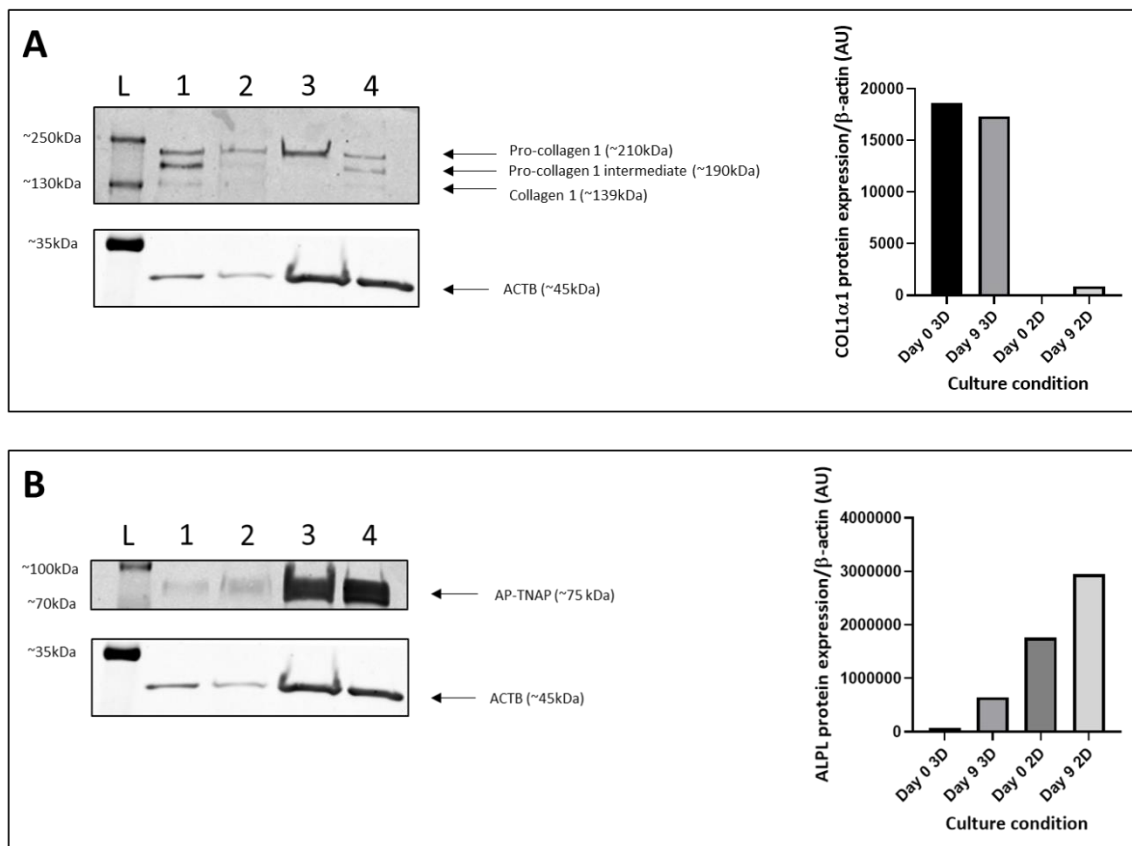


**Figure 4.7. 3D culture using Biogelx high stiffness standard hydrogels increases the expression of osteoblast associated COL1 $\alpha$ 1 compared to 2D culture.** Expression of proteins associated with the osteoblast phenotype and bone ECM produced by SaOS-2 cells cultured over 0-9 days in 2D and Biogelx standard high stiffness hydrogels was assessed via immunoblotting. Lanes are indicated by (L) ladder, (1) Day 0 3D, (2), Day 9 3D, (3) Day 0 2D and (4) Day 9 2D. Blotting was performed in triplicate and quantification was performed relative to  $\beta$ -actin expression. Densitometry was performed on one replicate representative of the dataset.

#### 4.4.5.3. The effect of hydrogel encapsulation on SaOS-2 cell morphology

SaOS-2 cells grown in 2D, and 3D were stained using CellTracker™ Deep Red following a 24 hour culture period. It was observed that distinct morphological differences exist between the two cell culture methods. 2D culture of SaOS-2 cells results in a flattened, elongated morphology whereas 3D culture results in a rounded morphology. Notably, encapsulated cells in 3D also express bleb-like structures indicative of apoptosis (**Figure 4.8**).

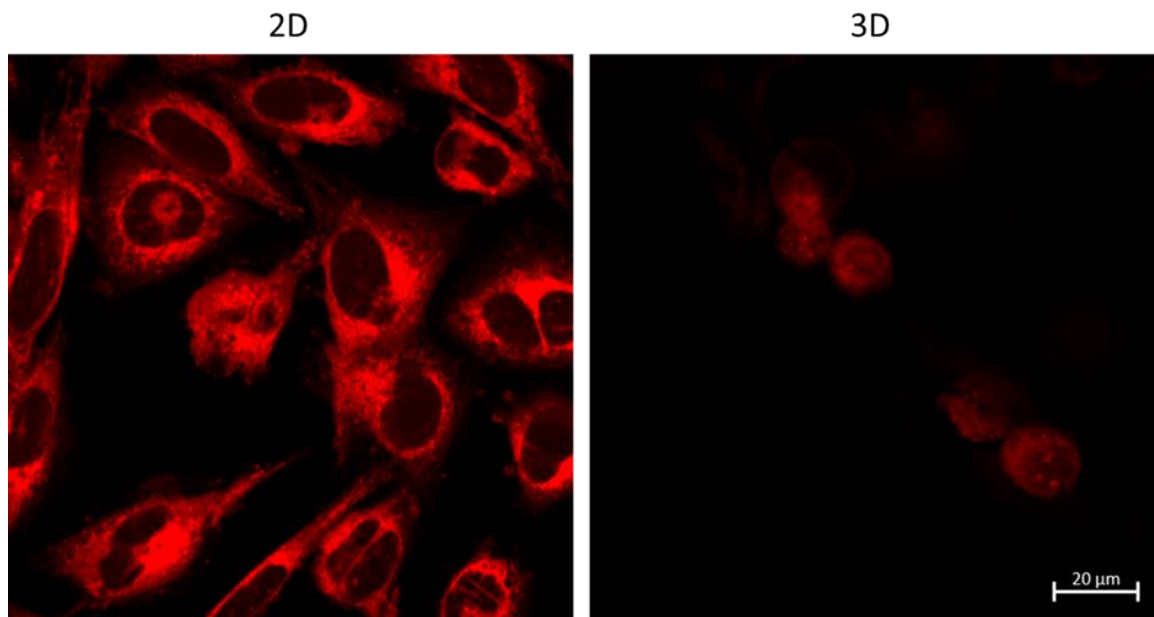


**Figure 4.8. Hydrogel encapsulation changes C-28/I2 morphology.** CellTracker™ Deep Red staining of SaOS-2 cells after 24 hours in 2D culture and 24 hours post-3D encapsulation in Biogelx high stiffness standard hydrogels. The scale bar represents 20μm.

#### **4.4.6. C-28/I2 and Saos-2 functionalised hydrogel screening**

Due to these apparent morphological differences in chondrogenic and osteoblastic cells cultured in standard high-stiffness 3D gels, it was determined that other hydrogel formulations manufactured by Biogelx had to be considered for 3D model development. Therefore, cell viability was assessed across all commercially available Biogelx hydrogel formulations at a variety of stiffnesses (low, medium, and high) over a 24 hour culture period (**Figure 4.9 & 4.10**). For both C-28/I2 and Saos-2 cells, culture in standard gels across all stiffnesses resulted in the death of all encapsulated cells (**Figure 4.9 & 4.10** panels i-iii). GFOGER functionalised gels yielded the most positive outcome for both C-28/I2 and SaOS-2 encapsulated cells with low, medium, and high stiffness culture resulting in viabilities of 47%, 69% and 59% for C-28/I2 cells and 77%, 83% and 82% for SaOS-2 cells respectively (**Figure 4.9 & 4.10** panels iv-vi). IKVAV hydrogels provided less favourable results than GFOGER hydrogels for both C-28/I2 and SaOS-2 encapsulated cells with low, medium, and high stiffnesses reducing cell viability to 42%, 35% and 13% for C-28/I2 cultures and 63%, 50% and 19% for SaOS-2 cultures (**Figure 4.9 & 4.10** panels vii-ix). C-28/I2 encapsulation in RGD hydrogels resulted in 100% mortality (**Figure 4.9** panels iv-vi), a finding that was reflected in low-stiffness RGD SaOS-2 cultures (**Figure 4.10** panel x). However, SaOS-2 cells encapsulated in medium and high stiffness RGD

hydrogel constructs resulted in cell viabilities of 42% and 48% respectively (Figure 4.10 panel xi-xii). Due to these results, medium stiffness GFOGER and IKVAV gels were considered as potential candidates for a long-term culture model and were taken forward for a time course analysis.

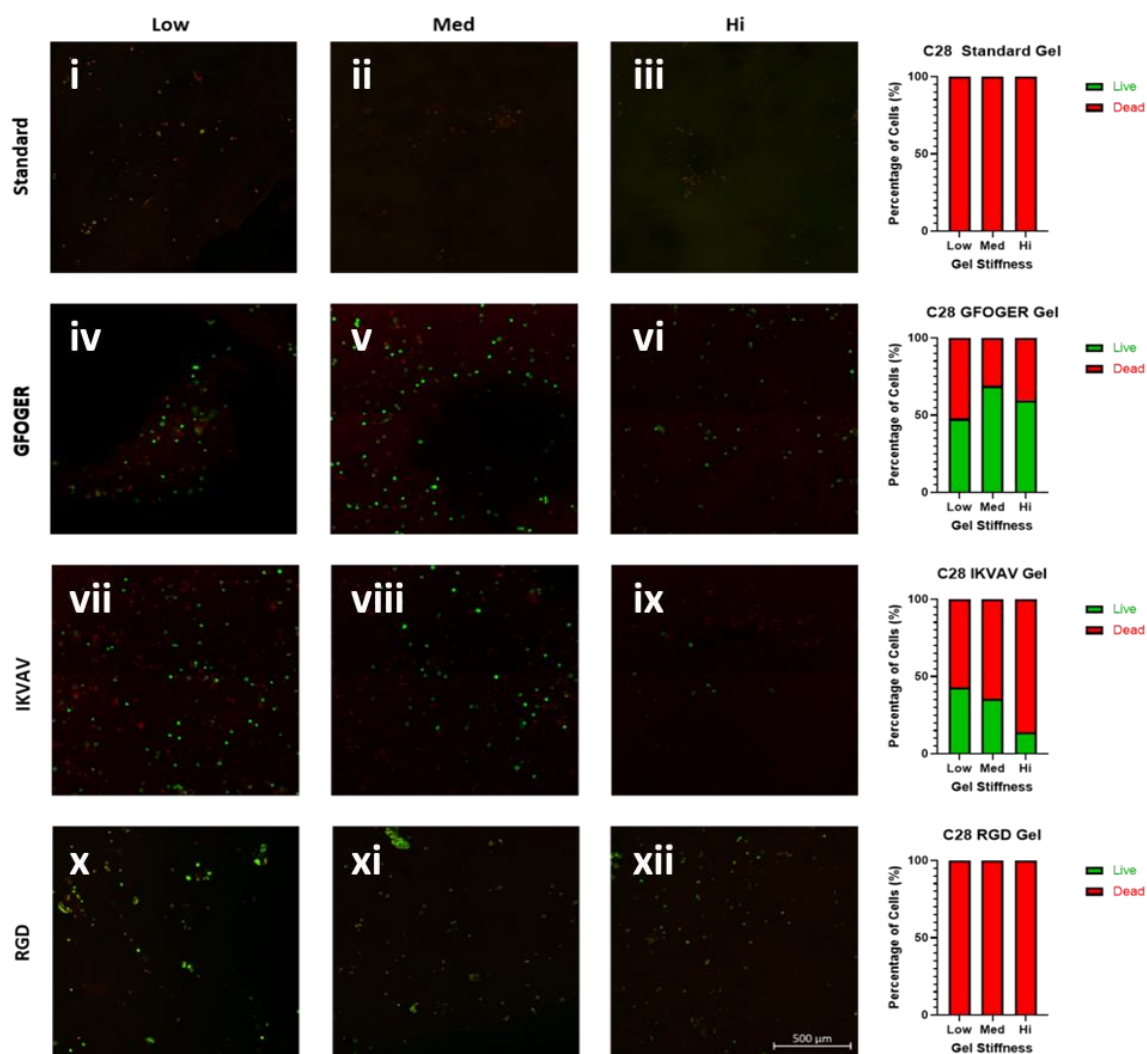


**Figure 4.9. Biogelx hydrogel stiffness and composition impacts encapsulated C-28/12 cell viability.** Screening of C-28/12 compatibility with functionalised hydrogels 24 hours post-encapsulation using live/dead staining. All commercially available Biogelx hydrogel formulations were tested including standard (Fmoc-FF/S), GFOGER (Fmoc-FF/S with a collagen-like functional group), IKVAV (Fmoc-FF/S with a laminin-like functional group) and RGD (Fmoc-FF/S with a fibronectin-like functional group). These formulations were tested at recommended standardised stiffnesses low (Low), medium (Med) and high (Hi). Viable cells can be seen in green with non-viable cells seen in red. Cells that were both red and green were non-viable as cell DNA would be damaged to allow propidium iodide binding and subsequent fluorescence. Culture conditions are labelled as (i) low stiffness standard hydrogel, (ii) medium stiffness standard hydrogel, (iii) high stiffness standard hydrogel, (iv) low stiffness GFOGER hydrogel, (v) medium

stiffness GFOGER hydrogel, (vi) high stiffness GFOGER hydrogel, (vii) low stiffness IKVAV hydrogel, (viii) medium stiffness IKVAV hydrogel, (ix) high stiffness IKVAV hydrogel, (x) low stiffness RGD hydrogel, (xi) medium stiffness RGD hydrogel and (xii) high stiffness RGD hydrogel. Images are presented as 2x2 tile scans and are representative of 4 fields of view. The scale bar represents 500µm.

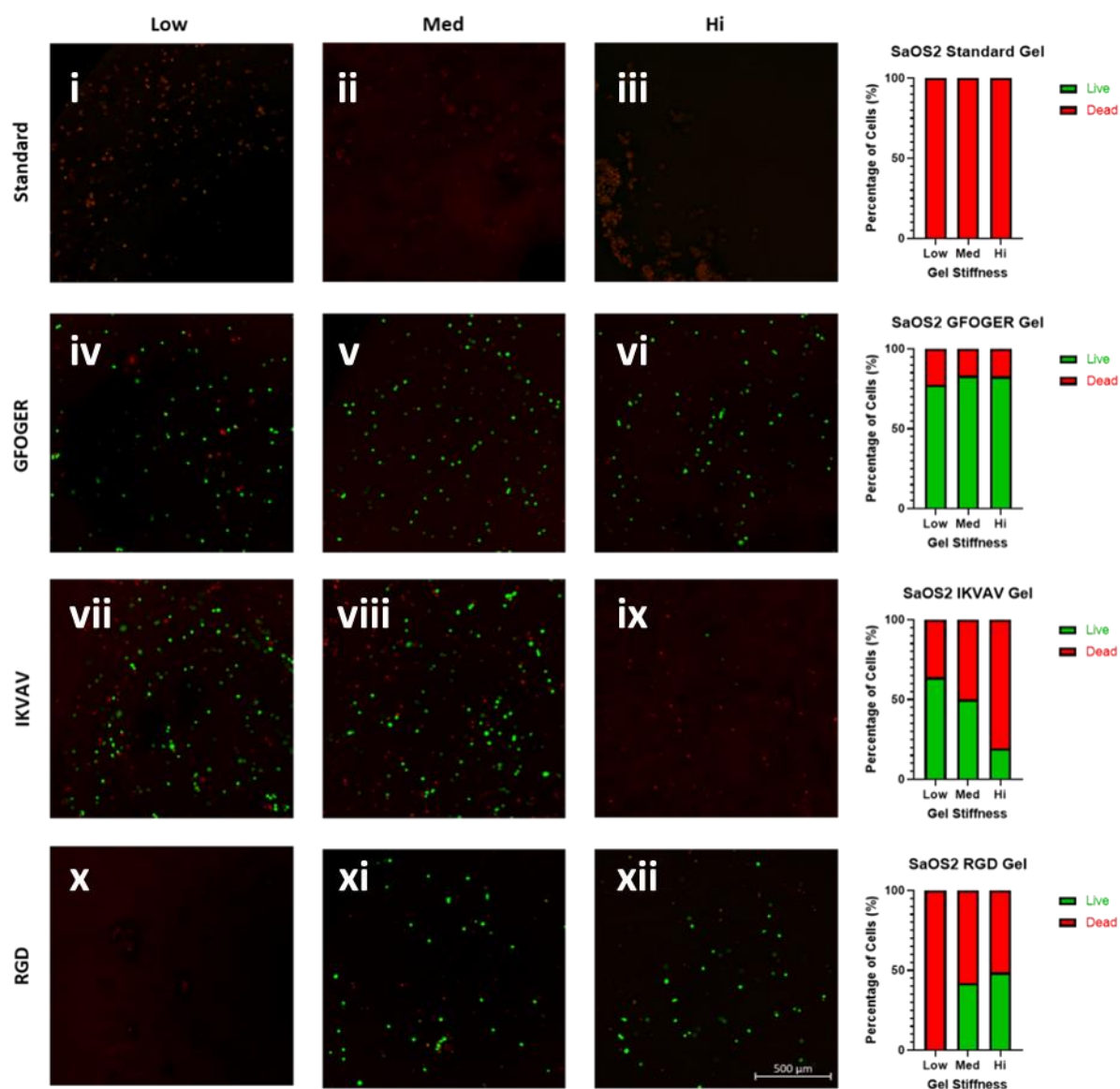


**Figure 4.10. Biogelx hydrogel stiffness and composition impacts encapsulated SaOS-2 cell viability.**

Screening of SaOS-2 compatibility with functionalised hydrogels 24 hours post-encapsulation using live/dead staining. All commercially available Biogelx hydrogel formulations were tested including standard (Fmoc-FF/S), GFOGER (Fmoc-FF/S with a collagen-like functional group), IKVAV (Fmoc-FF/S with a laminin-like functional group) and RGD (Fmoc-FF/S with a fibronectin-like functional group). These formulations were tested at recommended standardised stiffnesses low (Low), medium (Med) and high (Hi). Viable cells can be seen in green with non-viable cells seen in red. Cells that were both red and green were non-viable as cell DNA would be damaged to allow propidium iodide binding and subsequent fluorescence. Culture conditions are labelled as (i) low stiffness standard hydrogel, (ii) medium stiffness standard hydrogel, (iii) high stiffness standard hydrogel, (iv) low stiffness GFOGER hydrogel, (v) medium

stiffness GFOGER hydrogel, (vi) high stiffness GFOGER hydrogel, (vii) low stiffness IKVAV hydrogel, (viii) medium stiffness IKVAV hydrogel, (ix) high stiffness IKVAV hydrogel, (x) low stiffness RGD hydrogel, (xi) medium stiffness RGD hydrogel and (xii) high stiffness RGD hydrogel. Images are presented as 2x2 tile scans and are representative of 4 fields of view. The scale bar represents 500µm.

#### **4.4.10. The impact of long-term encapsulation of C-28/I2 and SaOS-2 cells in GFOGER and IKVAV hydrogels**

Long-term characterisation of C-28/I2 viability in GFOGER and IKVAV hydrogels was performed following initial functionalised gel screening (**Figure 4.11 & 4.12**). C-28/I2 cells cultured in GFOGER hydrogels displayed a drastic drop in viability after 24 hours in culture to 17% (**Figure 4.11** panel i) with viability dropping to 0% at all subsequent time points (**Figure 4.11** panels ii-v). Contrastingly SaOS-2 cells cultured in GFOGER hydrogels maintained high levels of viability after 24 hours in culture with 87% of cells recorded as viable (**Figure 4.12** panel i). However, three days post-encapsulation in GFOGER gels resulted in only 4% of encapsulated SaOS-2 cells being viable (**Figure 4.12** panel ii) and at all subsequent time points, 0% of SaOS-2 cells survived (**Figure 4.12** panel iii-v). C-28/I2 cells encapsulated in IKVAV hydrogels were found to be non-viable at all culture time points tested (**Figure 4.11** panels vi-x). SaOS-2 IKVAV encapsulated cells were found to show drastic drops in viability after 24 hours (39%) (**Figure 4.12** panel vi) this was found to drop again by day 3 (15%) (**Figure 4.12** panel vii). Saos-2 cells were non-viable at all subsequent time points tested (**Figure 4.12** panels viii-x), combined with previous results this shows IKVAV gels display greater variability in terms of suitability for cell culture.

C-28/I2 2D control cultures were shown to have a high degree of viable cells after 24 hours in culture with 94% of cells being viable (**Figure 4.11** panel xi). Subsequently, C-28/I2 2D culture viability decreased over day 3 (74%), day 6 (57%), day 9 (59%) and day 12 (49%) (**Figure 4.11** panel xii-xv). Similar trends were seen in SaOS-2 2D control cultures however these suffered less drastic drops in viability over time with cells showing 94% viability at Day 0 (**Figure 4.12** panel xi) and decreasing over time: day 3 (88%), day 6 (79%), day 9 (76%) and day 12 (71%) (**Figure 4.12** panels xii-xv).

These results indicate that all hydrogels tested are not suitable for long term cell culture and even have limited use as short-term culture models due to observed drops in

viability even 24-hours post encapsulation. However, to profile the changes observed in viability in a more specific manner, a shorter time encapsulation course was performed.

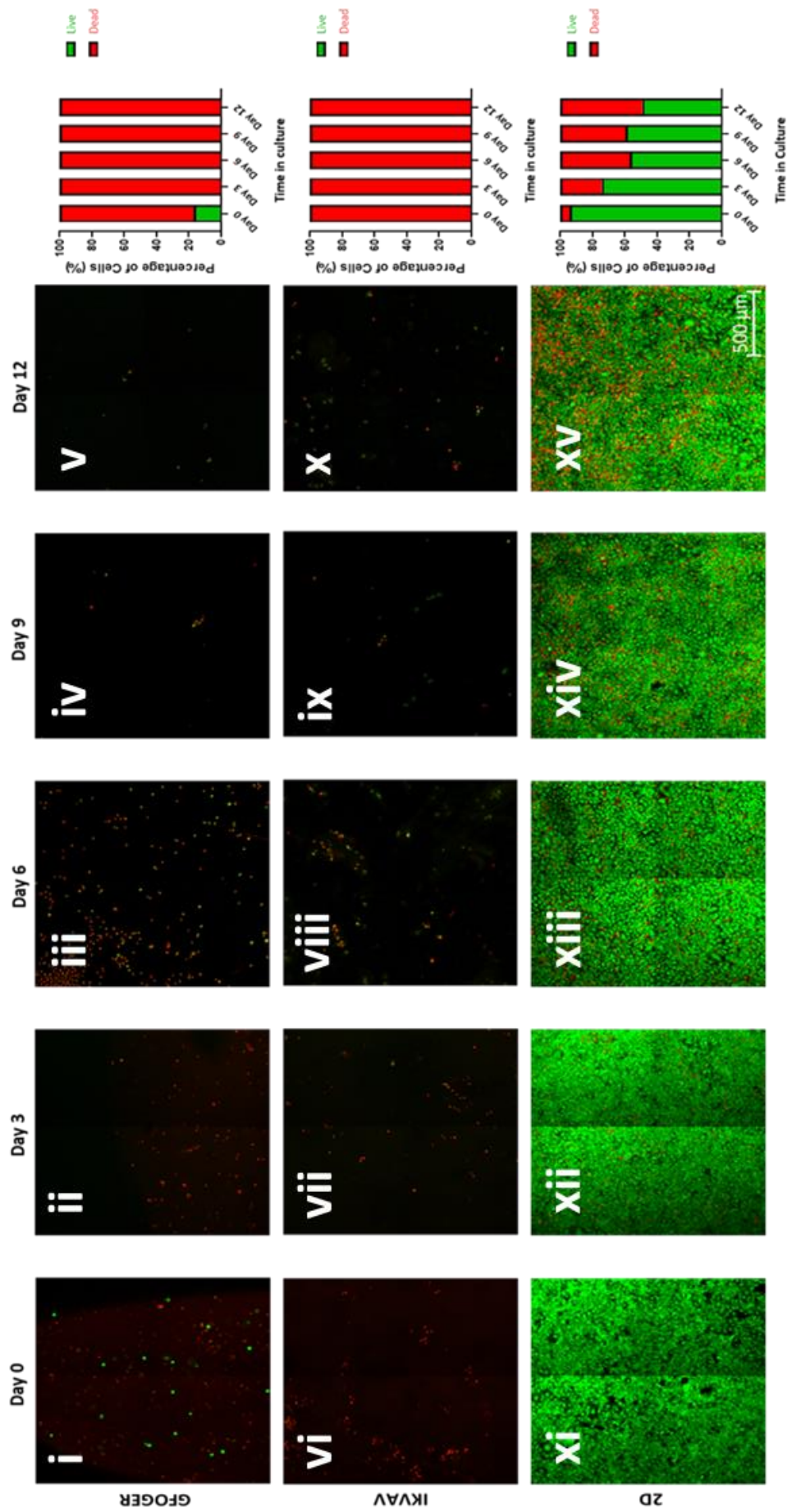


**Figure 4.11. Hydrogel encapsulation over a 12-day time course causes total C-28/I2 cell death.** Analysis of C-28/I2 compatibility with functionalised GFOGER (Fmoc-FF/S with a collagen-like functional group) and IKVAV (Fmoc-FF/S with a laminin-like functional group) hydrogels over a 12 day time course assessed via live/dead staining. These formulations were tested at medium stiffness as this was previously determined to be suitable. Viable cells can be seen in green with non-viable cells seen in red. Cells that were both red and green were non-viable as cell DNA would be damaged to allow propidium iodide incorporation. C-28/I2 cells were grown in 2D under similar conditions as a control. Culture conditions are labelled as (i) day 0 medium stiffness GFOGER hydrogel, (ii) day 3 medium stiffness GFOGER hydrogel, (iii) day 6 medium stiffness GFOGER hydrogel, (iv) day 9 medium stiffness GFOGER hydrogel, (v) day 12 medium stiffness GFOGER hydrogel, (vi) day 0 medium stiffness IKVAV hydrogel, (vii) day 3 medium stiffness IKVAV hydrogel, (viii) day 6 medium stiffness IKVAV hydrogel, (ix) day 9 medium stiffness IKVAV hydrogel, (x) day 12 medium stiffness IKVAV hydrogel, (xi) day 0 2D culture, (xii) day 3 2D culture, (xiii) day 6 2D culture, (xiv) day 9 2D culture and (xv) day 12 2D culture. Images shown represent a tile scan of 2x2 fields of view. Image brightness was enhanced by 20% using Microsoft PowerPoint. Scale bar represents 500µm.

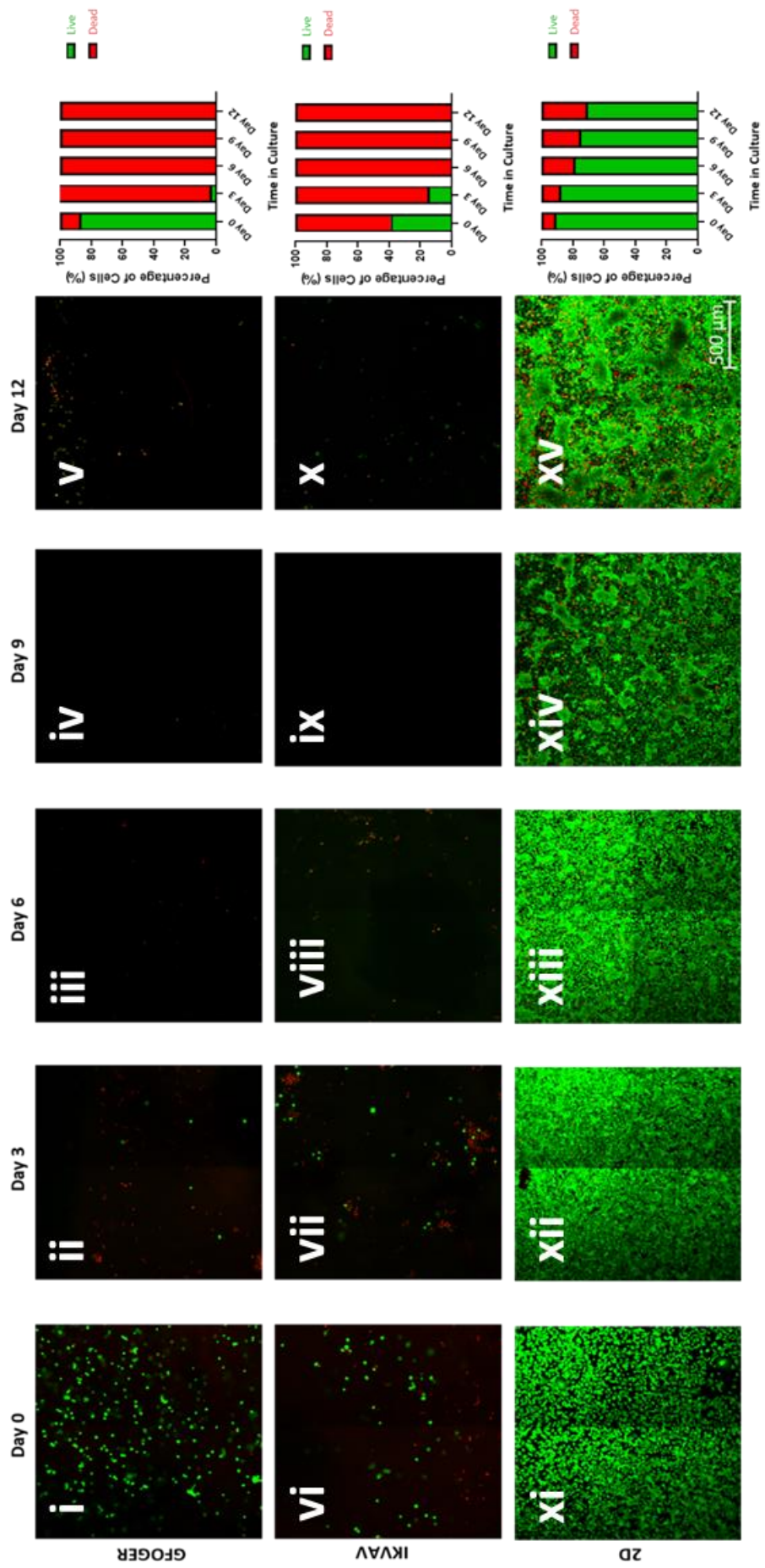


**Figure 4.12. Hydrogel encapsulation over a 12-day time course causes total SaOS-2 cell death.** Analysis of SaOS-2 compatibility with functionalised GFOGER (Fmoc-FF/S with a collagen-like functional group) and IKVAV (Fmoc-FF/S with a laminin-like functional group) hydrogels over a 12 day time course assessed via live/dead staining. These formulations were tested at medium stiffness as this was previously determined to be suitable. Viable cells can be seen in green with non-viable cells seen in red. Cells that were both red and green were non-viable as cell DNA would be damaged to allow propidium iodide incorporation. SaOS-2 cells were grown in 2D under similar conditions as a control. Culture conditions are labelled as (i) day 0 medium stiffness GFOGER hydrogel, (ii) day 3 medium stiffness GFOGER hydrogel, (iii) day 6 medium stiffness GFOGER hydrogel, (iv) day 9 medium stiffness GFOGER hydrogel, (v) day 12 medium stiffness GFOGER hydrogel, (vi) day 0 medium stiffness IKVAV hydrogel, (vii) day 3 medium stiffness IKVAV hydrogel, (viii) day 6 medium stiffness IKVAV hydrogel, (ix) day 9 medium stiffness IKVAV hydrogel, (x) day 12 medium stiffness IKVAV hydrogel, (xi) day 0 2D culture, (xii) day 3 2D culture, (xiii) day 6 2D culture, (xiv) day 9 2D culture and (xv) day 12 2D culture. Images shown represent a tile scan of 2x2 fields of view. Image brightness was enhanced by 20% using Microsoft PowerPoint. Scale bar represents 500µm.

#### **4.4.11. The impact of short-term encapsulation of C-28/I2 and SaOS-2 cells in GFOGER and IKVAV hydrogels**

Following the 12-day time course screen, a shorter 3-day time course was performed to determine the viability of C-28/I2 and SaOS-2 cells in short-term culture (**Figure 4.13 & 4.14**). The viability of C-28/I2 cells in both GFOGER and IKVAV hydrogels immediately dropped 24 hours post-encapsulation as shown by the basal (day 0) viability levels (**Figure 4.13** panel i). Further 3D culture leads to statistically significant drops in viability across all time points tested for both GFOGER and IKVAV formulations ( $P < 0.05$ ) (**Figure 4.13** panels ii-viii). Levels of viable C-28/I2 cells cultured in 2D remained stable throughout the culture period (**Figure 4.13** panels ix-xii). Short-term culture of SaOS-2 cells in GFOGER resulted in a significant drop in cell viability when comparing days 0 to days 2 and 3 of hydrogel culture (**Figure 4.14** compare panel i to iii and iv). In addition, when comparing days 1 and 2 to day 3 a continuous drop in viability can be observed over time (**Figure 4.14** compare panels ii and iii to iv). Short-term culture of SaOS-2 cells embedded in IKVAV hydrogels resulted in a significant drop in cell viability when comparing days 0 to days 2 and 3 (**Figure 4.14** compare panel v to panels vii and viii); with 2D cultured cells maintaining consistent viability across all time points tested (**Figure 4.14** panels ix-xii).

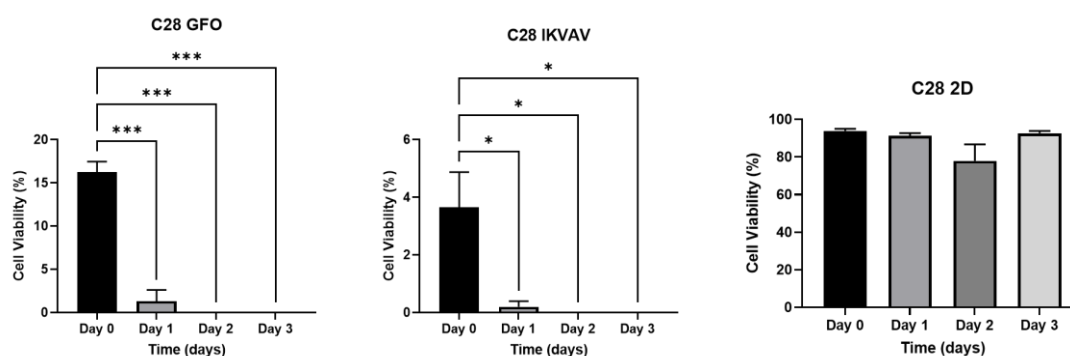
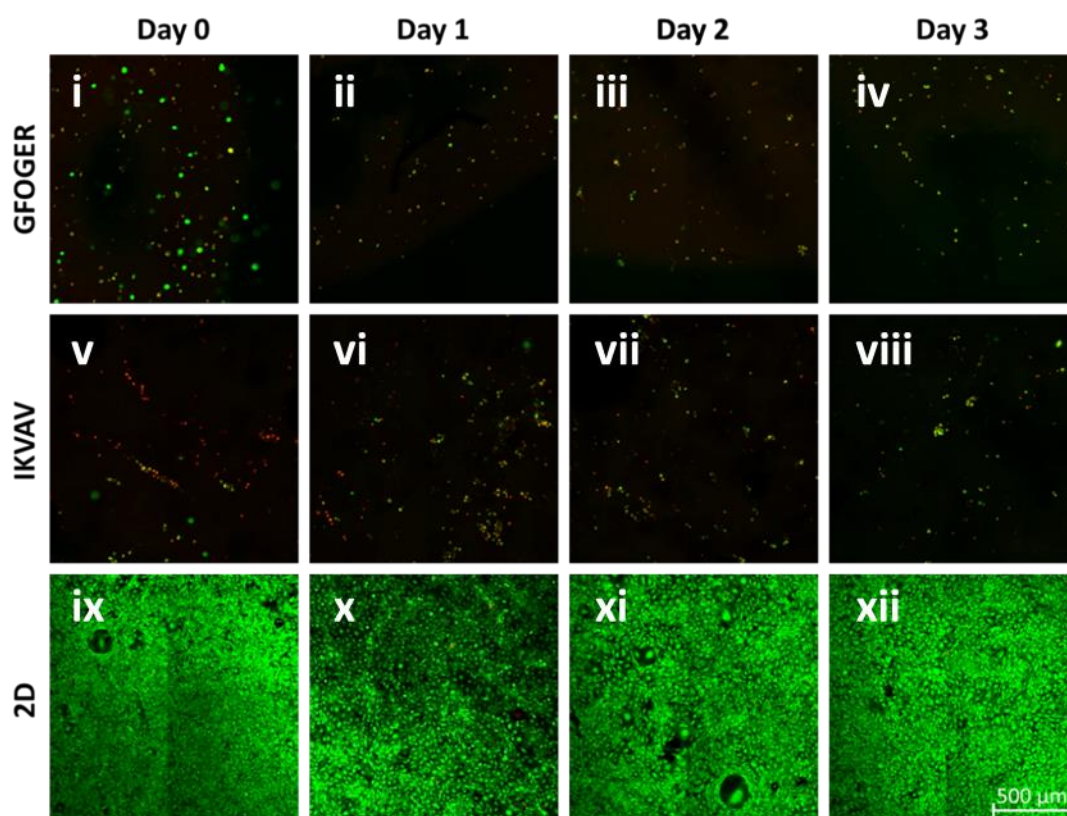


**Figure 4.13. Hydrogel encapsulation over a 3-day time course causes total C-28/I2 cell death.** Analysis of C-28/I2 compatibility with functionalised GFOGER (Fmoc-FF/S with a collagen-like functional group) and IKVAV (Fmoc-FF/S with a laminin-like functional group) hydrogels over a 3-day time course assessed via live/dead staining. These formulations were tested at medium stiffness as this was previously determined to be suitable. Viable cells can be seen in green with non-viable cells seen in red. Cells that were both red and green were non-viable as cell DNA would be damaged to allow propidium iodide incorporation. C-28/I2 cells were grown in 2D under similar conditions as a control. Culture conditions are labelled as (i) day 0 medium stiffness GFOGER hydrogel, (ii) day 1 medium stiffness GFOGER hydrogel, (iii) day 2 medium stiffness GFOGER hydrogel, (iv) day 3 medium stiffness GFOGER hydrogel, (v) day 0 medium stiffness IKVAV hydrogel, (vi) day 1 medium stiffness IKVAV hydrogel, (vii) day 2 medium stiffness IKVAV hydrogel, (viii) day 3 medium stiffness IKVAV hydrogel, (ix) day 0 2D culture, (x) day 1 2D culture, (xi) day 2 2D culture

and (xii) day 3 2D culture. Images shown represent a tile scan of 2x2 fields of view. Brightness of 3D images had increased by 40% using Microsoft PowerPoint. The scale bar represents 500µm.

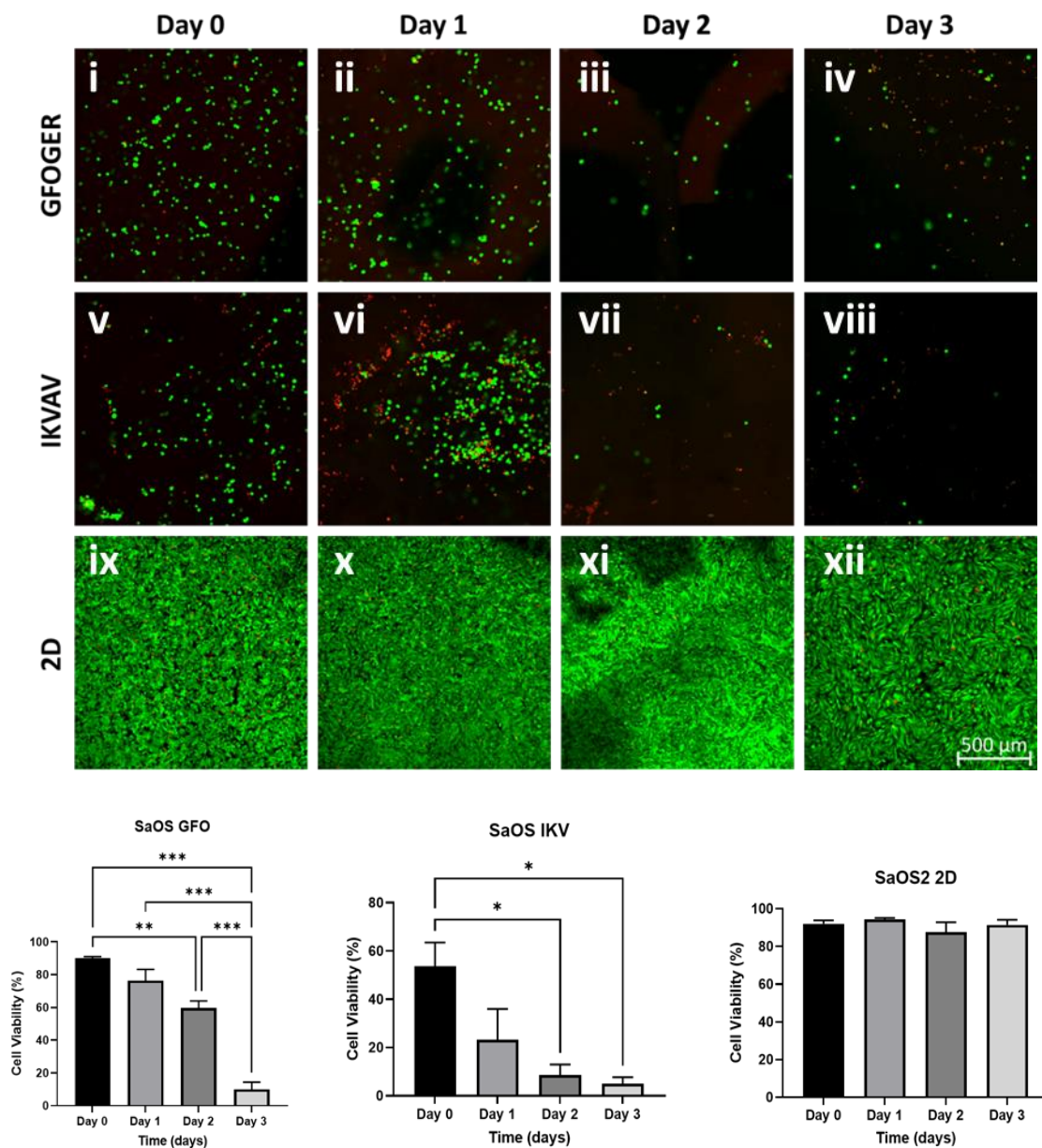


**Figure 4.14. Hydrogel encapsulation over a 3-day time course causes gross SaOS-2 cell death.** Analysis of SaOS-2 compatibility with functionalised GFOGER (Fmoc-FF/S with a collagen-like functional group) and IKVAV (Fmoc-FF/S with a laminin-like functional group) hydrogels over a 3-day time course assessed via live/dead staining. These formulations were tested at medium stiffness as this was previously determined to be suitable. Viable cells can be seen in green with non-viable cells seen in red. Cells that were both red and green were non-viable as cell DNA would be damaged to allow propidium iodide incorporation. SaOS-2 cells were grown in 2D under similar conditions as a control. Culture conditions are labelled as (i) day 0 medium stiffness GFOGER hydrogel, (ii) day 1 medium stiffness GFOGER hydrogel, (iii) day 2 medium

stiffness GFOGER hydrogel, (iv) day 3 medium stiffness GFOGER hydrogel, (v) day 0 medium stiffness IKVAV hydrogel, (vi) day 1 medium stiffness IKVAV hydrogel, (vii) day 2 medium stiffness IKVAV hydrogel, (viii) day 3 medium stiffness IKVAV hydrogel, (ix) day 0 2D culture, (x) day 1 2D culture, (xi) day 2 2D culture and (xii) day 3 2D culture. Images shown represent a tile scan of 2x2 fields of view. Brightness of 3D images had increased by 40% using Microsoft PowerPoint. The scale bar represents 500 $\mu$ m.

## 4.5 Discussion

The initial overall objective of this chapter was to characterise and determine the expression of genes and proteins associated with both C-28/I2 chondrocytes and SaOS-2 osteoblasts in a 3D hydrogel-base culture context. Ultimately, these individual 3D culture systems were to be included in a more physiologically relevant 3D co-culture model of OA. However, concerns regarding cell viability presented a challenge for this goal.

The process of RNA extraction for gene expression analysis from both animal cells and tissues is routine, however, due to the novelty of Biogelx hydrogel culture systems, there was first a need to assess the impact of the hydrogel on RNA yields and compare extraction methods to determine which is most suitable. Two of the most common RNA extraction methods used for mammalian cells cultured *in vitro* include Trizol phase separation-based methods and Qiagen RNeasy kit extractions. Trizol RNA extractions rely on the dissolution of RNA, DNA and proteins using a mixture of guanidium thiocyanate phenols, which are mixed with chloroform resulting in an emulsion which undergoes phase separation creating two distinct phases: a hydrophilic and a hydrophobic phase which is split by an interphase. The hydrophilic phase is where RNA remains soluble and can therefore be used to isolate the RNA component of a sample [314]. Alternatively, kit-based methods such as the Qiagen RNeasy kit rely on the dissolution of mammalian cells and subsequent RNA release via a highly salted guanidine thiocyanate lysis buffer containing reducing agents such as  $\beta$ -mercaptoethanol [315]. Published research has shown that extracting RNA from hydrogel-based culture systems has presented challenges when using these methods including hydrogels of both natural and synthetic nature [316–319]. Standard Trizol extraction performed on mammalian cells encapsulated in polysaccharide-based alginate, agarose and gellan hydrogels results in RNA that is not suitable for RT-qPCR [316, 317] and a wide variety of extraction methods – including the RNeasy kit – result in greatly varied yields of RNA depending on

the homogenisation method used [316]. It is often the case that  $\beta$ -sheet forming self-assembling peptides contain many protonated structures which may give an overall cationic or anionic charge to peptide fragments – this in turn will impact RNA extraction methods as mainstay techniques are often dependent on charge-based interactions [320]. Results presented in this chapter demonstrate the impact of hydrogel construct volume on the process of RNA extraction when using standard Qiagen RNeasy kit methods. Increasing hydrogel volume greatly diminishes RNA yields, suggesting future work should consider the hydrogel/cell ratio. This diminished RNA yield may be attributed to the direct charge interaction between peptide monomers and RNA, thus increasing gel volume results in increased loss of RNA [320]. Following the determination of the optimal hydrogel construct volume the efficiency of 4 different RNA extraction methods was assessed on hydrogel-encapsulated cells after 24 hours of culture.

Standard Trizol methods resulted in very low RNA yields, which can be expected [316]. This may be due to the role of charge interactions involved in the phase separation component of a typical Trizol extraction. Charged peptide subunits may be binding to and sequestering released RNA thus preventing it from dissolving in the aqueous phase of the Trizol-chloroform emulsion. RNeasy Kit/Trizol combination methods resulted in sufficient RNA concentrations for downstream applications, however, the RNeasy kit alone resulted in the second highest yield of RNA from encapsulated samples which can also be seen in previously published work [320]. The differences here may be explained by additional RNA loss when performing the Kit + Trizol method due to RNA sequestration during the phase separation of the Trizol emulsion, whereas the binding interaction of RNA to hydrated silica columns may outcompete the binding of peptide subunits to RNA [320]. RNA extraction using the alternate Trizol method described previously resulted in the highest yields of RNA this may be due to the increased chilled isopropanol incubation step performed. This step maximizes the precipitation of RNA and increases nucleic acid flocculation which promotes the formation of larger RNA complexes which pellet more efficiently when put under centrifugal force. However, this method may also increase salt precipitation which may have downstream impacts on RNA in terms of integrity and suitability for cDNA synthesis and subsequent RT-qPCR reactions. All methods produced acceptable 260/280 ratios, however methods involving phenol extractions produced low 260/230 values, this is due to carryover phenol or salt

contamination, as well as potential peptide contamination [314, 320]. RNeasy kits produced more desirable 260/230 ratios however these were slightly below the expected standard however this may also be due to peptide contamination [314, 320].

When considering RNA extraction from cells encapsulated in hydrogels over time, sharp drops in RNA concentration were observed; this effect was heightened when using the Kit extraction method which resulted in non-usable concentrations of RNA derived from cells encapsulated over 9 days, raising concerns over cell viability. The Alternate Trizol method resulted in the loss of RNA over time however, workable concentrations of RNA were harvested after 9 days of cell encapsulation, therefore this method was used to extract from multiple RNA samples. These results have highlighted decreases in RNA concentrations following hydrogel encapsulation and subsequent culture. Previous publications have shown that rapid degradation of RNA is associated with pathological processes such as apoptosis and necrosis [321, 322] and this was therefore considered following the downstream applications of this RNA which was assessed in the form of reverse transcription and RT-qPCR experiments.

Quantitative PCR experiments performed using RNA extracted via the Alternate Trizol method resulted in no significant changes in the expression of any target genes except for a significant decrease in periostin expression. The standard error for all RT-qPCR experiments can be seen to be highly variable which may have contributed to these findings. Results found in Chapter 3 show that the RT-qPCR methodology used previously is suitable for both target cell lines producing robust results. Therefore, this inconclusive alteration in gene expression may be due to changes in RNA extraction methodology. The drop in RNA concentration retrieved from cells cultured over time in 3D suggests that cells may not have been surviving in hydrogel constructs. Notably, RT-qPCR performed on harvests derived from 2D culture also resulted in highly variable results indicating it may be the overall extraction methodology that influenced the highly variable results shown.

Following RT-qPCR experiments, protein expression was considered. Extraction of protein from hydrogel constructs was achieved via conventional means and was deemed suitable for analysis via immunoblotting. Immunoblotting results show 3D cultures exhibiting trends that differ from their 2D counterparts. When considering cartilage proteins, COMP was shown to increase from Day 0 to Day 3 when cells were

encapsulated in hydrogels, however an inverse effect was seen in 2D cultures. These findings are consistent with 2D *in vitro* conditions not necessarily being suitable for chondrocyte culture, with loss of expression of chondrocytic markers being a key issue with 2D culture [323, 324]. 3D culture has been shown to support chondrogenic activity [323]; however, it is worth noting here that 2D expression of COMP was higher overall regardless of time point tested, which again may suggest that the particular hydrogel systems used here are not a suitable culture system for C-28/I2 chondrocytes. Expression of MMP-13 was found to increase in both 3D and 2D *in vitro* cultures over time, with this increase being much more substantial in 2D cultures. Expression of MMP-13 by chondrocytes is a natural process and has been shown in monolayer [324, 325]. It has been highlighted that 3D culture can maintain MMP-13 expression [326]. Notably, here it is shown that 3D cultured C-28/I2 cells express low basal MMP-13 and that this increases over time in 3D culture. This increase in MMP-13 expression may be stimulated by unfavourable cell culture conditions induced by cell encapsulation. These concerns have been further addressed in this chapter with cell viability analysis and will be discussed. Upon analysis of osteoblast related proteins, it was observed that processed COL1 $\alpha$ 1 was detectable in 3D encapsulated SaOS-2 cells at day 0 and maintained over a 9-day culture period with a slight decrease in expression over time. It has been highlighted that 3D culture can promote the osteoblastic phenotype and this may be occurring here [251]. Conversely, 2D cultures expressed no processed COL1 $\alpha$ 1 at day 0 with an increase in expression to a detectable level observed at day 9. These 2D culture results are consistent with findings detailed in chapter 3. Finally, expression of AP-TNAP showed the same trend between both 3D and 2D cultures, increasing as a function of time, with overall greater levels of expression detected at both time points in 2D cultures. Three dimensional cell-culture has been shown to improve the phenotype of encapsulated cells, typically promoting many markers associated with the phenotype of the encapsulated cell, including chondrocytes and osteoblasts [251, 323]. These effects have been considered to be tied to the physical properties of the external matrix itself and subsequent mechanotransduction [228]. Alterations in phenotypic expression of encapsulated cells are subject to a variety of matrix properties including composition and stiffness [265, 327–331]. Therefore, to truly assess the suitability of a hydrogel system for cell culture and inclusion in a 3D model of OA, composition and stiffness should be assessed.

To visualise hydrogel-encapsulated cells, initial immunostaining steps were performed comparing F-actin and DAPI staining on cells cultured in 2D compared to 2.5D, which revealed a high degree of auto-fluorescence can be found originating from the hydrogel construct, an artefact which has been detailed in nanofibrillar self-assembling peptide hydrogels [332]. Therefore, subsequent staining was tested via the use of cell-permeable dyes that fluoresce in the red light spectrum, resulting in successful staining of encapsulated cells with minimal background staining. As Biogelx hydrogel products are a porous hydrogel scaffold; this result is expected as this would be permissive to small molecule dyes. This method was then adapted using cell permeable dyes as a live/dead stain to assess cell viability in hydrogel encapsulated cells. An initial screen was performed using both cell lines in 4 different functionalised hydrogels: Standard, GFOGER, IKVAV and RGD, over 3 different stiffnesses: low, medium, and high. C-28/I2 and SaOS-2 cells encapsulated in each type of hydrogel resulted in varying degrees of cell death 24 hours post-encapsulation across all hydrogel stiffnesses. GFOGER and IKVAV hydrogels of medium stiffness yielded the highest levels of cell survival in a construct that would be suitable for the development of a future co-culture model – low stiffness hydrogels despite showing fewer toxic effects, were not viscous enough to be included in a direct interface co-culture model (**Figure 4.2A-B**). Therefore, longer term cytotoxicity studies were conducted using both GFOGER and IKVAV hydrogels at medium stiffness. C-28/I2 cells cultured in both GFOGER and IKVAV hydrogels displayed drastic drops in viability 24-hours post encapsulation, with complete cell death being observed from 3 days post-encapsulation and at each subsequent timepoint. SaOS-2 cells displayed favourable cell viability in GFOGER constructs after 24 hours of culture, however viability dropped substantially by 3 days post-encapsulation, from day 6, total cell death was observed. SaOS-2 cells encapsulated in IKVAV hydrogels displayed immediate considerable drops in cell viability 24 hours post-encapsulation; with this trend continuing into day 3 of culture. By day 6 complete cell death had occurred, and this was observed across each subsequent timepoint. Finally, comprehensive 3-day time courses were conducted to analyse the specific time profile of cell death of encapsulated C-28/I2 and SaOS-2 cells encapsulated in GFOGER and IKVAV hydrogels. C-28/I2 cells displayed statistically significant drops in cell viability at all time points tested relative to control, suggesting that these hydrogels are in no way suitable as a culture system for this cell line. SaOS-2 cells showed slightly higher levels of survivability in both hydrogel

types, no statistically significant difference in viability was observed until days 2 and 3 of culture, with GFOGER encapsulated cells displaying the highest percentage of viable cells, again these results suggest these hydrogel systems are not suitable for SaOS-2 cell culture with significant cell death occurring in short experimental time frames. Research has shown that the presence of different Fmoc-FF functional groups can drastically alter cell viability; an effect that was observed here [268, 333]. These functional groups may also impact cell adhesion [334] and it has been suggested that a reduction in adhesion may directly impact cell viability [333]. Therefore, it is no surprise here that encapsulation in GFOGER sustained cell viability longer than the other tested functionalized hydrogels, and the standard hydrogel. The GFOGER functional group was highlighted as an integrin recognition site in type I and type IV collagen [335], therefore its support of chondrocytes and osteoblasts beyond that of IKVAV, RGD and Standard hydrogels is also not surprising. Despite studies highlighting Fmoc-protected self-assembling peptide hydrogels to be supportive of chondrocyte and osteoblast growth [266, 336], dissolution and degradation of these peptides has been shown to result in necrosis for cells exposed to by-products of this process, showing differential effects between candidate cell lines in a time dependent manner [337]. Additionally, Fmoc-FF peptides have also shown general cytotoxic effects [338].

To remedy these cytotoxic effects, future work would have involved collaborative efforts with Biogelx to optimize these self-assembling peptide hydrogel systems with the aim of creating a product with a composition and stiffness that is suited to the culture of both C-28/I2 chondrocytes and SaOS-2 osteoblasts specifically. However, due to the COVID-19 pandemic and unforeseen circumstances Biogelx went into liquidation and was subsequently dissolved as a commercial entity preventing future collaborative efforts.

This chapter aimed to show proof of concept hydrogel culture systems for future inclusion in co-culture models of OA. The hydrogel system tested were suitable for co-culture model development which was shown in an acellular experiment. Subsequently, the next goal involved the optimisation of RNA extraction, protein extraction, RT-qPCR and immunoblotting which was achieved, however the integrity of the RNA retrieved was suspect. Cell viability of encapsulated cells was considered and presented the next goal of this chapter, overall, the results presented here suggest that the commercially

available Biogelx hydrogel systems are not suitable for C-28/12 or SaOS-2 cell culture as indicated by live/dead staining. Finally, this chapter sought to establish a hydrogel co-culture system that was representative of OA, however due to concerns regarding RNA integrity and cell viability, this model was not established and the scope to optimize this was diminished as Biogelx were liquidated as a commercial entity.

## Chapter 5: Development of an inflammation-based co-culture model of osteoarthritis and investigation of autophagy as a potential therapeutic pathway

### 5.1. Introduction

Osteoarthritis (OA) involves the degradation of the articular cartilaginous matrix which is comprised of a variety of collagenous and non-collagenous proteins, with Type II collagen existing as a key structural molecule that is often impacted directly by disease progression. Research has highlighted the role of inflammatory processes in the destruction of the articular cartilage under the OA phenotype, in addition to mechanical stressors [186, 339].

Currently no validated *in vitro* model of osteoarthritis exists as it is hard to recapitulate the disease under *in vitro* conditions due to the multitude of complex factors that influence the disease and the lack of defined culture conditions that simulate the disease environment. Modelling OA can present a challenge for conventional 2D culture, however, the pathological inflammatory processes that often occur can be recapitulated.

Under physiological conditions, chondrocytes are quiescent and are found in the cartilage slowly turning over the matrix. However, under pathological OA conditions, a variety of factors including cytokines and chemokines have been shown to cause a phenotypic shift in these cells. Cytokines such as tumour necrosis factor alpha (TNF- $\alpha$ ) and interleukin-1 beta (IL-1 $\beta$ ) are two common inflammatory molecules found in OA; increased TNF- $\alpha$  and IL-1 $\beta$  levels have been associated with increased disease severity across a variety of grades of OA disease [340, 341]. These cytokines have been shown to function via induction of further inflammation, or by directly impacting critical collagenous and non-collagenous matrix proteins, including down-regulation of Type II collagen and up-regulation of MMP-13 [342, 343], a collagen type II collagenase. Both IL-1 $\beta$  and TNF- $\alpha$  have been shown to exert their function upon cells via canonical NF- $\kappa$ B signalling and have a synergistic effect on stimulation of this pathway [181, 344]. Notably, TNF- $\alpha$  stimulation of the NF- $\kappa$ B pathway specifically has been shown to inhibit type II collagen expression [343]; additionally, both TNF- $\alpha$  and IL-1 $\beta$  stimulation of this pathway has been shown to drive the upregulation MMP-13 [182, 184, 185]. This

dysregulation of important anabolic and catabolic proteins such as Type II collagen and MMP-13 can cause an imbalance within the cartilaginous matrix leading to an increased degradative phenotype and OA disease progression. Once established, an inflammatory model of OA will have utility for investigating OA related pathways and processes. A variety of pathways have been highlighted as having a role in OA pathogenesis, however the autophagy pathway stands out as its activity has direct links to aging, inflammation and shows potential for regulating many hallmark disease symptoms [197].

Research has shown that even healthy adult chondrocytes constitutively express MMP-13, however, it is endocytosed and degraded by chondrocytes via autophagy, resulting in an amelioration of its degradative effects [345]. Autophagy is a physiological intracellular pathway that is important in cell metabolism. Under abnormal environmental conditions, this pathway plays a protective role via the degradation and recycling of intracellular macromolecules, membranes, and organelles [346]. Basal autophagy levels have been shown to decrease with age resulting in the accumulation of damaged and aged macromolecules and organelles and subsequently, loss of cellular function, senescence, and apoptosis [346, 347]. It has been shown that autophagy can protect cartilage and that levels of autophagy in OA cartilage are decreased [348, 349]. *In vitro*, *in vivo* and *in silico* modelling have highlighted a variety of links between OA, MMP-13 expression, and autophagy; increased MMP-13 expression is associated with a concomitant reduction of LC3-II expression and overall autophagy [350, 351], as well as a decline in lysosome activity and Bcl-2 expression – key indicators of autophagy induction and activity [352]. IL-1 $\beta$  induced MMP-13 gene expression has also been shown to be ameliorated by autophagy induction [353]. As well as MMP-13 modulation, research has shown that ablation of key autophagy genes such as ATG7 impairs collagen type II secretion and ECM formation [354].

It is known that the processes of inflammation and autophagy are interlinked, with TNF- $\alpha$  and IL-1 $\beta$  acting as autophagy inducers [355]. Autophagy is known to directly inhibit the production of both cytokines *in vitro* and *in vivo* [356], and research has shown cytokine-induced NF- $\kappa$ B translocation can be inhibited via autophagy induction using the potent autophagy stimulator rapamycin [357]. Consequently, autophagy may be considered a therapeutic target under OA-associated inflammatory conditions. Many clinically approved autophagy inducing drugs exist such rapamycin and azathioprine.

Azathioprine is an immunomodulatory therapy used in the treatment of Crohn's disease due to its anti-inflammatory effects [358]. However, azathioprine has also shown autophagy modulating activity, and the therapeutic potential of this in the context of OA has yet to be considered, providing a novel candidate for the treatment of OA symptoms.

However, to reliably assess the potential benefit of autophagy modulation, a reliable and robust *in vitro* model of inflammation-driven OA must first be developed in physiologically relevant cells. C-28/I2 cells are determined as a suitable candidate for the development of this model in Chapter 3. Therefore, this chapter aims to create a cytokine-induced OA-like disease model in C-28/I2 cells to investigate the activity of autophagy, and the effect of autophagy modulation on critical matrix proteins including MMP-13 and type II collagen.

## **5.2. Aims and objectives**

### **5.2.1. Aims**

Investigate the activity of autophagy, and the effect of autophagy modulation on critical matrix proteins including MMP-13 and type II collagen in a cytokine-induced OA-like disease model.

### **5.2.2. Objectives**

1. Create an inflammation-based model of OA-associated pathology in C-28/I2 chondrocytes.
2. Determine the impact of inflammation on autophagy activity in C-28/I2 chondrocytes.
3. Investigate the effect of autophagy modulating drugs on the expression of OA-relevant chondrocyte proteins and autophagy associated markers in C-28/I2 chondrocytes.

## **5.3. Methods**

### **5.3.1. Cell culture**

Cells were maintained as detailed in section 2.2.1. Briefly, all cells were maintained in tissue culture flasks and subcultured via trypsinization at 70-80% confluency.

For RT-qPCR and immunoblotting, C-28/I2 cells cultured in 2D were seeded in 6-well cultures dishes at a density of  $5 \times 10^5$  cells per well in 3mL of growth media and incubated for 24 hours at 37°C. For immunostaining experiments C-28/I2 cells were seeded in monolayer culture in 6 well plates containing 13mm coverslips at a density of  $5 \times 10^5$  cells in 3mL growth medium and incubated for 24 hours at 37°C. After 24 hours culture media was switched to differentiation media as per section 2.2.1. for the duration of the experiment. At this stage any required cytokines or autophagy modulating molecules were added (section 5.3.2).

### **5.3.2. Cytokine and drug treatments**

Cytokines were prepared prior to experiments using sterile diluents, aliquoted and stored at -80°C. IL-1 $\beta$  (ThermoFisher Scientific) was reconstituted in 500 $\mu$ L of deionized water and diluted 1:1 in 500 $\mu$ L 1% BSA-PBS to give a stock solution of 3mg/mL. TNF- $\alpha$  (Sigma Aldrich) was reconstituted in 100 $\mu$ L deionized water. Working solutions were created by diluting cytokines in differentiation culture media as per section 5.3.1. Azathioprine, bafilomycin and rapamycin were all reconstituted in DMSO to give stock solutions at concentrations of 100mM, 1mM and 100 $\mu$ M respectively. These compounds were diluted in culture media as per section 5.3.1. to create working solutions of 120 $\mu$ M, 100nM and 27 $\mu$ M. IL-1 $\beta$  and TNF- $\alpha$  were applied at the expected efficacious concentration of 10ng/mL as per previous studies [359–362]

### **5.3.3. RNA extraction**

Cells were washed twice with 3mL ice-cold PBS and scraped on ice in 1mL of ice-cold PBS. Cell suspensions were then spun at 800xg for 5 minutes at 4°C to generate a cell pellet. PBS supernatants were removed, and samples were frozen at -80°C until 3 biological replicates for each experimental condition had been harvested, at which point RNA extraction was conducted as per section 2.5.1.

#### **5.3.4. cDNA synthesis and RT-qPCR**

cDNA was synthesised as per section 2.5.3. and frozen at -20°C for storage. RT-qPCR was conducted on chondrocyte genes *COL2A1* and *MMP-13*. Primer sequences are detailed in Appendix II. RT-qPCR was performed over 3 biological replicates as detailed in section 2.5.4. Data were normalized to the expression of *B2M* and *SHDA* for C-28/I2 cell lines as determined in Chapter 3. Target gene data were analysed as per section 2.5.6. as detailed by Livak and Schmittgen (2001) [270]

#### **5.3.5. Protein extraction and quantification**

Cells were washed twice with 3mL ice-cold PBS and scraped on ice in 1mL of ice-cold PBS. Cell suspensions were then spun at 800xg for 5 minutes at 4°C to generate a cell pellet. PBS supernatants were removed, and samples were frozen at -80°C until 3 biological replicates for each experimental condition had been harvested. Once all biological replicates were acquired, protein was extracted and quantified as per section 2.6.1.

#### **5.3.6. Immunoblotting**

Following quantification of protein concentration in whole cell lysates, samples were loaded onto pre-cast 4-20% gradient Tris-Glycine gels. Immunoblotting was performed as per section 2.6.5 with membranes probed overnight using primary antibodies as detailed in Appendix III. Secondary antibody staining was performed, and proteins visualized using the Licor Odyssey system. (Section 2.6.5 & Appendix III). The expression of a protein of interest was then normalized to  $\beta$ -actin expression. Immunoblotting images were quantified as per section 2.6.6.

#### **5.3.7. Immunofluorescence**

Immunofluorescent staining was conducted as per section 2.10 C-28/I2 coverslips were washed, fixed, for 10 minutes using 4% PFA. Cultures were washed again and permeabilised with 0.2% Triton-X-PBS and washed. Fixed cells were then blocked with 10% FCS-PBS and primary antibodies were diluted in 1% FBS-PBS as detailed in Appendix III and added to fixed cells overnight at 4°C. Cultures were then washed 20 times with

PBS and 20 times with 1% FCS-PBS. Secondary antibodies were diluted in 1% FBS-PBS as detailed in appendix III and incubated for 1 hour at room temperature. Again, cultures were washed 20 times with PBS and 20 times with 1% FCS-PBS. Finally, coverslips were then mounted on slides using Vectashield DAPI mounting medium and sealed using nail varnish. Slides were then imaged using a Zeiss LSCM 880 (Jena, Germany) and ZEN Black software (Zeiss). Images were then processed using ZEN Blue software (Zeiss).

#### **5.3.8. Statistical analysis**

Statistical analysis was performed using GraphPad Prism 9.3.0 (GraphPad Software, USA) as per section 2.11.

## 5.4. Results

### 5.4.1. Development of a cytokine-based inflammation model in C-28/I2 chondrocytes

#### 5.4.1.1. The effect of 24 hour cytokine treatment on C-28/I2 morphology

C-28/I2 cells were treated with a combination of TNF- $\alpha$  (10ng/mL) and IL-1 $\beta$  (10ng/mL) for 0, 1 and 24 hours and assessed using light microscopy. No morphological changes were observed under cytokine treatments for these time periods (**Figure 5.1**).

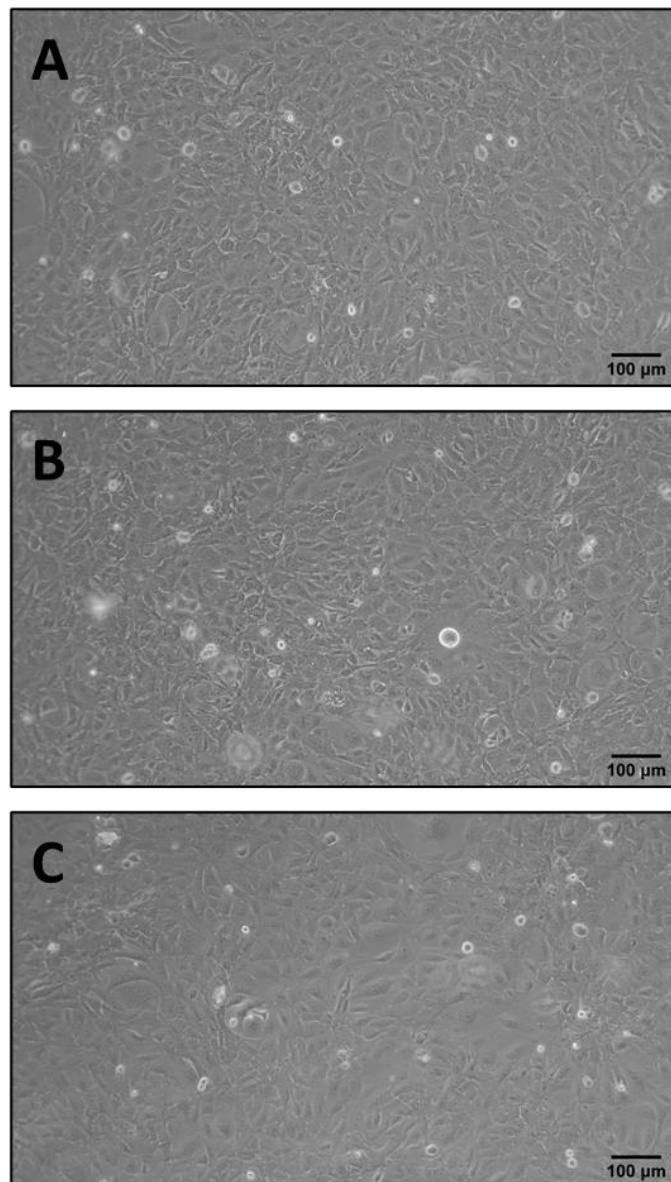


**Figure 5.1. Cytokine treatment does not impact C-28/I2 cell morphology.** Cells were treated with TNF- $\alpha$  (10ng/mL) and IL-1 $\beta$  (10ng/mL) for 0, 1 and 24 hours (A-C). Cells were cultured for 0 hours (A), 1 hours (B) and 24 hours (C) in the presence of a combined treatment of 10ng/mL TNF- $\alpha$  and IL-1 $\beta$ . Images shown are taken at 10X magnification, scale bars represent 100 $\mu$ m.

#### 5.4.1.2. Nuclear Factor Kappa B activation in response to 24 hour cytokine treatment on C-28/I2 chondrocytes

To assess the inflammatory response, C-28/I2 cells were treated with a combination of TNF- $\alpha$  and IL-1 $\beta$ , and translocation of the P65 cellular subunit of the NF- $\kappa$ B pathway was assessed using immunofluorescence. Following 1 hour of cytokine treatment, clear translocation of the P65 subunit was observed, moving from a predominantly cytoplasmic location with little nuclear staining, to a predominantly nuclear location (Figure. 5.2, compare panels i and ii) indicating the inflammatory response is being activated. 24 hours post-cytokine treatment, P65 returned to a predominantly cytoplasmic location with some residual nuclear staining (Figure 5.2, panel iii).

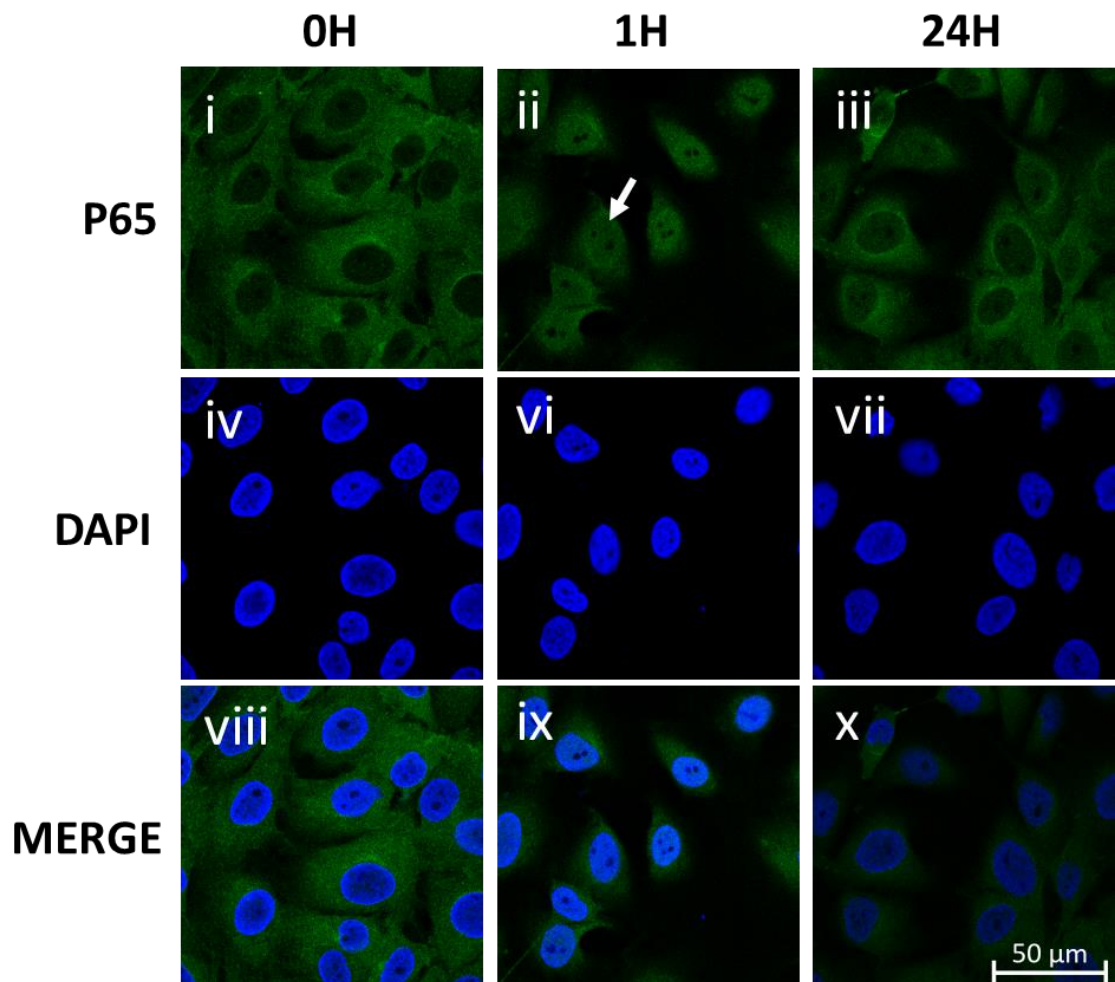


**Figure 5.2. Cytokine treatment drives rapid P65 translocation in C-28/I2 cells.** Translocation of P65 cellular subunit in C-28/I2 chondrocytes treated with pro-inflammatory cytokines over 24 hours. C-28 cells were treated with TNF- $\alpha$  (10ng/mL) and IL-1 $\beta$  (10ng/mL) for 0, 1 and 24 hours (i-x). Cytokine treated cells showed translocation of p65 from the cell cytoplasm to the nucleus after 1 hour (compare i and ii)

confirmed via immunofluorescence. This process was seen to be partially reversed 24 hours post-treatment, although some P65 is still present in the nucleus of treated cells. Images were taken at 63X magnification, and the scale bar represents 50µm. Data shown is representative of n=1.

#### 5.4.1.3. The impact of 24 hour cytokine treatment on Matrix Metalloproteinase 13 gene expression in C-28/I2 chondrocytes

RT-qPCR was used to assess the effects of 24 hours of inflammatory stimulation on the chondrocyte phenotype of in C-28/I2 chondrocytes treated with a combination of TNF- $\alpha$  and IL-1 $\beta$  (Figure 5.3). Results show treatment with TNF- $\alpha$  and IL-1 $\beta$  modestly increased MMP-13 expression between the control sample (0 hours) and 1 hour post-treatment. This effect is lost 24 hours post-treatment when a slight reduction in MMP-13 expression is observed compared to control and 1-hour treatments.

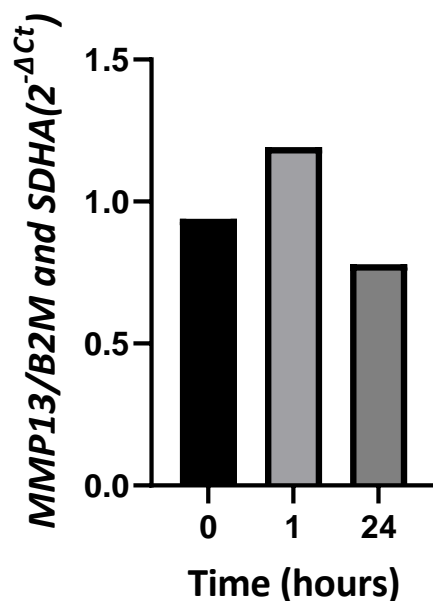


**Figure 5.3 Cytokine treatment induces MMP-13 gene expression in C-28/I2 cells over a 24 hour time period.** C-28/I2 cells were treated with TNF- $\alpha$  (10ng/mL) and IL-1 $\beta$  (10ng/mL) for 0, 1 and 24 hours. MMP-13 levels were assessed using RT-qPCR on cDNA collected from C-28/I2 cells treated with TNF- $\alpha$  (10ng/mL) and IL-1 $\beta$  (10ng/mL) for 0, 1 and 24 hours. Data is presented as  $2^{-\Delta Ct}$  showing normalised changes in MMP-13 expression. Data shown represents n=1.

#### 5.4.1.4. The impact of 24 hour cytokine treatment on Matrix Metalloproteinase 13 protein expression in C-28/I2 chondrocytes

Expression of MMP-13 protein expression was analysed using immunoblotting and densitometry in C-28/I2 chondrocytes treated with a combination of TNF- $\alpha$  and IL-1 $\beta$ . Results show that MMP-13 expression increased as a function of time (Figure 5.4A, compare lanes 2 and 4) and quantified in Figure 5.4B.

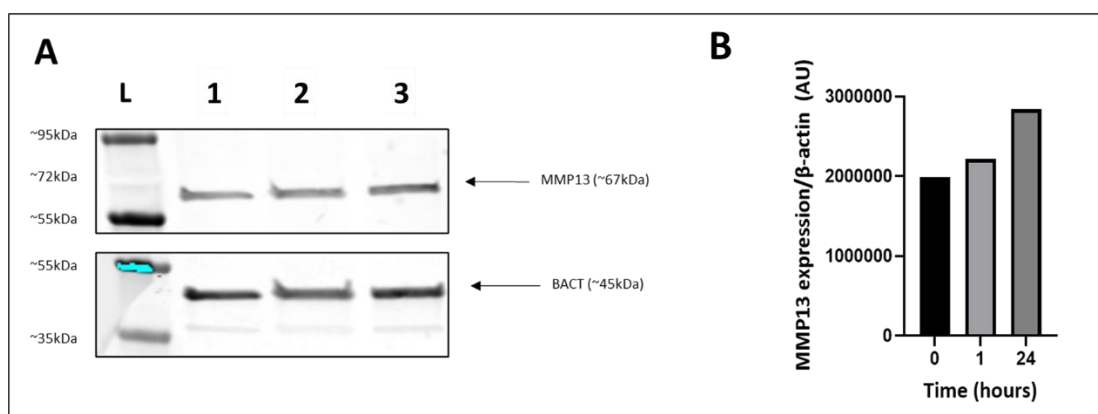


**Figure 5.4. Cytokine treatment induces MMP-13 protein expression in C-28/I2 cells over a 24 hour time period.** C-28/I2 cells were treated with TNF- $\alpha$  (10ng/mL) and IL-1 $\beta$  (10ng/mL) for 0, 1 and 24 hours. MMP-13 was detected and analysed via immunoblotting (A). Lanes are represented by (L) ladder, (1) 0 hours, (2) 1 hour, (3) 24 hours. Densitometry was conducted relative to  $\beta$ -actin expression (B). Data shown represents n=1.

#### 5.4.2. 48 hour time course analysis of cytokine-induced inflammation in C-28/I2 chondrocytes

Previous results showed that 24 hours post-cytokine treatment, P65 returned to a predominantly cytoplasmic location with some residual nuclear staining (Figure 5.2), suggesting that the inflammatory signal was not being sustained. Therefore, a more detailed time course was required to determine when this reversal of P65 translocation occurred within the 24-hour time period.

##### 5.4.2.1. The effect of cytokine treatment on C-28/I2 morphology over a 48 hour time course

C-28/I2 cells were treated with a combination of TNF- $\alpha$  and IL-1 $\beta$  over a time course of 0 to 48 hours (Figure 5.5) and cell morphology was assessed using light microscopy.

Wells became more confluent over time; however no distinct morphological changes were observed under cytokine treatments over the 48-hour time course.

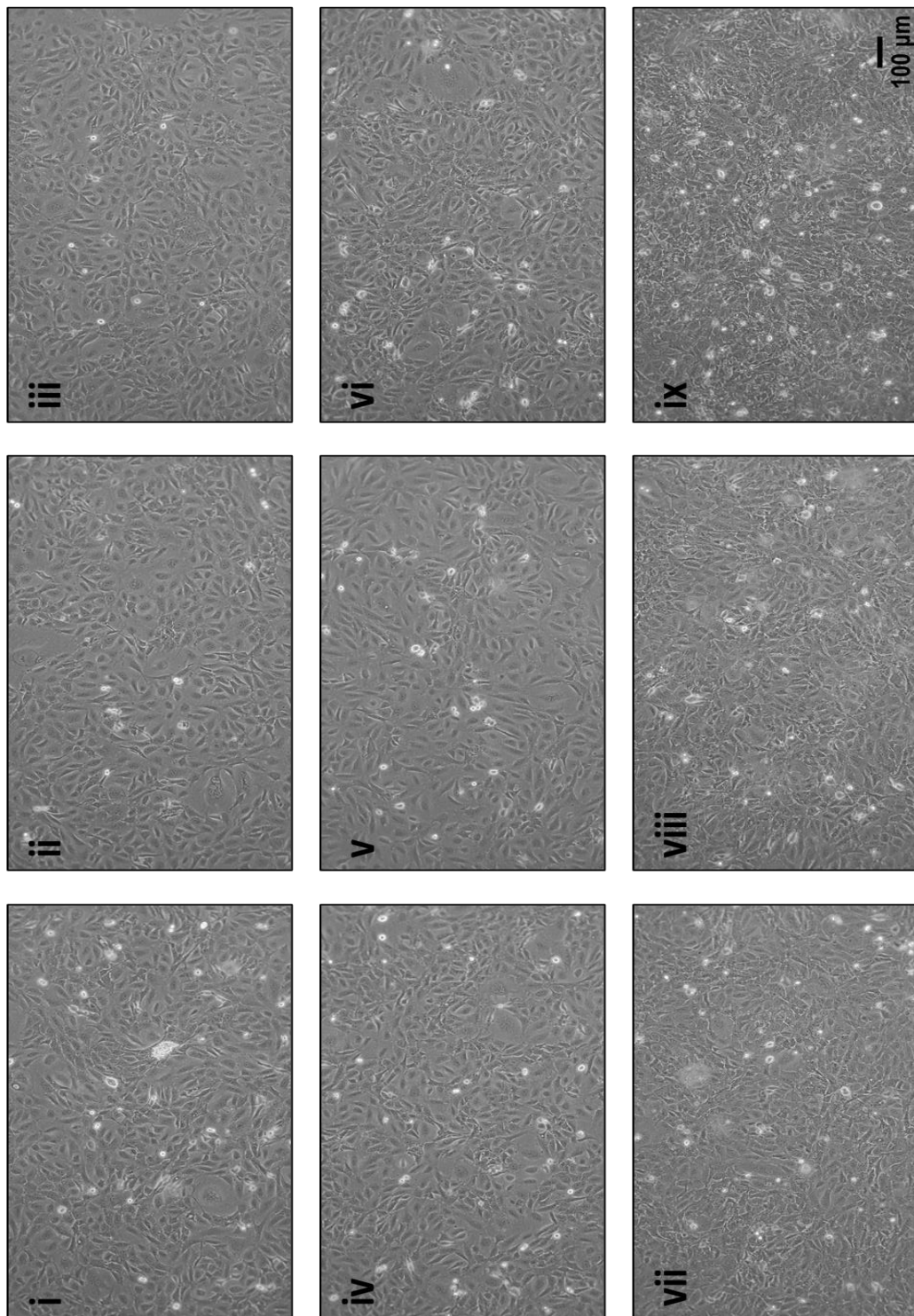


**Figure 5.5. Cytokine treatment does not influence morphology of C-28/I2 over a 48 hour culture period.** C-28/I2 cells were treated with TNF- $\alpha$  (10ng/mL) and IL-1 $\beta$  (10ng/mL) from 0 to 48 hours (i-ix) Cells were cultured for 0 hours (i), 1 hours (ii), 2 hours (iii), 4 hours (iv), 6 hours (v), 8 hours (vi), 24 hours (vii), 32 hours (viii) and 48 hours (ix) in the presence of a combination of 10ng/mL TNF- $\alpha$  and IL-1 $\beta$ . Images shown are taken at 10X magnification, scale bars represent 100 $\mu$ m.

#### **5.4.2.2. Nuclear Factor Kappa B activation in C-28/I2 cells treated with Tumour Necrosis Factor- $\alpha$ and Interleukin-1 $\beta$ over a 48 hour time course**

C-28/I2 cells were incubated with TNF- $\alpha$  and IL-1 $\beta$  over 48 hours and P65 cellular location was assessed over this time via immunofluorescence. Cellular location was split into 3 different compartments: cytoplasmic, nuclear, and intermediate (a combination of cytoplasmic and nuclear staining); this provides a clear indication of the localisation of p65 under inflammatory conditions. Upon stimulation with cytokines, almost all P65 translocated and was no longer exclusively located in the cell cytoplasm (Figure 5.6A panels i – ix & Figure 5.6B), a significant effect which lasted over the duration of the experiment as confirmed by a one-way ANOVA ( $P < 0.0001$ ). Further analysis revealed that at 1- and 2-hour timepoints, 60% and 65% of P65 was exclusively nuclear (Figure 5.6A panels ii - iii & Figure 5.6C), and these values were significantly higher than 0-hour controls confirmed via a one-way ANOVA ( $p < 0.05$ ). No other time point expressed significantly higher levels of exclusively nuclear P65 than controls. Consideration of intermediate staining revealed that 4-hour time points expressed this phenotype at a significantly higher level ( $P < 0.01$ ). Additionally, 6, 8-, 24-, 32- and 48-hour time points also expressed significantly higher levels of intermediate staining compared to controls (Figure 5.6A panels v-ix & Figure 5.6D), confirmed via one-way ANOVA ( $P < 0.001$ ). Overall, cytokine treatment induced translocation from being exclusively cytoplasmic to a combination of cytoplasmic, nuclear, and intermediate after 1 hour, with stained cells showing predominantly nuclear/intermediate localization through the 2-hour time point where some exclusively cytoplasmic staining could also be observed. At 4 and 6 hours P65 staining shifted predominantly to the intermediate phenotype with some exclusively cytoplasmic staining observed across later time points.

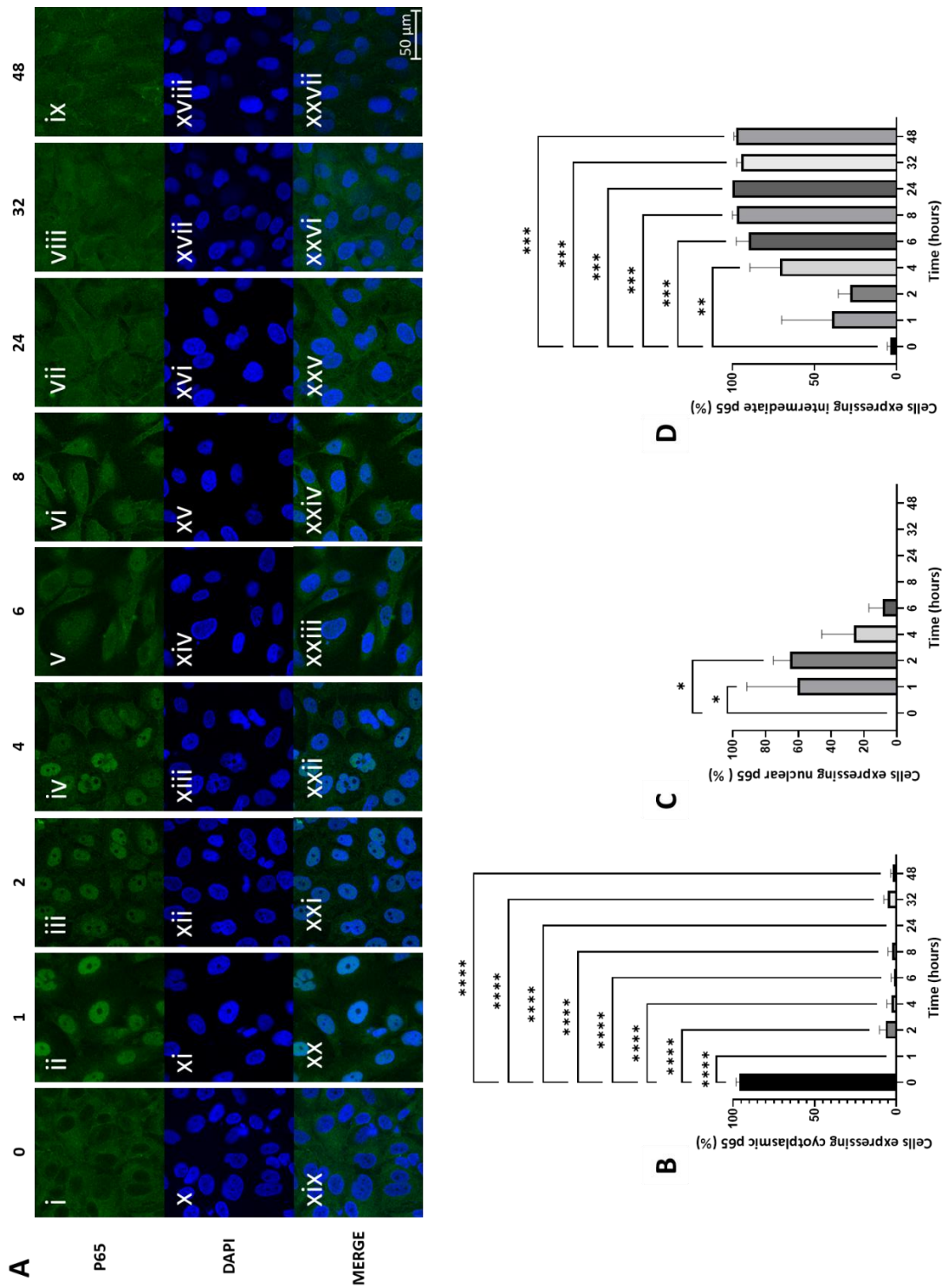


**Figure 5.6. Cytokines induce partially-reversible translocation of P65 in C-28/I2 cells cultured over a 48 hour time period.** Cells were treated with TNF- $\alpha$  (10ng/mL) and IL-1 $\beta$  (10ng/mL) for 0 to 48 hours and translocation of the p65 subunit was determined via immunofluorescence. Treatment time (in hours) is indicated in panel A above each image column. The cellular location of P65 was split into 3 different compartments: (B) cytoplasmic, (C) nuclear, and (D) intermediate (a combination of cytoplasmic and nuclear staining) and cell nuclei were stained with DAPI. Cytokine treatment resulted in almost all P65 translocating to nuclear or intermediate compartments (Figure 5.6A panels i – ix & Figure 5.6B), a significant effect which lasted over the duration of the experiment as confirmed by a one-way ANOVA

( $P < 0.0001$ ) Significantly higher levels of nuclear p65 can be seen 1 and 2 hours post treatment compared to 0 hour controls (Figure 5.6A panels ii - iii & Figure 5.6C) confirmed by one-way ANOVA ( $p < 0.05$ ). Intermediate staining was found to be significantly higher 4-hours post-cytokine treatment ( $p < 0.01$ ), as well as 6, 8-, 24-, 32- and 48-hours post-treatment (Figure 5.6A panels v-ix & Figure 5.6D), confirmed via one-way ANOVA ( $P < 0.001$ ). Images were taken at 63X magnification and scale bars represent 50 $\mu$ m. Data shown is representative of  $n=3$ . Statistical significance is denoted by: \*\*\*\* =  $p < 0.0001$ , \*\*\* =  $p < 0.0005$ , \*\* =  $p < 0.01$ , \* =  $p < 0.05$ .

#### **5.4.2.3. The impact of cytokine treatment on gene expression associated with the chondrocyte phenotype over a 48 hour timecourse**

C-28/12 cells were incubated with TNF- $\alpha$  and IL-1 $\beta$  over 48 hours and the expression of chondrocyte-associated genes was assessed at regular intervals. A one-way ANOVA on Analysis of RT-qPCR data revealed that expression of MMP-13 was significantly higher when comparing 0-hour controls to 4 ( $P < 0.05$ ), 6 ( $P < 0.001$ ) and 8 ( $P < 0.0001$ ) hour treatments (Figure 5.7A). Further one-way ANOVA analysis comparing 4- and 8-hour time points revealed that 8-hour MMP-13 levels were significantly higher than 4 hours ( $P < 0.01$ ). No statistically significant effect was seen for COL2A1 expression over the timecourse; however, a downward trend can be observed. (Figure 5.8B).

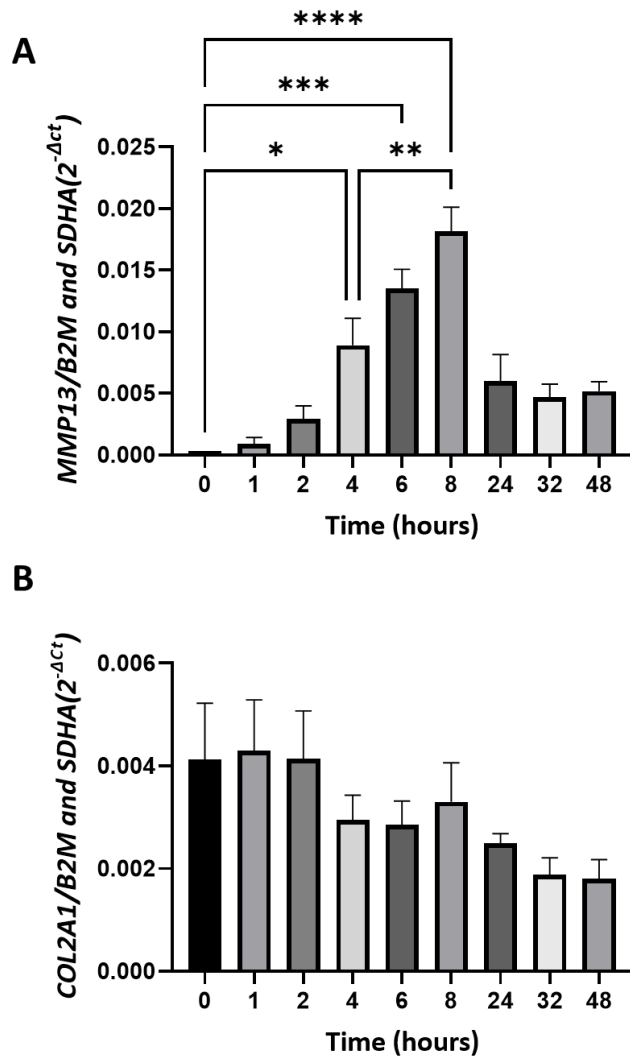


**Figure 5.7. Cytokine treatment drives expression of the catabolic MMP-13 in a time dependent manner in C-28/I2 cells cultured over 48 hours.** Cells were treated with TNF- $\alpha$  (10ng/mL) and IL-1 $\beta$  (10ng/mL) for 0 to 48 hours and levels of (A) MMP-13 and (B) COL2A1 expression were assessed via RT-qPCR. One-way ANOVA revealed that MMP-13 expression was significantly higher when comparing 0-hour controls to 4- (P=<0.05), 6- (P=<0.001) and 8- (P=<0.0001) hour cytokine treatments. Additionally, MMP-13 expression at 8 hours was higher than at 4 hours post-treatment (P=<0.0001). Data is presented as 2<sup>- $\Delta$ Ct</sup> mean values  $\pm$  SEM showing normalized changes in the expression of target genes. Results were obtained from a dataset of n=3. Statistical significance is denoted by: \*\*\*\* = p<0.0001, \*\*\* = p<0.0005, \*\* = p <0.01, \* = p<0.05.

#### **5.4.2.4. Expression of chondrocyte and apoptosis associated proteins in C-28/I2 cells treated with Tumour Necrosis Factor- $\alpha$ and Interleukin-1 $\beta$ over a time course of 0 to 48 hours**

Expression of a proteolytically processed form of PARP (cleaved PARP), which is indicative of caspase activation and the induction of apoptosis, together with MMP-13 and COL2A1 protein was analysed using immunoblotting and densitometry in C-28/I2 chondrocytes treated with a combination of TNF- $\alpha$  and IL-1 $\beta$  over a time course of 48 hours. A low, but stable level of cleaved PARP expression was observed up to 2 hours (Figure 5.8A lanes, 1-2), before sharply increasing at 4 hours (Figure 5.8A, lane 3), and then reducing slightly between 6 and 24 hours (Figure 5.8A, lanes 4-7). Cleaved PARP expression increased sharply again at 32 hours and 48 hours (Figure 5.8A, lanes 8 and 9). MMP-13 expression shows little change between 0 and 6-hour time points (Figure 5.8C, lanes 1-5), however, the expression did increase at 8, 24, and 32 hours plateauing at 48 hours (Figure 5.8C, lanes 6-9). Expression of COL2 $\alpha$ 1 was observed to drop over 0 to 4 hours (Figure 5E, lanes 0-3) and slightly increased as a function of time between 6 to 24 hours, dropping off slightly at 32 hours and stabilizing again at 48 hours (Figure 5.8E, lanes 4-9).

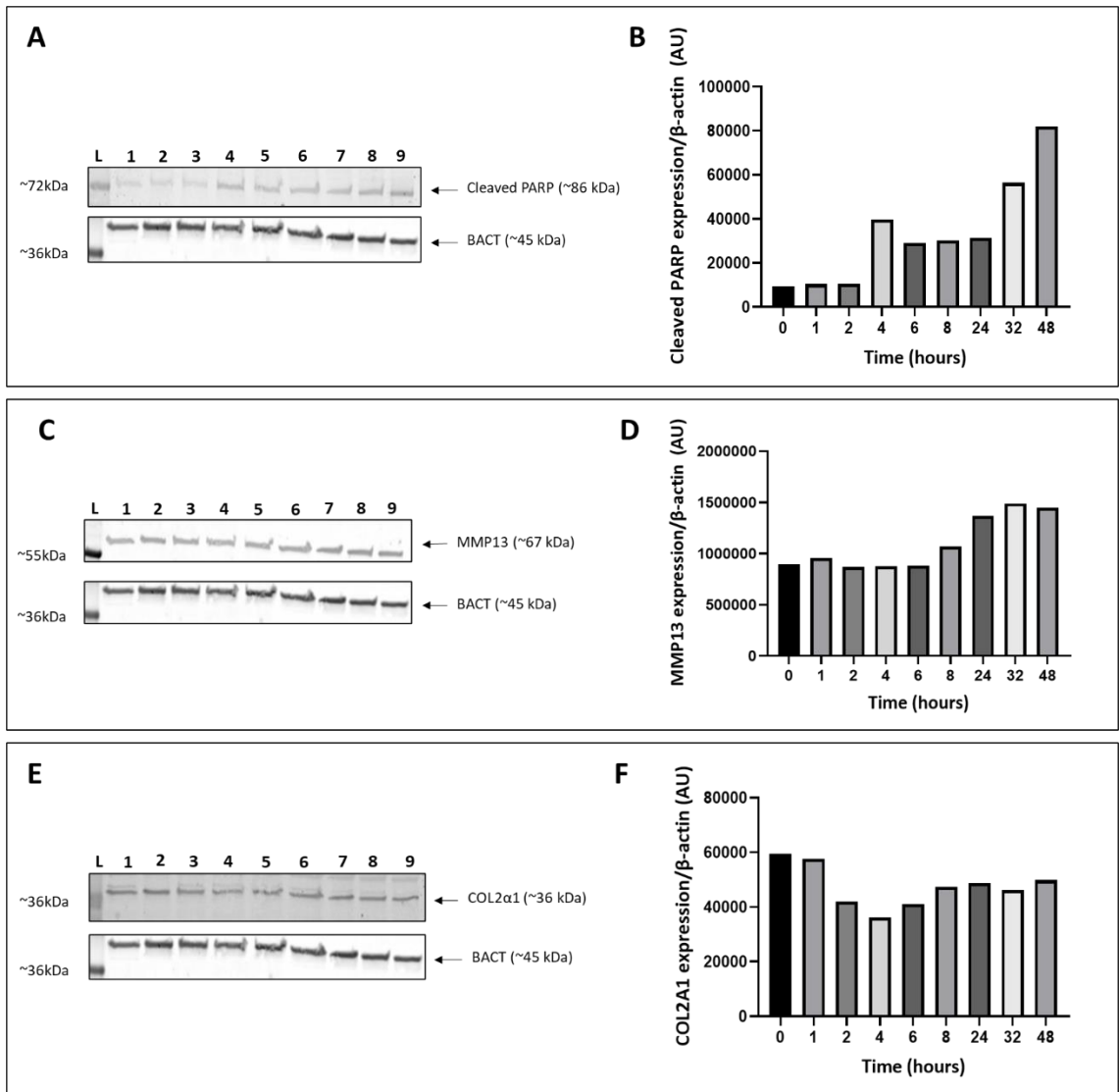


**Figure 5.8. Cytokine treatment induces the expression of catabolic and apoptotic proteins in C-28/I2 cells over a 48 hour time course.** Cells were treated with TNF- $\alpha$  (10ng/mL) and IL-1 $\beta$  (10ng/mL) for up to 48 hours. Protein levels of cleaved PARP (A), MMP-13 (C) and COL2 $\alpha$ 1 (E) were detected and analysed via immunoblotting. Lanes are represented by (L) ladder (1) 0 hours, (2) 1 hour, (3) 2 hours, (4) 4 hours (5) 6 hours, (6) 8 hours, (7) 24 hours, (8) 32 hours, (9) 48 hours. Densitometry was conducted relative to  $\beta$ -actin expression for Cleaved PARP (B), MMP-13 (D) and COL2A1 (E). The data shown represents n=3. Densitometry was performed on one replicate representative of the dataset.

#### **5.4.2.5. Induction of autophagy in C-28/I2 cells treated with Tumour Necrosis Factor- $\alpha$ and Interleukin-1 $\beta$ over a time course of 0 to 48 hours**

C-28/I2 cells treated with a combination of TNF- $\alpha$  and IL-1 $\beta$  were immunostained to assess the impact of these cytokines on autophagy induction over a time course of 48 hours (Figure 5.9). Autophagy induction was confirmed via the accumulation of LC3 puncta. Statistical analysis using a one-way ANOVA revealed that 6 hours of cytokine treatment induced autophagy to a significant level compared to 0-hour controls (Figure 5.9A, compare panels i and v) ( $P < 0.05$ ). A statistically significant effect was also observed when comparing 0-hour controls to 24-hour bafilomycin treatments (Figure 5.9A, compare panels i and x) ( $P < 0.0001$ ). Together these results suggest that there is an induction in autophagy with TNF- $\alpha$  and IL-1 $\beta$  treatment in C-28/I2 cells.

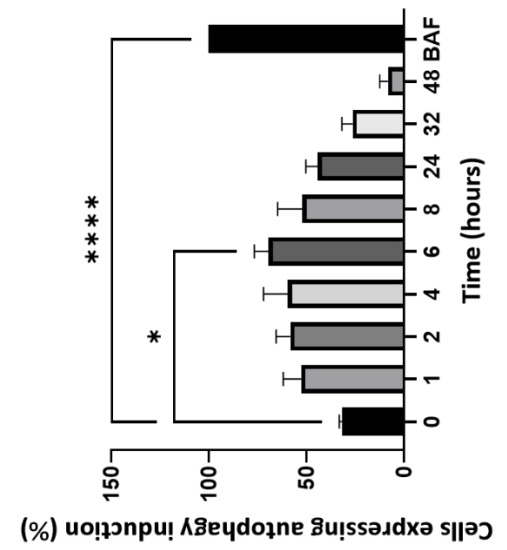
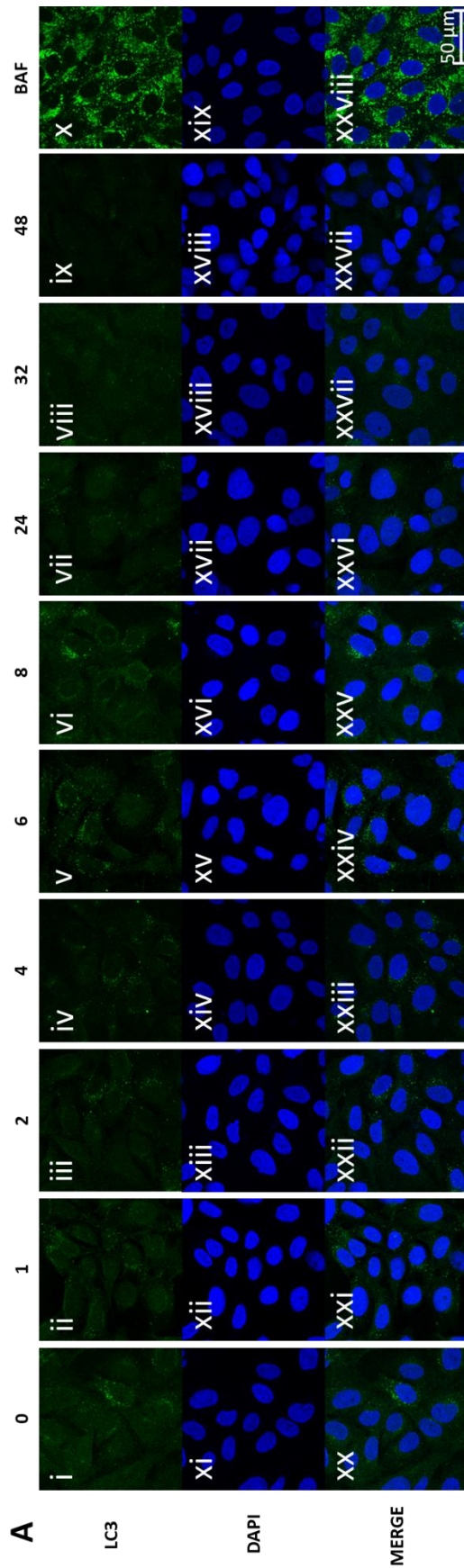


**Figure 5.9. Autophagy is induced in a time dependent manner in response to cytokine treatment in C-28/12 cells over a 48 hour culture period.** Cells were treated with TNF- $\alpha$  (10ng/mL) and IL-1 $\beta$  (10ng/mL) for up to 48 hours (A-B). The effect of cytokine treatment on autophagy was assessed via

immunofluorescent staining of LC3 puncta (A, panels i-x), an indicator of autophagy induction. Panel lanes (A) represent time in hours. BAF = bafilomycin (160nm) treated cells, a positive control for LC3 staining. Cell nuclei were stained with DAPI. Images were taken at 63X magnification and scale bars represent 50µm. The data shown is representative of n=3. Statistical significance is denoted by: \*\*\*\* =  $p < 0.0001$  and \* =  $p < 0.05$ .

### 5.4.3. The effect of drug induced autophagy induction on C-28/I2 cells

#### 5.4.3.1. The effect of autophagy induction on C-28/I2 cell morphology

To examine the potential therapeutic effects of the autophagy inducers rapamycin and azathioprine, cells were treated with these drugs for 8 and 24 hours. Light microscopy was performed on untreated cells, as well as cells treated with rapamycin and azathioprine for both 8 and 24 hours (Figure 5.10). No distinct morphological differences were observed between conditions.

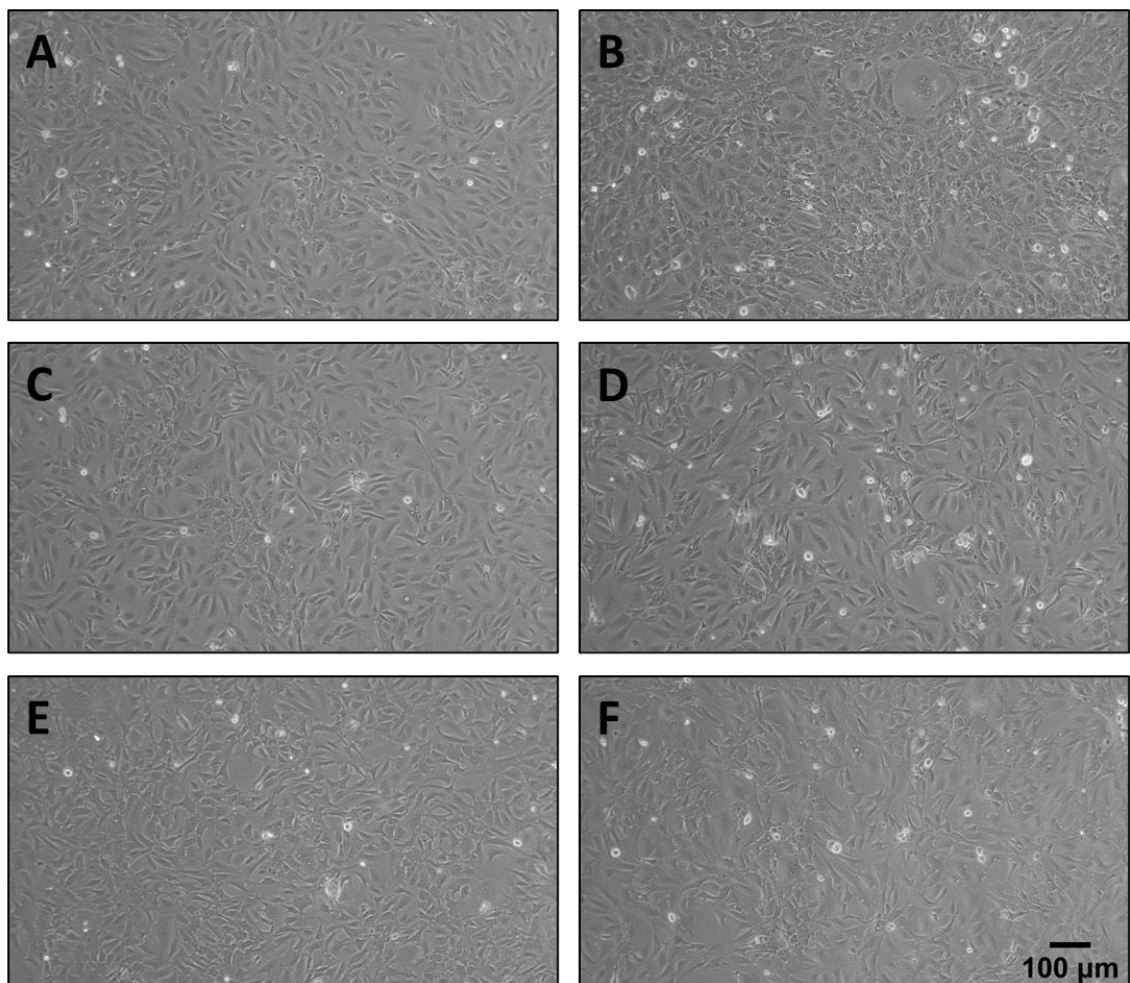


**Figure 5.10 Autophagy inducing drugs do not impact C-28/I2 cell morphology.** Cells were cultured under a variety of conditions (A) 8 hours untreated, (C), 8 hours rapamycin (27µM) (E), 8 hours azathioprine

(120 $\mu$ M) and (B) 24 hours untreated, (D) 24 hours rapamycin (27 $\mu$ m), (F) 24 hours azathioprine (120 $\mu$ m). Cell morphology was assessed via light microscopy. Images shown are taken at 10X magnification, scale bars represent 100 $\mu$ m.

#### **5.4.3.2. The impacts of azathioprine and rapamycin on autophagy induction in C-28/I2 cells**

LC3 immunostaining was conducted on cells treated with rapamycin and azathioprine for both 8 and 24 hours. After 8 hours of rapamycin treatment, autophagy is induced to a level higher than that found in controls, confirmed by one-way ANOVA ( $P < 0.01$ ). A similar effect was seen after 24 hours of rapamycin treatment ( $P < 0.05$ ). Azathioprine had no effect on the induction of autophagy at both time points. This suggests that C-28/I2 cells are susceptible to autophagy induction via the potent autophagy inducing drug rapamycin, an effect which is sustained for up to 24 hours. Additionally, rapamycin stimulates autophagy to a greater extent than azathioprine.

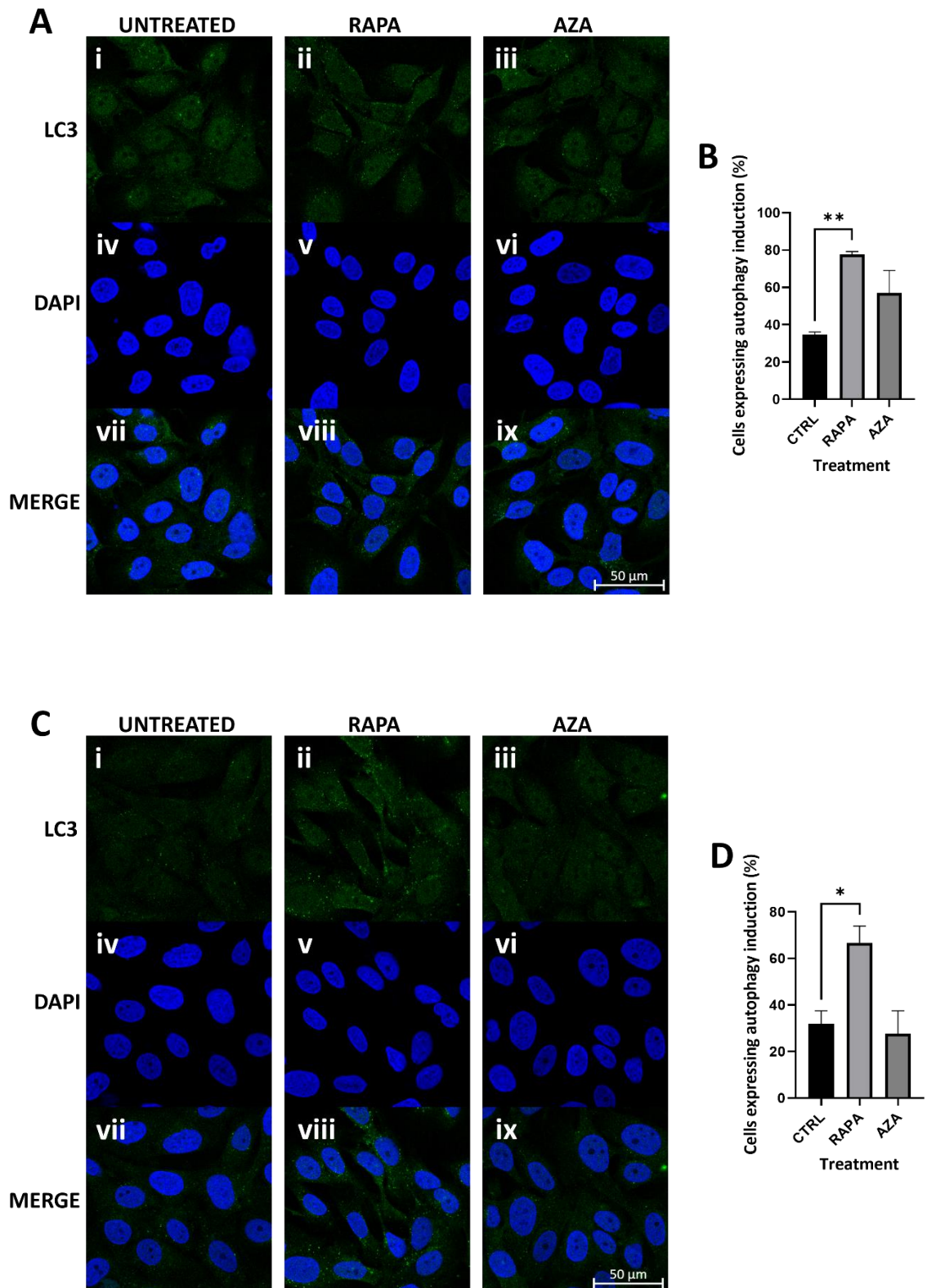


**Figure 5.11 Rapamycin induces autophagy in C-28/I2 cells 8 and 24 hours post-treatment.** Autophagy induction was assessed in cells treated with rapamycin (27 $\mu$ M) and azathioprine (120 $\mu$ M) for 8 (A-B) and 24 hours (C-D). Induction of autophagy was confirmed via analysis of the accumulation of LC3 puncta. Cells were counterstained with DAPI. Images were taken at 63X magnification and scale bars represent 50 $\mu$ m. Data shown is representative of n=3.

#### 5.4.3.3. Analysis of chondrocyte associated gene expression by C-28/I2 cells treated with rapamycin and azathioprine for 8 and 24 hours.

C-28/I2 cells were treated with rapamycin and azathioprine for 8 and 24 hours. RNA was harvested, cDNA synthesised, and RT-qPCR was performed. Analysis revealed that there were no statistically significant differences in levels of MMP-13 or COL2A1 compared to untreated controls when cells were treated with rapamycin or azathioprine for 8 or 24 hours. Suggesting that administration of these drugs does not influence the expression of disease associated genes under physiological conditions.

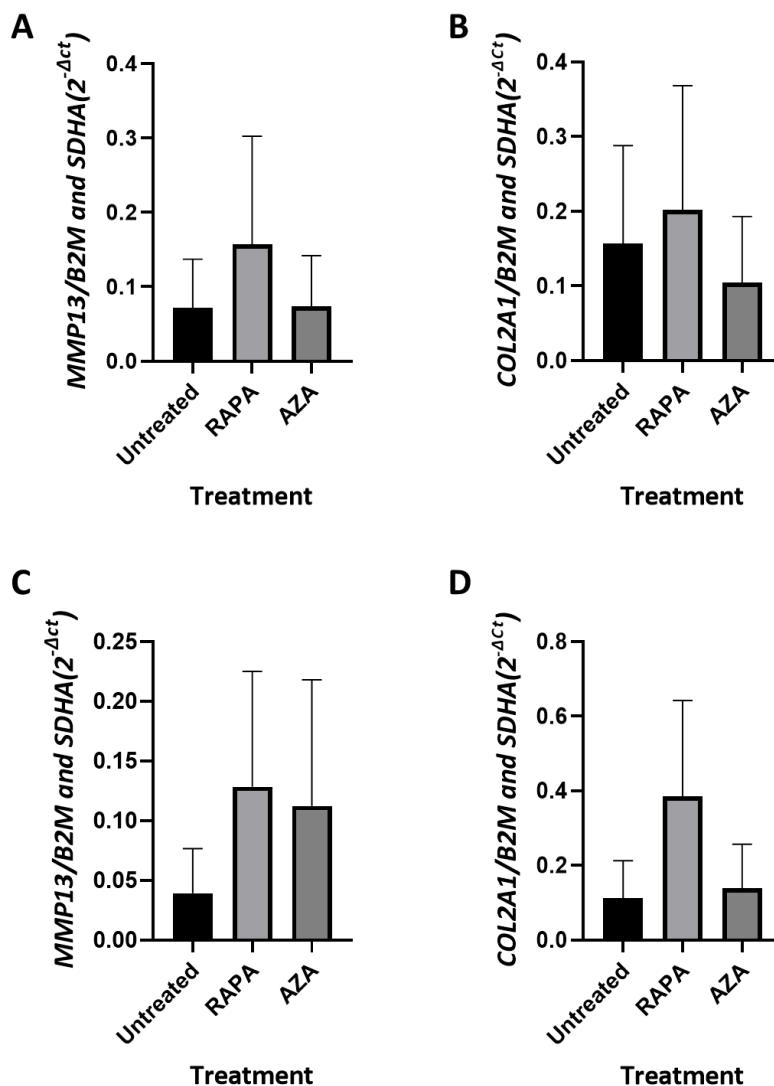
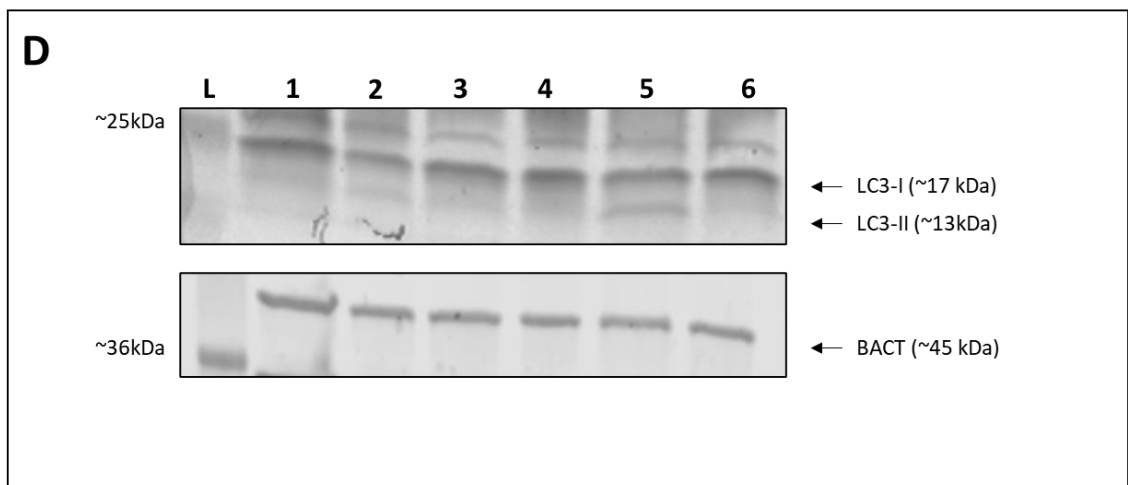
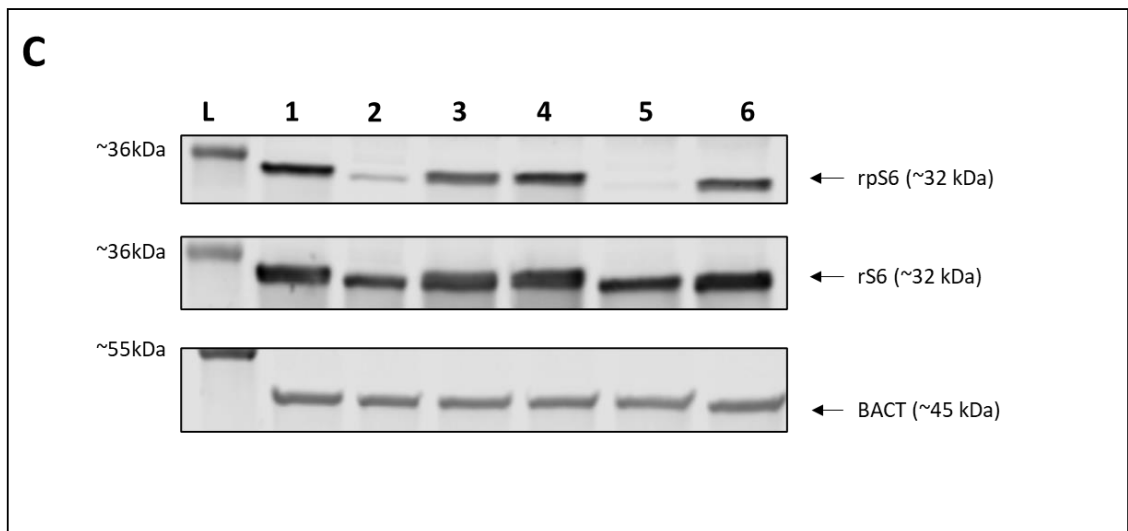
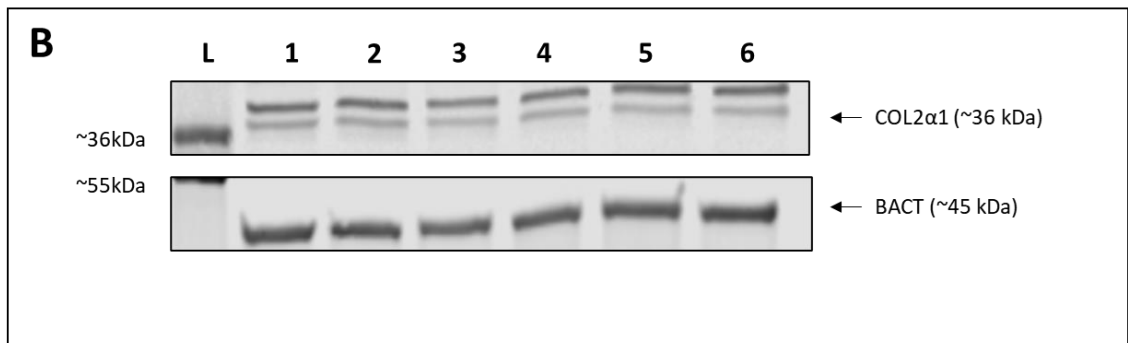
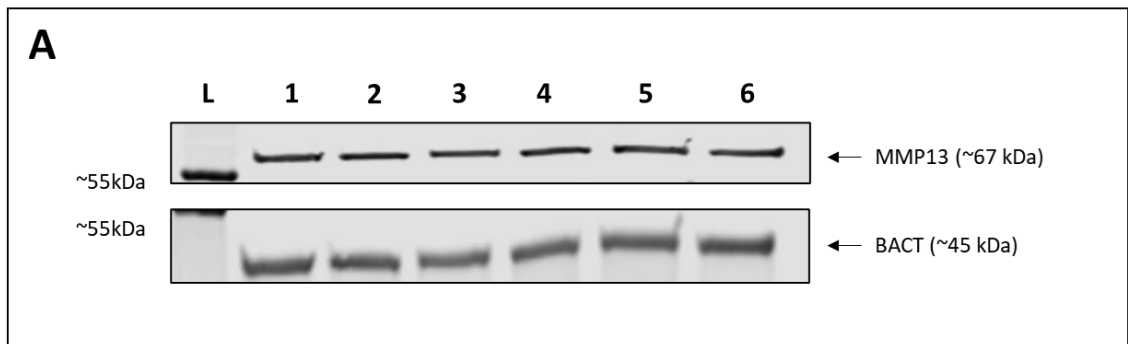


Figure 5.12. Autophagy inducing drugs have no effect on the expression of chondrocyte associated genes in C-28/I2 cells. C-28/I2 cells were treated with rapamycin (27 $\mu$ M) and azathioprine (120 $\mu$ M) for 8 and 24 hours (A-D). RT-qPCR was performed to assess the impacts of these drugs on the

expression of genes associated with the chondrocyte phenotype (A) 8 hours post-treatment MMP-13 expression (B) 8 hours post-treatment COL2A1 expression, (C) 24 hours post-treatment MMP-13 expression, (D) 24 hours COL2A1 expression. Data is presented as  $2^{-\Delta Ct}$  mean values  $\pm$  SEM showing normalized changes in the expression of target genes. Results were obtained from a dataset of n=3.

#### **5.4.3.4. Analysis of chondrocyte and autophagy associated protein expression by C-28/I2 cells treated with rapamycin and azathioprine for 8 and 24 hours.**

Expression of chondrocyte and autophagy related proteins were assessed in C-28/I2 cells treated with rapamycin and azathioprine. MMP-13 expression was found to be stable at the 8-hour time point for all treatments (**Figure 5.13A** lanes 1-3 & **Figure 5.13E**). 24 hours post-treatment MMP-13 expression dropped slightly in both rapamycin and azathioprine treatments (**Figure 5.13A** compare lane 4 to lanes 5 and 6, & **Figure 5.13F**). Collagen II remained stable at 8 hours between control and rapamycin treatments (**Figure 5.13B** lanes 1 and 2, & **Figure 5.13G**), however azathioprine induced a slight drop in expression (**Figure 5.13B** compare lane 1 to lane 3 & **Figure 5.13G**). After 24 hours, both rapamycin and azathioprine caused a drop in COL2 $\alpha$ 1 expression (**Figure 5.13B** compare lane 4 to lanes 5 and 6, & **Figure 5.13H**), with rapamycin showing the lowest levels of COL2 $\alpha$ 1 expression. Regarding autophagy related proteins, the mTORC1 subunit rS6 and levels of its phosphorylation (rpS6) were assessed, additionally, the levels of LC3-I to LC3-II conversion were assessed to confirm the downstream effects of mTORC1 manipulation. Rapamycin and azathioprine were shown to reduce phosphorylation of S6 compared to control with rapamycin having a more profound effect, this pattern was observed across both 8- hour (**Figure 5.13C** compare lane 1 to 2 and 3 & **Figure 5.13I**) and 24-hour (**Figure 5.13C** compare lane 4 and 5 to 6, & **5.13J**) time points. Conversion of LC3-I to LC3-II presented the same observable trend between 8-hour (**Figure 5.13D** compare lane 1 to 2 and 3, & **Figure 5.13K**) and 24-hour (**Figure 5.13D** compare lane 4 to 5 and 6, & **Figure 5.13L**) timepoints; conversion levels were comparable between control and azathioprine treatments, however rapamycin increased LC3 conversion.



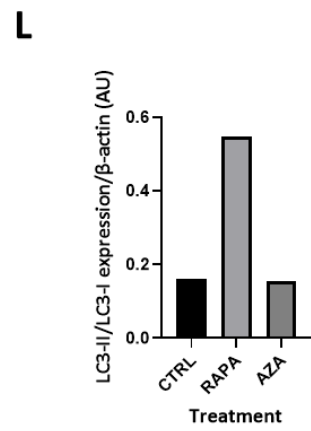
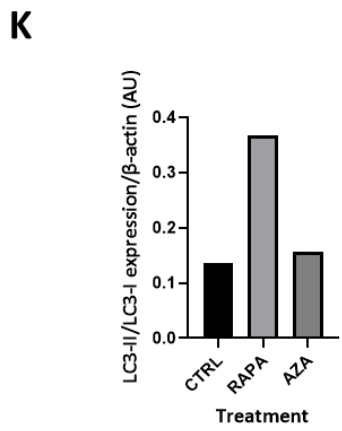
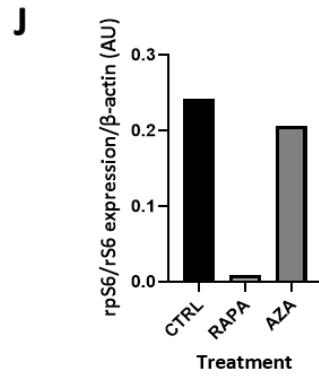
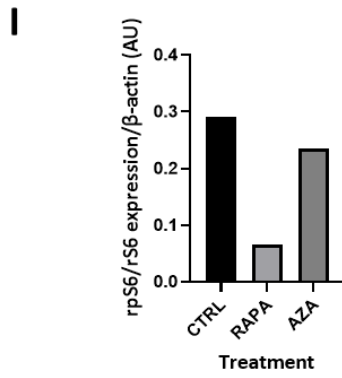
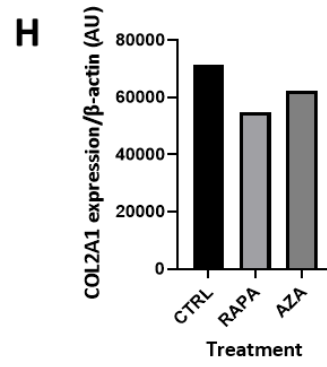
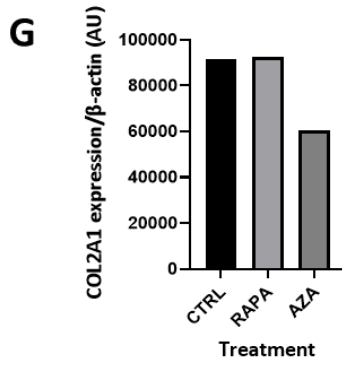
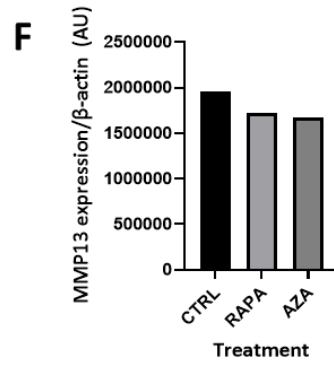
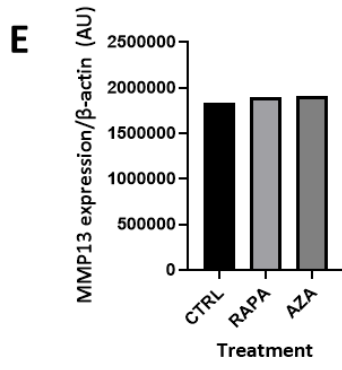


**Figure 5.13. Rapamycin alters the expression of chondrocyte associated proteins and induces the expression of proteins associated with mTOR inhibition and autophagy in a time dependent manner.** Analysis of chondrocyte and autophagy-associated protein expression by C-28/I2 cells treated with rapamycin and azathioprine for 8 and 24 hours (A-L). C-28/I2 cells were treated with rapamycin (27 $\mu$ M) and azathioprine (120 $\mu$ M), and protein expression was assessed via immunoblotting. Immunoblotting (A-D) lanes are represented by (L) ladder, (1) 8-hour untreated control, (2) 8-hour rapamycin treatment, (3) 8-hour azathioprine treatment, (4) 24-hour untreated control, (5) 24-hour rapamycin treatment and (6) 24-hour azathioprine treatment. The data shown represents n=2. Densitometry was conducted on one replicate representative of the dataset (E-L).

## 5.5. Discussion

This chapter aimed to create a 2D, *in vitro*, inflammation-based model of OA-associated pathology and to determine whether inflammation drives the induction of autophagy in this model, thus identifying autophagy as a potential therapeutic target for OA.

Initial experiments assessed the impact of TNF- $\alpha$  and IL-1 $\beta$  on the expression of disease-relevant protein MMP-13 [340, 341], as well as the ability of these cytokines to activate the pro-inflammatory NF- $\kappa$ B pathway, as indicated by P65 translocation. Activation of the NF- $\kappa$ B pathway has been shown to contribute to disease pathology including the upregulation of MMP-13 [184]. Therefore, short-term cytokine time course experiments were piloted over 0, 1 and 24 hours. These pilot experiments revealed that a combination of TNF- $\alpha$  and IL-1 $\beta$  was able to stimulate P65 translocation 1-hour post-treatment, a process that was reversed within 24 hours. These results were mirrored in initial RT-qPCR experiments which highlighted an increase in MMP-13 expression 1-hour post-treatment followed by a reduction to basal levels after 24 hours. As a final part of these initial experiments, the expression of MMP-13 protein was analysed, which displayed a steady increase over the course of the experiment. Together these results suggest that a combination of TNF- $\alpha$  and IL-1 $\beta$  can stimulate the NF- $\kappa$ B pathway and increase the genetic and protein expression of MMP-13, a finding that has been shown in the literature previously [186].

Following these initial experiments, a longer-term time course was conducted due to the observed reversal in P65 translocation within 24 hours. This longer time course across 48 hours considered the same outcomes as pilot experiments, with the added inclusion of collagen type II, and the poly (ADP-ribose) polymerase (PARP) protein which

acted as a positive control for IL-1 $\beta$  stimulation [363]. IL-1 $\beta$  has been shown to induce activation of caspase-3 which in turn cleaves PARP [363]. Under physiological conditions, PARP exists to help maintain the cell through mechanisms such as DNA repair and cleavage of PARP prevents this, which in turn helps drive cells toward an apoptotic fate [364]. Therefore, when cells are treated with IL-1 $\beta$ , PARP cleavage should be detectable. Across this time course, cell cultures were treated with the TNF- $\alpha$ /IL-1 $\beta$  cytokine cocktail at regular intervals to attempt to replicate OA conditions and produce a sustained inflammatory response. Immunostaining revealed rapid nuclear translocation of P65 indicative of NF- $\kappa$ B activation within 1 and 2 hours of treatment. This effect was followed by a predominant sustained intermediate staining phenotype for the remainder of the experiment suggesting some P65 remained nuclear and therefore NF- $\kappa$ B stimulation was retained. This result may be beneficial when considering the development of a novel *in vitro* model of OA as this disease is considered chronic where recurring tissue damage results in the production of pro-inflammatory cytokines in the articular joint space [223]. RT-qPCR analysis following cytokine stimulation over a 48-hour time course revealed that MMP-13 levels significantly increased over 4, 6 and 8 hours compared to controls, with 8 hours of treatment providing the highest level of MMP-13 gene expression; this effect is not unexpected as several articles detail the ability of TNF- $\alpha$  and IL-1 $\beta$  to induce MMP-13 expression [182, 184, 185]. No significant difference was observed in COL2A1 expression as determined by RT-qPCR however, a trend can be seen in the data with expression decreasing over time. Literature has shown that TNF- $\alpha$  can inhibit the production of ECM components including proteoglycans [365] and IL-1 $\beta$  can specifically decrease articular chondrocyte COL2A1 gene expression [366]. The results presented in this study may differ due to the use of C-28/12 cell lines, published studies showing the anti-collagen effects of TNF- $\alpha$  and IL-1 $\beta$  often use primary chondrocytes as models which are known to be more sensitive than cell lines and have higher levels of COL2A1 expression [277].

Protein expression was also considered over a 48-hour time course to elucidate the impact of TNF- $\alpha$  and IL-1 $\beta$  on chondrocyte-associated, disease-relevant proteins as well as the apoptotic mediator PARP. It is shown here that PARP cleavage is initiated 4 hours post-treatment as indicated by an increase in cleaved-PARP presence in immunoblotting experiments, an effect that was increased at both 32- and 48-hour time points. This

trend is consistent with findings present in published literature, with increasing IL-1 $\beta$  exposure times resulting in an increase in PARP cleavage [363]. Analysis of the expression of chondrocyte proteins such as MMP-13 over this time course revealed a similar trend to the short-term cytokine studies, however, MMP-13 levels were found to increase to a further extent 8 hours post-treatment and beyond. This result is not unexpected as previously mentioned, TNF- $\alpha$  and IL-1 $\beta$  both stimulate MMP-13 protein production [367]. COL2 $\alpha$ 1 protein expression was seen to decrease over time with TNF- $\alpha$  and IL-1 $\beta$  treatment, however, this effect was recovered between 6 and 24 hours with expression remaining relatively stable for the remainder of the experiment. Notably, COL2 $\alpha$ 1 expression levels post-treatment never returned to basal levels. Again, this result is not unexpected as both cytokines have been shown to inhibit not only ECM components but collagen type II synthesis directly; it has been suggested that TNF- $\alpha$  can directly interfere with the transcription of COL2A1 mRNA [368] as does IL-1 $\beta$  directly impact the Sonic Hedgehog (SHH) pathway [369].

Literature has highlighted the ability of IL-1 $\beta$  to induce MMP-13 and disrupt the cartilaginous ECM through a variety of signalling pathways. IL-1 $\beta$  binds to its associated receptor IL-1RI and activates downstream pathways including NF- $\kappa$ B, as well as members of the mitogen-activated protein kinase (MAPK) signalling family such as extracellular signal-regulated kinases (ERK), c-Jun N-terminal kinases (JNKs) and p38 MAPKs [186, 370, 371]. These not only drive a host of catabolic processes including expression of a variety of MMPs, as well as the ADAMTS enzymes, but also promote inflammation and inhibit chondrogenic processes, disrupting SOX9 activity, as well as disrupting type II collagen and proteoglycans, and inhibiting their synthesis [186, 342, 372]. A similar effect has been shown with TNF- $\alpha$  can stimulate both TNFR-1 and TNFR-2 which induce varying effects. TNFR-1 binding can result in the production of two different signalling complexes: 1 and 2 [186, 373]. Complex 1 interacts with TNFR-1 associated death domain (TRADD) [373]. TRADD forms a complex with receptor interacting protein-1 (RIP-1) and TNF receptor-associated factor 2 (TRAF-2) which in turn drives downstream signalling via NF- $\kappa$ B [373, 374] and the MAPK pathways as previously described, or via the activator protein 1 (AP-1) pathway [375]. Complex 2 results in activation of Fas-associated death domain (FADD) which stimulates caspase-8 and downstream caspase-3 activity which can lead to apoptosis [373]. TNFR-2 stimulation

exerts function through activation of NF- $\kappa$ B and JNK signalling [376]. TNFR-1 Complex 1 and TNFR-2 signalling both lead to similar effects seen with IL-1 $\beta$  stimulation including upregulation of catabolic molecules such as MMP-13 and the ADAMTS enzymes, as well as disruption of collagens and proteoglycans and inhibition of their synthesis [375, 377–380]. It is worth highlighting that TNF- $\alpha$  exists in two forms, soluble and membrane bound [381]. TNFR-1 activity is stimulated by both forms whereas TNFR-2 activity is mainly activated by the membrane form [382, 383]. The inflammatory response shown in this chapter may therefore derive from predominantly TNFR-1 activity which may explain the increase in MMP-13 as well as PARP cleavage.

The final component of the 48-hour time course detailed in this chapter involved investigating the effect of TNF- $\alpha$  and IL-1 $\beta$  on the induction of autophagy in the target cell line. This was achieved via the analysis of the accumulation of LC3, a key component of autophagosome formation, which is indicative of stimulation of the process [206]. Results show that 6 hours of cytokine treatment can cause a significant induction in autophagy as confirmed by an increase in LC3 puncta. Literature has shown that both TNF- $\alpha$  and IL-1 $\beta$  stimulate autophagy, and it is suggested that in this scenario autophagy may act in a protective manner via the reduction of cytokine-induced apoptosis [384, 385]. TNF- $\alpha$  has been shown to directly stimulate autophagy activity through the upregulation of key autophagy proteins LC3 and beclin 1 as well as the conversion of LC3-I to LC3-II and indicator of autophagy induction [386]. TNF- $\alpha$  stimulation of autophagy is considered to occur via occur via JNK, ERK1/2 and Akt signalling pathways [387, 388]. However, it is notable that autophagy has been shown to work to reduce expression of TNF- $\alpha$  via inhibition of p38 MAPK signalling [389] therefore this pathway may present a therapeutic target when considered reduction of endogenous TNF- $\alpha$  production. Alternatively, IL-1 $\beta$  induction of autophagy may occur through the activation of inflammasomes and it has been suggested that through the engulfment of these inflammasomes, autophagy may work in an anti-inflammatory manner, preventing further inflammation by inhibiting caspase-1 activity [390].

The results of this time course analysis suggested that by 8 hours, maximal MMP-13 expression is attained, and that MMP-13 protein expression is found to be higher at later time points including 24 hours. Additionally, a significant induction of autophagy was observed 6 hours post-treatment and it was determined subsequent experiments would

focus on 8 hour and 24 hour time points to allow for experimental probing of these targets.

The final aim of this chapter was to investigate the effect of autophagy modulating drugs on the expression of OA-relevant chondrocyte proteins and autophagy associated markers in C-28/I2 chondrocytes. As literature has suggested that autophagy may have a protective effect on OA chondrocytes [209, 325, 348, 353, 391, 392] it stands to reason that autophagy inducing compounds should be the first potential therapeutics to be considered. Therefore, the final portion of this chapter aimed to investigate the impact of the autophagy inducers rapamycin and azathioprine on autophagy induction in C-28/I2 chondrocytes [348, 358]. Furthermore, this study aimed to determine the effects of autophagy stimulation on the expression of the chondrocyte phenotype, as literature has shown autophagy acts in a protective manner under cytokine-induced stress [353]. Autophagy induction was initially assessed via LC3 puncta accumulation, which was significantly increased with rapamycin treatment at both 8- and 24 hours relative to experimental controls. However, azathioprine did not significantly increase autophagy at either time point. Rapamycin functions via the inhibition of the mammalian target of rapamycin (mTOR) mTORC1 which results in the activation of autophagy [393] a well characterised effect [394]. Autophagy induction via azathioprine has been shown in THP-1 monocytes as well as peripheral blood mononuclear cells (PBMCs) [358] however the mechanism by which this occurs potentially differs from rapamycin. Research has shown azathioprine activity may be dependent on its ability to interact with both mTORC1 and PERK, a gene associated with the unfolded protein response (UPR) – a process tied closely to autophagy [358].

Autophagy and the production of chondrocyte-associated disease-relevant genes and proteins such as those related to MMP-13, and type II collagen are intimately linked: with autophagy being protective against MMP-13 overexpression and playing a vital role in type II collagen production [22, 50–52]. Therefore, induction of autophagy may present a potential therapeutic strategy that would decrease, or at least stabilize catabolic MMP-13 expression and potentially enhance type II collagen production. Treatment of cells with rapamycin or azathioprine did not induce any changes in genetic levels of basal expression of either MMP-13 or COL2A1 at either 8- or 24-hour timepoints. Notably, this experiment was not performed in the presence of

inflammatory stimuli which may explain the reason for no changes in expression; it could be the case that induction of autophagy doesn't necessarily reduce basal expression of these genes, as exemplified by previous work considering MMP-13 and the prevention of pathological modulation of this gene via autophagy induction[353]. Future work should endeavour to conduct these experiments in the presence of cytokines and expand experiments to include a repertoire of techniques that will allow for the full elucidation of the role of autophagy in osteoarthritis such techniques may include CRISPR/Cas9 genome editing. C-28/I2 cells used here are an immortalized line with all autophagy machinery conserved. CRISPR/Cas9 may be used to knock out important autophagy-related genes that have relevance to OA such as ATG7 [354]. This would allow for a direct investigation into the role of autophagy under inflammatory OA-like conditions *in vitro* using a high throughput cell line that can be adapted into a comprehensive *in vitro* model of osteoarthritis.

When considering the impact of rapamycin and azathioprine on MMP-13 protein production, no changes were observed 8 hours post-treatment relative to controls and a slight decrease in MMP-13 expression was observed 24 hours post-treatment. Again, this experiment was conducted in the absence of cytokines, therefore the scope of impact of these drugs is limited to alterations from basal levels under no inflammatory challenge which may explain the lack of drastic changes in MMP-13 expression. COL2 $\alpha$ 1 levels remained stable between untreated, and rapamycin-treated cells at 8 hours, however, a decrease was seen in azathioprine-treated cells. Inhibition of the mTOR pathway was confirmed via the reduction in phosphorylation of S6 ribosomal proteins in rapamycin-treated cells. A similar effect was seen in azathioprine-treated cells indicating that azathioprine is acting to inhibit mTOR as described previously [358]. Autophagy induction was also analysed using immunoblotting. The conversion of LC3-I to LC3-II is a process that is indicative of autophagy induction. Rapamycin stimulation was found to induce the highest level of conversion of LC3-I to LC3-II at 8 and 24-hour time points; this result is consistent with a higher level of LC3 puncta in immunostaining and greater amounts of S6 phosphorylation. Azathioprine did not stimulate LC3-I:LC3-II conversion beyond basal levels, again this result is concomitant with no significant change in LC3 puncta in azathioprine-treated cells or lower levels of rpS6 phosphorylation. While rapamycin is a known potent inducer of autophagy, the

differential effects seen here when comparing rapamycin and azathioprine treatments may be due to azathioprine driving endoplasmic reticulum (ER) stress induced apoptosis [395].

In summary, this chapter has confirmed that C-28/I2 cells respond to stimulation with TNF- $\alpha$  and IL-1 $\beta$ , inducing a sustained inflammatory response as indicated by the nuclear translocation of the P65 NF- $\kappa$ B subunit. In addition, this inflammatory response correlated with an increase in MMP-13 gene and protein expression, a hallmark of OA. Cytokine treatment was also found to induce autophagy, highlighting this pathway as a potential therapeutic target for OA treatment. Induction of autophagy was robustly achieved in these cells with the well-characterised autophagy inducer rapamycin; however, rapamycin treatment had little effect on OA disease-relevant genes and proteins. In contrast, azathioprine treatment did not induce autophagy under the conditions tested, however, it must be noted that rapamycin and azathioprine treatment were performed in the absence of cytokine stimulation, suggesting that the inflammatory phenotype of OA may be a necessary component for the potentially beneficial effects of autophagy induction in these cells.

## Chapter 6. General Discussion

### 6.1. Introduction

Due to the challenges associated with culturing human chondrocytes and osteoblasts in 2D *in vitro* cultures, no definitive *in vitro* model of OA exists. Current *in vitro* models only consider chondrocytes when examining OA but do not take the whole joint into account. It is now generally accepted that has been suggested that investigation of OA pathology should consider other tissues of the articulated joint such as bone, as they also express early pathological hallmarks that are characteristic of OA. The lack of a suitable *in vitro* model is slowing the development of novel therapeutics, therefore, a physiological *in vitro* model of OA must be developed, as this could expedite the process and be financially beneficial whilst adhering to the three Rs of animal research. Recent research has focused on the use of a variety of 3D *in vitro* culture systems for bone and cartilage, with the understanding that these systems may avoid some common pitfalls of standard 2D *in vitro* culture.

Typically, standard 2D *in vitro* models of adherent cells such as chondrocytes and osteoblasts involve the growth of cells in a monolayer on cell culture-treated plastics such as polystyrene flasks and multiwell plates. These models are cheap and have relatively high throughput, representing an attractive disease modelling option for researchers. However, several drawbacks exist when using these 2D systems. The 2D environment provides no option for nutrient and oxygen gradients that are often found in tissues and altered mechanotransduction may result in the de-differentiation of cells [227, 228]. Specifically, chondrocytes have been shown to de-differentiate when grown in 2D, adopting a fibroblast-like shape, and showing a downregulation in the expression of key matrix-associated genes such as COL2A1, ACAN and COMP [229]. Additionally, COL1A1 mRNA is upregulated, further signifying de-differentiation [230]. Therefore, the development of a 3D *in vitro* model is appealing, as this may preserve the advantages of 2D culture, whilst ameliorating some of the disadvantages.

### 6.2. Determination of optimum cell lines and growth conditions

Chapter 3 set out to determine the most suitable cell lines and culture conditions for inclusion in a novel 3D *in vitro* model of OA. Two candidate cell lines were identified as

suitable, C-28/I2 chondrocytes and SaOS-2 osteoblasts, as they expressed key chondrogenic and osteogenic markers respectively, over a 12-day time course. Additionally, some de-differentiation of human primary chondrocytes was observed in longer term 2D culture, therefore, cell lines are more practical for establishing a high throughput model for studying the impact of OA disease-like conditions on chondrocytes and osteoblasts. Cell lines, however, are not substitutes for primary cell cultures, as some loss of phenotype can occur in cell lines [396, 397]. Therefore, while C-28/I2 and SaOS-2 cell lines may be used in the development stages of cartilage/bone *in vitro* modelling they should not be considered a replacement for primary cells or tissues derived from *in vivo* sources, for example, common murine models or human patients undergoing knee replacement surgery.

The co-culture conditions described in Chapter 3 may be suitable for the inclusion of structural and immune cells involved in diseases such as rheumatoid arthritis, as synoviocytes and macrophages have been maintained using DMEM/F-12 as a basal component of their preferred growth media [398–400], however, further optimisation is necessary. The culture conditions detailed in Chapter 3 are a starting point for the development of bone-cartilage *in vitro* models, to ultimately describe interactions between different cell types implicated in a variety of diseases.

### **6.3. Development of a three-dimensional *in vitro* model of osteoarthritis**

Chapter 4 aimed to develop a 3D *in vitro* model of C-28/I2 and SaOS-2 cells using the culture conditions established in Chapter 3. Acellular 3D conditions were optimised, ensuring Biogelx hydrogel constructs were suitable for co-culture methods. Hydrogel culture systems can be formulated to a variety of stiffness' which is considered a benefit of the platform [265]. To create an *in vitro* model that incorporates physical contact, the mechanical stiffness of the hydrogel is important, as hydrogel deformation or leakage should be avoided. In Chapter 4, a hydrogel stiffness is detailed that has physical stability and is commercially available, thus identifying a candidate for future research and development of 3D *in vitro* physical contact models. Hydrogels can be manipulated in a variety of ways that will allow future researchers to investigate the activity of co-cultured, hydrogel-encapsulated, cell populations that are in direct contact with one

another, or that are physically separated using a transwell culture system. A direct contact culture system will allow for the co-culture of multiple adherent cell types, a model that is difficult to establish in traditional 2D culture conditions. This would create a platform for modelling diseases such as OA, rheumatoid arthritis with the inclusion of chondrocytes and synoviocytes [401], or to investigate the unique bone-tendon interface with varying degrees of stiffness as detailed by Paxton et. al. (2020) [312]. Additionally, this model could be used for non-musculoskeletal diseases such as atherosclerosis, with an interface of smooth muscle cells and endothelial cells being co-cultured [402].

Alternatively, the non-physical contact model using a transwell system may provide a platform for the study of secreted cell signalling molecules where direct cell contacts and potential migration of populations are not desired for example, when an experiment requires analysis of a distinct set of analytes from a pure cell population.

#### **6.4. Viability of three-dimensional cell cultures**

Cell viability was assessed which highlighted the impact of hydrogel stiffness and composition on encapsulated C-28/I2 and SaOS-2 cells. It was observed that GFOGER and IKVAV medium stiffness hydrogels resulted in the highest yield of viable cells 24 hours post-encapsulation, whereas standard and RGD hydrogels resulted in the greatest decrease in cell viability. These results highlighted the importance of both matrix stiffness and composition on cell viability and identified these properties as being key in the selection of a hydrogel culture system for the development of a 3D *in vitro* model of OA, or for the development of any hydrogel-based model using chondrocytes and osteoblasts.

Hydrogel composition was also found to impact the viability of C-28/I2 and SaOS-2 cells. Overall, GFOGER functionalised hydrogels resulted in the best viability for all encapsulated cells, an unsurprising result as this is a triple helical synthetic peptide derived from type I collagen with a strong binding affinity for  $\alpha 2\beta 1$  integrins [403]. Collagens are a major component of both cartilage and bone matrices, and despite some structural differences between type I and type II collagens, these molecules share a lot of homogeneous properties which may explain the *in vitro* support provided by GFOGER

hydrogels for both chondrocytes and osteoblasts. IKVAV is a laminin-like motif, and hydrogels functionalised with this yielded the second-highest levels of viability for encapsulated chondrocytes and osteoblasts. *In vivo* chondrocytes are surrounded by a narrow pericellular matrix which has been shown to contain high levels of laminin [404]. Laminin has also been shown to be osteogenic, promoting cell survival, the upregulation of osteoblast-associated genes, as well as the production of a calcified matrix [405, 406].

Again, it is perhaps unsurprising that these IKVAV peptide motifs are more supportive of chondrocytes and osteoblasts than standard unmodified hydrogels. While RGD hydrogels of medium and high stiffness were capable of maintaining some viability in encapsulated SaOS-2 cells, they were not suitable at all for C-28/I2 culture. Many studies that use RGD motifs use modified versions of this peptide and while having been shown to promote cell proliferation and viability, their effect on cell differentiation is controversial [407]. Chondrocytes commonly express integrin  $\alpha 5\beta 1$  and studies have shown that binding of  $\alpha 5\beta 1$  integrins can promote chondrogenesis [408], however, this integrin is overexpressed in OA and is pro-inflammatory in this scenario, leading to catabolism and subsequent cartilage matrix degradation [409–411]. Additionally, blocking integrins on chondrocytes such as  $\alpha \nu\beta 3$  has also been shown to inhibit OA progression [412]. When considering osteoblasts, specific integrins such as  $\alpha 5\beta 1$  may promote osteogenesis [413], whereas  $\alpha \nu\beta 3$  may inhibit osteogenic differentiation and proliferation [414]. With this widely known variety of effects and conflict regarding the full function of integrins under physiological and pathological conditions, RGD functionalised hydrogels may not present the best option for an *in vitro* model, adding a variety of potential confounding factors to disease modelling. These findings further highlight the importance of substrate composition on cell viability. It is therefore suggested herein that molecular similarities between functionalised hydrogel systems and native ECM components provide a more suitable environment for *in vitro* culture; notably, via the inclusion of motifs that mimic major structural molecules such as collagens, when considering bone and cartilage. One key aim of this thesis was to work with an industrial collaborator, Biogelx, and develop a suitable hydrogel-based culture system that would allow for the successful culture of chondrocytes and osteoblasts. However, due to the COVID-19 pandemic and resultant financial challenges, Biogelx became insolvent and was eventually liquidated as a commercial entity. This resulted in

a loss of knowledge, skill and raw materials that prevented further development of hydrogel formulations.

## **6.5. Phenotype of three-dimensional cell cultures**

Previous work has emphasized the role of substrate stiffness and its impact on a variety of cell behaviours such as differentiation [265]. When considering chondrocyte-specific behaviours, matrix stiffness has been shown to influence cell proliferation [415], chondrogenic differentiation [416], morphology and ECM synthesis [417]. This is perhaps not surprising as the role of cell-ECM interactions is important and should not be overlooked when considering disease of structural tissues and mechanotransduction has been shown to influence cell phenotype [228]. It has been shown that OA pathology alters the cartilage matrix; increasing stiffness resulting from collagen crosslinking via increased lysyl oxidase production, as well as accumulation of advanced glycation end-products, encourages collagen cross-linking [418]. This stiffening disrupts the chondrocyte catabolism vs. anabolism balance in favour of catabolism via the mechanotransductive Rho-ROCK-MLC axis [418]. Overall, activation of this pathway results in increased expression of catabolic MMPs and decreased expression of chondrogenic *SOX9* [418]. Additionally, it is worth noting that the overall elastic modulus of human articular cartilage is in the gigapascal (GPa) range, which greatly exceeds the modulus of hydrogels detailed in Chapter 4 and many other published in *vitro* systems [415–417]. Similarly, bone has a young's modulus in the gigapascal range [419]. Therefore, research should consider these great differences in stiffness when designing hydrogel-based models of articular cartilage, and this principle should be applied to other tissues.

## **6.6. Autophagy as a potential therapeutic target**

Finally, Chapter 5 aimed to develop an *in vitro* model to mimic the inflammatory conditions associated with OA and investigate autophagy as a potential therapeutic target under these inflammatory conditions. Due to chondrocytes being the primary focus of OA in the literature, this chapter aimed to use C-28/I2 cells as a chondrocyte model and to integrate osteoblasts, represented by SaOS-2 cells, however, due to time

constraints this was not achievable. Results showed that C-28/I2 cells are responsive to inflammatory cytokine stimulation, and this correlated with an increase in autophagy activity. This was not unexpected as autophagy and inflammation are intimately linked processes [420]. It was also shown in C-28/I2 cells that autophagy can be induced using the autophagy-inducing drug rapamycin. In contrast, the novel autophagy-inducing drug, azathioprine, did not affect autophagy in C-28/I2 cells.

In C-28/I2 cells, the expression of disease-associated proteins were affected by autophagy-modulating compounds, it can be seen that rapamycin treatment can reduce MMP13 protein levels however this is also associated with a concomitant reduction in COL2 $\alpha$ 1 expression. Therefore, autophagy may be regarded as a potential therapeutic target if MMP13 reduction is the key clinical outcome being considered. Research has shown that autophagy may play a protective role in OA and that MMP13 expression can be attenuated via modulation of the autophagy process [208–211, 391, 421, 422]. MMP13 is also upregulated in response to inflammatory cytokine activation via IL-R1, TNFR-1 and TNFR-2 receptor activation acting via the NF- $\kappa$ B pathway, which autophagy has also been shown to inhibit [186, 423]. Therefore, the findings of Chapter 5 concur with published literature, however, further analysis of the role of autophagy under inflammatory conditions is required before any definitive conclusions can be drawn.

## **6.7. Development of novel therapeutics for osteoarthritis**

There are no definitive OA treatments on the market yet, with pharmaceutical interventions focusing on symptomatic relief such as pain relief and anti-inflammatory treatments [424]. Surgical interventions, whilst often removing arthritic tissues, are invasive, financially costly, and come with the risk of potential complications [425]. Therefore, targeting pathways such as autophagy may help in the amelioration of disease symptoms. Current OA treatments undergoing clinical trials are more targeted than currently available palliative treatments; new treatments are specifically targeting cartilage repair and regeneration, alteration of subchondral bone remodelling or specifically neutralizing inflammatory factors IL-1 $\alpha$  and IL-1 $\beta$  [426]. From this perspective of clinical development, targeting a particular pathway such as autophagy is an attractive therapeutic option. Small molecule stimulation of autophagy may

attenuate articular joint catabolism through MMP13 regulation, slowing down disease progression entirely as MMP13 is critical in pathology [353, 427]. Additionally, autophagy has been shown to play a role in the regulation of collagen synthesis, highlighting its potential role in the treatment of OA [422]. Therefore, autophagy-modulating drugs such as rapamycin may present potential therapeutics for OA and other diseases with aberrant MMP13 expression and altered collagen synthesis such as Ehlers-Danlos syndrome and liver fibrosis [428, 429].

## **6.8. Further Applications**

This body of work has detailed the potential of particular cell lines as representative model systems of both bone and cartilage, and their suitability for inclusion in a 3D *in vitro* model of OA using commercially available hydrogel systems. However, findings elucidated upon here may have applications beyond the scope of this project alone. C-28/I2 and SaOS-2 cells were established as representative human chondrocytes and osteoblasts that are able to express a variety of genes and proteins associated with their respective extracellular matrices and are able to do so under identical growth conditions. This presents a model system that may be used to further probe diseases of the bone and cartilage. Including benefits to research into osteoarthritis, this could include inflammatory articular joint disorders such as rheumatoid arthritis [430], developmental diseases such as osteogenesis imperfecta [431] and chondrodysplasias [432]. The development of shared culture conditions between these cells would allow for the elucidation of cell-cell interactions, either in a direct manner via use of 3D systems such as hydrogels or cell-scaffolds, or in a non-contact system via the use of porous transwell inserts.

The importance of extracellular environment was also highlighted here in 3D culture conditions, as part of an overall aim of creating a suitable three-dimensional culture system for both chondrocytes and osteoblasts. This was not achieved as hydrogel products were not fit for this purpose. However, in addition to this, a variety of RNA retrieval methods were described each of which have varying results; these have been discussed previously. However, the consideration of a variety of extraction methods and resulting differences in RNA concentration and quality provides useful information for

RNA extraction methodologies going forward in both *in vitro* and *in vivo* research. It will allow future researchers to consider if they are using the appropriate methods and highlights that they should consider a variety of factors in detail such as: the physicochemical properties of the material to be extracted [320], homogenisation and disruption methods, and RNA retrieval steps [315, 317, 319, 433].

Finally, this work has highlighted the potential links between inflammation, autophagy, and pathological effects on chondrocytes. It was shown that cytokines such as TNF- $\alpha$  and IL-1 $\beta$  drive MMP-13 expression and that this is concomitant with an increase in autophagy activity in C-28/I2 chondrocytes. These results have implications for any inflammation driven disease, particularly those characterised by increases in expression of the catabolic enzyme MMP-13. Through the attenuation of autophagy and thus potentially inflammation and its associated expression of MMP-13 a therapeutic target may exist to reduce the catabolic symptoms of OA. However, other severe and fatal diseases such as Graft-Versus-Host disease which has been found to be characterised by inflammation induced MMP-13 expression [434]. MMP-13 overexpression is also linked to liver steatosis and the subsequent ability of cancerous cells to extravasate and metastasise; reduction of MMP-13 expression results in a protective effect [435]. Therefore, the current study has laid foundational work linking inflammation and autophagy whilst considering MMP-13 expression specifically. This may help further research into therapeutic options via methods such as autophagy attenuation as this has been shown to decrease inflammation induced MMP-13 expression previously [325, 353].

Had the goal of development of a 3D *in vitro* model of OA been achieved, this would have opened up a variety of potential experimental manipulations to facilitate the investigation of cell-cell and cell-ECM interactions. Cell-laden directly interfacing constructs may have been designed that would allow for assessment of disease characteristics in two distinct cell populations similar to work produced by Alsaykhan et. al. (2020) [312]; this work encompassed the creation of novel 3D constructs that modelled cell interfaces across both horizontal and vertical planes which provides ideal *in vitro* modelling conditions for the study of musculoskeletal disease as these models allows bone and cartilage tissues to be mimicked in 3D to varying degrees of complexity. Alternatively, models investigating the interaction between multiple cell types in one

single construct could be developed akin to those produced by Stüdle et. al. (2018) [251]. Investigation of cell-ECM-cell interactions may be achieved via seeding a monolayer of cells on top of a hydrogel containing encapsulated cells; researchers would thus have a tool that allows for the examination of the impact of cell-cell interactions in the context of a shared substrate as well as varying culture conditions. Beyond the manual preparation of 3D *in vitro* models, Biogelx hydrogels may have had potential for inclusion in a 3D extrusion-based printing system as a bioink. Print-based models using bioinks have been shown to allow for a great degree of control over matrix dimensions [436] as well and the creation of detailed co-culture systems that are highly robust – an issue that currently plagues manual 3D model preparation [436]. These printed systems may be further manipulated to investigate disease influencing pathologies such as chronic inflammation [436].

## 6.9. Conclusions

The lack of currently available treatments for OA may be due to a lack of a suitable *in vitro* model for drug screening. It has been suggested that this lack of an *in vitro* model restrains research translation from *in vitro* to *in vivo* which in turn greatly inhibits therapeutic development [426]. Many pre-clinical experiments in drug development rely on classic 2D *in vitro* cell culture before moving to *in vivo* animal models and eventually human clinical trials. However, due to the previously mentioned disadvantages of this culture method, it can be difficult to truly mimic chondrocyte and osteoblast behaviour, as well as OA pathology, as is also the case for other diseases such as cancer [437]. Therefore, the need for a definitive *in vitro* model of OA is desperately required; this model should seek to go beyond typical 2D *in vitro* culture methods and foray into the field of 3D *in vitro* modelling as this has been shown to present more *in vivo*-like conditions, for example, via the inclusion of an ECM and other microenvironment features.

This study has highlighted that Fmoc-based supramolecular hydrogel systems may be unsuitable for chondrocyte and osteoblast cell line culture due to cell viability concerns. Several hydrogel systems, including those both biologic [240–242] and synthetic [247, 249–251] in nature have shown suitability for chondrocyte and osteoblast culture, however, other 3D systems exist that may provide alternative culture methods to

directly model OA-like disease. A variety of prefabricated scaffolds including polymer-based scaffold systems and microcarriers may provide suitable culture frameworks for chondrocytes and osteoblasts [238, 257] and research has also highlighted the potential of scaffold-free pellet-based systems for chondrocyte culture, but these display a comparatively limited capacity for osteoblast culture [261, 263]. Recent research has highlighted “joint-on-a-chip” (JOC) models, which act as an “organ-on-a-chip” (OOC) for diseases of the joint [438]. These models combine 3D culture elements such as cell scaffolds or bioreactor environments and microfluidic features to create a more comprehensive *in vitro* culture system. JOC models present a potential way to recapitulate more reliable models of OA via the inclusion of multiple cell types in one model, for example, chondrocytes and osteoblasts while also considering disease-modifying factors such as cytokine treatment [439], immune cells [440], or the impacts of mechanical pressure and shear stress on cultured cells [440, 441]. Thus, the use of a validated *in vitro* model combined with a defined therapeutic target such as inflammation attenuation via autophagy may allow for significant leaps forward in drug development and treatment of OA.

### **6.10. Directions for future research**

The results presented in this thesis have highlighted the potential of C-28/I2 chondrocyte and SaOS-2 osteoblast cell models for use in a comprehensive *in vitro* model of OA. Additionally, the therapeutic potential of autophagy has been highlighted as a possible treatment for pathological events associated with OA disease onset and progression. The overall aim of this thesis was to develop a 3D *in vitro* model of OA that would allow for the investigation of potential therapeutics for the treatment of OA, such as autophagy. However, the supramolecular self-assembling peptide-based Fmoc hydrogels provided Biogelx were unsuitable for C-28/I2 and SaOS-2 cell culture in their commercially available state; further use of these hydrogels would have necessitated an alteration of hydrogel formulations only achievable with the support of Biogelx, unfortunately, due to the global COVID-19 pandemic the company became insolvent, and this could not be achieved. Understandably, this leaves a variety of open avenues for future research.

Future experimental work should consider alternative options for 3D *in vitro* culture. It may be the case that hydrogels containing Fmoc groups are unfavourable for cell culture. Although, the literature has shown that alternative hydrogel formulations have promise. Perhaps the inclusion of these alternate hydrogel systems in a JOC model would allow for more suitable conditions for cell culture with a hydrogel component, capturing not only the variety of cell types involved in OA but also the ECM-like conditions provided by the hydrogel system. This would also provide the opportunity to not only consider the impacts of cytokines on chondrocytes and osteoblasts but also mechanical stimulation as JOC models can facilitate this via fluid flow. Alternate considerations may be given to polymer-based scaffold systems, or even scaffold-free systems, however, these often present a challenge when it comes to the physical manipulation of cells. Subsequently, co-culture methods should be further developed. This thesis outlines models in which chondrocytes and osteoblasts may be co-cultured, with or without the presence of a physical contact site, however, this was shown using acellular hydrogels. Therefore, future work should aim to further develop these co-culture methods in the presence of cells; this would necessitate further optimisation of the molecular and cell biology techniques used in this thesis to ensure pure cell populations are used for downstream analysis such as RT-qPCR or immunoblotting. JOC models present an alternative to manually preparing co-cultures using scaffold and scaffold-free systems as these are designed to facilitate co-culture.

Following the establishment of an appropriate 3D *in vitro* model system, further optimization of candidate cells should be performed, particularly regarding disease-mimicking conditions as well as *in vivo* similarity. To simulate an OA phenotype, primary cells would of course act as better representatives of native chondrocytes and osteoblasts, therefore future research should seek to develop a model with primary cells. Murine models may act as an initial source of both healthy and diseased cells, and human-derived cells may eventually be acquired via surgical means from patients undergoing knee or hip replacements. Upon establishment of optimal 3D co-culture conditions, "OA-like" conditions may be further optimized, and therapeutic avenues may be investigated. Inducing an OA-like phenotype may be produced via cytokine stimulation or even mechanical stimulation, a desirable pathogenic stimulus that is hard to mimic in 2D culture. Alternatively, the overexpression of disease-relevant proteins

such as MMP13 in chondrocytes or Col1 $\alpha$ 1 in osteoblasts may be achieved via transfection experiments, creating a diseased phenotype. Alternatively, key genes such as chondrocyte COL2A1 and RANKL may be downregulated via the use of siRNAs or knocked out using CRISPR-Cas9 genome editing technology. This would allow for the analysis of loss of function under disease conditions and how this may impact co-cultured cells such as osteoblasts. When considering the autophagy pathway, the impacts of 3D culture on the activity of this pathway under physiological conditions must be assessed. Subsequently, genome editing using CRISPR-Cas9 targeting key autophagy genes such as ATG7 would allow for the assessment of the role of autophagy in OA. Ablation of these genes has been shown to contribute to OA pathology; however, this has not been fully investigated in a 3D *in vitro* co-culture model of OA.

OA is a disease with a broad aetiology and many confounding factors making it difficult to develop disease therapeutics. Unfortunately, many available treatments deal with symptoms but do not necessarily halt disease progression and many patients suffer decreased quality of life. Therapeutic development is hindered due to hurdles presented when translating *in vitro* experimental results to *in vivo* models and it is suggested here that this is due to the limitations posed by conventional 2D *in vitro* cell culture. Here, it was shown that C-28/I2 chondrocytes and SaOS-2 osteoblasts may present suitable cell models for inclusion in an *in vitro* model of OA. This thesis also highlighted the potential disadvantages of working with Fmoc-protected self-assembling supramolecular peptide-based hydrogels, indicating a shift in research focus to non-Fmoc hydrogels is potentially needed. Finally, it was shown that autophagy is a potential therapeutic target in OA as it shares close ties with inflammatory stimulation as well as MMP13 regulation in C-28/I2 chondrocytes.



## References

1. Arthritis Research UK (2013) Osteoarthritis in general practice July 2013 Arthritis Research UK
2. Zhang Y, Jordan JM (2011) Epidemiology of Osteoarthritis. *Clinical Geriatric Medicine* 26:355–369. <https://doi.org/10.1016/j.cger.2010.03.001>.Epidemiology
3. Kerkhof HJM, Lories RJ, Meulenbelt I, Jonsdottir I (2010) Chromosome 7Q22 To Influence Susceptibility for Osteoarthritis. *Arthritis Rheumatology* 62:499–510. <https://doi.org/10.1002/art.27184.A>
4. Yuan XL, Meng HY, Wang YC, et al (2014) Bone-cartilage interface crosstalk in osteoarthritis: Potential pathways and future therapeutic strategies. *Osteoarthritis Cartilage* 22:1077–1089. <https://doi.org/10.1016/j.joca.2014.05.023>
5. Sluka K (1996) Pain mechanisms involved in musculoskeletal disorders. *Journal of Orthopaedic & Sports Physical Therapy* 24:240–254. <https://doi.org/10.2519/jospt.1996.24.4.240>
6. Turkiewicz A, Petersson IF, Björk J, et al (2014) Current and future impact of osteoarthritis on health care: A population-based study with projections to year 2032. *Osteoarthritis Cartilage* 22:1826–1832. <https://doi.org/10.1016/j.joca.2014.07.015>
7. Decker RS (2018) Articular cartilage and joint development from embryogenesis to adulthood. 62:50–56. <https://doi.org/10.1016/j.semcd.2016.10.005>.Articular
8. Prekasan D, Saju KK (2016) Review of the Tribological Characteristics of Synovial Fluid. *Procedia Technology* 25:1170–1174. <https://doi.org/10.1016/j.protcy.2016.08.235>
9. Clarke B (2008) Normal bone anatomy and physiology. *Clin J Am Soc Nephrol* 3 Suppl 3:S131-9. <https://doi.org/10.2215/CJN.04151206>
10. Taichman RS (2005) Blood and bone: two tissues whose fates are intertwined to create the hematopoietic stem-cell niche. *Blood* 105:2631–2639. <https://doi.org/10.1182/blood-2004-06-2480.Supported>
11. Donell S (2019) Subchondral bone remodelling in osteoarthritis. *EFORT Open Rev* 4:221–229. <https://doi.org/10.1302/2058-5241.4.180102>
12. Mahjoub M, Berenbaum F, Houard X (2012) Why subchondral bone in osteoarthritis? the importance of the cartilage bone interface in osteoarthritis. *Osteoporosis International* 23:841–846. <https://doi.org/10.1007/s00198-012-2161-0>
13. Stewart HL, Kawcak CE (2018) The Importance of Subchondral Bone in the Pathophysiology of Osteoarthritis. *Front Vet Sci* 5:1–9. <https://doi.org/10.3389/fvets.2018.00178>

14. Ott SM (2018) Cortical or Trabecular Bone: What's the Difference? *Am J Nephrol* 47:373–375. <https://doi.org/10.1159/000489672>
15. Li G, Yin J, Gao J, et al (2013) Subchondral bone in osteoarthritis: insight into risk factors and microstructural changes. *Arthritis Res Ther* 15:. <https://doi.org/10.1186/ar4405>
16. Suri S, Walsh DA (2012) Osteochondral alterations in osteoarthritis. *Bone* 51:204–211. <https://doi.org/10.1016/j.bone.2011.10.010>
17. Clark JM, Huber JD (1990) The structure of the human subchondral plate. *Journal of Bone and Joint Surgery - Series B* 72:866–873. <https://doi.org/10.1302/0301-620x.72b5.2211774>
18. Ascenzi M-G (2012) The osteon: the micromechanical unit of compact bone. *Frontiers in Bioscience* 17:1551. <https://doi.org/10.2741/4003>
19. Milz S, Putz R (1994) Quantitative morphology of the subchondral plate of the tibial plateau. *J Anal* 185:103–110
20. El-Ganzuri MA, Ahmed RR, Bastawy EM (2016) Regulatory Mechanisms of Bone Development and Function. *Annals of Cytology and Pathology* 1:5–17
21. Kii I, Nishiyama T, Li M, et al (2010) Incorporation of tenascin-C into the extracellular matrix by periostin underlies an extracellular meshwork architecture. *Journal of Biological Chemistry* 285:2028–2039. <https://doi.org/10.1074/jbc.M109.051961>
22. Mackie EJ, Ramsey S (1996) Modulation of osteoblast behaviour by tenascin. *J Cell Sci* 109:1597–1604. <https://doi.org/10.1242/jcs.109.6.1597>
23. Beck, G.R., Sullivan, E.C., Moran, E., Zerler B (1998) Relationship between alkaline phosphatase levels, osteopontin expression, and mineralization in differentiating MC3T3-E1 osteoblasts. *J Cell Biochem* 68:269–280. [https://doi.org/10.1002/\(sici\)1097-4644\(19980201\)68:2<269::aid-jcb13>3.0.co;2-a](https://doi.org/10.1002/(sici)1097-4644(19980201)68:2<269::aid-jcb13>3.0.co;2-a)
24. Rosenberg N, Rosenberg O, Soudry M (2012) Osteoblasts in bone physiology-mini review. *Rambam Maimonides Med J* 3:e0013. <https://doi.org/10.5041/RMMJ.10080>
25. Atkins GJ, Findlay DM (2012) Osteocyte regulation of bone mineral: A little give and take. *Osteoporosis International* 23:2067–2079. <https://doi.org/10.1007/s00198-012-1915-z>
26. Caplan AI (1991) Mesenchymal Stem Cells. *Journal of Orthopaedic Research* 9:641–650. [https://doi.org/10.1016/0009-2614\(70\)87009-9](https://doi.org/10.1016/0009-2614(70)87009-9)
27. Florencio-Silva R, da Silva Sasso GR, Sasso-Cerri E, et al (2015) Biology of Bone Tissue: Structure, Function, and Factors That Influence Bone Cells. *Biomed Res Int* 2015:1–17. [https://doi.org/10.1016/S0923-2532\(05\)80182-6](https://doi.org/10.1016/S0923-2532(05)80182-6)
28. Komori T, Yagi H, Nomura S, et al (1997) Targeted Disruption of Cbfa1 Results in a Complete Lack of Bone Formation owing to Maturation Arrest of Osteoblasts. *Proc Natl Acad Sci U S A* 89:755–764. [https://doi.org/10.1016/s0092-8674\(00\)80258-5](https://doi.org/10.1016/s0092-8674(00)80258-5)
29. Ducy P, Zhang R, Geoffroy V, et al (1997) *Osf2/Cbfa1*: A transcriptional activator of osteoblast differentiation. *Cell* 89:747–754. [https://doi.org/10.1016/S0092-8674\(00\)80257-3](https://doi.org/10.1016/S0092-8674(00)80257-3)

30. Nakashima K, Zhou X, Kunkel G, et al (2002) The Novel Zinc Finger-Containing Transcription Factor Osterix Is Required for Osteoblast Differentiation and Bone Formation. *Cell* 108:17–29. [https://doi.org/10.1016/s0092-8674\(01\)00622-5](https://doi.org/10.1016/s0092-8674(01)00622-5)
31. Liu W, Toyosawa S, Furuichi T, et al (2001) Overexpression of Cbfa1 in osteoblasts inhibits osteoblast maturation and causes osteopenia with multiple fractures. *Journal of Cell Biology* 155:157–166. <https://doi.org/10.1083/jcb.200105052>
32. Long F (2012) Building strong bones: Molecular regulation of the osteoblast lineage. *Nat Rev Mol Cell Biol* 13:27–38. <https://doi.org/10.1038/nrm3254>
33. Miller SC, Jee WSS (1987) The bone lining cell: A distinct phenotype? *Calcif Tissue Int* 41:1–5. <https://doi.org/10.1007/BF02555122>
34. Dierkes C, Kreisel M, Schulz A, et al (2009) Catabolic properties of microdissected human endosteal bone lining cells. *Calcif Tissue Int* 84:146–155. <https://doi.org/10.1007/s00223-008-9213-7>
35. Andersen TL, Sondergaard TE, Skorzynska KE, et al (2009) A physical mechanism for coupling bone resorption and formation in adult human bone. *American Journal of Pathology* 174:239–247. <https://doi.org/10.2353/ajpath.2009.080627>
36. Nakashima, T., Hayashi, M., Takano, F., Kurata, K., Oh-hora, M., Feng, J.Q., Bonewald, L.F., Kodama, T., Wutz, A., Wagner, E.F., Penninger, J.M., Takayanagi H (2011) Evidence for osteocyte regulation of bone homeostasis through RANKL expression. *Nat Med* 17:1231–1234. <https://doi.org/10.1038/nm.2452>
37. Kennedy OD, Herman BC, Laudier DM, et al (2012) Activation of resorption in fatigue-loaded bone involves both apoptosis and active pro-osteoclastogenic signaling by distinct osteocyte populations. *Bone* 50:1115–1122. <https://doi.org/10.1016/j.bone.2012.01.025>
38. Franz-Odenaal TA, Hall BK, Witten PE (2006) Buried alive: How osteoblasts become osteocytes. *Developmental Dynamics* 235:176–190. <https://doi.org/10.1002/dvdy.20603>
39. Palumbo C, Palazzini S, Zaffe D, G. M (1990) Osteocyte differentiation in the tibia of newborn rabbit: an ultrastructural study of the formation of cytoplasmic processes. *Acta Anat (Basel)* 137:350–358. <https://doi.org/10.1159/000146907>
40. Dallas SL, Prideaux M, Bonewald LF (2013) The osteocyte: An endocrine cell . . . and more. *Endocr Rev* 34:658–690. <https://doi.org/10.1210/er.2012-1026>
41. Currey JD (2003) The many adaptations of bone. *J Biomech* 36:1487–1495. [https://doi.org/10.1016/S0021-9290\(03\)00124-6](https://doi.org/10.1016/S0021-9290(03)00124-6)
42. Schulze E, Witt M, Kasper M, et al (1999) Immunohistochemical investigations on the differentiation marker protein E11 in rat calvaria, calvaria cell culture and the osteoblastic cell line ROS 17/2.8. *Histochem Cell Biol* 111:61–69. <https://doi.org/10.1007/s004180050334>
43. Toyosawa S, Shintani S, Fujiwara T, et al (2001) Dentin matrix protein 1 is predominantly expressed in chicken and rat osteocytes but not in osteoblasts. *Journal of Bone and Mineral Research* 16:2017–2026. <https://doi.org/10.1359/jbmr.2001.16.11.2017>

44. Ubaidus S, Li M, Sultana S, et al (2009) FGF23 is mainly synthesized by osteocytes in the regularly distributed osteocytic lacunar canalicular system established after physiological bone remodeling. *J Electron Microsc (Tokyo)* 58:381–392. <https://doi.org/10.1093/jmicro/dfp032>
45. Igarashi M, Kamiya N, Ito K, Takagi M (2002) In situ localization and in vitro expression of osteoblast/osteocyte factor 45 mRNA during bone cell differentiation. *Histochemical Journal* 34:255–263. <https://doi.org/10.1023/A:1021745614872>
46. Winkler DG, Sutherland MK, Geoghegan JC, et al (2003) Osteocyte control of bone formation via sclerostin, a novel BMP antagonist. *EMBO Journal* 22:6267–6276. <https://doi.org/10.1093/emboj/cdg599>
47. Guo D, Keightley A, Guthrie J, et al (2012) Identification of Osteocyte-Selective Proteins. 10:3688–3698. <https://doi.org/10.1002/pmic.201000306>. Identification
48. Yang W, Harris M, Heinrich J, et al (2009) Gene expression signatures of a fibroblastoid preosteoblast and cuboidal cell model compared to the MLO-Y4 osteocyte cell model. *Bone* 44:32–45. <https://doi.org/10.1161/CIRCULATIONAHA.110.956839>
49. Yavropoulou MP, Yovos JG (2008) Osteoclastogenesis - Current knowledge and future perspectives. *Journal of Musculoskeletal Neuronal Interactions* 8:204–216
50. Sodek J, McKee MD (2000) Molecular and cellular biology of alveolar bone. *Periodontol* 2000 24:99–126. <https://doi.org/10.1034/j.1600-0757.2000.2240106.x>
51. Udagawa N, Takahashi N, Yasuda H, et al (2000) Osteoprotegerin produced by osteoblasts is an important regulator in osteoclast development and function. *Endocrinology* 141:3478–3484. <https://doi.org/10.1210/endo.141.9.7634>
52. Boyce BF, Xing L (2008) Functions of RANKL/RANK/OPG in bone modeling and remodeling. *Arch Biochem Biophys* 473:139–146. <https://doi.org/10.1016/j.abb.2008.03.018>
53. Matsumoto M, Kogawa M, Wada S, et al (2004) Essential role of p38 mitogen-activated protein kinase in cathepsin K gene expression during osteoclastogenesis through association of NFATc1 and PU.1. *Journal of Biological Chemistry* 279:45969–45979. <https://doi.org/10.1074/jbc.M408795200>
54. Miyamoto T (2006) The dendritic cell-specific transmembrane protein DC-STAMP is essential for osteoclast fusion and osteoclast bone-resorbing activity. *Mod Rheumatol* 16:341–342. <https://doi.org/10.1007/s10165-006-0524-0>
55. Arana-Chavez VE, Bradaschia-Correa V (2009) Clastic cells: Mineralized tissue resorption in health and disease. *International Journal of Biochemistry and Cell Biology* 41:446–450. <https://doi.org/10.1016/j.biocel.2008.09.007>
56. Holliday LS, Bubb MR, Jiang J, et al (2005) Interactions between vacuolar H<sup>+</sup>-ATPases and microfilaments in osteoclasts. *J Bioenerg Biomembr* 37:419–423. <https://doi.org/10.1007/s10863-005-9483-y>
57. Oshiro T, Shibasaki Y, John Martin T, Sasaki T (2001) Immunolocalization of Vacuolar-Type H1-ATPase, Cathepsin K, Matrix Metalloproteinase-9, and Receptor Activator of NFκB Ligand in Odontoclasts During Physiological Root Resorption of Human Deciduous Teeth. *Anat Rec* 264:305–311. <https://doi.org/10.1002/ar.0000>

58. Xia L, Kilb J, Wex H, et al (1999) Localization of rat cathepsin K in osteoclasts and resorption pits: Inhibition of bone resorption and cathepsin K-activity by peptidyl vinyl sulfones. *Biol Chem* 380:679–687. <https://doi.org/10.1515/BC.1999.084>
59. Bonucci E (2012) Bone mineralization. *Frontiers in Bioscience* 17:100–128. <https://doi.org/10.2741/3918>
60. Shoulders MD, Raines RT (2009) Collagen Structure and Stability. *Annu Rev Biochem* 78:929–958. <https://doi.org/10.1146/annurev.biochem.77.032207.120833>
61. An J, Leeuwenburgh S, Wolke J, Jansen J (2016) Mineralization Processes in Hard Tissue: Bone. *Biomaterialization and Biomaterials: Fundamentals and Applications* 129–146. <https://doi.org/10.1016/B978-1-78242-338-6.00005-3>
62. Price PA (1988) Role of vitamin-k-dependent proteins in bone metabolism. *Annu Rev Nutr* 8:565–583. <https://doi.org/10.1146/annurev.nu.08.070188.003025>
63. Szulc P, Chapuy MC, Meunier PJ, Delmas PD (1996) Serum undercarboxylated osteocalcin is a marker of the risk of hip fracture: A three year follow-up study. *Bone* 18:487–488. [https://doi.org/10.1016/8756-3282\(96\)00037-3](https://doi.org/10.1016/8756-3282(96)00037-3)
64. Ducy P, Desbois C, Boyce B, et al (1996) Increased bone formation in osteocalcin-deficient mice. *Nature* 382:448–452. <https://doi.org/10.1038/382448a0>
65. Klein GL (2014) Insulin and bone: Recent developments. *World J Diabetes* 5:14. <https://doi.org/10.4239/wjd.v5.i1.14>
66. Shunsuke I, Hosaka Y, Iwasaki T, et al (2008) The modulations of collagen fibril assembly and its structure by decorin: an electron microscopic study. *Arch Histol Cytol* 71:37–44. <https://doi.org/10.1679/aohc.71.37>
67. Danielson KG, Baribault H, Holmes DF, et al (1997) Targeted disruption of decorin leads to abnormal collagen fibril morphology and skin fragility. *Journal of Cell Biology* 136:729–743. <https://doi.org/10.1083/jcb.136.3.729>
68. Mochida Y, Parisuthiman D, Pornprasertsuk-Damrongsri S, et al (2009) Decorin modulates collagen matrix assembly and mineralization. *Matrix Biology* 28:44–52. <https://doi.org/10.1016/j.matbio.2008.11.003>
69. Hoshi K, Kemmotsu S, Takeuchi Y, et al (1999) The primary calcification in bones follows removal of decorin and fusion of collagen fibrils. *Journal of Bone and Mineral Research* 14:273–280. <https://doi.org/10.1359/jbmr.1999.14.2.273>
70. Corsi A, Xu T, Chen XD, et al (2002) Phenotypic effects of biglycan deficiency are linked to collagen fibril abnormalities, are synergized by decorin deficiency, and mimic Ehlers-Danlos-like changes in bone and other connective tissues. *Journal of Bone and Mineral Research* 17:1180–1189. <https://doi.org/10.1359/jbmr.2002.17.7.1180>
71. Sheldon H, Robinson RA (1957) Electron microscope studies of crystal-collagen relationships in bone. IV. The occurrence of crystals within collagen fibrils. *J Biophys Biochem Cytol* 3:1011–1016. <https://doi.org/10.1083/jcb.3.6.1011>
72. Chai YC, Carlier A, Bolander J, et al (2012) Current views on calcium phosphate osteogenicity and the translation into effective bone regeneration strategies. *Acta Biomater* 8:3876–3887. <https://doi.org/10.1016/j.actbio.2012.07.002>

73. Anderson HC (1995) Molecular biology of matrix vesicles. *Clin Orthop Relat Res* 266–280. <https://doi.org/10.1097/00003086-199505000-00034>
74. Anderson HC (2003) Matrix vesicles and calcification. *Curr Rheumatol Rep* 5:222–226. <https://doi.org/10.1007/s11926-003-0071-z>
75. Peress NS, Anderson HC, Sajdera SW (1974) The lipids of matrix vesicles from bovine fetal epiphyseal cartilage. *Calcif Tissue Res* 14:275–281. <https://doi.org/10.1007/BF02060301>
76. Ali SY, Sajdera SW, Anderson HC (1970) Isolation and characterization of calcifying matrix vesicles from epiphyseal cartilage. *Proc Natl Acad Sci U S A* 67:1513–1520. <https://doi.org/10.1073/pnas.67.3.1513>
77. Montessuit C, Caverzasio J, Bonjour JP (1991) Characterization of a P(i) transport system in cartilage matrix vesicles: Potential role in the calcification process. *Journal of Biological Chemistry* 266:17791–17797
78. Wu LNY, Genge BR, Lloyd GC, Wuthiers RE (1991) Collagen-binding Proteins in Collagenase-released Matrix Vesicles from Cartilage
79. Arsenault AL, Frankland BW, Ottensmeyer FP (1991) Vectorial sequence of mineralization in the turkey leg tendon determined by electron microscopic imaging. *Calcif Tissue Int* 48:46–55. <https://doi.org/10.1007/BF02555795>
80. Wenkert D (2011) Primary disorders of bone and connective tissues. In: *Textbook of Pediatric Rheumatology, Sixth Edit.* Elsevier Inc., pp 742–765
81. Hessle L, Johnson KA, Anderson HC, et al (2002) Tissue-nonspecific alkaline phosphatase and plasma cell membrane glycoprotein-1 are central antagonistic regulators of bone mineralization. *Proc Natl Acad Sci U S A* 99:9445–9449. <https://doi.org/10.1073/pnas.142063399>
82. Rucci N (2008) Molecular Biology of Bone Remodelling. *Clinical Cases in Mineral and Bone Metabolism* 5:49–56
83. Bonewald LF (2007) Osteocytes as dynamic multifunctional cells. *Ann N Y Acad Sci* 1116:281–290. <https://doi.org/10.1196/annals.1402.018>
84. Li X, Qin L, Bergenstock M, et al (2007) Parathyroid hormone stimulates osteoblastic expression of MCP-1 to recruit and increase the fusion of pre/osteoclasts. *Journal of Biological Chemistry* 282:33098–33106. <https://doi.org/10.1074/jbc.M611781200>
85. Wiktor-Jedrzejczak W, Bartocci A, Ferrante AW, et al (1990) Total absence of colony-stimulating factor 1 in the macrophage-deficient osteopetrotic (op/op) mouse. *Proc Natl Acad Sci U S A* 87:4828–4832. <https://doi.org/10.1073/pnas.87.12.4828>
86. Ma YL, Cain RL, Halladay DL, et al (2001) Catabolic effects of continuous human PTH (1-38) in vivo is associated with sustained stimulation of RANKL and inhibition of osteoprotegerin and gene-associated bone formation. *Endocrinology* 142:4047–4054. <https://doi.org/10.1210/endo.142.9.8356>
87. Partridge NC, Jeffrey JJ, Ehlich LS, et al (1987) Hormonal regulation of the production of collagenase and a collagenase inhibitor activity by rat osteogenic sarcoma cells. *Endocrinology* 120:1956–1962. <https://doi.org/10.1210/endo-120-5-1956>

88. Yang CM, Chien CS, Yao CC, et al (2004) Mechanical strain induces collagenase-3 (MMP-13) expression in MC3T3-E1 osteoblastic cells. *Journal of Biological Chemistry* 279:22158–22165. <https://doi.org/10.1074/jbc.M401343200>
89. Raggatt LJ, Partridge NC (2010) Cellular and molecular mechanisms of bone remodeling. *Journal of Biological Chemistry* 285:25103–25108. <https://doi.org/10.1074/jbc.R109.041087>
90. Saftig P, Hunziker E, Wehmeyer O, et al (1998) Impaired osteoclastic bone resorption leads to osteopetrosis in cathepsin-K-deficient mice. *Proc Natl Acad Sci U S A* 95:13453–13458. <https://doi.org/10.1073/pnas.95.23.13453>
91. Teitelbaum SL (2000) Bone Resorption by Osteoclasts. *Science* (1979) 289:1504–1509. <https://doi.org/10.1126/science.289.5484.1504>
92. Everts V, Delaissé JM, Korper W, et al (2002) The bone lining cell: Its role in cleaning Howship's lacunae and initiating bone formation. *Journal of Bone and Mineral Research* 17:77–90. <https://doi.org/10.1359/jbmr.2002.17.1.77>
93. Van PT, Vignery A, Baron R (1982) Cell and Tissue An electron-microscopic study of the bone-remodeling sequence in the rat. *Cell* 225:283–292
94. Tang Y, Wu X, Lei W, et al (2009) TGF- $\beta$ 1-induced migration of bone mesenchymal stem cells couples bone reabsorption and formation. *Nat Med* 15:757–765. <https://doi.org/10.1016/j.physbeh.2017.03.040>
95. Pederson L, Ruan M, Westendorf JJ, et al (2008) Regulation of bone formation by osteoclasts involves Wnt/BMP signaling and the chemokine sphingosine-1-phosphate. *Proc Natl Acad Sci U S A* 105:20764–20769. <https://doi.org/10.1073/pnas.0805133106>
96. Zhao C, Irie N, Takada Y, et al (2006) Bidirectional ephrinB2-EphB4 signaling controls bone homeostasis. *Cell Metab* 4:111–121. <https://doi.org/10.1016/j.cmet.2006.05.012>
97. Keller H, Kneissel M (2005) SOST is a target gene for PTH in bone. *Bone* 37:148–158. <https://doi.org/10.1016/j.bone.2005.03.018>
98. Robling AG, Niziolek PJ, Baldrige LA, et al (2008) Mechanical stimulation of bone in vivo reduces osteocyte expression of Sost/sclerostin. *Journal of Biological Chemistry* 283:5866–5875. <https://doi.org/10.1074/jbc.M705092200>
99. Fox AJS, Bedi A, Rodeo SA (2009) The basic science of the patella: structure, composition, and function. *Orthopaedics* 1:461–468. <https://doi.org/10.1055/s-0032-1313741>
100. Decker RS, Koyama E, Pacifici M (2015) Articular Cartilage: Structural and Developmental Intricacies and Questions. *Curr Osteoporos Rep* 13:407–414. <https://doi.org/10.1007/s11914-015-0290-z>
101. Baumann CA, Hinckel BB, Bozynski CC, Farr J (2019) Articular Cartilage: Structure and Restoration. In: *Joint Preservation of the Knee*. pp 3–24
102. Staines KA, Pollard AS, McGonnell IM, et al (2013) Cartilage to bone transitions in health and disease. *Journal of Endocrinology* 219:. <https://doi.org/10.1530/JOE-13-0276>

103. Archer CW, Francis-West P (2003) The chondrocyte. *International Journal of Biochemistry and Cell Biology* 35:401–404. [https://doi.org/10.1016/S1357-2725\(02\)00301-1](https://doi.org/10.1016/S1357-2725(02)00301-1)
104. Pacifici M, Koyama E, Iwamoto M (2005) Mechanisms of synovial joint and articular cartilage formation: Recent advances, but many lingering mysteries. *Birth Defects Res C Embryo Today* 75:237–248. <https://doi.org/10.1002/bdrc.20050>
105. Bhosale AM, Richardson JB (2008) Articular cartilage: Structure, injuries and review of management. *Br Med Bull* 87:77–95. <https://doi.org/10.1093/bmb/ldn025>
106. Kozhemyakina E, Lassar AB, Zelzer E (2015) A pathway to bone: Signaling molecules and transcription factors involved in chondrocyte development and maturation. *Development (Cambridge)* 142:817–831. <https://doi.org/10.1242/dev.105536>
107. Akiyama H, Chaboissier MC, Martin JF, et al (2002) The transcription factor Sox9 has essential roles in successive steps of the chondrocyte differentiation pathway and is required for expression of Sox5 and Sox6. *Genes Dev* 16:2813–2828. <https://doi.org/10.1101/gad.1017802>
108. Cooper KL, Oh S, Sung Y, et al (2013) Multiple phases of chondrocyte enlargement underlie differences in skeletal proportions. *Nature* 495:375–378. <https://doi.org/10.1038/nature11940>
109. Stickens D, Behonick DJ, Ortega N, et al (2004) Altered endochondral bone development in matrix metalloproteinase 13-deficient mice. *Development* 131:5883–5895. <https://doi.org/10.1242/dev.01461>
110. Zelzer E, McLean W, Ng YS, et al (2002) Skeletal defects in VEGF(120/120) mice reveal multiple roles for VEGF in skeletogenesis. *Development* 129:1893–1904. <https://doi.org/10.1242/dev.129.8.1893>
111. Holder N (1977) An experimental investigation into the early development of the chick elbow joint. *Embryol exp Morph* 39:115–127. <https://doi.org/https://doi.org/10.1242/dev.39.1.115>
112. Hyde G, Boot-Handford RP, Wallis GA (2008) Col2a1 lineage tracing reveals that the meniscus of the knee joint has a complex cellular origin. *J Anat* 213:531–538. <https://doi.org/10.1111/j.1469-7580.2008.00966.x>
113. Storm EE, Kingsley DM (1996) Joint patterning defects caused by single and double mutations in members of the bone morphogenetic protein (BMP) family. *Development* 122:3969–3979. <https://doi.org/10.1242/dev.122.12.3969>
114. Snow HE, Riccio LM, Mjaatvedt CH, et al (2005) Versican expression during skeletal/joint morphogenesis and patterning of muscle and nerve in the embryonic mouse limb. *Anatomical Record - Part A Discoveries in Molecular, Cellular, and Evolutionary Biology* 282:95–105. <https://doi.org/10.1002/ar.a.20151>
115. Ito MM, Kida MY (2000) Morphological and biochemical re-evaluation of the process of cavitation in the rat knee joint : cellular and cell strata alterations in the interzone. *McDermott* 197:659–679

116. Hayes AJ, MacPherson S, Morrison H, et al (2001) The development of articular cartilage: evidence for an appositional growth mechanism. *Anat Embryol (Berl)* 203:469–479. <https://doi.org/10.1007/s004290100178>
117. Shoulders MD, Raines RT (2009) Collagen structure and stability. *Annu Rev Biochem* 78:929–958
118. Poole AR, Kobayashi M, Yasuda T, et al (2002) Type II collagen degradation and its regulation in articular cartilage in osteoarthritis. *Ann Rheum Dis* 61:78–81. [https://doi.org/10.1136/ard.61.suppl\\_2.ii78](https://doi.org/10.1136/ard.61.suppl_2.ii78)
119. Nakagawa Y, Muneta T, Otabe K, et al (2016) Cartilage derived from bone marrow mesenchymal stem cells expresses lubricin in vitro and in vivo. *PLoS One* 11:1–19. <https://doi.org/10.1371/journal.pone.0148777>
120. Verma P, Dalal K (2013) Serum cartilage oligomeric matrix protein (COMP) in knee osteoarthritis: A novel diagnostic and prognostic biomarker. *Journal of Orthopaedic Research* 31:999–1006. <https://doi.org/10.1002/jor.22324>
121. Rosenberg K, Olsson H, Mörgelin M, Heinegård D (1998) Cartilage oligomeric matrix protein shows high affinity zinc-dependent interaction with triple helical collagen. *Journal of Biological Chemistry* 273:20397–20403. <https://doi.org/10.1074/jbc.273.32.20397>
122. Ogston AG, Stanier JE The physiological function of hyaluronic acid in synovial fluid; viscous, elastic and lubricant properties. *J Physiol (1953)* 19:244–252. <https://doi.org/10.1113/jphysiol.1953.sp004842>
123. Gupta RC, Lall R, Srivastava A, Sinha A (2019) Hyaluronic acid: Molecular mechanisms and therapeutic trajectory. *Front Vet Sci* 6:. <https://doi.org/10.3389/fvets.2019.00192>
124. Akkiraju H, Nohe A (2015) Role of Chondrocytes in Cartilage Formation, Progression of Osteoarthritis and Cartilage Regeneration. *J Dev Biol* 3:177–192. <https://doi.org/10.3390/jdb3040177>
125. Zuscik MJ, Hilton MJ, Zhang X, et al (2008) Regulation of chondrogenesis and chondrocyte differentiation by stress. *Journal of Clinical Investigation* 118:429–438. <https://doi.org/10.1172/JCI34174.of>
126. Fawns HT, Landells JW (1953) Histochemical studies of rheumatic conditions. I. Observations on the fine structures of the matrix of normal bone and cartilage. *Ann Rheum Dis* 12:105–113. <https://doi.org/10.1136/ard.12.2.105>
127. Gerber HP, Vu TH, Ryan AM, et al (1999) VEGF couples hypertrophic cartilage remodeling, ossification and angiogenesis during endochondral bone formation. *Nat Med* 5:623–628. <https://doi.org/10.1038/9467>
128. Loeser RF, Olex AL, McNulty MA, et al (2013) Disease Progression and Phasic Changes in Gene Expression in a Mouse Model of Osteoarthritis. *PLoS One* 8:. <https://doi.org/10.1371/journal.pone.0054633>
129. Tchetina E V, Squires G, Poole AR (2005) Increased Type II Collagen Degradation and Very Early Focal Cartilage Degeneration Is Associated with Upregulation of Chondrocyte Differentiation Related Genes in Early Human Articular Cartilage Lesions. *J Rheumatol* 32:876–886

130. Qi-ping D, Min-lei Q, Ping S, Dong H (2003) Clinical observation on treatment of 60 cases of osteoarthritis of knee joint by electroacupuncture. *Journal of Acupuncture and Tuina Science* 1:38–40. <https://doi.org/10.1007/BF02874745>
131. Buckland-Wright JC, Macfarlane DG, Lynch A, Clark B (1990) Quantitative microfocal radiographic assessment of progression in osteoarthritis of the hand. *Arthritis and Rheumatism* 33:57–65. <https://doi.org/10.1002/art.1780330107>
132. Harrison M, Schajowicz F, Trueta J (1953) Osteoarthritis of the hip: a study of the nature and evolution of the disease. *J Bone Joint Surg Br* 35-B:598–626. <https://doi.org/10.1302/0301-620X.35B4.598>
133. Goldring MB, Goldring SR (2007) Osteoarthritis. *J Cell Physiol* 213:626–634. <https://doi.org/10.1002/JCP>
134. Goldenberg DL, Egan MS, Cohen AS (1982) Inflammatory synovitis in degenerative joint disease. *J Rheumatol* 9:204–209
135. Prieto-Potin I, Largo R, Roman-Blas JA, et al (2015) Characterization of multinucleated giant cells in synovium and subchondral bone in knee osteoarthritis and rheumatoid arthritis. *BMC Musculoskelet Disord* 16:1–10. <https://doi.org/10.1186/s12891-015-0664-5>
136. Hu Y, Chen X, Wang S, et al (2021) Subchondral bone microenvironment in osteoarthritis and pain. *Bone Res* 9:. <https://doi.org/10.1038/s41413-021-00147-z>
137. Dieppe P, Cushnaghan J, Young P, et al (1993) Prediction of the progression of joint space narrowing in osteoarthritis of the knee by bone scintigraphy. *Ann Rheum Dis* 52:557–563. <https://doi.org/10.1136/ard.52.8.557>
138. Petersson IF, Boegard T, Svensson B, et al (1993) Changes in cartilage and bone metabolism identified by serum markers in early osteoarthritis of the knee joint. *Ann Rheum Dis* 52:557–563. <https://doi.org/10.1093/rheumatology/37.1.46>
139. Mrosek EH, Lahm A, Erggelet C, et al (2006) Subchondral bone trauma causes cartilage matrix degeneration: An immunohistochemical analysis in a canine model. *Osteoarthritis Cartilage* 14:171–178. <https://doi.org/10.1016/j.joca.2005.08.004>
140. Muraoka T, Hagino H, Okano T, et al (2007) Role of subchondral bone in osteoarthritis development: A comparative study of two strains of guinea pigs with and without spontaneously occurring osteoarthritis. *Arthritis Rheum* 56:3366–3374. <https://doi.org/10.1002/art.22921>
141. Couchourel D, Aubry I, Delalandre A, et al (2009) Altered mineralization of human osteoarthritic osteoblasts is attributable to abnormal type I collagen production. *Arthritis Rheum* 60:1438–1450. <https://doi.org/10.1002/art.24489>
142. Bailey AJ, Sims TJ, Knott L (2002) Phenotypic expression of osteoblast collagen in osteoarthritic bone: production of type I homotrimer. *Int J Biochem Cell Biol* 34:176–182. [https://doi.org/10.1016/s1357-2725\(01\)00107-8](https://doi.org/10.1016/s1357-2725(01)00107-8)
143. Martel-Pelletier J, Pelletier J-P (2010) Is osteoarthritis a disease involving only cartilage or other articular tissues? *Joint Diseases and Related Surgery* 21:2–14
144. Gs M, Mologhianu G (2014) Osteoarthritis pathogenesis-a complex process that involves the entire joint. *J Med Life* 7:37–41

145. Roemer FW, Neogi T, Nevitt MC, et al (2010) Subchondral bone marrow lesions are highly associated with, and predict subchondral bone attrition longitudinally: the MOST study. *Osteoarthritis Cartilage* 18:47–53. <https://doi.org/10.1016/j.joca.2009.08.018>
146. Carrino JA, Blum J, Parellada JA, et al (2006) MRI of bone marrow edema-like signal in the pathogenesis of subchondral cysts. *Osteoarthritis Cartilage* 14:1081–1085. <https://doi.org/10.1016/j.joca.2006.05.011>
147. Tanamas SK, Wluka AE, Pelletier JP, et al (2010) Bone marrow lesions in people with knee osteoarthritis predict progression of disease and joint replacement: A longitudinal study. *Rheumatology* 49:2413–2419. <https://doi.org/10.1093/rheumatology/keq286>
148. Hilal G, Martel-Pelletier J, Pelletier JP, et al (1998) Osteoblast-like cells from human subchondral osteoarthritic bone demonstrate an altered phenotype in vitro: Possible role in subchondral bone sclerosis. *Arthritis Rheum* 41:891–899. [https://doi.org/10.1002/1529-0131\(199805\)41:5<891::AID-ART17>3.0.CO;2-X](https://doi.org/10.1002/1529-0131(199805)41:5<891::AID-ART17>3.0.CO;2-X)
149. Massicotte F, Fernandes JC, Martel-Pelletier J, et al (2006) Modulation of insulin-like growth factor 1 levels in human osteoarthritic subchondral bone osteoblasts. *Bone* 38:333–341. <https://doi.org/10.1016/j.bone.2005.09.007>
150. Hock JM, Centrella M, Canalis E (1988) Insulin-Like Growth Factor I Has Independent Effects on Bone Matrix Formation and Cell Replication. *J Bone Miner Res* 3:254–260
151. Zgoda M, Paczek L, Bartłomiejczyk I, et al (2005) Transforming growth factor- $\beta$ 1, interleukin-1 $\beta$  and collagenase activity in subchondral bone of the femur and the severity of osteoarthritis of the hip. *Clin Exp Rheumatol* 23:912–913
152. Sakao K, Takahashi KA, Arai Y, et al (2009) Asporin and transforming growth factor- $\beta$  gene expression in osteoblasts from subchondral bone and osteophytes in osteoarthritis. *Journal of Orthopaedic Science* 14:738–747. <https://doi.org/10.1007/s00776-009-1401-4>
153. Xiong J, Onal M, Jilka RL, et al (2011) Matrix-embedded cells control osteoclast formation. *Nat Med* 17:1235–1241. <https://doi.org/10.1038/nm.2448>
154. Nakashima T, Hayashi M, Fukunaga T, et al (2011) Evidence for osteocyte regulation of bone homeostasis through RANKL expression. *Nat Med* 17:1231–1234. <https://doi.org/10.1038/nm.2452>
155. Lacey DL, Timms E, Tan HL, et al (1998) Osteoprotegerin ligand is a cytokine that regulates osteoclast differentiation and activation. *Cell* 93:165–176. [https://doi.org/10.1016/S0092-8674\(00\)81569-X](https://doi.org/10.1016/S0092-8674(00)81569-X)
156. Lacey DL, Tan HL, Lu J, et al (2000) Osteoprotegerin ligand modulates murine osteoclast survival in vitro and in vivo. *American Journal of Pathology* 157:435–448. [https://doi.org/10.1016/S0002-9440\(10\)64556-7](https://doi.org/10.1016/S0002-9440(10)64556-7)
157. Massicotte F, Lajeunesse D, Benderdour M, et al (2002) Can altered production of interleukin-1 $\beta$ , interleukin-6, transforming growth factor- $\beta$  and prostaglandin E2 by isolated human subchondral osteoblasts identify two subgroups of osteoarthritic patients. *Osteoarthritis Cartilage* 10:491–500. <https://doi.org/10.1053/joca.2002.0528>

158. Stashenko P, Dewhirst FE, Rooney ML, et al (1987) Interleukin-1 $\beta$  Is a Potent Inhibitor of Bone Formation In Vitro. *Journal of bone and mineral research* 2:559–565. <https://doi.org/10.1002/jbmr.5650020612>
159. Gowen M, Wood DD, Ihrie EJ, et al (1983) An interleukin 1 like factor stimulates bone resorption in vitro. *Nature* 306:378–380. <https://doi.org/10.1038/306378a0>
160. Dewhirst FE, Stashenko PP, Mole JE, Tsurumachi T (1985) Purification and partial sequence of human osteoclast-activating factor: identity with interleukin 1 beta. 135:2562–2568
161. Akatsu T, Takahashi N, Udagawa N, et al (1991) Role of Prostaglandins in Interleukin-1-Induced Bone Resorption in Mice In Vitro. *Journal of Bone and Mineral Research* 6:183–190. <https://doi.org/10.1002/jbmr.5650060212>
162. Sandell LJ, Aigner T (2001) Articular cartilage and changes in arthritis matrix degradation. *Arthritis Res* 3:107–113. <https://doi.org/10.1186/ar325>
163. Redini F, Galera P, Mauviel A, et al (1988) Transforming growth factor  $\beta$  stimulates collagen and glycosaminoglycan biosynthesis in cultured rabbit articular chondrocytes. *FEBS Lett* 234:172–175. [https://doi.org/10.1016/0014-5793\(88\)81327-9](https://doi.org/10.1016/0014-5793(88)81327-9)
164. Chandrasekhar S, Harvey AK (1988) Transforming growth factor- $\beta$  is a potent inhibitor of IL-1 induced protease activity and cartilage proteoglycan degradation. *Biomedical and Biophysical Research Communications* 157:1352–1359. [https://doi.org/10.1016/s0006-291x\(88\)81024-6](https://doi.org/10.1016/s0006-291x(88)81024-6)
165. Vuolteenaho K, Moilanen T, Jalonen U, et al (2005) TGF $\beta$  inhibits IL-1 -induced iNOS expression and NO production in immortalized chondrocytes. *Inflammation Research* 54:420–427. <https://doi.org/10.1007/s00011-005-1373-6>
166. Flechtenmacher J, Huch K, Thonar EJMA, et al (1996) Recombinant human osteogenic protein 1 is a potent stimulator of the synthesis of cartilage proteoglycans and collagens by human articular chondrocytes. *Arthritis Rheum* 39:1896–1904. <https://doi.org/10.1002/art.1780391117>
167. Huch K, Wilbrink B, Flechtenmacher J, et al (1997) Effects of recombinant human osteogenic protein 1 on the production of proteoglycan, prostaglandin E2, and interleukin-1 receptor antagonist by human articular chondrocytes cultured in the presence of interleukin-1 $\beta$ . *Arthritis Rheum* 40:2157–2161. <https://doi.org/10.1002/art.1780401209>
168. Wei F-Y, Lee JK, Wei L, et al (2017) Correlation of insulin-like growth factor 1 and osteoarthritic cartilage degradation: a spontaneous osteoarthritis in guinea-pig HHS Public Access. *Eur Rev Med Pharmacol Sci* 21:4493–4500
169. Zhong L, Huang X, Karperien M, Post JN (2016) Correlation between gene expression and osteoarthritis progression in human. *Int J Mol Sci* 17:. <https://doi.org/10.3390/ijms17071126>
170. Enomoto H, Enomoto-Iwamoto M, Iwamoto M, et al (2000) Cbfa1 is a positive regulatory factor in chondrocyte maturation. *Journal of Biological Chemistry* 275:8695–8702. <https://doi.org/10.1074/jbc.275.12.8695>

171. Miller RE, Miller RJ, Malfait AM (2014) Osteoarthritis joint pain: The cytokine connection. *Cytokine* 70:185–193. <https://doi.org/10.1016/j.cyto.2014.06.019>
172. Tetlow LC, Adlam DJ, Woolley DE (2001) Matrix metalloproteinase and proinflammatory cytokine production by chondrocytes of human osteoarthritic cartilage; Associations with degenerative changes. *Arthritis Rheum* 44:585–594. [https://doi.org/10.1002/1529-0131\(200103\)44:3<585::AID-ANR107>3.0.CO;2-C](https://doi.org/10.1002/1529-0131(200103)44:3<585::AID-ANR107>3.0.CO;2-C)
173. Neuhold LA, Killar L, Zhao W, et al (2001) Postnatal expression in hyaline cartilage of constitutively active human collagenase-3 (MMP-13) induces osteoarthritis in mice. *Journal of Clinical Investigation* 107:35–44. <https://doi.org/10.1172/JCI10564>
174. Roughley PJ, Mort JS (2014) The role of aggrecan in normal and osteoarthritic cartilage. *J Exp Orthop* 1:1–11. <https://doi.org/10.1186/s40634-014-0008-7>
175. Dahlberg L, Billingham RC, Webb G, et al (2000) Selective enhancement of collagenase-mediated cleavage of resident type II collagen in cultured osteoarthritic cartilage and arrest with a synthetic inhibitor that spares collagenase 1 (Matrix metalloproteinase 1). *Arthritis Rheum* 43:673–682. [https://doi.org/10.1002/1529-0131\(200003\)43:3<673::AID-ANR25>3.0.CO;2-8](https://doi.org/10.1002/1529-0131(200003)43:3<673::AID-ANR25>3.0.CO;2-8)
176. Koshy PJT, Lundy CJ, Rowan AD, et al (2002) The modulation of matrix metalloproteinase and ADAM gene expression in human chondrocytes by interleukin-1 and oncostatin M: A time-course study using real-time quantitative reverse transcription-polymerase chain reaction. *Arthritis Rheum* 46:961–967. <https://doi.org/10.1002/art.10212>
177. Pufe T, Harde V, Petersen W, et al (2004) Vascular endothelial growth factor (VEGF) induces matrix metalloproteinase expression in immortalized chondrocytes. *Journal of Pathology* 202:367–374. <https://doi.org/10.1002/path.1527>
178. Kashiwagi M, Tortorella M, Nagase H, Brew K (2001) TIMP-3 Is a Potent Inhibitor of Aggrecanase 1 (ADAM-TS4) and Aggrecanase 2 (ADAM-TS5). *Journal of Biological Chemistry* 276:12501–12504. <https://doi.org/10.1074/jbc.C000848200>
179. Fransès RE, McWilliams DF, Mapp PI, Walsh DA (2010) Osteochondral angiogenesis and increased protease inhibitor expression in OA. *Osteoarthritis Cartilage* 18:563–571. <https://doi.org/10.1016/j.joca.2009.11.015>
180. Zelzer E, Mamluk R, Ferrara N, et al (2004) VEGFA is necessary for chondrocyte survival during bone development. *Development* 131:2161–2171. <https://doi.org/10.1242/dev.01053>
181. Weber A, Wasiliew P, Kracht M (2010) Interleukin-1 (IL-1) Pathway. *Immunology* 3:1–19. <https://doi.org/10.1126/scisignal.3105cm1>
182. Goldring MB, Otero M, Plumb DA, et al (2011) Roles of inflammatory and anabolic cytokines in cartilage metabolism: signals and multiple effectors converge upon MMP-13 regulation in osteoarthritis. *21:202–220*. <https://doi.org/10.22203/ecm.v021a16>
183. Séguin CA, Bernier SM (2003) TNF $\alpha$  Suppresses Link Protein and Type II Collagen Expression in Chondrocytes: Role of MEK1/2 and NF- $\kappa$ B Signaling Pathways. *J Cell Physiol* 197:356–369. <https://doi.org/10.1002/jcp.10371>

184. Liacini A, Sylvester J, Li WQ, et al (2003) Induction of matrix metalloproteinase-13 gene expression by TNF- $\alpha$  is mediated by MAP kinases, AP-1, and NF- $\kappa$ B transcription factors in articular chondrocytes. *Exp Cell Res* 288:208–217. [https://doi.org/10.1016/S0014-4827\(03\)00180-0](https://doi.org/10.1016/S0014-4827(03)00180-0)
185. Zhang G, Sun Y, Wang Y, et al (2016) MiR-502-5p inhibits IL-1 $\beta$ -induced chondrocyte injury by targeting TRAF2. *Cell Immunol* 302:50–57. <https://doi.org/10.1016/j.cellimm.2016.01.007>
186. Molnar V, Matišić V, Kodvanj I, et al (2021) Cytokines and Chemokines involved in osteoarthritis pathogenesis. *Int J Mol Sci* 22:. <https://doi.org/10.3390/ijms22179208>
187. Lyons TJ, McClure SF, Stoddart RW, McClure J (2006) The normal human chondro-osseous junctional region: Evidence for contact of uncalcified cartilage with subchondral bone and marrow spaces. *BMC Musculoskelet Disord* 7:1–8. <https://doi.org/10.1186/1471-2474-7-52>
188. Findlay DM, Kuliwaba JS (2016) Bone-cartilage crosstalk: A conversation for understanding osteoarthritis. *Bone Res* 4:1–12. <https://doi.org/10.1038/boneres.2016.28>
189. Wang, B., Zhou, X., Price, C., Li, W., Pan, J., Wang L (2014) Quantifying load-induced solute transport and solute-matrix interactions within the osteocyte lacunar-canalicular system. *Journal of Bone and Mineral Research* 28:1075–1086. <https://doi.org/https://doi.org/10.1002/jbmr.1804>
190. Zhang L, Gardiner BS, Smith DW, et al (2010) On the role of diffusible binding partners in modulating the transport and concentration of proteins in tissues. *J Theor Biol* 263:20–29. <https://doi.org/10.1016/j.jtbi.2009.11.023>
191. O'Hara BP, G Urban JP, Maroudas A (1990) Influence of cyclic loading on the nutrition of articular cartilage. *Ann Rheum Dis* 49:536–539. <https://doi.org/10.1136/ard.49.7.536>
192. Botter SM, Van Osch GJVM, Clockaerts S, et al (2011) Osteoarthritis induction leads to early and temporal subchondral plate porosity in the tibial plateau of mice: An in vivo microfocal computed tomography study. *Arthritis Rheum* 63:2690–2699. <https://doi.org/10.1002/art.30307>
193. Sanchez C, Deberg MA, Piccardi N, et al (2005) Osteoblasts from the sclerotic subchondral bone downregulate aggrecan but upregulate metalloproteinases expression by chondrocytes. This effect is mimicked by interleukin-6, -1 $\beta$  and oncostatin M pre-treated non-sclerotic osteoblasts. *Osteoarthritis Cartilage* 13:979–987. <https://doi.org/10.1016/j.joca.2005.03.008>
194. Sanchez C, Horcajada MN, Scalfo FM, et al (2015) Carnosol inhibits pro-inflammatory and catabolic mediators of cartilage breakdown in human osteoarthritic chondrocytes and mediates cross-talk between subchondral bone osteoblasts and chondrocytes. *PLoS One* 10:1–15. <https://doi.org/10.1371/journal.pone.0136118>
195. Tat SK, Padrines M, Theoleyre S, et al (2006) OPG/membranous-RANKL complex is internalized via the clathrin pathway before a lysosomal and a proteasomal degradation. *Bone* 39:706–715. <https://doi.org/10.1016/j.bone.2006.03.016>

196. Zhen G, Wen C, Jia X, et al (2013) Inhibition of TGF- $\beta$  signaling in mesenchymal stem cells of subchondral bone attenuates osteoarthritis. *Nat Med* 19:704–712. <https://doi.org/10.1038/nm.3143>
197. Duan R, Xie H, Liu ZZ (2020) The Role of Autophagy in Osteoarthritis. *Front Cell Dev Biol* 8:1–9. <https://doi.org/10.3389/fcell.2020.608388>
198. Glick D, Barth S, Macleod KF (2010) Autophagy: Cellular and molecular mechanisms. *Journal of Pathology* 221:3–12. <https://doi.org/10.1002/path.2697>
199. Sun K, Deng W, Zhang S, et al (2013) Paradoxical roles of autophagy in different stages of tumorigenesis: Protector for normal or cancer cells. *Cell Biosci* 3:. <https://doi.org/10.1186/2045-3701-3-35>
200. Shang L, Chen S, Du F, et al Nutrient starvation elicits an acute autophagic response mediated by Ulk1 dephosphorylation and its subsequent dissociation from AMPK. <https://doi.org/10.1073/pnas.1100844108/-/DCSupplemental>
201. Jung CH, Ro SH, Cao J, et al (2010) MTOR regulation of autophagy. *FEBS Lett* 584:1287–1295. <https://doi.org/10.1016/j.febslet.2010.01.017>
202. Ruvinsky I, Meyuhas O (2006) Ribosomal protein S6 phosphorylation: from protein synthesis to cell size. *Trends Biochem Sci* 31:342–348. <https://doi.org/10.1016/j.tibs.2006.04.003>
203. Ichimiya T, Yamakawa T, Hirano T, et al (2020) Autophagy and autophagy-related diseases: A review. *Int J Mol Sci* 21:1–21. <https://doi.org/10.3390/ijms21238974>
204. Menon MB, Dhamija S (2018) Beclin 1 phosphorylation - at the center of autophagy regulation. *Front Cell Dev Biol* 6:. <https://doi.org/10.3389/fcell.2018.00137>
205. Lamb CA, Yoshimori T, Tooze SA (2013) The autophagosome: Origins unknown, biogenesis complex. *Nat Rev Mol Cell Biol* 14:759–774. <https://doi.org/10.1038/nrm3696>
206. Klionsky DJ, Abdel-Aziz AK, Abdelfatah S, et al (2021) Guidelines for the use and interpretation of assays for monitoring autophagy (4th edition)1. *Autophagy* 17:1–382. <https://doi.org/10.1080/15548627.2020.1797280>
207. Dikic I, Elazar Z (2018) Mechanism and medical implications of mammalian autophagy. *Nat Rev Mol Cell Biol* 19:349–364. <https://doi.org/10.1038/s41580-018-0003-4>
208. Ren J, Zhang Y (2018) Targeting Autophagy in Aging and Aging-Related Cardiovascular Diseases. *Trends Pharmacol Sci* 39:1064–1076. <https://doi.org/10.1016/j.tips.2018.10.005>
209. Feng L, Feng C, Wang CX, et al (2020) Circulating microRNA let-7e is decreased in knee osteoarthritis, accompanied by elevated apoptosis and reduced autophagy. *Int J Mol Med* 45:1464–1476. <https://doi.org/10.3892/ijmm.2020.4534>
210. Qin N, Wei L, Li W, et al (2017) Local intra-articular injection of resveratrol delays cartilage degeneration in C57BL/6 mice by inducing autophagy via AMPK/mTOR pathway. *J Pharmacol Sci* 134:166–174. <https://doi.org/10.1016/j.jphs.2017.06.002>

211. Zhang Y, Vasheghani F, Li YH, et al (2015) Cartilage-specific deletion of mTOR upregulates autophagy and protects mice from osteoarthritis. *Ann Rheum Dis* 74:1432–1440. <https://doi.org/10.1136/annrheumdis-2013-204599>
212. Ribeiro M, López de Figueroa P, Blanco FJ, et al (2016) Insulin decreases autophagy and leads to cartilage degradation. *Osteoarthritis Cartilage* 24:731–739. <https://doi.org/10.1016/j.joca.2015.10.017>
213. Ribeiro M, López de Figueroa P, Nogueira-Recalde U, et al (2016) Diabetes-accelerated experimental osteoarthritis is prevented by autophagy activation. *Osteoarthritis Cartilage* 24:2116–2125. <https://doi.org/10.1016/j.joca.2016.06.019>
214. Ouyang J, Jiang H, Fang H, et al (2017) Isoimperatorin ameliorates Osteoarthritis by downregulating the mammalian target of rapamycin C1 signaling pathway. *Mol Med Rep* 16:9636–9644. <https://doi.org/10.3892/mmr.2017.7777>
215. Cinque L, Forrester A, Bartolomeo R, et al (2015) FGF signalling regulates bone growth through autophagy. *Nature* 528:272–275. <https://doi.org/10.1038/nature16063>
216. Wu TT, Li WM, Yao YM (2016) Interactions between autophagy and inhibitory cytokines. *Int J Biol Sci* 12:884–897. <https://doi.org/10.7150/ijbs.15194>
217. Harris J, Hartman M, Roche C, et al (2011) Autophagy controls IL-1 $\beta$  secretion by targeting Pro-IL-1 $\beta$  for degradation. *Journal of Biological Chemistry* 286:9587–9597. <https://doi.org/10.1074/jbc.M110.202911>
218. Ni Z, Li H, Mu D, et al (2022) Rapamycin Alleviates 2,4,6-Trinitrobenzene Sulfonic Acid-Induced Colitis through Autophagy Induction and NF- $\kappa$  B Pathway Inhibition in Mice. *Mediators Inflamm* 2022:. <https://doi.org/10.1155/2022/2923216>
219. Lampropoulou-Adamidou K, Lelovas P, Karadimas E V., et al (2014) Useful animal models for the research of osteoarthritis. *European Journal of Orthopaedic Surgery and Traumatology* 24:263–271. <https://doi.org/10.1007/s00590-013-1205-2>
220. Saji Joseph J, Tebogo Malindisa S, Ntwasa M (2019) Two-Dimensional (2D) and Three-Dimensional (3D) Cell Culturing in Drug Discovery. In: *Cell Culture*. IntechOpen
221. Edmondson R, Broglie JJ, Adcock AF, Yang L (2014) Three-dimensional cell culture systems and their applications in drug discovery and cell-based biosensors. *Assay Drug Dev Technol* 12:207–218. <https://doi.org/10.1089/adt.2014.573>
222. Tibbitt MW, Anseth KS (2009) Hydrogels as extracellular matrix mimics for 3D cell culture. *Biotechnol Bioeng* 103:655–663. <https://doi.org/10.1002/bit.22361>.Hydrogels
223. Sokolove J, Lepus CM (2013) Role of inflammation in the pathogenesis of osteoarthritis: Latest findings and interpretations. *Ther Adv Musculoskelet Dis* 5:77–94. <https://doi.org/10.1177/1759720X12467868>
224. Zhou S, Thornhill TS, Meng F, et al (2016) Influence of osteoarthritis grade on molecular signature of human cartilage. *Journal of Orthopaedic Research* 34:454–462. <https://doi.org/10.1002/jor.23043>
225. Deshmukh V, Hu H, Barroga C, et al (2018) A small-molecule inhibitor of the Wnt pathway (SM04690) as a potential disease modifying agent for the treatment of osteoarthritis of the knee. *Osteoarthritis Cartilage* 26:18–27. <https://doi.org/10.1016/j.joca.2017.08.015>

226. Al-Modawi RN, Brinchmann JE, Karlsen TA (2019) Multi-pathway protective effects of microRNAs on human chondrocytes in an in vitro model of osteoarthritis. *Mol Ther Nucleic Acids* 17:776–790. <https://doi.org/10.1016/j.omtn.2019.07.011>
227. Antoni D, Burckel H, Josset E, Noel G (2015) Three-dimensional cell culture: A breakthrough in vivo. *Int J Mol Sci* 16:5517–5527. <https://doi.org/10.3390/ijms16035517>
228. Gieni RS, Hendzel MJ (2008) Mechanotransduction from the ECM to the genome: Are the pieces now in place? *J Cell Biochem* 104:1964–1987. <https://doi.org/10.1002/jcb.21364>
229. Stokes DG, Liu G, Coimbra IB, et al (2002) Assessment of the gene expression profile of differentiated and dedifferentiated human fetal chondrocytes by microarray analysis. *Arthritis Rheum* 46:404–419. <https://doi.org/10.1002/art.10106>
230. Marlovits S, Hombauer M, Truppe M, et al (2004) Changes in the ratio of type-I and type-II collagen expression during monolayer culture of human chondrocytes. *J Bone Joint Surg Br* 86-B:286–295. <https://doi.org/10.1302/0301-620x.86b2.14918>
231. Manferdini C, Maumus M, Gabusi E, et al (2013) Adipose-derived mesenchymal stem cells exert antiinflammatory effects on chondrocytes and synoviocytes from osteoarthritis patients through prostaglandin E2. *Arthritis Rheum* 65:1271–1281. <https://doi.org/10.1002/art.37908>
232. Kuroda K, Kabata T, Hayashi K, et al (2015) The paracrine effect of adipose-derived stem cells inhibits osteoarthritis progression *Orthopedics and biomechanics. BMC Musculoskelet Disord* 16:1–10. <https://doi.org/10.1186/s12891-015-0701-4>
233. Geurts J, Jurić D, Müller M, et al (2018) Novel ex vivo human osteochondral explant model of knee and spine osteoarthritis enables assessment of inflammatory and drug treatment responses. *Int J Mol Sci* 19:. <https://doi.org/10.3390/ijms19051314>
234. Lee CM, Kisiday JD, McIlwraith CW, et al (2013) Development of an in vitro model of injury-induced osteoarthritis in cartilage explants from adult horses through application of single-impact compressive overload. *Am J Vet Res* 74:40–47. <https://doi.org/https://doi.org/10.2460/ajvr.74.1.40>
235. Byron CR, Trahan RA (2017) Comparison of the effects of Interleukin-1 on equine articular cartilage explants and cocultures of osteochondral and synovial explants. *Front Vet Sci* 4:1–10. <https://doi.org/10.3389/fvets.2017.00152>
236. Haltmayer E, Ribitsch I, Gabner S, et al (2019) Co-culture of osteochondral explants and synovial membrane as in vitro model for osteoarthritis. *PLoS One* 14:1–19. <https://doi.org/10.1371/journal.pone.0214709>
237. Duval K, Grover H, Han LH, et al (2017) Modeling physiological events in 2D vs. 3D cell culture. *Physiology* 32:266–277. <https://doi.org/10.1152/physiol.00036.2016>
238. Buyuksungur S, Endogan Tanir T, Buyuksungur A, et al (2017) 3D printed poly( $\epsilon$ -caprolactone) scaffolds modified with hydroxyapatite and poly(propylene fumarate) and their effects on the healing of rabbit femur defects. *Biomater Sci* 5:2144–2158. <https://doi.org/10.1039/c7bm00514h>

239. Mandal BB, Kundu SC (2009) Cell proliferation and migration in silk fibroin 3D scaffolds. *Biomaterials* 30:2956–2965. <https://doi.org/10.1016/j.biomaterials.2009.02.006>
240. Zeng L, Yao Y, Wang DA, Chen X (2014) Effect of microcavitary alginate hydrogel with different pore sizes on chondrocyte culture for cartilage tissue engineering. *Materials Science and Engineering C* 34:168–175. <https://doi.org/10.1016/j.msec.2013.09.003>
241. Remya NS, Nair PD (2013) Engineering cartilage tissue interfaces using a natural glycosaminoglycan hydrogel matrix - An in vitro study. *Materials Science and Engineering C* 33:575–582. <https://doi.org/10.1016/j.msec.2012.09.015>
242. An H, Lee JW, Lee HJ, et al (2018) Hyaluronate-alginate hybrid hydrogels modified with biomimetic peptides for controlling the chondrocyte phenotype. *Carbohydr Polym.* <https://doi.org/10.1016/j.carbpol.2018.06.016>
243. Song K, Li L, Yan X, et al (2016) Fabrication and development of artificial osteochondral constructs based on cancellous bone/hydrogel hybrid scaffold. *J Mater Sci Mater Med* 27:. <https://doi.org/10.1007/s10856-016-5722-5>
244. Ivanovska J, Zehnder T, Lennert P, et al (2016) Biofabrication of 3D Alginate-Based Hydrogel for Cancer Research: Comparison of Cell Spreading, Viability, and Adhesion Characteristics of Colorectal HCT116 Tumor Cells. *Tissue Eng Part C Methods* 22:708–715. <https://doi.org/10.1089/ten.tec.2015.0452>
245. Galuzzi M, Perteghella S, Antonioli B, et al (2018) Human engineered cartilage and decellularized matrix as an alternative to animal osteoarthritis model. *Polymers (Basel)* 10:1–16. <https://doi.org/10.3390/polym10070738>
246. Qiu Y, Lim JJ, Scott Jr L, et al (2011) PEG-based hydrogels with tunable degradation characteristics to control delivery of marrow stromal cells for tendon overuse injuries. *Acta Biomater* 7:959–966. <https://doi.org/10.1016/j.actbio.2010.11.002>
247. Steinmetz NJ, Aisenbrey EA, Westbrook KK, et al (2015) Mechanical loading regulates human MSC differentiation in a multi-layer hydrogel for osteochondral tissue engineering. *Acta Biomater* 21:1–12. <https://doi.org/10.1016/j.actbio.2015.04.015>
248. Maisani M, Pezzoli D, Chassande O, Mantovani D (2016) Cellularizing hydrogel-based scaffolds to repair bone tissue: How to create a physiologically relevant micro-environment? *J Tissue Eng* 8:. <https://doi.org/10.1177/2041731417712073>
249. Dey P, Schneider T, Chiappisi L, et al (2016) Mimicking of Chondrocyte Microenvironment Using in Situ Forming Dendritic Polyglycerol Sulfate-Based Synthetic Polyanionic Hydrogels. *Macromol Biosci* 16:580–590. <https://doi.org/10.1002/mabi.201500377>
250. Inagaki Y, Kitamura N, Kurokawa T, et al (2014) Effects of culture on PAMPS/PDMAAm double-network gel on chondrogenic differentiation of mouse C3H10T1/2 cells: In vitro experimental study. *BMC Musculoskelet Disord* 15:1–7. <https://doi.org/10.1186/1471-2474-15-320>
251. Stüdle C, Vallmajó-Martín Q, Haumer A, et al (2018) Spatially confined induction of endochondral ossification by functionalized hydrogels for ectopic engineering of osteochondral tissues. *Biomaterials* 1–31. <https://doi.org/10.1016/j.biomaterials.2018.04.025>

252. Samavedi S, Diaz-Rodriguez P, Erndt-Marino JD, Hahn MS (2017) A three-dimensional chondrocyte-macrophage coculture system to probe inflammation in experimental osteoarthritis. *Tissue Eng Part A* 23:101–114. <https://doi.org/10.1089/ten.tea.2016.0007>
253. Malikmammadov E, Tanir TE, Kiziltay A, et al (2018) PCL and PCL-based materials in biomedical applications. *J Biomater Sci Polym Ed* 29:863–893. <https://doi.org/10.1080/09205063.2017.1394711>
254. Woodruff MA, Hutmacher DW (2010) The return of a forgotten polymer - Polycaprolactone in the 21st century. *Progress in Polymer Science (Oxford)* 35:1217–1256. <https://doi.org/10.1016/j.progpolymsci.2010.04.002>
255. Calvert JW, Marra KG, Cook L, et al (2000) Characterization of osteoblast-like behavior of cultured bone marrow stromal cells on various polymer surfaces. *J Biomed Mater Res* 52:279–284. [https://doi.org/10.1002/1097-4636\(200011\)52:2<279::AID-JBM6>3.0.CO;2-8](https://doi.org/10.1002/1097-4636(200011)52:2<279::AID-JBM6>3.0.CO;2-8)
256. Brennan M, Renaud A, Gamblin AL, et al (2015) 3D cell culture and osteogenic differentiation of human bone marrow stromal cells plated onto jet-sprayed or electrospun micro-fiber scaffolds. *Biomedical Materials (Bristol)* 10:. <https://doi.org/10.1088/1748-6041/10/4/045019>
257. Bouffi C, Thomas O, Bony C, et al (2010) The role of pharmacologically active microcarriers releasing TGF- $\beta$ 3 in cartilage formation in vivo by mesenchymal stem cells. *Biomaterials* 31:6485–6493. <https://doi.org/10.1016/j.biomaterials.2010.05.013>
258. Morille M, Toupet K, Montero-Menei CN, et al (2016) PLGA-based microcarriers induce mesenchymal stem cell chondrogenesis and stimulate cartilage repair in osteoarthritis. *Biomaterials* 88:60–69. <https://doi.org/10.1016/j.biomaterials.2016.02.022>
259. Li S, Lao J, Chen BPC, et al (2003) Genomic analysis of smooth muscle cells in 3-dimensional collagen matrix. *The FASEB journal : official publication of the Federation of American Societies for Experimental Biology* 17:97–99. <https://doi.org/10.1096/fj.02-0256fje>
260. Fallica B, Maffei JS, Villa S, et al (2012) Alteration of Cellular Behavior and Response to PI3K Pathway Inhibition by Culture in 3D Collagen Gels. *PLoS One* 7:e48024
261. Caron MMJ, Emans PJ, Coolen MME, et al (2012) Redifferentiation of dedifferentiated human articular chondrocytes: Comparison of 2D and 3D cultures. *Osteoarthritis Cartilage* 20:1170–1178. <https://doi.org/10.1016/j.joca.2012.06.016>
262. Hirao M, Tamai N, Tsumaki N, et al (2006) Oxygen tension regulates chondrocyte differentiation and function during endochondral ossification. *Journal of Biological Chemistry* 281:31079–31092. <https://doi.org/10.1074/jbc.M602296200>
263. Utting JC, Robins SP, Brandao-Burch A, et al (2006) Hypoxia inhibits the growth, differentiation and bone-forming capacity of rat osteoblasts. *Exp Cell Res* 312:1693–1702. <https://doi.org/10.1016/j.yexcr.2006.02.007>
264. Nakagawa Y, Muneta T, Otabe K, et al (2016) Cartilage derived from bone marrow mesenchymal stem cells expresses lubricin in vitro and in vivo. *PLoS One* 11:1–19. <https://doi.org/10.1371/journal.pone.0148777>

265. Alakpa E V., Jayawarna V, Lampel A, et al (2016) Tunable Supramolecular Hydrogels for Selection of Lineage-Guiding Metabolites in Stem Cell Cultures. *Chem* 1:298–319. <https://doi.org/10.1016/j.chempr.2016.07.001>
266. Jayawarna V, Ali M, Jowitt TA, et al (2006) Nanostructured hydrogels for three-dimensional cell culture through self-assembly of fluorenylmethoxycarbonyl-dipeptides. *Advanced Materials* 18:611–614. <https://doi.org/10.1002/adma.200501522>
267. Smith AM, Williams RJ, Tang C, et al (2008) Fmoc-diphenylalanine self assembles to a hydrogel via a novel architecture based on  $\pi$ - $\pi$  interlocked  $\beta$ -sheets. *Advanced Materials* 20:37–41. <https://doi.org/10.1002/adma.200701221>
268. Jayawarna V, Richardson SM, Hirst AR, et al (2009) Introducing chemical functionality in Fmoc-peptide gels for cell culture. *Acta Biomater* 5:934–943. <https://doi.org/10.1016/j.actbio.2009.01.006>
269. Huettner N, Dargaville TR, Forget A (2018) Discovering Cell-Adhesion Peptides in Tissue Engineering: Beyond RGD. *Trends Biotechnol* 36:372–383. <https://doi.org/10.1016/j.tibtech.2018.01.008>
270. Livak KJ, Schmittgen TD (2001) Analysis of relative gene expression data using real-time quantitative PCR and the  $2^{-\Delta\Delta CT}$  method. *Methods* 25:402–408. <https://doi.org/10.1006/meth.2001.1262>
271. Pautke C, Schieker M, Tischler T, et al (2004) Characterization of osteosarcoma cell lines MG-63, Saos-2 and U-2 in comparison to human osteoblasts. *European Journal of Vascular and Endovascular Surgery* 24:3743–3748. [https://doi.org/10.1016/S1078-5884\(98\)80019-1](https://doi.org/10.1016/S1078-5884(98)80019-1)
272. Finger F, Schörle C, Zien A, et al (2003) Molecular Phenotyping of Human Chondrocyte Cell Lines T/C-28a2, T/C-28a4, and C-28/I2. *Arthritis Rheum* 48:3395–3403. <https://doi.org/10.1002/art.11341>
273. Loeser RF, Sadiev S, Tan L, Goldring MB (2000) Integrin expression by primary and immortalized human chondrocytes: Evidence of a differential role for  $\alpha 1\beta 1$  and  $\alpha 2\beta 1$  integrins in mediating chondrocyte adhesion to types II and VI collagen. *Osteoarthritis Cartilage* 8:96–105. <https://doi.org/10.1053/joca.1999.0277>
274. Greco KV, Iqbal AJ, Rattazzi L, et al (2011) High density micromass cultures of a human chondrocyte cell line: A reliable assay system to reveal the modulatory functions of pharmacological agents. *Biochem Pharmacol* 82:1919–1929. <https://doi.org/10.1037/a0032811.Child>
275. Archer CW, McDowell J, Bayliss MT, et al (1990) Phenotypic modulation in subpopulations of human articular chondrocytes in vitro. *J Cell Sci* 97:361–371. <https://doi.org/10.1242/jcs.97.2.361>
276. Goldring MB, Birkhead JR, Suen L, et al (1994) Interleukin-1, beta-modulated Gene Expression in Immortalized Human Chondrocytes. *Journal of Clinical Investigation* 94:2307–2316. <https://doi.org/10.1172/JCI117595>.
277. Finger F, Schörle C, Zien A, et al (2003) Molecular Phenotyping of Human Chondrocyte Cell Lines T/C-28a2, T/C-28a4, and C-28/I2. *Arthritis Rheum* 48:3395–3403. <https://doi.org/10.1002/art.11341>

278. Loeser RF, Sadiev S, Tan L, Goldring MB (2000) Integrin expression by primary and immortalized human chondrocytes: Evidence of a differential role for  $\alpha 1\beta 1$  and  $\alpha 2\beta 1$  integrins in mediating chondrocyte adhesion to types II and VI collagen. *Osteoarthritis Cartilage* 8:96–105. <https://doi.org/10.1053/joca.1999.0277>
279. Kokenyesi R, Tan L, Robbins JR, Goldring MB (2000) Proteoglycan production by immortalized human chondrocyte cell lines cultured under conditions that promote expression of the differentiated phenotype. *Arch Biochem Biophys* 383:79–90. <https://doi.org/10.1006/abbi.2000.2044>
280. Goldring MB, Fukuo K, Birkhead JR, et al (1994) Transcriptional suppression by interleukin-1 and interferon- $\gamma$  of type II collagen gene expression in human chondrocytes. *J Cell Biochem* 54:85–99. <https://doi.org/10.1002/jcb.240540110>
281. Czekanska EM, Stoddart MJ, Ralphs JR, et al (2014) A phenotypic comparison of osteoblast cell lines versus human primary osteoblasts for biomaterials testing. *J Biomed Mater Res A* 102:2636–2643. <https://doi.org/10.1002/jbm.a.34937>
282. Hashemibeni B, Jafary F, Esmail N, et al (2013) Comparison of phenotypic characterization between differentiated osteoblasts from stem cells and calvaria osteoblasts in vitro. *Int J Prev Med* 4:180–186
283. Prideaux M, Wijenayaka AR, Kumarasinghe DD, et al (2014) SaOS2 osteosarcoma cells as an in vitro model for studying the transition of human osteoblasts to osteocytes. *Calcif Tissue Int* 95:183–193. <https://doi.org/10.1007/s00223-014-9879-y>
284. Rodan SB, Imai Y, Thiede MA, et al (1987) Characterization of a Human Osteosarcoma Cell Line (Saos-2) with Osteoblastic Properties. *Cancer Res* 47:4961–4966
285. Simon MJK, Niehoff P, Kimmig B, et al (2010) Expression profile and synthesis of different collagen types I, II, III, and V of human gingival fibroblasts, osteoblasts, and SaOS-2 cells after bisphosphonate treatment. *Clin Oral Investig* 14:51–58. <https://doi.org/10.1007/s00784-009-0312-2>
286. Prideaux M, Wijenayaka AR, Kumarasinghe DD, et al (2014) SaOS2 osteosarcoma cells as an in vitro model for studying the transition of human osteoblasts to osteocytes. *Calcif Tissue Int* 95:183–193. <https://doi.org/10.1007/s00223-014-9879-y>
287. Goldring MB (2004) Culture of Immortalized Chondrocytes and Their Use As Models of Chondrocyte Function. *Cartilage and Osteoarthritis* 100:037–052. <https://doi.org/10.1385/1-59259-810-2:037>
288. Watt FM (1988) Effect of seeding density on stability of the differentiated phenotype of pig articular chondrocytes in culture. *J Cell Sci* 89 ( Pt 3):373–378. <https://doi.org/10.1242/jcs.89.3.373>.
289. Stokes DG, Liu G, Dharmavaram R, et al (2001) Regulation of type-II collagen gene expression during human chondrocyte de-differentiation and recovery of chondrocyte-specific phenotype in culture involves Sry-type high-mobility-group box (SOX) transcription factors. *Biochemical Journal* 360:461–470. <https://doi.org/10.1042/0264-6021:3600461>
290. Chen M, Huang J, Yang X, et al (2012) Serum starvation induced cell cycle synchronization facilitates human somatic cells reprogramming. *PLoS One* 7:. <https://doi.org/10.1371/journal.pone.0028203>

291. Kulkarni G V., McCulloch CAG (1994) Serum deprivation induces apoptotic cell death in a subset of Balb/c 3T3 fibroblasts. *J Cell Sci* 107:1169–1179.  
<https://doi.org/10.1242/jcs.107.5.1169>.
292. Saas J, Lindauer K, Bau B, et al (2004) Molecular phenotyping of HCS-2/8 cells as an in vitro model of human chondrocytes. *Osteoarthritis Cartilage* 12:924–934.  
<https://doi.org/10.1016/j.joca.2004.08.002>
293. Bau B, Gebhard PM, Haag J, et al (2002) Relative messenger RNA expression profiling of collagenases and aggrecanases in human articular chondrocytes in vivo and in vitro. *Arthritis Rheum* 46:2648–2657. <https://doi.org/10.1002/art.10531>
294. Sen M, Cheng YH, Goldring MB, et al (2004) WISP3-Dependent Regulation of Type II Collagen and Aggrecan Production in Chondrocytes. *Arthritis Rheum* 50:488–497.  
<https://doi.org/10.1002/art.20005>
295. Kang SW, Yoo SP, Kim BS (2007) Effect of chondrocyte passage number on histological aspects of tissue-engineered cartilage. *Biomed Mater Eng* 17:269–276
296. Jilka RL, Weinstein RS, Bellido T, et al (1998) Osteoblast programmed cell death (apoptosis): Modulation by growth factors and cytokines. *Journal of Bone and Mineral Research* 13:793–802. <https://doi.org/10.1359/jbmr.1998.13.5.793>
297. Newton PT, Staines KA, Spevak L, et al (2012) Chondrogenic ATDC5 cells: An optimised model for rapid and physiological matrix mineralisation. *Int J Mol Med* 30:1187–1193.  
<https://doi.org/10.3892/ijmm.2012.1114>
298. Coe MR, Summers TA, Parsons SJ, et al (1992) Matrix mineralization in hypertrophic chondrocyte cultures: Beta glycerophosphate increases type X collagen messenger RNA and the specific activity of pp60c-src kinase. *Bone Miner* 18:91–106.  
[https://doi.org/10.1016/0169-6009\(92\)90850-d](https://doi.org/10.1016/0169-6009(92)90850-d).
299. Altaf FM, Hering TM, Kazmi NH, et al (2006) Ascorbate-enhanced chondrogenesis of ATDC5 cells. *Eur Cell Mater* 12:64–69. <https://doi.org/10.22203/ecm.v012a08>
300. Xu K, Zhang Y, Ilalov K, et al (2007) Cartilage oligomeric matrix protein associates with Granulin-Epithelin Precursor (GEP) and potentiates GEP-stimulated chondrocyte proliferation. *Journal of Biological Chemistry* 282:11347–11355.  
<https://doi.org/10.1074/jbc.M608744200>
301. Halász K, Kassner A, Mörgelin M, Heinegård D (2007) COMP acts as a catalyst in collagen fibrillogenesis. *Journal of Biological Chemistry* 282:31166–31173.  
<https://doi.org/10.1074/jbc.M705735200>
302. Goldring MB, Birkhead J, Sandell LJ, et al (1988) Interleukin 1 suppresses expression of cartilage-specific types II and IX collagens and increases types I and III collagens in human chondrocytes. *Journal of Clinical Investigation* 82:2026–2037.  
<https://doi.org/10.1172/JCI113823>
303. Chang X, Zheng Y, Yang Q, et al (2012) Carbonic anhydrase I (CA1) is involved in the process of bone formation and is susceptible to ankylosing spondylitis. *Arthritis Res Ther* 14:1–14. <https://doi.org/10.1186/ar3929>

304. Chen F, Walder B, James AW, et al (2012) NELL-1-dependent mineralisation of Saos-2 human osteosarcoma cells is mediated via c-Jun N-terminal kinase pathway activation. *Int Orthop* 36:2181–2187. <https://doi.org/10.1007/s00264-012-1590-x>
305. Wang QG, Wimpenny I, Dey RE, et al (2018) The unique calcium chelation property of poly(vinyl phosphonic acid-co-acrylic acid) and effects on osteogenesis in vitro. *J Biomed Mater Res A* 106:168–179. <https://doi.org/10.1002/jbm.a.36223>
306. Tolba E, Müller WEG, Abd El-Hady BM, et al (2016) High biocompatibility and improved osteogenic potential of amorphous calcium carbonate/vaterite. *J Mater Chem B* 4:376–386. <https://doi.org/10.1039/c5tb02228b>
307. Yeung P, Cheng KH, Yan CH, Chan BP (2019) Collagen microsphere based 3D culture system for human osteoarthritis chondrocytes (hOACs). *Sci Rep* 9:. <https://doi.org/10.1038/s41598-019-47946-3>
308. Askari M, Afzali Naniz M, Kouhi M, et al (2021) Recent progress in extrusion 3D bioprinting of hydrogel biomaterials for tissue regeneration: A comprehensive review with focus on advanced fabrication techniques. *Biomater Sci* 9:535–573. <https://doi.org/10.1039/d0bm00973c>
309. Ramiah P, du Toit LC, Choonara YE, et al (2020) Hydrogel-Based Bioinks for 3D Bioprinting in Tissue Regeneration. *Front Mater* 7:. <https://doi.org/10.3389/fmats.2020.00076>
310. Madduma-Bandara USK, Madihally S V. (2021) Synthetic hydrogels: Synthesis, novel trends, and applications. *J Appl Polym Sci* 138:. <https://doi.org/10.1002/app.50376>
311. MacPherson D, Bram Y, Park J, Schwartz RE (2021) Peptide-based scaffolds for the culture and maintenance of primary human hepatocytes. *Sci Rep* 11:. <https://doi.org/10.1038/s41598-021-86016-5>
312. Alsaykhan H, Paxton JZ (2020) Investigating materials and orientation parameters for the creation of a 3D musculoskeletal interface co-culture model. *Regen Biomater* 7:413–425. <https://doi.org/10.1093/RB/RBAA018>
313. Gores GJ, Herman B, Lemasters JJ (1990) Plasma membrane bleb formation and rupture: A common feature of hepatocellular injury. *Hepatology* 11:690–698. <https://doi.org/10.1002/hep.1840110425>
314. Chomczynski P, Sacchi N (2006) The single-step method of RNA isolation by acid guanidinium thiocyanate-phenol-chloroform extraction: Twenty-something years on. *Nat Protoc* 1:581–585. <https://doi.org/10.1038/nprot.2006.83>
315. Tan SC, Yiap BC (2009) DNA, RNA, and protein extraction: The past and the present. *J Biomed Biotechnol* 2009:. <https://doi.org/10.1155/2009/574398>
316. Köster N, Schmiermund A, Grubelnig S, et al (2016) Single-Step RNA Extraction from Different Hydrogel-Embedded Mesenchymal Stem Cells for Quantitative Reverse Transcription-Polymerase Chain Reaction Analysis. *Tissue Eng Part C Methods* 22:552–560. <https://doi.org/10.1089/ten.tec.2015.0362>
317. Wang C, Hao J, Zhang F, et al (2008) RNA extraction from polysaccharide-based cell-laden hydrogel scaffolds. *Anal Biochem* 380:333–334. <https://doi.org/10.1016/j.ab.2008.06.005>

318. Wang L, Stegemann JP (2010) Extraction of high quality RNA from polysaccharide matrices using cetyltrimethylammonium bromide. *Biomaterials* 31:1612–1618. <https://doi.org/10.1016/j.biomaterials.2009.11.024>
319. Yu C, Young S, Russo V, et al (2013) Techniques for the isolation of high-quality RNA from cells encapsulated in chitosan hydrogels. *Tissue Eng Part C Methods* 19:829–838. <https://doi.org/10.1089/ten.tec.2012.0693>
320. Burgess KA, Workman VL, Elsayy MA, et al (2018) RNA extraction from self-assembling peptide hydrogels to allow qPCR analysis of encapsulated cells. *PLoS One* 13:1–19. <https://doi.org/10.1371/journal.pone.0197517>
321. Thomas MP, Liu X, Whangbo J, et al (2015) Apoptosis Triggers Specific, Rapid, and Global mRNA Decay with 3' Uridylated Intermediates Degraded by DIS3L2. *Cell Rep* 11:1079–1089. <https://doi.org/10.1016/j.celrep.2015.04.026>
322. Plemel JR, Caprariello A V., Keough MB, et al (2017) Unique spectral signatures of the nucleic acid dye acridine orange can distinguish cell death by apoptosis and necroptosis. *Journal of Cell Biology* 216:1163–1181. <https://doi.org/10.1083/jcb.201602028>
323. Salgado C, Jordan O, Allémann E (2021) Osteoarthritis in vitro models: Applications and implications in development of intra-articular drug delivery systems. *Pharmaceutics* 13:1–23. <https://doi.org/10.3390/pharmaceutics13010060>
324. Caron MMJ, Emans PJ, Coolsen MME, et al (2012) Redifferentiation of dedifferentiated human articular chondrocytes: Comparison of 2D and 3D cultures. *Osteoarthritis Cartilage* 20:1170–1178. <https://doi.org/10.1016/j.joca.2012.06.016>
325. Yamamoto K, Okano H, Miyagawa W, et al (2016) MMP-13 is constitutively produced in human chondrocytes and co-endocytosed with ADAMTS-5 and TIMP-3 by the endocytic receptor LRP1. *Matrix Biology* 56:57–73. <https://doi.org/10.1016/j.matbio.2016.03.007>
326. Yeung P, Cheng KH, Yan CH, Chan BP (2019) Collagen microsphere based 3D culture system for human osteoarthritis chondrocytes (hOACs). *Sci Rep* 9:. <https://doi.org/10.1038/s41598-019-47946-3>
327. Sarem M, Arya N, Heizmann M, et al (2018) Interplay between stiffness and degradation of architected gelatin hydrogels leads to differential modulation of chondrogenesis in vitro and in vivo. *Acta Biomater* 69:83–94. <https://doi.org/10.1016/j.actbio.2018.01.025>
328. V Thomas L, VG R, D Nair P (2017) Effect of stiffness of chitosan-hyaluronic acid dialdehyde hydrogels on the viability and growth of encapsulated chondrocytes. *Int J Biol Macromol* 104:1925–1935. <https://doi.org/10.1016/j.ijbiomac.2017.05.116>
329. Schuh E, Hofmann S, Stok K, et al (2012) Chondrocyte redifferentiation in 3D: The effect of adhesion site density and substrate elasticity. *J Biomed Mater Res A* 100 A:38–47. <https://doi.org/10.1002/jbm.a.33226>
330. Yang M, Zhang ZC, Liu Y, et al (2021) Function and Mechanism of RGD in Bone and Cartilage Tissue Engineering. *Front Bioeng Biotechnol* 9

331. Knight CG, Morton LF, Onley DJ, et al (1998) Identification in collagen type I of an integrin  $\alpha 2\beta 1$ -binding site containing an essential GER sequence. *Journal of Biological Chemistry* 273:33287–33294. <https://doi.org/10.1074/jbc.273.50.33287>
332. Koch F, Wolff A, Mathes S, et al (2018) Amino acid composition of nanofibrillar self-assembling peptide hydrogels affects responses of periodontal tissue cells in vitro. *Int J Nanomedicine* 13:6717–6733. <https://doi.org/10.2147/IJN.S173702>
333. Aye SSS, Li R, Boyd-Moss M, et al (2018) Scaffolds formed via the non-equilibrium supramolecular assembly of the synergistic ECM peptides RGD and PHSRN demonstrate improved cell attachment in 3D. *Polymers (Basel)* 10:. <https://doi.org/10.3390/polym10070690>
334. Diaferia C, Rosa E, Gallo E, et al (2021) Self-supporting hydrogels based on fmoc-derivatized cationic hexapeptides for potential biomedical applications. *Biomedicines* 9:. <https://doi.org/10.3390/biomedicines9060678>
335. Knight CG, Morton LF, Peachey AR, et al (2000) The collagen-binding  $\alpha$ -domains of integrins  $\alpha 1/\beta 1$  and  $\alpha 2/\beta 1$  recognize the same specific amino acid sequence, GFOGER, in native (triple- helical) collagens. *Journal of Biological Chemistry* 275:35–40. <https://doi.org/10.1074/jbc.275.1.35>
336. Petropoulou K, Platania V, Chatzinikolaidou M, Mitraki A (2022) A Doubly Fmoc-Protected Aspartic Acid Self-Assembles into Hydrogels Suitable for Bone Tissue Engineering. *Materials* 15:. <https://doi.org/10.3390/ma15248928>
337. Truong WT, Su Y, Gloria D, et al (2015) Dissolution and degradation of Fmoc-diphenylalanine self-assembled gels results in necrosis at high concentrations in vitro. *Biomater Sci* 3:298–307. <https://doi.org/10.1039/c4bm00244j>
338. McCloskey AP, Draper ER, Gilmore BF, Laverty G (2017) Ultrashort self-assembling Fmoc-peptide gelators for anti-infective biomaterial applications. *Journal of Peptide Science* 23:131–140. <https://doi.org/10.1002/psc.2951>
339. Griffin TM, Guilak F (2005) The Role of Mechanical Loading in the Onset and Progression of Osteoarthritis. *Exerc Sport Sci Rev* 33:195–200. <https://doi.org/10.1097/00003677-200510000-00008>
340. Min S, Wang C, Lu W, et al (2017) Serum levels of the bone turnover markers dickkopf-1, osteoprotegerin, and TNF- $\alpha$  in knee osteoarthritis patients. *Clin Rheumatol* 36:2351–2358. <https://doi.org/10.1007/s10067-017-3690-x>
341. McNulty AL, Rothfusz NE, Leddy HA, Guilak F (2013) Synovial fluid concentrations and relative potency of interleukin-1 alpha and beta in cartilage and meniscus degradation. *Journal of Orthopaedic Research* 31:1039–1045. <https://doi.org/10.1002/jor.22334>
342. Wang X, Li F, Fan C, et al (2011) Effects and relationship of ERK1 and ERK2 in interleukin-1 $\beta$ -induced alterations in MMP3, MMP13, type II collagen and aggrecan expression in human chondrocytes. *Int J Mol Med* 27:583–589. <https://doi.org/10.3892/ijmm.2011.611>
343. Séguin CA, Bernier SM (2003) TNF $\alpha$  Suppresses Link Protein and Type II Collagen Expression in Chondrocytes: Role of MEK1/2 and NF- $\kappa$ B Signaling Pathways. *J Cell Physiol* 197:356–369. <https://doi.org/10.1002/jcp.10371>

344. Hayden MS, Ghosh S (2014) Regulation of NF- $\kappa$ B by TNF family cytokines. *Semin Immunol* 26:253–266. <https://doi.org/10.1016/j.smim.2014.05.004>
345. Yamamoto K, Okano H, Miyagawa W, et al (2016) MMP-13 is constitutively produced in human chondrocytes and co-endocytosed with ADAMTS-5 and TIMP-3 by the endocytic receptor LRP1. *Matrix Biology* 56:57–73. <https://doi.org/10.1016/j.matbio.2016.03.007>
346. Duan R, Xie H, Liu ZZ (2020) The Role of Autophagy in Osteoarthritis. *Front Cell Dev Biol* 8:1–9. <https://doi.org/10.3389/fcell.2020.608388>
347. Roca-Agujetas V, De Dios C, Lestón L, et al (2019) Recent Insights into the Mitochondrial Role in Autophagy and Its Regulation by Oxidative Stress. *Oxid Med Cell Longev* 2019:. <https://doi.org/10.1155/2019/3809308>
348. Carames B, Hasegawa A, Taniguchi N, et al (2012) Autophagy Activation by Rapamycin Reduces Severity of Experimental Osteoarthritis. *Ann Rheum Dis* 71:575–581. <https://doi.org/10.1136/annrheumdis-2011-200557>.Autophagy
349. Feng L, Feng C, Wang CX, et al (2020) Circulating microRNA let-7e is decreased in knee osteoarthritis, accompanied by elevated apoptosis and reduced autophagy. *Int J Mol Med* 45:1464–1476. <https://doi.org/10.3892/ijmm.2020.4534>
350. Ribeiro M, López de Figueroa P, Blanco FJ, et al (2016) Insulin decreases autophagy and leads to cartilage degradation. *Osteoarthritis Cartilage* 24:731–739. <https://doi.org/10.1016/j.joca.2015.10.017>
351. Ribeiro M, López de Figueroa P, Nogueira-Recalde U, et al (2016) Diabetes-accelerated experimental osteoarthritis is prevented by autophagy activation. *Osteoarthritis Cartilage* 24:2116–2125. <https://doi.org/10.1016/j.joca.2016.06.019>
352. Hui W, Young DA, Rowan AD, et al (2016) Oxidative changes and signalling pathways are pivotal in initiating age-related changes in articular cartilage. *Ann Rheum Dis* 75:449–458. <https://doi.org/10.1136/annrheumdis-2014-206295>
353. Cheng NT, Guo A, Meng H (2016) The protective role of autophagy in experimental osteoarthritis, and the therapeutic effects of Torin 1 on osteoarthritis by activating autophagy. *BMC Musculoskelet Disord* 17:. <https://doi.org/10.1186/s12891-016-0995-x>
354. Cinque L, Forrester A, Bartolomeo R, et al (2015) FGF signalling regulates bone growth through autophagy. *Nature* 528:272–275. <https://doi.org/10.1038/nature16063>
355. Wu TT, Li WM, Yao YM (2016) Interactions between autophagy and inhibitory cytokines. *Int J Biol Sci* 12:884–897. <https://doi.org/10.7150/ijbs.15194>
356. Harris J, Hartman M, Roche C, et al (2011) Autophagy controls IL-1 $\beta$  secretion by targeting Pro-IL-1 $\beta$  for degradation. *Journal of Biological Chemistry* 286:9587–9597. <https://doi.org/10.1074/jbc.M110.202911>
357. Ni Z, Li H, Mu D, et al (2022) Rapamycin Alleviates 2,4,6-Trinitrobenzene Sulfonic Acid-Induced Colitis through Autophagy Induction and NF- $\kappa$  B Pathway Inhibition in Mice. *Mediators Inflamm* 2022:. <https://doi.org/10.1155/2022/2923216>
358. Hooper KM, Casanova V, Kemp S, et al (2019) The Inflammatory Bowel Disease Drug Azathioprine Induces Autophagy via mTORC1 and the Unfolded Protein Response Sensor PERK. *Inflamm Bowel Dis* 25:1481–1496. <https://doi.org/10.1093/ibd/izz039>

359. Chockalingam PS, Varadarajan U, Sheldon R, et al (2007) Involvement of protein kinase C $\zeta$  in interleukin-1 $\beta$  induction of ADAMTS-4 and type 2 nitric oxide synthase via NF- $\kappa$ B signaling in primary human osteoarthritic chondrocytes. *Arthritis Rheum* 56:4074–4083. <https://doi.org/10.1002/art.23043>
360. Rasheed Z, Akhtar N, Haqqi TM (2010) Pomegranate extract inhibits the interleukin-1 $\beta$ -induced activation of MKK-3, p38 $\alpha$ -MAPK and transcription factor RUNX-2 in human osteoarthritis chondrocytes. *Arthritis Res Ther* 12:. <https://doi.org/10.1186/ar3166>
361. Li S, Yang X, Feng Z, et al (2018) Catalase Enhances Viability of Human Chondrocytes in Culture by Reducing Reactive Oxygen Species and Counteracting Tumor Necrosis Factor- $\alpha$ -Induced Apoptosis. *Cellular Physiology and Biochemistry* 49:2427–2442. <https://doi.org/10.1159/000493841>
362. Zhang X, Dong Y, Dong H, et al (2021) Telmisartan Mitigates TNF- $\alpha$ -Induced Type II Collagen Reduction by Upregulating SOX-9. *ACS Omega* 6:11756–11761. <https://doi.org/10.1021/acsomega.1c01170>
363. Shakibaei M, John T, Seifarth C, Mobasheri A (2007) Resveratrol inhibits IL-1 $\beta$ -induced stimulation of caspase-3 and cleavage of PARP in human articular chondrocytes in vitro. *Ann N Y Acad Sci* 1095:554–563. <https://doi.org/10.1196/annals.1397.060>
364. Los M, Mozoluk M, Ferrari D, et al (2002) Activation and caspase-mediated inhibition of PARP: A molecular switch between fibroblast necrosis and apoptosis in death receptor signaling. *Mol Biol Cell* 13:978–988. <https://doi.org/10.1091/mbc.01-05-0272>
365. Saklatvala J (1998) Tumour necrosis factor  $\alpha$  stimulates resorption and inhibits synthesis of proteoglycan in cartilage. *J Natl Med Assoc* 322:547–549. <https://doi.org/10.2165/00128415-199204100-00048>
366. Chadjichristos C, Ghayor C, Kypriotou M, et al (2003) Sp1 and Sp3 transcription factors mediate interleukin-1 $\beta$  down-regulation of human type II collagen gene expression in articular chondrocytes. *Journal of Biological Chemistry* 278:39762–39772. <https://doi.org/10.1074/jbc.M303541200>
367. Woodell-May J, Matuska A, Oyster M, et al (2011) Autologous protein solution inhibits MMP-13 production by IL-1 $\beta$  and TNF $\alpha$ -stimulated human articular chondrocytes. *Journal of Orthopaedic Research* 29:1320–1326. <https://doi.org/10.1002/jor.21384>
368. Solis-Herruzo JA, Brenner DA, Chojkier M (1988) Tumor necrosis factor  $\alpha$  inhibits collagen gene transcription and collagen synthesis in cultured human fibroblasts. *Journal of Biological Chemistry* 263:5841–5845. [https://doi.org/10.1016/s0021-9258\(18\)60642-8](https://doi.org/10.1016/s0021-9258(18)60642-8)
369. Osei ET, B. Mostaço-Guidolin L, Hsieh A, et al (2020) Epithelial-interleukin-1 inhibits collagen formation by airway fibroblasts: Implications for asthma. *Sci Rep* 10:1–14. <https://doi.org/10.1038/s41598-020-65567-z>
370. Fan Z, Yang H, Bau B, et al (2006) Role of mitogen-activated protein kinases and NF $\kappa$ B on IL-1 $\beta$ -induced effects on collagen type II, MMP-1 and 13 mRNA expression in normal articular human chondrocytes. *Rheumatol Int* 26:900–903. <https://doi.org/10.1007/s00296-006-0114-7>

371. Han Z, Boyle DL, Chang L, et al (2001) c-Jun N-terminal kinase is required for metalloproteinase expression and joint destruction in inflammatory arthritis. *Journal of Clinical Investigation* 108:73–81. <https://doi.org/10.1172/jci200112466>
372. Hwang SG, Yu SS, Poo H, Chun JS (2005) c-Jun/activator protein-1 mediates interleukin-1 $\beta$ -induced dedifferentiation but not cyclooxygenase-2 expression in articular chondrocytes. *Journal of Biological Chemistry* 280:29780–29787. <https://doi.org/10.1074/jbc.M411793200>
373. Micheau O, Rg Tschopp J (2003) Induction of TNF Receptor I-Mediated Apoptosis via Two Sequential Signaling Complexes of these receptors delivers a powerful and rapid proapoptotic signal through a DD-mediated recruitment of the adaptor protein FADD and the formation of the so-called complex I fails to induce the expression of antiapoptotic
374. Qin J, Shang L, Ping A-S, et al (2012) TNF/TNFR signal transduction pathway-mediated anti-apoptosis and anti-inflammatory effects of sodium ferulate on IL-1 $\beta$ -induced rat osteoarthritis chondrocytes in vitro. *Arthritis Res Ther* 14:. <https://doi.org/10.1186/ar4085>
375. Liacini A, Sylvester J, Li WQ, et al (2003) Induction of matrix metalloproteinase-13 gene expression by TNF- $\alpha$  is mediated by MAP kinases, AP-1, and NF- $\kappa$ B transcription factors in articular chondrocytes. *Exp Cell Res* 288:208–217. [https://doi.org/10.1016/S0014-4827\(03\)00180-0](https://doi.org/10.1016/S0014-4827(03)00180-0)
376. Cabal-Hierro L, Rodríguez M, Artime N, et al (2014) TRAF-mediated modulation of NF- $\kappa$ B AND JNK Activation by TNFR2. *Cell Signal* 26:2658–2666. <https://doi.org/10.1016/j.cellsig.2014.08.011>
377. Gun Bilgic D, Hatipoglu OF, Cigdem S, et al (2020) NF- $\kappa$ B upregulates ADAMTS5 expression by direct binding after TNF- $\alpha$  treatment in OUMS-27 chondrosarcoma cell line. *Mol Biol Rep* 47:4215–4223. <https://doi.org/10.1007/s11033-020-05514-3>
378. Westacott CI, Barakat AF, Wood L, et al (2000) Tumor necrosis factor alpha can contribute to focal loss of cartilage in osteoarthritis. *Osteoarthritis Cartilage* 8:213–221. <https://doi.org/10.1053/joca.1999.0292>
379. Xue J, Wang J, Liu Q, Luo A (2013) Tumor necrosis factor- $\alpha$  induces ADAMTS-4 expression in human osteoarthritis chondrocytes. *Mol Med Rep* 8:1755–1760. <https://doi.org/10.3892/mmr.2013.1729>
380. Murakami S, Lefebvre V, De Crombrughe B (2000) Potent inhibition of the master chondrogenic factor Sox9 gene by interleukin-1 and tumor necrosis factor- $\alpha$ . *Journal of Biological Chemistry* 275:3687–3692. <https://doi.org/10.1074/jbc.275.5.3687>
381. Kriegler M, Perez C, Defay K, et al (1988) A Novel Form of TNF/Cachectin Is a Cell Surface Cytotoxic Transmembrane Protein: Ramifications for the Complex Physiology of TNF. *Cell* 53:45–53. [https://doi.org/10.1016/0092-8674\(88\)90486-2](https://doi.org/10.1016/0092-8674(88)90486-2).
382. Grell M, Douni E, Wajant H, et al (1995) The Transmembrane Form of Tumor Necrosis Factor Is the Prime Activating Ligand of the 80 kDa Tumor Necrosis Factor Receptor. *Cell* 83:793–802. [https://doi.org/10.1016/0092-8674\(95\)90192-2](https://doi.org/10.1016/0092-8674(95)90192-2).

383. Grell M, Wajant H, Zimmermann G, Scheurich P (1998) The type 1 receptor (CD120a) is the high-affinity receptor for soluble tumor necrosis factor. *Cell Biology* 95:570–575. <https://doi.org/doi: 10.1073/pnas.95.2.570>
384. Zheng L, Wang W, Ni J, et al (2017) Role of autophagy in tumor necrosis factor- $\alpha$ -induced apoptosis of osteoblast cells. *Journal of Investigative Medicine* 65:1014–1020. <https://doi.org/10.1136/jim-2017-000426>
385. Shen J, Xu S, Zhou H, et al (2017) IL-1 $\beta$  induces apoptosis and autophagy via mitochondria pathway in human degenerative nucleus pulposus cells. *Sci Rep* 7:1–12. <https://doi.org/10.1038/srep41067>
386. Dai Y, Ding J, Yin W, et al (2018) Increased Autophagy Enhances the Resistance to Tumor Necrosis Factor-Alpha Treatment in Rheumatoid Arthritis Human Fibroblast-Like Synovial Cell. *Biomed Res Int* 2018:. <https://doi.org/10.1155/2018/4941027>
387. Jia G, Cheng G, Gangahar DM, Agrawal DK (2006) Insulin-like growth factor-1 and TNF- $\alpha$  regulate autophagy through c-jun N-terminal kinase and Akt pathways in human atherosclerotic vascular smooth cells. *Immunol Cell Biol* 84:448–454. <https://doi.org/10.1111/j.1440-1711.2006.01454.x>
388. Sivaprasad U, Basu A (2008) Inhibition of ERK attenuates autophagy and potentiates tumour necrosis factor- $\alpha$ -induced cell death in MCF-7 cells. *J Cell Mol Med* 12:1265–1271. <https://doi.org/10.1111/j.1582-4934.2008.00282.x>
389. Pun NT, Subedi A, Kim MJ, Park PH (2015) Globular adiponectin causes tolerance to LPS-induced TNF- $\alpha$  expression via autophagy induction in RAW 264.7 macrophages: Involvement of SIRT1/FoxO3A axis. *PLoS One* 10:. <https://doi.org/10.1371/journal.pone.0124636>
390. Shi CS, Shenderov K, Huang NN, et al (2012) Activation of autophagy by inflammatory signals limits IL-1 $\beta$  production by targeting ubiquitinated inflammasomes for destruction. *Nat Immunol* 13:255–263. <https://doi.org/10.1038/ni.2215>
391. Ribeiro M, López de Figueroa P, Blanco FJ, et al (2016) Insulin decreases autophagy and leads to cartilage degradation. *Osteoarthritis Cartilage* 24:731–739. <https://doi.org/10.1016/j.joca.2015.10.017>
392. Ribeiro M, López de Figueroa P, Nogueira-Recalde U, et al (2016) Diabetes-accelerated experimental osteoarthritis is prevented by autophagy activation. *Osteoarthritis Cartilage* 24:2116–2125. <https://doi.org/10.1016/j.joca.2016.06.019>
393. Lin X, Han L, Weng J, et al (2018) Rapamycin inhibits proliferation and induces autophagy in human neuroblastoma cells. *Biosci Rep* 38:1–8. <https://doi.org/10.1042/BSR20181822>
394. Ravikumar B, Vacher C, Berger Z, et al (2004) Inhibition of mTOR induces autophagy and reduces toxicity of polyglutamine expansions in fly and mouse models of Huntington disease. *Nat Genet* 36:585–595. <https://doi.org/10.1038/ng1362>
395. Nam HJ, Kim YE, Moon BS, et al (2021) Azathioprine antagonizes aberrantly elevated lipid metabolism and induces apoptosis in glioblastoma. *iScience* 24:. <https://doi.org/10.1016/j.isci.2021.102238>
396. Lin Z, Willers C, Xu J, Zheng M-H The Chondrocyte: Biology and Clinical Application

397. Czekanska EM, Stoddart MJ, Richards RG, Hayes JS (2012) In search of an osteoblast cell model for in vitro research. *Eur Cell Mater* 24:1–17. <https://doi.org/10.22203/eCM.v024a01>
398. Carsons SE, Wolf J (1995) Interaction between synoviocytes and extracellular matrix in vitro. *Ann Rheum Dis* 54:413–416. <https://doi.org/10.1136/ard.54.5.413>
399. Fu D, Yang Y, Xiao Y, et al (2012) Role of p21-activated kinase 1 in regulating the migration and invasion of fibroblast-like synoviocytes from rheumatoid arthritis patients. *Rheumatology (United Kingdom)* 51:1170–1180. <https://doi.org/10.1093/rheumatology/kes031>
400. Couto MA, Liu L, Lehrer, And RI, Ganz T (1994) Inhibition of Intracellular Histoplasma capsulatum Replication by Murine Macrophages That Produce Human Defensin. *Infect Immun* 62:2375–2378. <https://doi.org/10.1128/iai.62.6.2375-2378.1994>
401. Huh YH, Lee G, Song WH, et al (2015) Crosstalk between FLS and chondrocytes is regulated by HIF-2 $\alpha$ -mediated cytokines in arthritis. *Exp Mol Med* 47:. <https://doi.org/10.1038/EMM.2015.88>
402. Li M, Qian M, Kyler K, Xu J (2018) Endothelial–Vascular Smooth Muscle Cells Interactions in Atherosclerosis. *Front Cardiovasc Med* 5:. <https://doi.org/10.3389/fcvm.2018.00151>
403. Knight CG, Morton LF, Onley DJ, et al (1998) Identification in collagen type I of an integrin  $\alpha 2\beta 1$ -binding site containing an essential GER sequence. *Journal of Biological Chemistry* 273:33287–33294. <https://doi.org/10.1074/jbc.273.50.33287>
404. Kvist AJ, Nyström A, Hultenby K, et al (2008) The major basement membrane components localize to the chondrocyte pericellular matrix - A cartilage basement membrane equivalent? *Matrix Biology* 27:22–33. <https://doi.org/10.1016/j.matbio.2007.07.007>
405. Tang Y, Luo K, Tan J, et al (2021) Laminin alpha 4 promotes bone regeneration by facilitating cell adhesion and vascularization. *Acta Biomater* 126:183–198. <https://doi.org/10.1016/j.actbio.2021.03.011>
406. Tang J, Saito T (2018) A Novel Fragment Derived from Laminin-411 Facilitates Proliferation and Differentiation of Odontoblast-Like Cells. *Biomed Res Int* 2018:. <https://doi.org/10.1155/2018/9465383>
407. Yang M, Zhang ZC, Liu Y, et al (2021) Function and Mechanism of RGD in Bone and Cartilage Tissue Engineering. *Front Bioeng Biotechnol* 9:. <https://doi.org/10.3389/fbioe.2021.773636>
408. Tao T, Li Y, Gui C, et al (2018) Fibronectin enhances cartilage repair by activating progenitor cells through integrin  $\alpha 5\beta 1$  Receptor. *Tissue Eng Part A* 24:1112–1124. <https://doi.org/10.1089/ten.tea.2017.0322>
409. Ostergaard K, Salter DM, Petersen J, et al Expression of  $\alpha$  and  $\beta$  subunits of the integrin superfamily in articular cartilage from macroscopically normal and osteoarthritic human femoral heads. <https://doi.org/10.1136/ard.57.5.303>

410. Almonte-Becerril M, Costell M, Kouri JB (2014) Changes in the integrins expression are related with the osteoarthritis severity in an experimental animal model in rats. *Journal of Orthopaedic Research* 32:1161–1166. <https://doi.org/10.1002/jor.22649>
411. Candela ME, Wang C, Gunawardena AT, et al (2016) Alpha 5 integrin mediates osteoarthritic changes in mouse knee joints. *PLoS One* 11:. <https://doi.org/10.1371/journal.pone.0156783>
412. Wang Q, Onuma K, Liu C, et al (2019) Dysregulated integrin  $\alpha$ V $\beta$ 3 and CD47 signaling promotes joint inflammation, cartilage breakdown, and progression of osteoarthritis. *JCI Insight* 4:. <https://doi.org/10.1172/jci.insight.128616>
413. Hamidouche Z, Fromigué O, Ringe J, et al Priming integrin 5 promotes human mesenchymal stromal cell osteoblast differentiation and osteogenesis. <https://doi.org/10.1073/pnas.0812334106>
414. Cheng SL, Lai CF, Blystone SD, Avioli L V. (2001) Bone mineralization and osteoblast differentiation are negatively modulated by integrin  $\alpha$ V $\beta$ 3. *Journal of Bone and Mineral Research* 16:277–288. <https://doi.org/10.1359/jbmr.2001.16.2.277>
415. Schuh E, Hofmann S, Stok K, et al (2012) Chondrocyte redifferentiation in 3D: The effect of adhesion site density and substrate elasticity. *J Biomed Mater Res A* 100 A:38–47. <https://doi.org/10.1002/jbm.a.33226>
416. Sarem M, Arya N, Heizmann M, et al (2018) Interplay between stiffness and degradation of architected gelatin hydrogels leads to differential modulation of chondrogenesis in vitro and in vivo. *Acta Biomater* 69:83–94. <https://doi.org/10.1016/j.actbio.2018.01.025>
417. V Thomas L, VG R, D Nair P (2017) Effect of stiffness of chitosan-hyaluronic acid dialdehyde hydrogels on the viability and growth of encapsulated chondrocytes. *Int J Biol Macromol* 104:1925–1935. <https://doi.org/10.1016/j.ijbiomac.2017.05.116>
418. Kim JH, Lee G, Won Y, et al (2015) Matrix cross-linking-mediated mechanotransduction promotes posttraumatic osteoarthritis. *Proc Natl Acad Sci U S A* 112:9424–9429. <https://doi.org/10.1073/pnas.1505700112>
419. Rho JY, Ashman RB, Turner CH (1993) Young's modulus of trabecular and cortical bone material: Ultrasonic and microtensile measurements. *J Biomech* 26:111–119. [https://doi.org/10.1016/0021-9290\(93\)90042-D](https://doi.org/10.1016/0021-9290(93)90042-D)
420. Wu TT, Li WM, Yao YM (2016) Interactions between autophagy and inhibitory cytokines. *Int J Biol Sci* 12:884–897. <https://doi.org/10.7150/ijbs.15194>
421. Ribeiro M, López de Figueroa P, Blanco FJ, et al (2016) Insulin decreases autophagy and leads to cartilage degradation. *Osteoarthritis Cartilage* 24:731–739. <https://doi.org/10.1016/j.joca.2015.10.017>
422. Cinque L, Forrester A, Bartolomeo R, et al (2015) FGF signalling regulates bone growth through autophagy. *Nature* 528:272–275. <https://doi.org/10.1038/nature16063>
423. Ni Z, Li H, Mu D, et al (2022) Rapamycin Alleviates 2,4,6-Trinitrobenzene Sulfonic Acid-Induced Colitis through Autophagy Induction and NF- $\kappa$  B Pathway Inhibition in Mice. *Mediators Inflamm* 2022:. <https://doi.org/10.1155/2022/2923216>

424. Grässel S, Muschter D (2020) Recent advances in the treatment of osteoarthritis. *F1000 Research* 9:. <https://doi.org/10.12688/f1000research.22115.1>
425. Brumat P, Kunšič O, Novak S, et al (2022) The Surgical Treatment of Osteoarthritis. *Life* 12:. <https://doi.org/10.3390/life12070982>
426. Hunter DJ, Bierma-Zeinstra S (2019) Osteoarthritis. *The Lancet* 393:1745–1759. [https://doi.org/10.1016/S0140-6736\(19\)30417-9](https://doi.org/10.1016/S0140-6736(19)30417-9)
427. Hui W, Young DA, Rowan AD, et al (2016) Oxidative changes and signalling pathways are pivotal in initiating age-related changes in articular cartilage. *Ann Rheum Dis* 75:449–458. <https://doi.org/10.1136/annrheumdis-2014-206295>
428. Iozzo R V., Gubbiotti MA (2018) Extracellular matrix: The driving force of mammalian diseases. *Matrix Biology* 71–72:1–9. <https://doi.org/10.1016/j.matbio.2018.03.023>
429. Duarte S, Baber J, Fujii T, Coito AJ (2015) Matrix metalloproteinases in liver injury, repair and fibrosis. *Matrix Biology* 44–46:147–156. <https://doi.org/10.1016/j.matbio.2015.01.004>
430. Smolen JS, Aletaha D, McInnes IB (2016) Rheumatoid arthritis. *The Lancet* 388:2023–2038
431. Tauer JT, Robinson ME, Rauch F (2019) Osteogenesis Imperfecta: New Perspectives From Clinical and Translational Research. *JBMR Plus* 3
432. Seegmiller RE, Foster C, Burnham JL (2019) Understanding chondrodysplasia (cho): A comprehensive review of cho as an animal model of birth defects, disorders, and molecular mechanisms. *Birth Defects Res* 111:237–247
433. Gasparian A, Daneshian L, Ji H, et al (2015) Purification of high-quality RNA from synthetic polyethylene glycol-based hydrogels. *Anal Biochem* 484:1–3. <https://doi.org/10.1016/j.ab.2015.05.002>
434. Ma H-H, Fu J, Lentzsch S, Mapara MY (2019) Role of MMP-13 in Graft-Versus-Host Disease. *Blood* 134:1928–1928. <https://doi.org/10.1182/blood-2019-127703>
435. Mendonsa AM, VanSaun MN, Ustione A, et al (2015) Host and tumor derived MMP13 regulate extravasation and establishment of colorectal metastases in the liver. *Mol Cancer* 14:. <https://doi.org/10.1186/s12943-014-0282-0>
436. Singh YP, Moses JC, Bandyopadhyay A, Mandal BB (2022) 3D Bioprinted Silk-Based In Vitro Osteochondral Model for Osteoarthritis Therapeutics. *Adv Healthc Mater* 11:. <https://doi.org/10.1002/adhm.202200209>
437. Silvestri A, Vicente F, Vicent MJ, et al (2021) Academic collaborative models fostering the translation of physiological in vitro systems from basic research into drug discovery. *Drug Discov Today* 26:1369–1381. <https://doi.org/10.1016/j.drudis.2021.02.024>
438. Banh L, Cheung KK, Chan MWY, et al (2022) Advances in organ-on-a-chip systems for modelling joint tissue and osteoarthritic diseases. *Osteoarthritis Cartilage* 30:1050–1061. <https://doi.org/10.1016/j.joca.2022.03.012>
439. Lin Z, Li Z, Li EN, et al (2019) Osteochondral Tissue Chip Derived From iPSCs: Modeling OA Pathologies and Testing Drugs. *Front Bioeng Biotechnol* 7:. <https://doi.org/10.3389/fbioe.2019.00411>

440. Paggi CA, Venzac B, Karperien M, et al (2020) Monolithic microfluidic platform for exerting gradients of compression on cell-laden hydrogels, and application to a model of the articular cartilage. *Sens Actuators B Chem* 315:.  
<https://doi.org/10.1016/j.snb.2020.127917>
441. Mondadori C, Palombella S, Salehi S, et al (2021) Recapitulating monocyte extravasation to the synovium in an organotypic microfluidic model of the articular joint. *Biofabrication* 13:.  
<https://doi.org/10.1088/1758-5090/ac0c5e>

## **Appendix**

### **Appendix I**

#### **Protein extraction, gel electrophoresis and immunoblotting buffers**

##### **Urea buffer**

8M Urea, 1M Tris pH 7.5, 1M NaCl, 1% Triton and 1M DTT.

##### **Laemmli Sample Buffer**

6% SDS, 22.5% glycerol, 93.8mM Tris-HCl pH 6.8 and bromophenol blue.

##### **Running Buffer (10X)**

144g glycine, 30g tris in 1L dH<sub>2</sub>O. Dilute to 1X using dH<sub>2</sub>O.

### Transfer Buffer (10X)

0.1% SDS, 144g glycine, 30g tris in 1L dH<sub>2</sub>O. Dilute to 1X using 7 parts dH<sub>2</sub>O, 2 parts methanol, and 1 part 10X transfer buffer.

### Stacking Gel

2.8mL H<sub>2</sub>O, 0.5mL 1M Tris-glycine pH 6.8, 0.67mL protogel, 40μL 10% SDS, 20μL 25% APS and 10μL TEMED.

### Resolving Gel

	6% gel	7% gel	8% gel	10% gel
H <sub>2</sub> O (mL)	3.87	3.8	3.6	2.84
1M Tris-glycine pH 8.8 (mL)	3.73	3.73	3.73	3.73
Protogel (mL)	2	2.3	2.67	3.33
10% SDS (μL)	100	100	100	100
APS (μL)	40	40	40	40
TEMED (μL)	10	10	10	10

## Appendix II – Primers

### Chondrocyte primers and housekeeping genes

Gene	Source		Sequence (5'-3')
COL2A1	Primer Design	F	ATGGCTGACCTGACCTGAT
		R	GACAATAAATAAATAGAACACCGAGAT
COL10A1	Primer Design	F	TGCTAGTATCCTTGAACCTGGTTC
		R	GGAATGAAGAACTGTGTCTTGGT
MMP13	Primer Design	F	ATGAAGACCCCAACCCTAAACA
		R	CGGAGACTGGTAATGGCATCA
ACAN	Primer Design	F	CCAACCAGCCTGACAACCTT
		R	GTGAAGGGGAGGTGGTAATTG
COMP	Primer Design	F	CCCCAATGAAAAGGACAACCTGC
		R	TGGTCGTCGTTCTTCTGGGA
B2M	Origene	F	CCACTGAAAAAGATGAGTATGCCT
		R	CCAATCAAATGCGGCATCTTCA
SDHA	Origene	F	GAGATGTGGTGTCTCGGTCCA
		R	GCTGTCTCTGAAATGCCAGGCA

## Osteoblast primers and housekeeping genes

Gene	Source		Sequence (5'-3')
COL1A1	Primer Design	F	TGGCTCTCCTGGTGAACAAG
		R	GCCAGGGAGACCGTTGAG
ALPL	Primer Design	F	CGAGATACAAGCACTCCCCTT
		R	GTCACGTTGTTCTGTTTCAGC
POSTN	Primer Design	F	TGCTCCCACCAATGAGGCT
		R	CTGGAGAGTATTTAAGATGTGGTACTTC
BGLAP	Primer Design	F	CCAGCGGTGCAGAGTCCAG
		R	CAGGTAGCGCCTGGGTCTC
PDPN	Primer Design	F	TCCACGGAGAAAGTGGATGG
		R	CCCTTCAGCTCTTTAGGGCG
ATP5B	Origene	F	TCATGCTGAGGCTCCAGAGTTC
		R	ACAGTCTTGCCAACTCCAGCAC
TOP1	Origene	F	GAACAAGCAGCCCGAGGATGAT
		R	TGCTGTAGCGTGATGGAGGCAT

## Appendix III – Antibodies

### Primary Antibodies

Antibody	Species	Source	Use	Dilution
COL1 $\alpha$ 1	Rabbit	Abcam	Immunoblotting	1:1000
PDPN	Sheep	R & D Systems	Immunoblotting	1:1000
AP-TNAP	Rabbit	Abcam	Immunoblotting	1:5000
COL2 $\alpha$ 1	Rabbit	Abcam	Immunoblotting	1:1000
COMP	Rabbit	Abcam	Immunoblotting	1:900
MMP13	Rabbit	Abcam	Immunoblotting	1:1000
COL10 $\alpha$ 1	Rabbit	Abcam	Immunoblotting	1:1000
P65	Mouse	Santa Cruz Biotechnology	Immunofluorescence	1:50
rS6	Mouse	Cell Signalling Technology	Immunoblotting	1:1000
Phospho-rS6	Mouse	Cell Signalling Technology	Immunoblotting	1:1000
BACT	Mouse	Cell Signalling Technology	Immunoblotting	1:2000
LC3	Rabbit		Immunoblotting	1:1000

		MBL International	Immunofluorescence	1:1000
--	--	----------------------	--------------------	--------

### Secondary antibodies

Antibody	Source	Use	Dilution
Goat anti-mouse 680LT	LI-COR	Immunoblotting	1:10,000
Goat anti-rabbit 680LT	LI-COR	Immunoblotting	1:10,000
Goat anti-mouse 800CW	LI-COR	Immunoblotting	1:10,000
		Immunofluorescence	1:2000
Goat anti-rabbit 800CW	LI-COR	Immunoblotting	1:10,000
		Immunofluorescence	1:10,000
Donkey anti-sheep IgG H&L (HRP)	Abcam	Immunoblotting	1:5000

### Appendix IV – Count masks

NI C28 LD GFOMED RED 18NOV21 Day0 - Windows Photo Viewer

File Print Email Burn Open

Count Masks of NI C28 LD GFOMED RED 18NOV21 Day0.tif (75%)

3.24x3.24 inches (972x972) 16-bit, 1.8MB

NI C28 LD GFOMED RED 18NOV21 Day0.tif - Windows Photo Viewer

File Edit Image Process Analyze Plugins Window Help

Slice	Count	Total Area	Average Size	%Area	Mean
NI C28 LD GFOMED RED 18NOV21 Day0.tif	361	0.101	2.811E-4	0.967	255

